UNCLASSIFIED

SECURITY CLASSIFICATION OF THIS PAGE (When Data Entered)

REPORT DOCUMENTATION PAGE		READ INSTRUCTIONS BEFORE COMPLETING FORM
1. REPORT NUMBER AFOSR-TR- 86-0554	2. GOVT ACCESSION NO.	3. RECIPIENT'S CATALOG NUMBER
4. TITLE (and Subtitle) Relationship Between Near-Field and Teleseismic Observations of Seismic Source Parameters		5. TYPE OF REPORT & PERIOD COVERED Final Technical 1 Feb.,1982 - 31 May, 1985
		6. PERFORMING ORG. REPORT NUMBER
7. AUTHOR(s) Shelton S. Alexander		8. CONTRACT OR GRANT NUMBER(s) Grant AFOSR-82-0054
9. PERFORMING ORGANIZATION NAME AND ADDRESS Geophysics Program/Geosciences Department 403 Deike Building, Pennsylvania State Univ. University Park, PA 16802		10. PROGRAM ELEMENT, PROJECT, TASK AREA & WORK UNIT NUMBERS 61102F, 2309, A9 N/A
11. CONTROLLING OFFICE NAME AND ADDRESS AFOSR/NP, Bldg 410 Bolling AFB, DC 20332-6448		12. REPORT DATE
		13. NUMBER OF PAGES 265
MONITORING AGENCY NAME & ADDRESS(if different from Controlling Office)		15. SECURITY CLASS. (of this report) UNCLASSIFIED
		15a. DECLASSIFICATION/DOWNGRADING SCHEDULE

DISTRIBUTION STATEMENT (of this Report)

DISTRIBUTION STATEMENT A
Approved for public release
Distribution Unlimited

DTIC ELECTE AUG 11 1986 S D

DISTRIBUTION STATEMENT (of the abstract entered in Block 20, if different from Report)

Approved for public release,
distribution unlimited

SUPPLEMENTARY NOTES

AD-A170 751

DTIC FILE COPY

19. KEY WORDS (Continue on reverse side if necessary and identify by block number)
Seismic surface waves, attenuation (Q), Lg excitation, explosion source, earthquake source, non-isotropic source excitation, synthetic seismograms, tectonic stress release, Lg magnitude-yield, regional recordings, Nevada test site, eastern North America, upper mantle structure beneath LASA, polarization filtering, French Sahara test site, New Brunswick source zone.

20. ABSTRACT (Continue on reverse side if necessary and identify by block number)

This report summarizes all of the research completed under this Grant. Earlier semi-annual and annual technical reports provide detailed descriptions of the first 19 months' work. The most recent findings are summarized as follows: For each of a number of Soviet explosions two different spectral approaches were used to determine the average Q for Lg signals arriving in a velocity window ranging approximately from 3.5 to 3.0 km/sec. The mean spectral slope based on all the events analyzed is then used to calculate the average attenuation coefficient $(QU)^{-1}$. Results from individual stations of

DD FORM 1 JAN 73 1473 EDITION OF 1 NOV 65 IS OBSOLETE

SECURITY CLASSIFICATION OF THIS PAGE (When Data Entered)

UNCLASSIFIED

the Grafenberg array (6 to 13 stations) were averaged for each event and compared to the single station (A1) results. Additionally, transverse component data were available for three of the GRF stations. At MAIO only vertical component Lg data were available. For the propagation path from Semipalatinsk to GRF, the narrow-band filtering method and the noise-corrected power spectra of both vertical and transverse components give an average Q for Lg of approximately 1000. For the path from Azgir to GRF the average Q is around 1100. For the path from Semipalatinsk to MAIO the average Q is approximately 625. There appear to be no significant differences in the results among individual events for each path, indicating that the strong tectonic release effects in evidence at long periods for some of the Semipalatinsk events do not influence the Lg spectra of those events appreciably in the frequency band .3 to 1.2 Hz, and the best band to use to establish an m_{bLg} vs m_b relationship is centered at .6 to .7 Hz.

To overcome long-period non-isotropic source effects for Shagan River events several very low tectonic release events are used to obtain an empirical "pure" explosion" Rayleigh signature (shape) which then is incrementally scaled and subtracted from the total Rayleigh wave signature of high tectonic release events until the best double-couple solution that also fits the Love wave signals is found (i.e. when the trace of the moment tensor is closest to zero); the scaled signal is then the appropriate explosion contribution. The remaining "pure earthquake" Rayleigh and Love wave signals for each event are interpreted in terms of a best-fitting equivalent earthquake model.

To determine the approximate threshold for obtaining source parameters from long-period surface waves in an intraplate setting, the phase matched filtering method is used to analyze the 1982 New Brunswick aftershock sequence with the well-recorded mainshock seismograms as the reference signals. The source excitation function of each aftershock is extracted from the observed signal spectrum by correcting for the path transfer function and the main shock source excitatation. Preliminary results using this approach on recordings at GDSN stations in North America indicate that source parameters (including depth) can be extracted for events as small as about m_b 4 to 4.5. (This will be part of a M.S. thesis by B. Yan).

The 1982 New Brunswick earthquake series, including the m_b 5.7 mainshock and several high magnitude aftershocks were investigated to determine their source mechanisms and focal depths. Band-pass filters applied over a broad frequency range provided group velocity and spectral amplitude data for Rayleigh and Love modes for the path to SCP. Synthetic amplitude spectra were generated assuming structure parameters common to both the source area and the propagation path. Key aspects of the source mechanism could be inferred from the fundamental mode observations, particularly for the mainshock on January 9, 1982, and the largest magnitude aftershock which occurred on January 11. Although there are significant differences in modal excitation at the higher frequencies from event to event, only qualitative support for source mechanism could be inferred because higher order modes could not be identified at the higher frequencies. Additionally, published NEIS teleseismic m_b, network m_{bLg}, and M_s values were compared with m_{bLg} and M_s values computed with the SCP data. These results indicated that the single-station m_{bLg} values for the four New Brunswick events studied in detail agreed remarkably well with the network average magnitudes, whereas M_s values commonly disagreed. In spite of the observed variable excitation of the individual higher order modes, consistent with the theoretical excitation appropriate for the different mechanisms for these events, the ensemble of modes that comprises the Lg signal gives every indication of providing a stable measure of source strength when m_{bLg} is measured according to Nuttli's magnitude relationship.

The fundamental mode Love-to-Rayleigh surface wave spectral ratios for periods greater than ten seconds provided estimates of source mechanism and focal depth for the mainshock and its larger aftershocks. The accuracy of focal depth determinations is approximately ± 1 km.

COLLEGE OF EARTH AND MINERAL SCIENCES

FINAL TECHNICAL REPORT

1 February 1983 - 31 May 1985

RELATIONSHIP BETWEEN NEAR-FIELD AND TELESEISMIC OBSERVATIONS OF SEISMIC SOURCE PARAMETERS

Grant AFOSR-82-0054

Sponsored by
Advanced Research Projects Agency (DOD)
ARPA Order No. 4397/3
Monitored by AFOSR Under Grant NO. AFOSR-82-0054

Principal Investigator: Shelton S. Alexander

Geophysics Program, Geosciences Department
403 Deike Building
Pennsylvania State University
University Park, PA 16802

The Pennsylvania State University

University Park, Pennsylvania

THE PENNSYLVANIA STATE UNIVERSITY

College of Earth and Mineral Sciences

UNDERGRADUATE PROGRAMS OF STUDY

Ceramic Science and Engineering, Earth Sciences, Fuel Science, Geography, Geosciences, Metallurgy, Meteorology, Mineral Economics, Mining Engineering, Petroleum and Natural Gas Engineering, and Polymer Science.

GRADUATE PROGRAMS AND FIELDS OF RESEARCH

Ceramic Science, Fuel Science, Geochemistry and Mineralogy, Geography, Geology, Geophysics, Metallurgy, Meteorology, Mineral Economics, Mineral Processing, Mining Engineering, Petroleum and Natural Gas Engineering, and Polymer Science.

UNIVERSITY-WIDE INTERDISCIPLINARY GRADUATE PROGRAMS INVOLVING E&MS FACULTY AND STUDENTS

Earth Sciences, Ecology, Environmental Pollution Control Engineering, Mineral Engineering Management, Operations Research, Regional Planning, and Solid State Science.

ASSOCIATE DEGREE PROGRAMS

Metallurgical Engineering Technology and Mining Technology.

INTERDISCIPLINARY RESEARCH GROUPS WITHIN THE COLLEGE

Coal Research Section, Mineral Conservation Section, Ore Deposits Research Section, and Mining and Mineral Resources Research Institute.

ANALYTICAL AND STRUCTURE STUDIES

Classical chemical analysis of metals and silicate and carbonate rocks; X-ray crystallography; electron microscopy and diffraction; electron microprobe analysis; atomic absorption analysis; spectrochemical analysis.

U Ed 9-725

FINAL TECHNICAL REPORT

1 February 1983 - 31 May 1985

ARPA Order No.:	4397/3
Program Code:	3291/A1
Name of Contractor:	Pennsylvania State University
Effective Date of Contract:	1 February 1982
Contract Expiration Date:	31 May 1985
Amount of Contract:	$268,000
Contract Number:	Grant AFOSR-82-0054
Principal Investigator:	Shelton S. Alexander (814) 865-2622
Program Manager and Telephone Number:	William J. Best (202) 767-4904
Short Title of Work:	Relationship Between Near-Field and Teleseismic Observations of Seismic Source Parameters

Sponsored by
Advanced Research Projects Agency (DOD)
ARPA Order No. 4397/3
Monitored by AFOSR Under Grant NO. AFOSR-82-0054

Geophysics Program, Geosciences Department
403 Deike Building
Pennsylvania State University
University Park, Pennsylvania 16802

TABLE OF CONTENTS

I. SUMMARY

SUMMARY
Grant No. AFOSR-82-0054

The research completed on this project is summarized as follows:

1. A statistical study was made to estimate source, path, and receiver terms from two Lg data sets for North America: (a) LRSM measurements for nearly 100 Nevada Test Site (NTS), and (b) WWSSN and Canadian recordings of 17 eastern North American earthquakes. Decay rates of r^{-2} are acceptable for both data sets, with a tendency to a lesser rate over paths in the Canadian Shield, where a mean crustal Q of approximately 2000 is indicated. For the NTS events the source terms correlate very well with yield. No dependence of Lg excitation on non-isotropic source effects was found; this includes transverse component Lg. This analysis method has been extended to obtain similar decomposition of source, path and station effects as a function of frequency for Lg signatures of NTS and Eurasian events.

2. Previous studies have shown that excitation of fundamental mode Love and Rayleigh waves corresponding to earthquake-like source contributions is highly variable among nearby explosions at NTS and at Semipalatinsk. The associated focal mechanisms typically are consistent with regional tectonic stress orientations. As discussed above we have found there is not a corresponding excitation of Lg waves for NTS explosions, and consequently magnitude-yield estimates using Lg will not be biased significantly by these non-isotropic source effects. For Soviet explosions in thrust-type tectonic settings, we have found that above about 0.3 Hz the vertical- and transverse-component Lg signals also are not significantly biased, but unlike NTS, excitation of somewhat lower frequency vertical-component Lg in some cases appears to be correlated with non-isotropic source contributions observed in the long-period data from the Shagan River test sites. Lg data above about 0.3 Hz seem to provide a reliable additional means of estimating yield for events at both test sites that is comparable to P-wave yield estimates when propagation and station effects are properly taken into account.

3. Several approaches, applied separately or in combination, have been used in an attempt to overcome the biasing effects of non-isotropic source excitation on seismic yield estimates from long-period observations. They fall into two general categories: (a) decomposition of observed seismic signatures, especially long-period Love and Rayleigh wave data, using a moment tensor (or equivalent) inversion formalism to estimate the explosion signal, and (b) use of carefully selected seismic phases, frequency bands, azimuths, and distances that are least affected by non-isotropic effects. The success in either case depends on the nature and strength of the non-isotropic contributions. Different strategies are required for strike-slip tectonic settings (NTS) and thrust-type tectonic settings (Semipalatinsk). An empirical correction procedure was developed that uses a suite of low-tectonic-release events to model the explosion contribution in the high-tectonic release long-period signals.

4. We have found that for similar epicentral distances Lg excitation (relative to m_b) is comparable among granite explosions at Semipalatinsk and Hoggar in north Africa. Preliminary work was directed to the important

question of whether NTS granite explosions have comparable or larger Lg excitation for a given m_b (yield) than Hoggar or Degelen explosions.

5. Several experiments were carried out to separate near-receiver effects from source effects on body waves, to use mode-converted phases to estimate source and receiver structure, and to put bounds on Q at source and receiver locations. In one of these studies (a M.S. project) a frequency-domain phase-difference polarization filter has been implemented and used as an aid in discrimination of wave types present in three-component seismic signals. Crustal structure beneath five three-component seismic stations in eastern North America has been investigated using P-to-SV conversions identified for teleseismic earthquake and underground nuclear explosion sources. These results are contained in an M.S. thesis (D. O'Neill) completed in late 1983.

6. Methods to increase the dynamic range of DWWSSN long-period and short-period digital recordings were developed and implemented using station SCP as an example. A paper describing this approach has been prepared for publication and is included in the Semi-Annual Technical Report for March 1, 1983 - August 31, 1983.

7. Fundamental and higher mode surface waves from the January 9, 1982 New Brunswick m_b 5.7 mainshock and several aftershocks are being used to investigate source mechanisms and focal depth for these events. They provide an opportunity for comparing source parameters obtained from regional observations with those from teleseismic observations of the same events; this source region is also a good analog of Semipalatinsk and the earthquakes are in a granite pluton. A M.S. paper that was completed on this topic (C. Nichols) appearts at the end of this report.

8. Spatial wavenumber analysis of multi-spectral scanner Landsat images has been used to study the orientation and location of structural lineaments in the region of the Hoggar massif in southern Algeria, Africa. All results are compared to a previous photointerpretation of the imagery and to available seismic observations on the mechanism of "tectonic release" associated with nuclear explosions detonated in the massif. Major results of the wavenumber analysis, photo-interpretation and seismic observations are in agreement with one another. In particular, the N38°E strike-slip fault inferred by Harkrider (1976) from analysis of surface wave radiation patterns is consistent with the prominent northeast-striking features observed in both the wavenumber spectra and the original imagery. From this study and previous work relevant to the area, the maximum principal compressive stress axis is inferred to have been in the east-west direction in the past, but at present is oriented in the north-south direction. This orientation is consistent with the present-day direction of African-Eurasian plate motion and with focal mechanisms of recent larger earthquakes to the northwest near El Assam, Algeria. A revised crustal structure model for this source area was also obtained. A M.S. thesis (C. Ng) describing these results has been completed and a paper for publication has been prepared. These results are included in the Semi-Annual Technical Report for March 1, 1983 - August 31, 1983 and March 1, 1984 - August 31, 1984.

9. Seismic experiments were carried out to study the vertical and laterialheterogeneities in the Earth's interior that can affect body-wave arrivals and their codas (or precursors for S waves). Various signal analysis

techniques were employed to separate near-receiver effects from near-source effects, and near-receiver, mode-convereted (P-SV, SV-P) arrivals were interpreted in terms of receiver crust and upper mantle structure. Significant variations in continental crust and upper mantle structure were found upon comparing results for stations RKON, WH2YK, and LASA. High frequency S arrivals from P-SV conversions from the 400 km discontinuity at RKON from Soviet explosions confirm that Q is very high in the upper mantle beneath that part of the Canadian Shield. A study of PcP-P travel time residuals show that significant lateral heterogeneity exists near the core-mantle boundary. There is some evidence that these deep-seated heterogeneities correlate with surface tectonic features such as continental shields.

10. For each of a number of Soviet explosions two different spectral approaches were used to determine the average Q for Lg signals arriving in a velocity window ranging approximately from 3.5 to 3.0 km/sec. The mean spectral slope based on all the events analyzed is then used to calculate the average attenuation coefficient $(QU)^{-1}$. Results from individual stations of the Grafenberg array (6 to 13 stations) were averaged for each event and compared to the single station (A1) results. Additionally, transverse component data were available for three of the GRF stations. At MAIO only vertical component Lg data were available. For the propagation path from Semipalatinsk to GRF, the narrow-band filtering method and the noise-corrected power spectra of both vertical and transverse components give an average Q for Lg of approximately 1000. For the path from Azgir to GRF the average Q is around 1100. For the path from Semipalatinsk to MAIO the average Q is approximately 625. There appear to be no significant differences in the results among individual events for each path, indicating that the strong tectonic release effects in evidence at long periods for some of the Semipalatinsk events do not influence the Lg spectra of those events appreciably in the frequency band .3 to 1.2 Hz, and the best band to use to establish an m_{bLg} vs m_b relationship is centered at .6 to .7 Hz.

To overcome long-period non-isotropic source effects for Shagan River events several very low tectonic release events are used to obtain an empirical "pure explosion" Rayleigh signature (shape) which then is incrementally scaled and subtracted from the total Rayleigh wave signature of high tectonic release events until the best double-couple solution that also fits the Love wave signals is found (i.e. when the trace of the moment tensor is closest to zero); the scaled signal is then the appropriate explosion contribution. The remaining "pure earthquake" Rayleigh and Love wave signals for each event are interpreted in terms of a best-fitting equivalent earthquake model.

To determine the approximate threshold for obtaining source parameters from long-period surface waves in an intraplate setting, the phase matched filtering method is used to analyze the 1982 New Brunswick aftershock sequence with the well-recorded mainshock seismograms as the reference signals. The source excitation function of each aftershock is extracted from the observed signal spectrum by correcting for the path transfer function and the main shock source excitation. Preliminary results using this approach on recordings at GDSN stations in North America indicate that source parameters (including depth) can be extracted for events as small as about m_b 4 to 4.5. (This will be part of a M.S. thesis by B. Yan).

Details of these findings appear in the semi-annual/annual technical reports on this Grant and in the latter portion of this report. Grant AFOSR-82-0054 supported fully or in part three completed M.S. theses (O'Neill, Ng, Nichols) and one M.S. (Yan) and one Ph.D. (Tang) that are still in progress. A list of

publications resulting from this investigation is included in the next section. Work completed since the last semi-annual report is also described in some detail in the sections that follow.

II. PUBLICATIONS

PUBLICATIONS

Alexander, S.S., 1982, Determination of the Relationship Between Near-Field and Teleseismic Observations of Seismic Source Parameters, Presented at the DARPA Symposium on Seismic Detection, Analysis, Discrimination, and Yield Determination, 25-27 May, 1982, Hampton, Virginia.

Alexander, S.S., 1982, Method for Overcoming the Effects of Non-Isotropic Source Excitation on Seismic Yield Estimation, Earthquake Notes, Vol. 53, No. 1.

Alexander, S.S., 1982, Surface Wave Evidence on the Nature of Non-Isotropic Source Effects, Presented at DARPA/AFOSR Symposium on The Physics of Non-Isotropic Effects from Underground Nuclear Explosions, 25-26 March, 1982, Las Vegas, Nevada.

Alexander, S.S., 1983, The Use of Lg as an Independent Estimator of Yield and Practical Methods of Overcoming Effects of Non-Isotropic Source Excitation on Long-Period Surface Wave Signals, Presented at the Fifth Annual DARPA/AFOSR Symposium on Seismic Detection, Analysis, Discrimination, and Yield Determination, 16-18 May, 1983, Eastsound, Washington.

Alexander, S.S., 1984, Relationship Among Near-Field, Regional, and Teleseismic Observations of Seismic Source Parameters, in Basic Research in the Vela Program 1959-1984, Proceedings of the May 1984 DARPA Review Meeting, Vol. 1, 14 pp.

Alexander, S.S., 1984, Surface Wave Analysis and Interpretation, EOS, Vol. 65, No. 16, p. 243-244.

Alexander, S.S., 1985, Estimates of Source and Path Characteristics in the USSR and North America Using Short Period (Lg) and Long-Period Surface Wave Spectra, Papers Presented at 7th Annual DARPA/AFGL Seismic Research Symposium, U.S. Air Force Academy, Colorado Springs, Colorado, May 6-8, DARPA publication.

Alexander, S.S. and C.C. Nichols, 1983, Excitation and Propagation of Lg in Eastern North America, Earthquake Notes, Vol. 54, No. 3, p. 8.

Alexander, S.S., C.C. Nichols, and B. Yan, 1984, Inferences on Focal Mechanism and Depth of Several New Brunswick Earthquakes from Rayleigh and Love Wave Spectral Excitation, Earthquake Notes, Vol. 55, No. 3, p. 10.

Alexander, S.S. and D. von Seggern, 1982, Aspects of Lg Excitation and Propagation in Eastern North America, EOS, Vol. 63, No. 45, p. 1035.

Alexander, S.S. and D. von Seggern, 1983, Dependence of Stress Drop on Seismic Magnitude, Earthquake Notes, Vol. 54, No. 3, p. 36.

*These publications represent work completed wholly or in part under Grant AFOSR-82-0054.

Alexander, S.S. and D. von Seggern, 1983, Spectral Estimates of Source, Path (Q), and Receiver Contributions to Lg Signals From Earthquakes and Explosions, EOS, Vol. 64, No. 18, p. 260.

Baumgardt, D.R. and S.S. Alexander, 1984, Structure of the Mantle Beneath Montana LASA from Analysis of Long-Period, Mode-Converted Phases, Bull. Seism. Soc. Am., Vol. 74, No. 5, p. 1683-1702.

Liaw, Z.-S., 1984, A Modified Cepstral Method and Its Application to DWWSSN Broadband Data, M.S. Thesis, Department of Geosciences, The Pennsylvania State University, 76 pp.

Liaw, Z.-S. and S.S. Alexander, 1984, A Modified Cepstral Method and Its Application to Detections of P-to-S Conversions, Bull. Inst. Earth Sciences, Academia Sinica, Vol. 4, p 29-49.

Ng, C.Y., 1983, Combined Use of Wavenumber Analysis of Landsat Digital Imagery and Seismic Data to Infer the Orientation of Tectonic Stress in the Hoggar Region in Africa, M.S. Thesis, Department of Geosciences, The Pennsylvania State University, 120 pp.

Ng, C. and S.S. Alexander, 1983, Combined Use of Wavenumber Analysis of Landsat Digital Imagery and Seismic Data to Infer the Orientation of Tectonic Stress in the Hoggar Region in Africa, EOS, Vol. 64, No. 18, p. 319.

Nichols, C.C., 1984, Analysis of the New Brunswick, 1982, Earthquake Sequence with Inferences on Source Parameters from Multi-Mode Surface Wave Dispersion and Spectral Excitation, M.S. Thesis, Department of Geosciences, The Pennsylvania State University.

Nichols, C.C. and S.S. Alexander, 1982, Long-Period and Lg Surface Wave Excitation by Recent Earthquakes in the Northeastern United States, EOS, Vol. 63, No. 18, p. 384.

Nichols, C.C. and S.S. Alexander, 1984, Analysis of the New Brunswick, 1982, Earthquake Sequence with Inferences on Source Parameters from Multi-mode Surface Wave Spectral Excitation, Earthquake Notes, Vol. 55, No. 1, p. 13.

O'Neill, D.C., 1983, Implementation of a Frequency-Domain Phase-Difference Polarization Filter and Its Application to a Determination of Crustal Structure in Parts of Eastern North America, M.S. Thesis, Department of Geosciences, The Pennsylvania State University, 145 pp.

O'Neill, D.C. and S.S. Alexander, 1982, Crustal Structure Beneath Parts of Eastern North America From P-SV Conversion, Earthquake Notes, Vol. 53, No. 3.

O'Neill, D.C. and S.S. Alexander, 1982, Inferences Concerning the Crust Beneath Eastern North American From P-SV Conversions, EOS, Vol. 63, No. 18, p. 380.

Tang, L. and S.S. Alexander, 1982, Methods to Increase the Effective Dynamic Range of Digital World-Wide Standardized Seismograph Network (DWWSSN) Long-Period Recordings, Earthquake Notes, Vol. 53, No. 3.

Tang, L. and S.S. Alexander, 1984, Source Parameters and Path Attenuation (Q) from Single-Station and Array Spectral Observations of Lg in Eurasia and North America, EOS, Vol. 65, No. 16, p. 233.

Tang, L. and S.S. Alexander, 1985, Estimates of Average Q from Lg Propagation in Eurasia, EOS, Vol. 66, No. 18, p. 305-306.

Yan, B. and S.S. Alexander, 1985, Surface Wave Study of the 1982 New Brunswick Earthquake Sequence Using a Phase Matched Filtering Method, EOS, Vol. 66, No. 18, p. 307.

Estimates of Average Q for Lg Propagation in Eurasia

TANG, L.
ALEXANDER, S.S. (Both at: Department of Geosciences, The Pennsylvania State University, University Park, PA 16802

Estimates of average Q of Lg signals in the frequency range .3 to 1.2 Hz have been obtained for propagation paths from the Semipalatinsk and Azgir areas of the USSR to Grafenberg, West Germany (GRF) and from Semipalatinsk to Mashed, Iran (MAIO). For each of a number of presumed explosions two different spectral approaches were used to determine the average Q for Lg signals arriving in a velocity window ranging approximately from 3.5 to 3.0 km/sec. One involves using a sequence of narrow-band filters at different center frequencies and plotting the spectral slope based on both the maximum amplitude and the rms amplitude of the filtered signal in the velocity window. The other involves computing the spectral slope from noise-corrected power spectra of the same velocity window. The mean slope based on all the events analyzed is then used to calculate the average Q. In the case of GRF results from individual stations of the Grafenberg array (6 to 13 stations) were averaged for each event and compared to the single station (AI) results. Additionally transverse component data were available for three of the GRF stations. At the MAIO station only vertical component Lg data were available. For the propagation path from Semipalatinsk at GRF, the narrow-band filtering method gives an average Q of 849-999 and 839-978 for vertical and transverse component, respectively. The noise-corrected power spectra also give a comparable average Q (912-1064). For the path from Semipalatinsk to MAIO average Q values are in the range 390-411, and for the path from Azgir to GRF the average Q is in the range 674-687. There appear to be no significant differences in the results among individual events, indicating that the strong tectonic release effects in evidence at long periods for some of the Semipalatinsk events do not influence the Lg spectra of those events appreciably in the frequency band .3 to 1.2 Hz.

Eos Vol. 66, No. 18, April 30, 1985

Surface Wave Study of the 1982 New Brunswick Earthquake Sequence Using a Phase Matched Filtering Method.

YAN, B.
ALEXANDER, S.S. (Both at: Department of Geosciences, The Pennsylvania State University, University Park, PA 16802)

The phase matched filtering method is used to analyze the 1982 New Brunswick aftershock sequence by using the well-recorded mainshock seismograms as the reference signals. This method not only significantly increases S/N for the aftershock records, but also separates primary Rayleigh or Love wave trains from multipaths and other contaminations. The well-documented mainshock source parameters have been used to synthesize the source excitation function of the reference filter. Hence, we obtain the path transfer function by division of the observed mainshock signal spectrum at each station by the complex-valued, mainshock source excitation function for that source-station azimuth. The source excitation function of each aftershock can then be extracted from the observed signal spectrum through division by the path transfer function. Finally, the resulting Love and Rayleigh source spectral excitation vs frequency and azimuth is used in an inverse calculation to derive the strike, dip, slip, depth, and moment of each aftershock. Preliminary results using this approach on recordings at GDSN stations in North America indicates that source parameters can be extracted for New Brunswick aftershocks as small as about m_b 4 to 4.5.

Eos Vol. 66, No. 18, April 30, 1985

INFERENCES ON FOCAL MECHANISM AND DEPTH OF SEVERAL NEW BRUNSWICK EARTHQUAKES FROM RAYLEIGH AND LOVE WAVE SPECTRAL EXCITATION

ALEXANDER, S.S., NICHOLS, C.C. and YAN, B., Department of Geosciences, Pennsylvania State University, University Park, PA 16802

Digital data from 3-component GDSN and RSTN stations have been processed using various filtering techniques to isolate Love and Rayleigh modes for the New Brunswick mainshock of January 9, 1982 and several of its aftershocks. Love to Rayleigh spectral ratios vs. frequency and azimuth are interpreted in terms of focal mechanism parameters and depth. Fundamental mode Rayleigh wave spectra in the period range from 10-30 seconds are particularly sensitive to depth, such that relative depths among events can be estimated to within approximately 1 km. However, the mainshock focal depth from the surface wave interpretation is shallower than that inferred from teleseismic body waves (6 km vs. 9 km) and the observed spectra suggest a composite excitation consistent with radiation from an upward propagating rupture initiated at 8-9 km depth. The depth inferred for the January 11 aftershock is similar (6 km) although it was located on a different (conjugate) fault plane. The January 9 aftershock was on the same fault as the mainshock but at a shallower depth (approximately 3-4 km). It appears that by applying matched filtering using the larger-event signals as reference waveforms and by applying polarization filters to the matched filtered traces useful surface wave spectral estimates (hence source information) can be obtained for events as small as about m_{Lg} 4.0, using existing 3-component digital stations. Comparison of spectral time-frequency or slowness-frequency patterns for vertical- and transverse-component Lg signals allows identification of events of similar mechanism for even smaller events; however, Lg spectra provide only general constraints on focal mechanism parameters unless individual higher modes can be isolated and identified.

EARTHQUAKE NOTES, Vol. 55, No. 3, 1984

FOCAL DEPTH DETERMINATIONS FROM REGIONAL RECORDINGS OF CRUSTAL SEISMIC EVENTS

ALEXANDER, S.S., TANG, L. and YAN, B., Department of Geosciences, The Pennsylvania State University, University Park, PA 16802

Fundamental-mode Rayleigh and Love wave spectra or spectral ratios combined with the patterns of spectral peaks and nulls in stacked, broad-band frequency vs. slowness (seismoprint) displays for the P-wave window before S can be used to obtain reliable focal depths for crustal earthquakes or explosions. Ideally several source-receiver azimuths should be used, but theoretical test cases and limited analysis of actual data suggest that reasonable estimates can be obtained with only a few stations at different azimuths. If the fault geometry can be constrained by standard fault-plane solutions using first motion observations, digital broad-band data from a single 3-component station can give reliable depth information.

Preliminary results indicate that absolute depth accuracies of approximately ± 1 km can be achieved and that relative depths among a number of events from the same epicentral area can be determined with better accuracy. Special signal processing techniques such as iterative matched filtering and polarization filtering typically improve the depth resolution, because of improved spectral signal-to-noise ratios and rejection of unwanted signals. Examples from the analysis of eastern North American events whose focal depths are known independently illustrate the effectiveness of our approach.

EARTHQUAKE NOTES, Vol. 55, No. 1, 1985

if the wavetrain of interest cannot be completely isolated in the seismic trace. Spectral leakage will obscure features in the amplitude rolloff above the corner frequency. Moreover, a straightforward FFT, even after the application of a prudent taper (e.g., Hamming) is subject to large periodogram variance and will misrepresent the frequency content of a pulse known to be greatly dispersed. We will describe multiple-taper time series techniques, developed in the recent engineering literature, that overcome many of these difficulties. We have tested these techniques on data collected from the Anza Seismic Telemetered Network of ten digitally-recording stations sampled at 250 times per second. With this high quality data, we have examined regional wavetrains from earthquakes and one NTS blast. Several distinct spectral features are found, both above and below the inferred corner frequency, that correlate between horizontal and vertical components. We will compare the multitaper spectra with single window spectra.

S12B-08

The Validity of Ray Theory Approximations for the Computation of Teleseismic SV Waves

CHARLES A. LANGSTON
CHANG E. BAAG (Both at: Dept. of Geosciences, The Pennsylvania State University, University Park, PA 16802)

Teleseismic SV waves have been generally ignored in wave propagation and source studies because of known complications in wave propagation for structure near the source and near the receiver. The validity of common optic ray and WKBJ seismogram methods for computing SV synthetic seismograms is examined by computing synthetic seismograms using these techniques and comparing them to SV synthetics produced from a wavenumber integration technique. Both ray methods give a poor approximation to the wave propagation for distances less than 60°. Diffracted Sp and the SPL wave interfere with near source phases, such as S, pS, and sS for a shallow seismic source, producing anomalously high amplitudes and complex waveforms in agreement with observational experience. Because of the Moho Sp phase and diffracted Sp phase, the vertical component of motion shows greater distortion, relative to the ray theory result, than does the radial component of motion. Ray theory appears to be appropriate for the initial 20 seconds of the SV wavetrain from a shallow source for ranges greater than 60°. SV waves from deep sources are less affected by diffracted Sp and SPL than SV from shallow sources.

S12B-09

Teleseismic Estimates of the Energy Radiated by Shallow Earthquakes

JOHN BOATWRIGHT (USGS, Menlo Park, CA 94025)
GEORGE CHOY (USGS, Golden, CO 80225)

The energy flux contained in the P-wave groups (P+pP +sP) or the S-wave groups (S+pS+sS) radiated by a shallow earthquake is estimated from the assumption that the energy flux in the direct and depth phases adds incoherently. By defining generalized radiation patterns which incorporate this neutral interference, the wave groups may be analyzed as though comprised of a single phase. The energy density spectra of broad-band GDSN recordings are corrected for both the body-wave attenuation and the frequency band of the recording. The corrected energy flux measurements are then used to estimate the radiated seismic energy.

This analysis is applied to digital recordings of the teleseismic wave-groups radiated by the May 2, 1983, Coalinga, California, earthquake and the October 28, 1983, Borah Peak, Idaho, earthquake. For the Coalinga earthquake, $E_S = (1.51e.40)\times10^{21}$ dyne-cm was calculated from six P-wave groups, while the SH wave-group recorded at station COL returned $E_S = 1.39\times10^{21}$ dyne-cm. For the Borah Peak earthquake, $E_S = (3.07e.44)\times10^{21}$ dyne-cm was calculated from seven P-wave groups. The energies yield estimates of the apparent stress of 17 and 8 bars for the Coalinga and the Borah Peak earthquake, respectively. This difference appears to result from the different tectonic environment of the events, where the thrust faulting at Coalinga is more strongly stressed than the normal faulting at Borah Peak.

S12B-10

A Hybrid Space and Spatial Transform Domain Method for the Computation of Source Time Functions for General Three-Dimensional Rupture Propagation

R. R. QUIN (Lamont-Doherty Geol. Obs. and Dept. of Geol. Sci. of Columbia University, Palisades, NY 10964)

A hybrid space and spatial transform method for the computation of source time functions based on an integral equation formulation of the mixed boundary value problem for fault displacements and tractions was developed. The spatial domain method is an adaptation of that of Das (1980) in which the displacements on the fault and the tractions off the fault are computed by convolving the Green's function for a point source with the tractions from all previous times to the onset of faulting. The spatial transform domain method does the convolutions by Fourier transforming in two dimensions the stresses and Green's functions, multiplying them in the transform domain, and then inverse transforming back to the space domain. The spatial domain is much more accurate for summing over the tip of the Green's function cone, while the transform domain method is faster for summing over the rest of the Green's function cone.

As a check of the accuracy of this method the results are compared against the known results of Kostrov for a circular crack which grows without stopping. Good agreement is found.

S12B-11

Seismicity Simulations With a Rate and State Dependent Friction Law

T. CAO (Department of Earth, Atmospheric, and Planetary Sciences, Massachusetts Institute of Technology, Cambridge, Mass. 02139)

The dynamic motion and stability of a single degree of freedom elastic system undergoing frictional slip is examined. The system consists of a sliding block connected to an elastic spring which is driven at a constant velocity. The frictional slip is governed by a laboratory inferred friction law proposed by Dieterich and Ruina. We further extended the solution to a one-dimensional mass-spring model with the same friction law. With this model, we can simulate quite different behavior exhibited at distinct sections along a major strike-slip fault, such as the San Andreas. On some sections of a fault, there is little seismic activity; the fault appears to be locked. On other sections of the fault, small earthquakes and aseismic creep relieve at least a fraction of the accumulating strain. In a previous seismicity simulation, we used a displacement hardening-softening friction law proposed by Stuart and found that when we chose a critical displacement of the same order of magnitude as the slip-weakening critical displacement estimated by Papageorgiou and Aki from strong motion data, we got a normal seismicity pattern including small to large earthquakes. In the present approach, we chose those nondimensional constants in the friction law according to experimental results and found that the characteristic sliding distance, as it is called in the friction law, is consistent with the slip-weakening critical displacement determined by Papageorgiou and Aki.

S12B-12

Mixed-Mode Shear Crack Propagating Between Rayleigh and S-Wave Velocities

D. J. ANDREWS (U.S. Geological Survey, Menlo Park, CA 94125)

A pure mode II (in-plane) shear crack cannot propagate spontaneously at a velocity between the Rayleigh velocity γ and the S-wave velocity β, but a 3-D or 2-D mixed-mode shear crack can propagate in this range of velocities, being driven by the mode III (anti-plane) component. There has been some disagreement in the literature concerning the solution for the mode II component in this case. The analytic expression that is the solution for crack velocity less than γ, applied to velocity greater than γ, has a negative stress intensity factor, which would imply that energy is generated at the crack tip. Burridge, on the other hand, found that a different analytic expression, having a stress intensity factor of zero (a singularity of order smaller than 1/2), is applicable for crack velocity between γ and β.

Numerical calculations of 2-D cracks have been done by a boundary integral method. The numerical result for a mode II crack prescribed to propagate at constant velocity agrees with Burridge's solution. Spontaneous propagation of a mixed-mode rupture has been calculated with a slip-weakening friction law, in which the slip velocity vector is collinear with the total traction vector and the magnitude of traction depends on the magnitude of slip. The spontaneous rupture velocity can be between γ and β, in which case energy is absorbed from both components of the elastic field, but the cohesive energy is taken primarily from the mode III component.

S12B-13

Fault Interaction and the Frequency of Aftershock Occurrence

T. YAMASHITA
L. KNOPOFF (both at Institute of Geophysics and Planetary Physics, University of California, Los Angeles, CA 90024)

The aftershock source models are theoretically studied in detail. The effect of source complexity is fully introduced in these source models. It is shown that the Omori formula of aftershock activity is very well explained by our source models.

Two kinds of source models are considered. In one model we assume the existence of unbroken patches on a main-shock fault plane. These patches are assumed to be the source of aftershocks. In another source model we consider the interaction of main-shock fault and its surrounding small faults. The catastrophic coalescence of main-shock fault and each small fault can be the source of aftershocks in this model. Aftershock activities in the interior and exterior of the main-shock fault plane are described by the former and latter source models, respectively.

Power law distributions are assumed for the distances over which catastrophic and quasistatic rupture extensions occur. The assumption of power law distribution is justified by some experimental and seismological observations. The stress corrosion cracking is assumed as the physical mechanism of quasistatic rupture extension.

S12B-14

of Magnitude, Ms-m_b, and Tectonic Regime

R. A. Strelitz
Dept. of Geology
Duke University,
Durham, NC 27706

Aftershocks are associated with almost all seismic events. Prozerov and Driewonski (1982) have determined a productivity or influence function and examined its behaviour as a function of magnitude and location. Since theoretical arguments indicate that aftershock production is a reflection of the physical processes and stress distribution at the source, it is not unreasonable to find substantial variations with depth and location according to a plate tectonic framework.

Analysis of NOAA epicenter catalogues for the years 1970-1983 for main events with Ms or $m_b \geq 6.0$ reveal that plots of # of aftershocks versus Ms-m_b dislays far more correlation than do similar plots of number against Ms or m_b. Since Ms» m_b indicates 'slow' or non-impulsive events, it is evident that such an event differs in physical processes from other 'normal' events. However, the fact that these deviations from the norm lie on both sides of the standard line would argue that there are two classes of 'slow' events, neither of which is normal.

Examination of the specifics of these events and all other well situated events that are substantially different from the mean events of their class reveal a tectonic influence though conclusions are necessarily restricted by the amount of data.

Prozerov and Driewonski (1982) A Method of Studying Variations in the Clustering Property of Eqs. J. Geophys. Res. 87 , 2829-2839.

S12B-15

Minimum Focal Depth vs. Magnitude (Moment) For Earthquakes in Eastern North America

ALEXANDER, S.S., (Department of Geosciences, The Pennsylvania State University, University Park, PA 16802)

Based on the entire available record of both historical and instrumentally-recorded earthquakes, there appears to be no documented case of a fault rupture breaking the Earth's surface in eastern North America. This implies a minimum focal depth as a function of magnitude (or moment) to account for the increase in the size of the fault rupture area with increasing magnitude. This minimum depth depends on: the type of faulting involved (generally thrust or strike-slip in eastern North America); the stress drop; the distribution of deviatoric stress with depth; and possibly the direction of propagation of the rupture, especially for earthquakes involving dominantly thrust faulting. To establish this depth relationship quantitatively and empirically, accurate focal depth determinations are required; however, reliable, well-constrained depths are not routinely available for a great many of the past earthquakes in eastern North America. In this study we have attempted to obtain a bound on the minimum depth vs magnitude relationship by using well-constrained depths determined by other workers and by further analysis of other instrumentally-recorded earthquakes. When available, both pP-P and Love and Rayleigh wave spectral observations are used to constrain the depth, because seismograms from only a few stations are required when the epicenter is well-defined. Although these may be geographical variations, our preliminary results suggest that m_{bLg} 4-and-above events are typically deeper than 3 km, magnitude 5-and-above events deeper than 5 km and magnitude 6-and-above events are deeper than 10 km.

AFGL/DARPA REVIEW OF NUCLEAR TEST MONITORING BASIC RESEARCH
US AIR FORCE ACADEMY, 6-8 MAY 1985

TITLE: ESTIMATES OF SOURCE AND PATH CHARACTERISTICS IN THE USSR AND NORTH AMERICA USING SHORT PERIOD (Lg) AND LONG-PERIOD SURFACE WAVE SPECTRA

AUTHOR: Shelton S. Alexander, Department of Geosciences,
The Pennsylvania State University, University Park, PA 16802

SUMMARY: For each of a number of Soviet explosions two different spectral approaches were used to determine the average Q for Lg signals arriving in a velocity window ranging approximately from 3.5 to 3.0 km/sec. The mean spectral slope based on all the events analyzed is then used to calculate the average attenuation coefficient $(QU)^{-1}$. Results from individual stations of the Grafenberg array (6 to 13 stations) were averaged for each event and compared to the single station (A1) results. Additionally, transverse component data were available for three of the GRF stations. At MAIO only vertical component Lg data were available. For the propagation path from Semipalatinsk to GRF, the narrow-band filtering method and the noise-corrected power spectra of both vertical and transverse components give an average Q for Lg of approximately 1000. For the path from Azgir to GRF the average Q is around 1100. For the path from Semipalatinsk to MAIO the average Q is approximately 625. There appear to be no significant differences in the results among individual events for each path, indicating that the strong tectonic release effects in evidence at long periods for some of the Semipalatinsk events do not influence the Lg spectra of those events appreciably in the frequency band .3 to 1.2 Hz, and the best band to use to establish an m_{bLg} vs m_b relationship is centered at .6 to .7 Hz.

To overcome long-period non-isotropic source effects for Shagan River events several very low tectonic release events are used to obtain an empirical "pure explosion" Rayleigh signature (shape) which then is incrementally scaled and subtracted from the total Rayleigh wave signature of high tectonic release events until the best double-couple solution that also fits the Love wave signals is found (i.e. when the trace of the moment tensor is closest to zero); the scaled signal is then the appropriate explosion contribution. The remaining "pure earthquake" Rayleigh and Love wave signals for each event are interpreted in terms of a best-fitting equivalent earthquake model.

To determine the approximate threshold for obtaining source parameters from long-period surface waves in an intraplate setting, the phase matched filtering method is used to analyze the 1982 New Brunswick aftershock sequence with the well-recorded mainshock seismograms as the reference signals. The source excitation function of each aftershock is extracted from the observed signal spectrum by correcting for the path transfer function and the main shock source excitation. Preliminary results using this approach on recordings at GDSN stations in North America indicate that source parameters (including depth) can be extracted for events as small as about m_b 4 to 4.5.

CONCLUSIONS AND RECOMMENDATIONS: The conclusions are included above. The principal recommendations are: 1) carry out further evaluations of Lg as an independent measure of yield, including especially transverse component Lg observed at local (e.g. NORESS) and more distributed arrays (e.g. GRF, NORSAR); 2) further investigate source parameter estimation methods using 3-component broad-band recordings at regional distances; and 3) assess relative effects of scattering vs. absorption for Eurasian and North American Lg propagation paths.

III. ESTIMATES OF SOURCE AND PATH CHARACTERISTICS IN THE USSR AND NORTH AMERICA USING SHORT-PERIOD (Lg) AND LONG-PERIOD SURFACE WAVE SPECTRA

ESTIMATES OF SOURCE AND PATH CHARACTERISTICS IN THE USSR AND NORTH AMERICA USING SHORT PERIOD (Lg) AND LONG-PERIOD SURFACE WAVE SPECTRA

S.S. Alexander
Geosciences Department
The Pennsylvania State University
University Park, PA 16802

Several approaches can be used to obtain improved absolute estimates of yield from Lg. One is the approach of von Seggern and Alexander (1983) where path effects are estimated and automatically taken into account to obtain the source moment (yield) for each event. Another is to use a local array such as Grafenberg or NORSAR (NORESS) to obtain the mean, noise-corrected Lg spectrum (with station structure effects averaged out) from which the path Q can be estimated, provided the source spectral shape for Lg excitation can be inferred. Estimates of average Q of Lg signals in the frequency range .3 to 1.2 Hz have been obtained for propagation paths from the Semipalatinsk and Azgir areas of the USSR to the Grafenberg, West Germany (GRF) array and from Semipalatinsk to Mashed, Iran (MAIO). For each of a number of presumed explosions two different spectral approaches were used to determine the average Q for Lg signals arriving in a velocity window ranging approximately from 3.5 to 3.0 km/sec. One involves using a sequence of narrow-band filters at different center frequencies and determining the spectral slope based on both the maximum amplitude and the rms amplitude of the filtered signal in the velocity window. The other involves computing the spectral slope from noise-corrected power spectra of the same velocity window. The mean slope based on all the events analyzed is then used to calculate the average attenuation coefficient $(QU)^{-1}$. In the case of GRF results from individual stations of the Grafenberg array (6 to 13 stations) were averaged for each event and compared to the single station (A1) results. Additionally, transverse component data were available for three of the GRF stations. At the MAIO station only vertical component Lg data were available. For the propagation path from Semipalatinsk at GRF, the narrow-band filtering method gives an average QU of 2980 and 2940 for vertical and transverse components, respectively. The noise-corrected power spectra also give a comparable average QU of 3190. These results indicate an average Q for Lg propagation to GRF of approximately 1000. For the path from Semipalatinsk to MAIO the average QU value is approximately 1480 corresponding to an average Q of around 450. For the path from Azgir to GRF the average QU is approximately 2360 corresponding to an average Q of around 680. Examples of these spectral results for different events are shown in Figure 1.

There appear to be no significant differences in the results among individual events for each path, indicating that the strong tectonic release effects in evidence at long periods for some of the Semipalatinsk events do not influence the Lg spectra of those events appreciably in the frequency band .3 to 1.2 Hz. In addition, plots of Lg spectral amplitude at selected frequencies vs m_b for GRF and MAIO paths indicate that the best frequency band to use to establish an m_{bLg} vs m_b relationship is centered at .6 to .7 Hz. Results for this frequency range are shown in Figure 2. The Lg signal level in this frequency range, corrected back to the source using the estimated $(QU)^{-1}$ value appropriate for each path, as discussed above, gives an estimate

of source strength (yield). Similar analysis of NTS and Hoggar events of known yield is in progress to develop the appropriate conversion of source terms from this method to yield.

To overcome the biasing perturbations on long-period surface waves caused by non-isotropic source effects, a formal moment tensor decomposition (properly constrained) can be used to estimate the isotropic (explosion) contribution if there is sufficient azimuthal coverage. However, in many instances surface wave data from relatively few stations are available, so other techniques are needed, especially for thrust-type tectonic release associated with Shagan River events. Our alternative approach for the Shagan River area is to use several very low tectonic release events to obtain an empirical "pure explosion" Rayleigh signature (shape) which then is incrementally scaled and subtracted from the total Rayleigh wave signature of high tectonic release events until the best double-couple solution that also fits the Love wave signals is found (i.e. when the trace of the moment tensor is closest to zero). This scale factor times the "pure explosion" signature then gives approximately the equivalent Rayleigh wave for the explosion without tectonic release. For each event, these derived "pure explosion" Rayleigh waves for the network stations are then used to estimate M_s (yield). The assumptions in this approach are (a) that "pure explosion" Rayleigh waveform shapes are the same for events of comparable yield in the same source region and (b) the long-period Rayleigh and Love wave signatures generated by non-isotropic source effects can be represented by a double-couple earthquake source. The remaining "pure earthquake" Rayleigh and Love wave signals for each event, interpreted in terms of a best-fitting equivalent earthquake model (strike, dip, rake, depth, moment), characterize the corresponding tectonic stress field at the source. To the extent that similar mechanisms are found for events located in sub-areas of the test site, a further iteration can be made to correct for the tectonic release contribution to the Rayleigh waves observed for the low-tectonic release calibration events.

In order to determine the approximate threshold for determining source parameters from long-period surface waves in an intraplate setting, the phase matched filtering method is used to analyze the 1982 New Brunswick aftershock sequence by using the well-recorded mainshock seismograms as the reference signals. This method not only significantly increases S/N for the aftershock records, but also separates primary Rayleigh or Love wave trains from multipaths and other contaminations. The well-documented mainshock source parameters have been used to synthesize the source excitation function of the reference filter. Hence, we obtain the path transfer function by division of the observed mainshock signal spectrum at each station by the complex-valued, mainshock source excitation function for that source-station azimuth. The source excitation function of each aftershock can then be extracted from the observed signal spectrum through division by the path transfer function. Finally, the resulting Love and Rayleigh source spectral excitation vs frequency and azimuth is used in an inverse calculation to derive the strike, dip, slip, depth, and moment of each aftershock. Preliminary results using this approach on recordings at GDSN stations in North America indicates that source parameters (including depth) can be extracted for New Brunswick aftershocks as small as about m_b 4 to 4.5. Figure 3 and Table 1 give examples of results for four of the New Brunswick events.

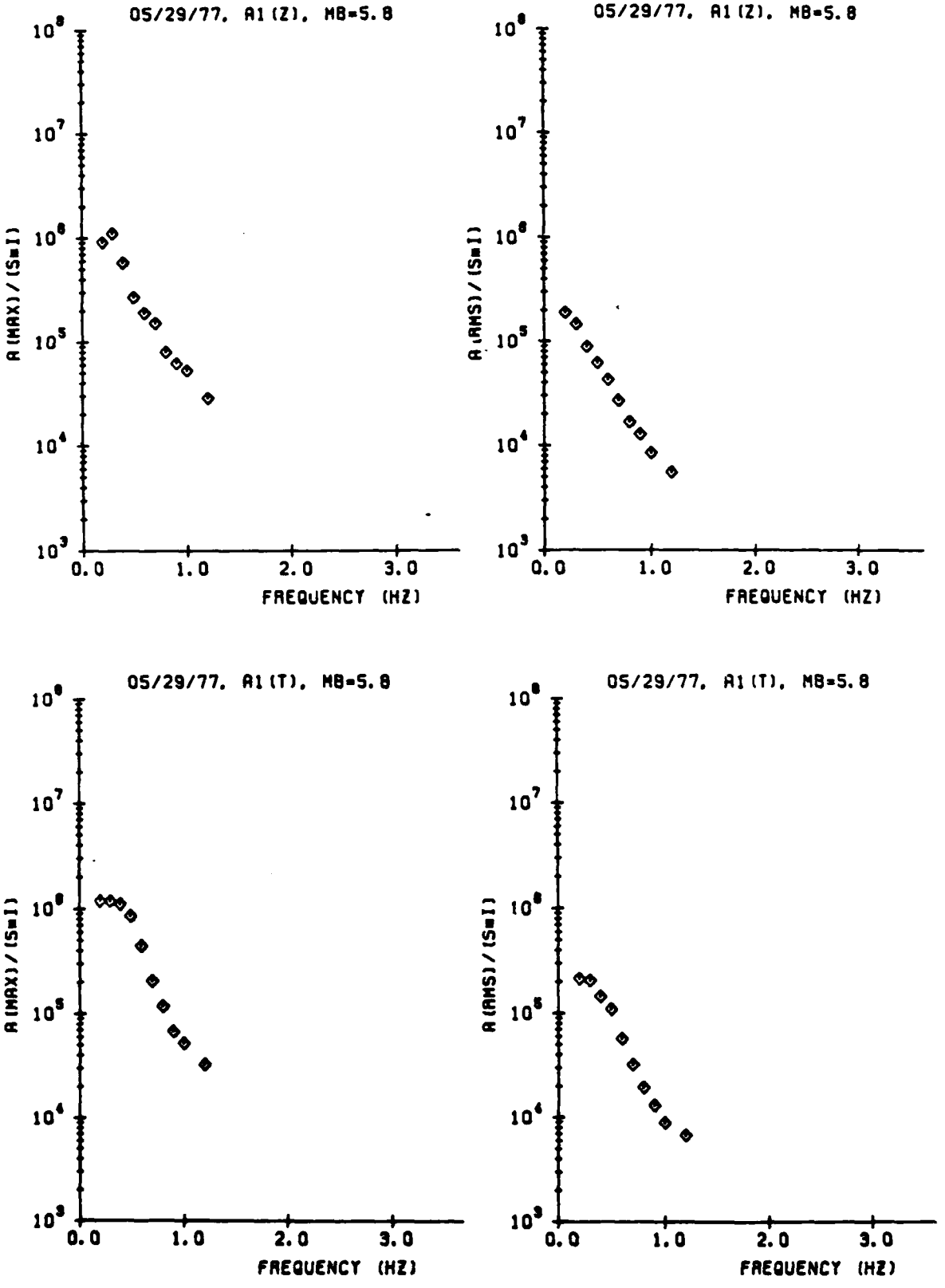
05/29/77, A1(Z), MB=5.8
A(MAX)/(Sm1)
FREQUENCY (HZ)
05/29/77, A1(Z), MB=5.8
A(RMS)/(Sm1)
FREQUENCY (HZ)
05/29/77, A1(T), MB=5.8
A(MAX)/(Sm1)
FREQUENCY (HZ)
05/29/77, A1(T), MB=5.8
A(RMS)/(Sm1)
FREQUENCY (HZ)

Figure 1a

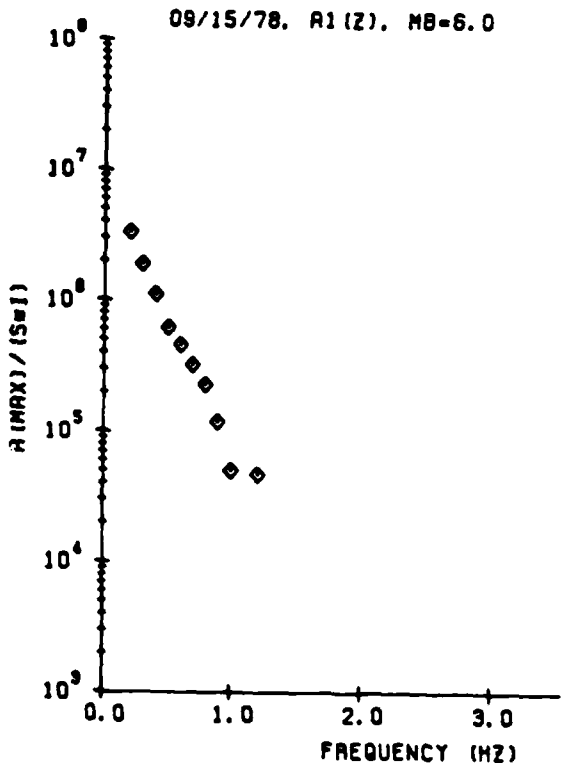
09/15/78. A1(Z). MB=6.0
A(MAX)/(S=1)
FREQUENCY (HZ)

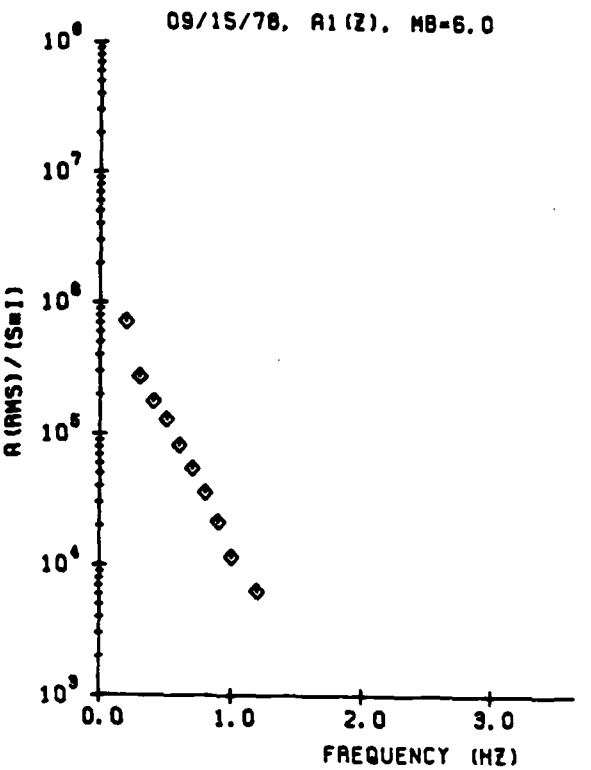
09/15/78. A1(Z). MB=6.0
A(RMS)/(S=1)
FREQUENCY (HZ)

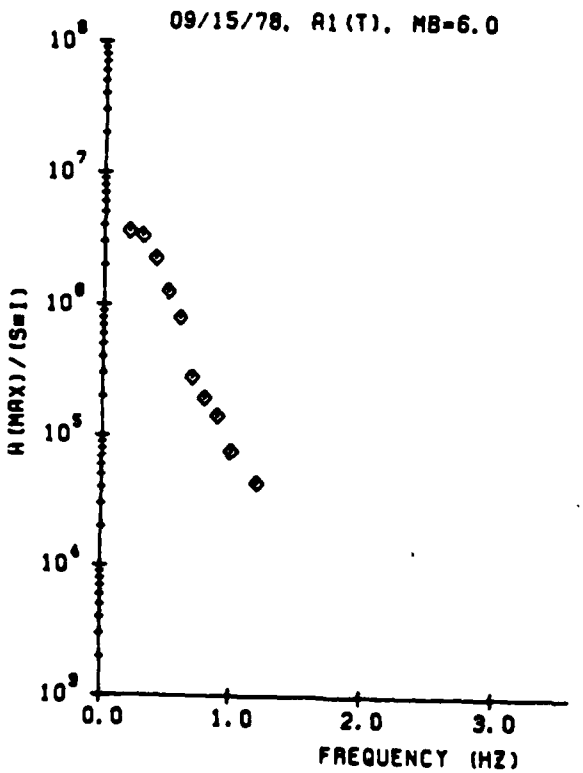
09/15/78. A1(T). MB=6.0
A(MAX)/(S=1)
FREQUENCY (HZ)

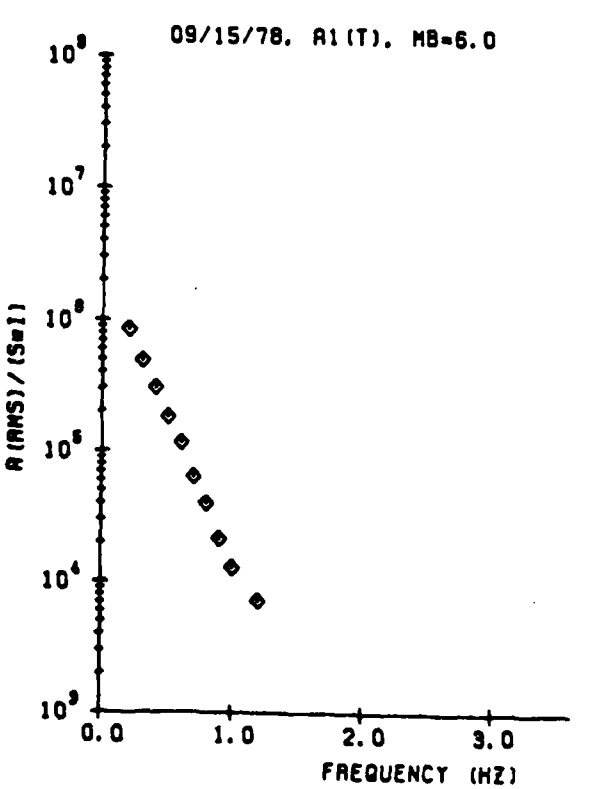
09/15/78. A1(T). MB=6.0
A(RMS)/(S=1)
FREQUENCY (HZ)

Figure 1b

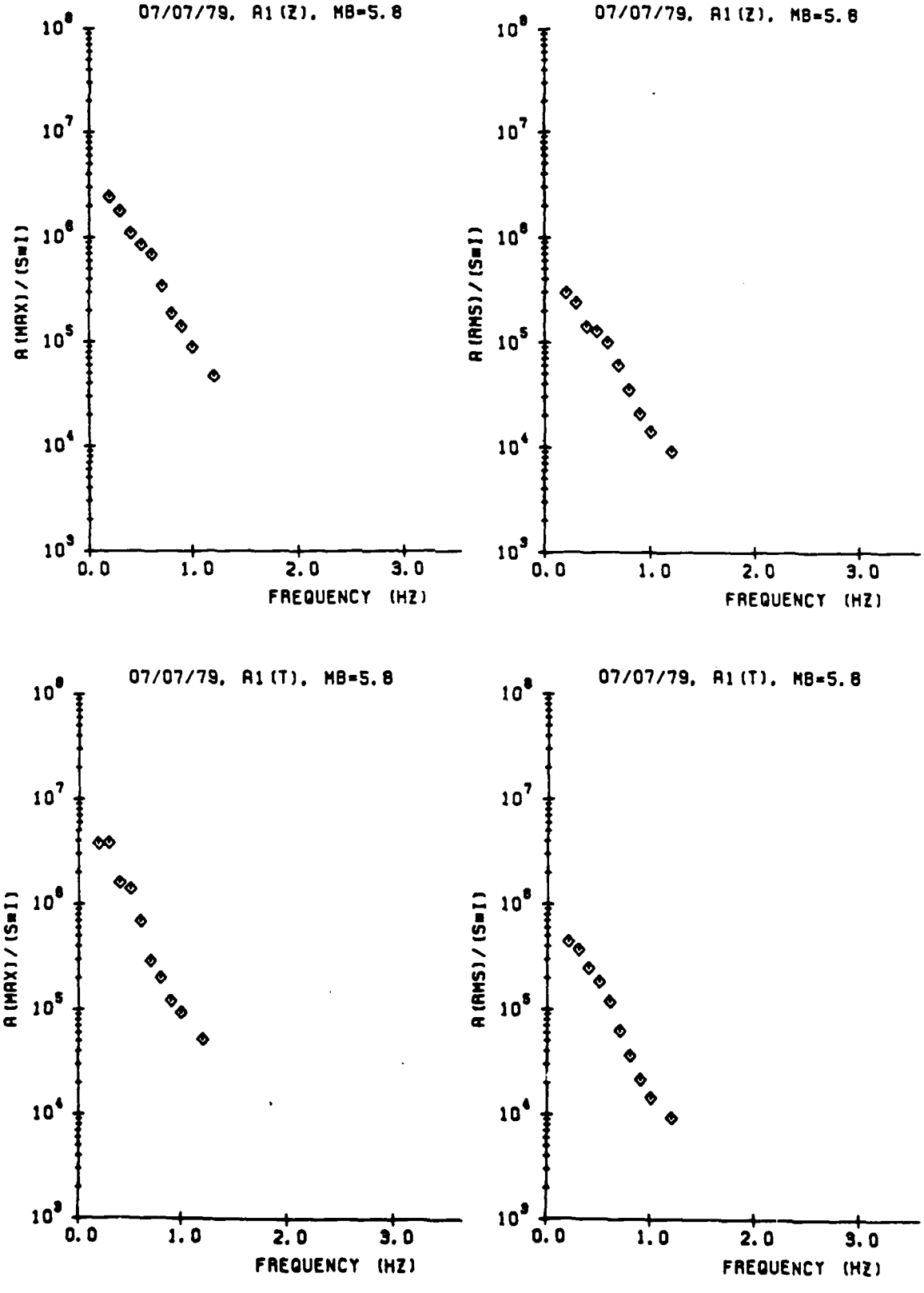
07/07/79, A1(Z), MB=5.8
A(MAX)/(S=1)
FREQUENCY (HZ)
07/07/79, A1(Z), MB=5.8
A(RMS)/(S=1)
FREQUENCY (HZ)
07/07/79, A1(T), MB=5.8
A(MAX)/(S=1)
FREQUENCY (HZ)
07/07/79, A1(T), MB=5.8
A(RMS)/(S=1)
FREQUENCY (HZ)

Figure 1c

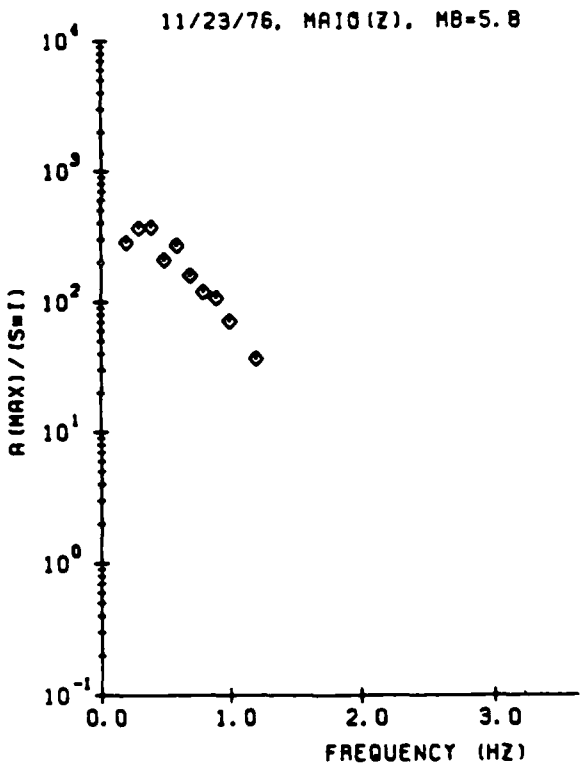
11/23/76. MA10(Z). MB=5.8
A(MAX)/(S=1)
FREQUENCY (HZ)

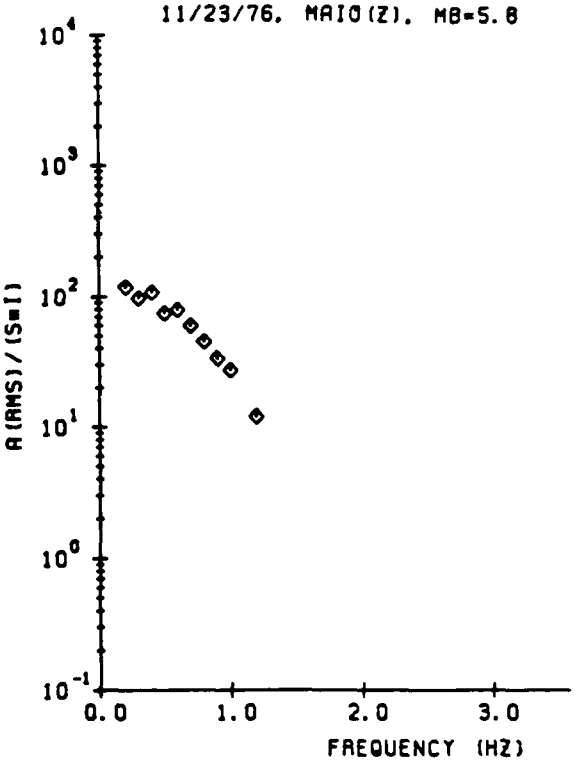
11/23/76. MA10(Z). MB=5.8
A(RMS)/(S=1)
FREQUENCY (HZ)

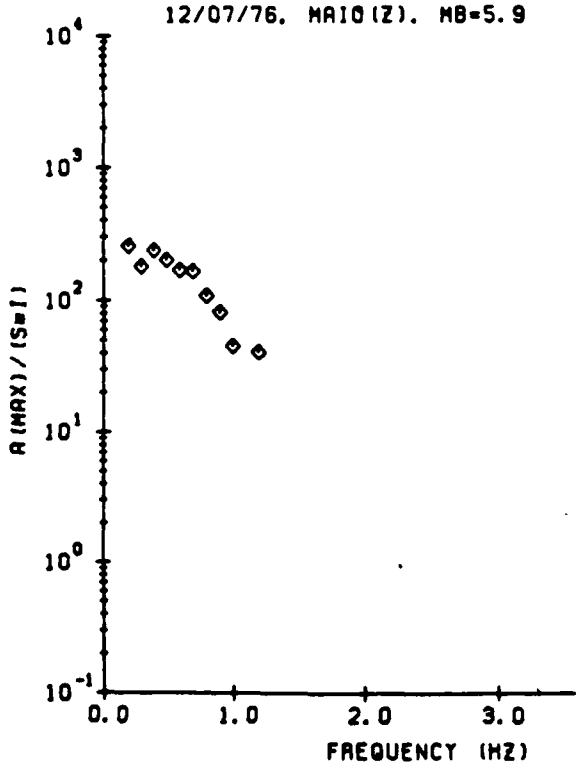
12/07/76. MA10(Z). MB=5.9
A(MAX)/(S=1)
FREQUENCY (HZ)

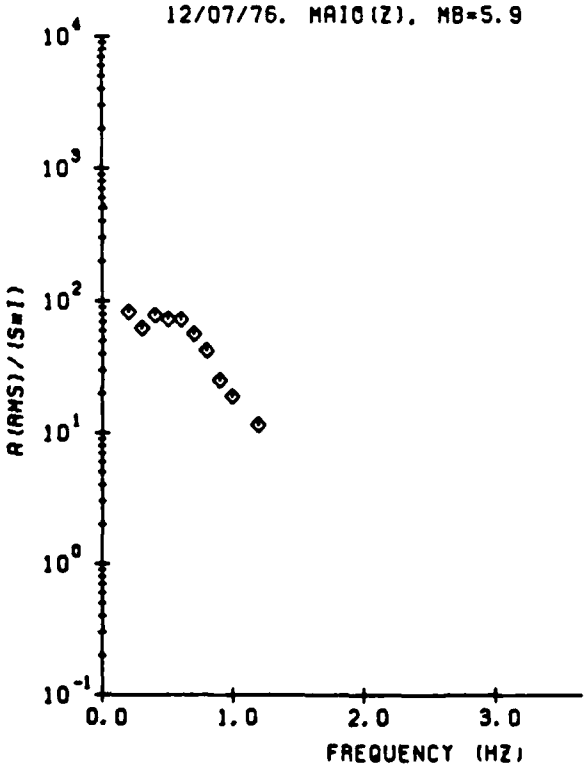
12/07/76. MA10(Z). MB=5.9
A(RMS)/(S=1)
FREQUENCY (HZ)

Figure 1d

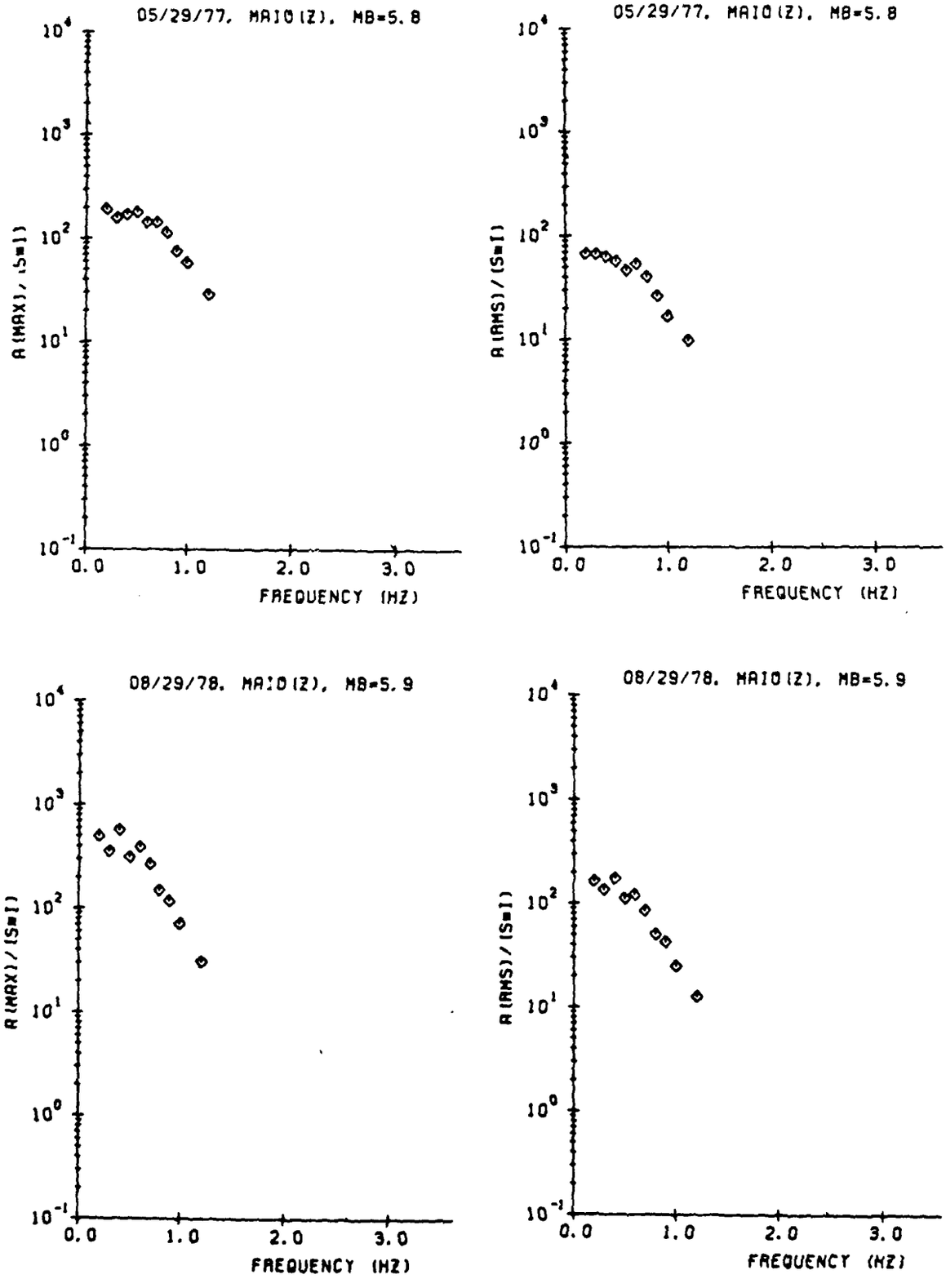
05/29/77, MAIO(Z), MB=5.8
A(MAX), (S=I)
FREQUENCY (HZ)
05/29/77, MAIO(Z), MB=5.8
A(RMS)/(S=I)
FREQUENCY (HZ)
08/29/78, MAIO(Z), MB=5.9
A(MAX)/(S=I)
FREQUENCY (HZ)
08/29/78, MAIO(Z), MB=5.9
A(RMS)/(S=I)
FREQUENCY (HZ)

Figure 1e

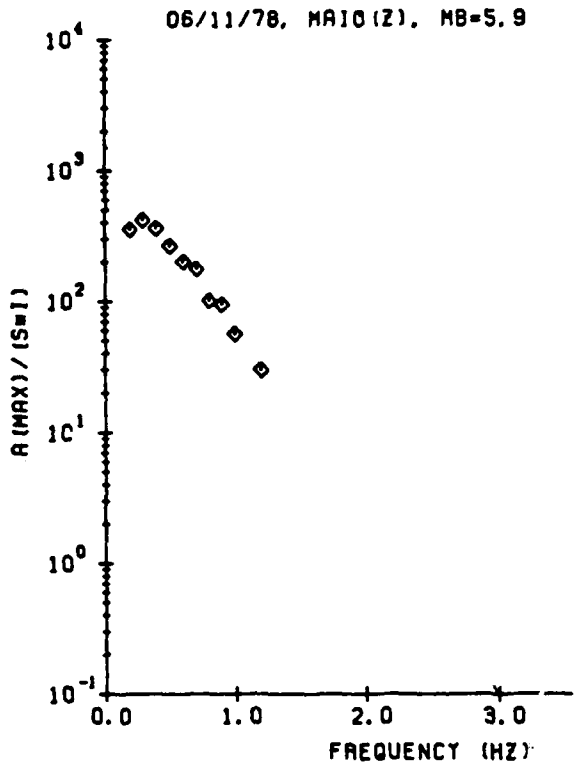
06/11/78, MAIO(Z), MB=5.9
A(MAX)/(S=I)
FREQUENCY (HZ)

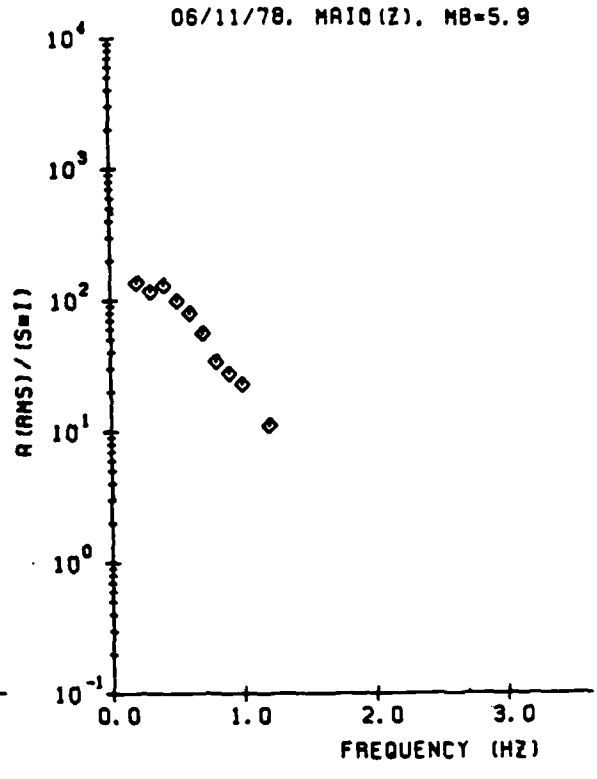
06/11/78, MAIO(Z), MB=5.9
A(RMS)/(S=I)
FREQUENCY (HZ)

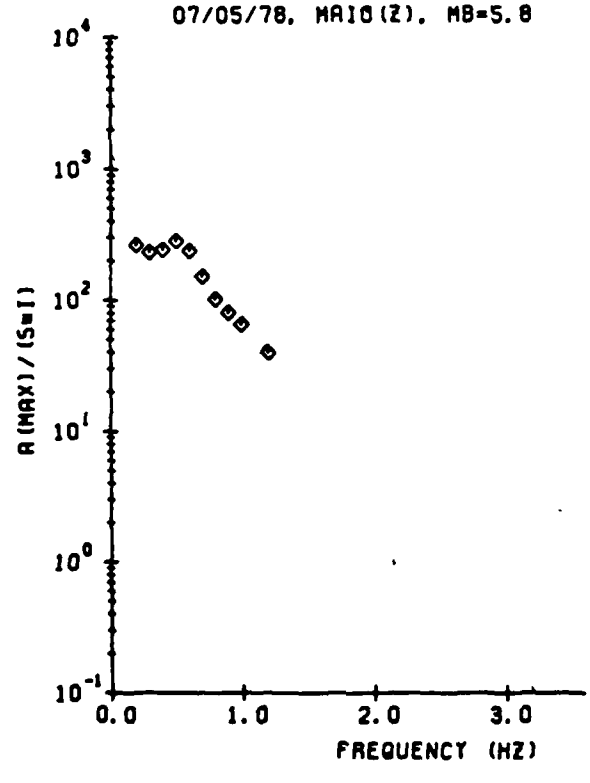
07/05/78, MAIO(Z), MB=5.8
A(MAX)/(S=I)
FREQUENCY (HZ)

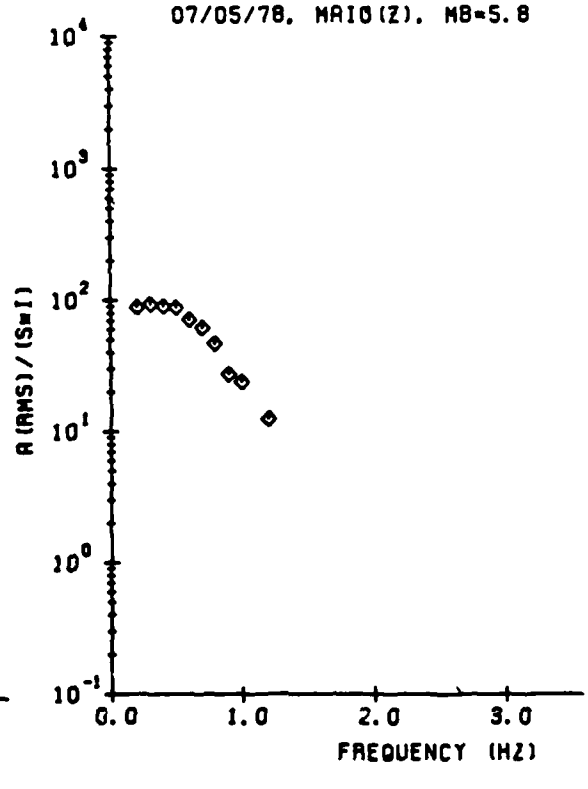
07/05/78, MAIO(Z), MB=5.8
A(RMS)/(S=I)
FREQUENCY (HZ)

Figure 1f

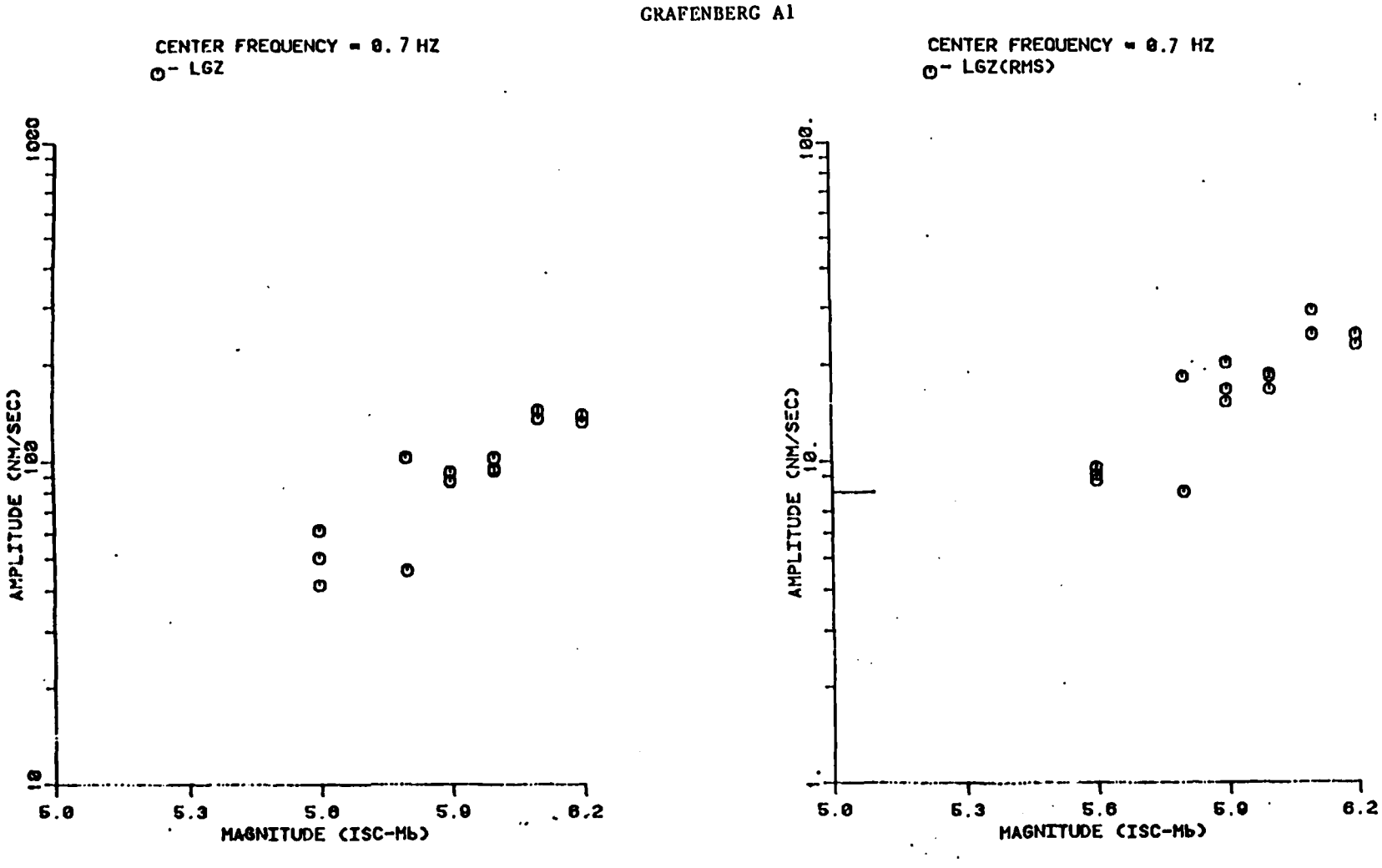

Figure 2a Observed Lg amplitude vs m_b for the center frequency indicated for Semipalatinsk explosions. Left-hand figure is the maximum amplitude and the right-hand figure is the RMS in the Lg velocity window.

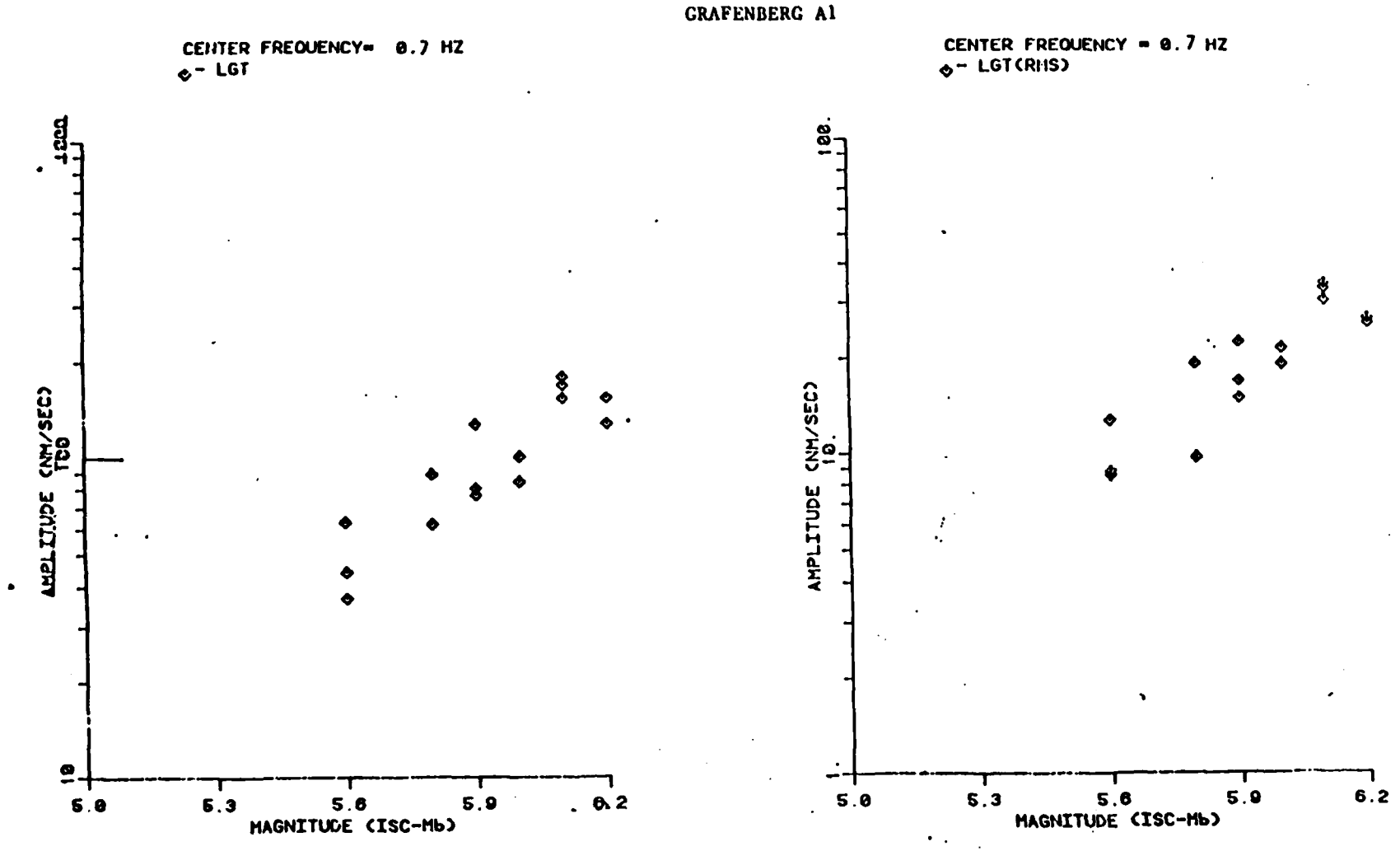

Figure 12b Observed Lg amplitude vs m_b for the center frequency indicated for Semipalatinsk explosions. Left-hand figure is the maximum amplitude and the right-hand figure is the RMS in the Lg velocity window.

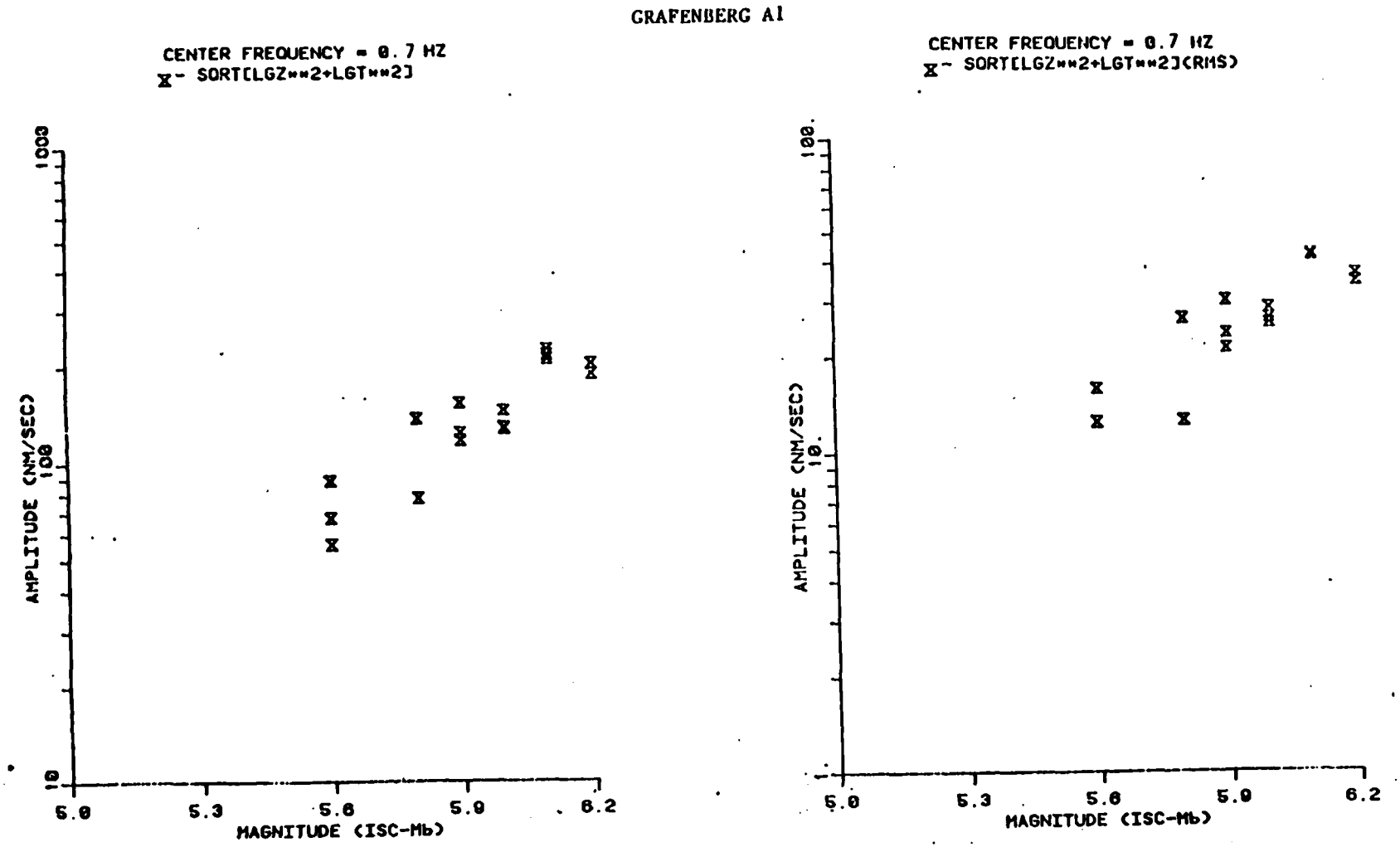

Figure 2c Observed Lg amplitude vs m_b for the center frequency indicated for Semipalatinsk explosions. Left-hand figure is the maximum amplitude and the right-hand figure is the RMS in the Lg velocity window.

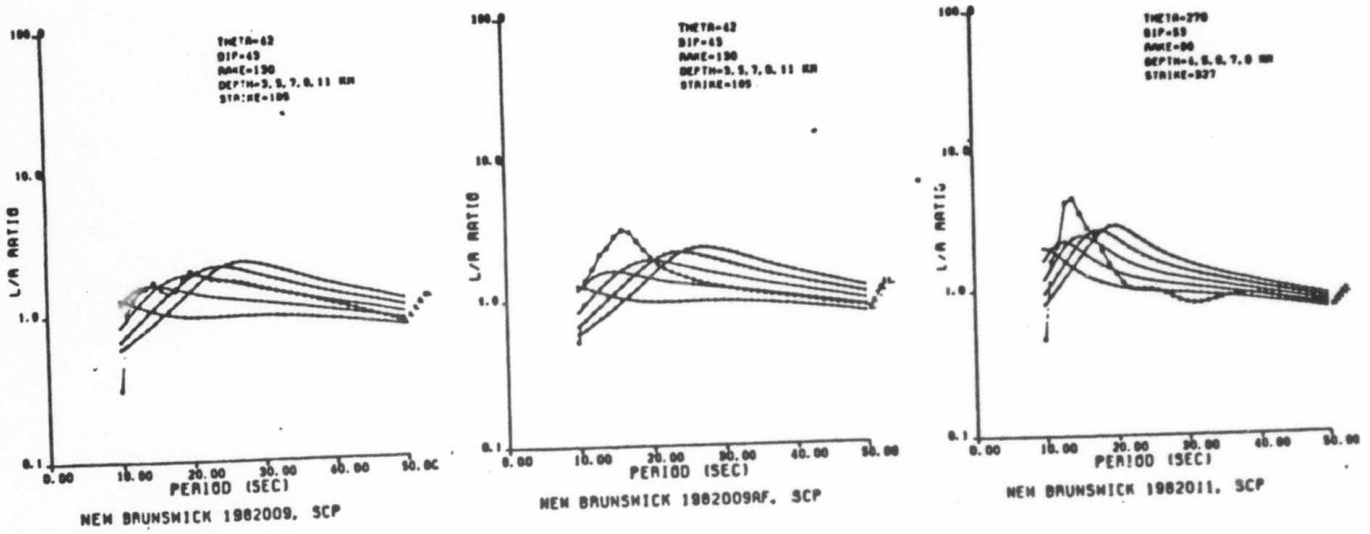

Figure 3. Focal depth and other source parameters for New Brunswick events.

Table 1

Summary of Depths Determined by Various Methods

Event	m_{bLg}	Body Wave Evidence	Aftershock Evidence	Surface Wave Evidence of Present Study
1/9/82 mainshock	5.8	9 km	7 km	7 ± 1.5 km
1/9/82 aftershock	5.3	7.5 km	7 km	3 - 5 ± 2 km
1/11/82 aftershock	5.5	6 km	6 - 7 km	6 ± 1 km
6/16/82	4.6	-	7 km	8 ± 2 km

IV. ANALYSIS OF THE NEW BRUNSWICK, 1982, EARTHQUAKE SEQUENCE WITH INFERENCES ON SOURCE PARAMETERS FROM MULTI-MODE SURFACE WAVE DISPERSION AND SPECTRAL EXCITATION (M.S. Thesis of C. Nichols)

The Pennsylvania State University

The Graduate School

Department of Geosciences

Analysis of the New Brunswick, 1982, Earthquake Sequence with Inferences on Source Parameters from Multi-Mode Surface Wave Dispersion and Spectral Excitation

A Paper in

Geophysics

by

Christine C. Nichols

Submitted in Partial Fulfillment
of the Requirements
for the Degree of

Master of Science

December 1984

TABLE OF CONTENTS

Page

APPENDICES

ABSTRACT

The 1982 New Brunswick earthquake series, including the m_b 5.7 mainshock and several high magnitude aftershocks, posed interesting problems in determining source mechanism and focal depth. The high quality, long period and broad-band DWWSSN digital recordings from SCP inspired a single station surface wave study to address these questions. Band-pass filters applied over the entire frequency range provided group velocity and spectral amplitude data for Rayleigh and Love modes. Synthetic amplitude spectra were generated assuming structure parameters common to both the source area and the propagation path. Key aspects of the source mechanism could be inferred from the fundamental mode observations, particularly for the mainshock on January 9, 1982, and the largest magnitude aftershock which occurred on January 11. Although there are significant differences in modal excitation at the higher frequencies from event to event, only qualitative support for source mechanism could be inferred because higher order modes could not be identified. Additionally, published NEIS teleseismic m_b, network m_{bLg}, and M_S values were compared with m_{bLg} and M_S values computed with the SCP data. These results indicated that the single-station m_{bLg} values for the four New Brunswick events studied agreed remarkably well with the network average magnitudes, whereas M_S values commonly disagreed. In spite of the observed variable excitation of the individual higher order modes, consistent with the theoretical excitation appropriate for the different mechanisms for these events, the ensemble of modes that comprises the Lg signal gives every indication of providing a stable measure of

source strength when m_{bLg} is measured according to Nuttli's magnitude relationship.

The fundamental mode Love-to-Rayleigh surface wave spectral ratios for periods greater than ten seconds provided useful qualitative evidence for source mechanism and focal depth. The mechanism proposed by Choy et.al. (1983) was supported for the mainshock, with fault plane striking at 195 degrees and dipping 65 degrees to the northwest with a rake of 70 degrees, but with preferred focal depth of 7 km rather than the 9 km given by Choy et.al. (1983). The results for the aftershock on January 11 are well-explained by the mechanism proposed by Wetmiller et.al. (1983), indicating thrusting on a plane conjugate to the fault plane of the mainshock, with strike of 332 degrees, dipping 48 degrees to the southeast with a rake of 59 degrees. The focal depth for this event was found to be 6 km from Love-to-Rayleigh spectral ratios at SCP. While results for the aftershock on January 9 were less conclusive, they suggest a shallower depth than the mainshock. Although the thrusting mechanisms are consistent with eastern North American crustal stress patterns, the inferred dip and rake of the mainshock are not consistent with faulting under the action of the ENE to NE horizontal compressive stress prevailing over much of the northeastern United States. The inferred source parameters for the January 11 aftershock are consistent with this stress orientation.

ACKNOWLEDGEMENTS

It is always difficult to adequately recognize the special efforts that are undertaken by friends, colleagues, and superiors in the interests of urging one on to successful completion of a degree. In my case, where anomalous circumstances were the rule, I have more acknowledgements to make than most. It was Shelton Alexander who first found me wandering through Deike Building in search of advice on an edifying introductory geophysics course and who later captured my imagination for research with his vision for and thoroughly intuitive grasp of surface wave analysis. All the professors are due special thanks for their own individual contributions in providing timely guidance at the drop of a hat and urgently needed scheduling flexibility. Appreciation is extended to Dr. David Harkrider, who provided the programs used to generate surface wave spectra and the patient advice needed to get them up and running; to R.J. Wetmiller, who supplied the most complete study to date on the New Brunswick events in advance of publication; to Dr. Gabriel LeBlanc, Dr. Jay Pulli, the Center for Seismic Studies and Teledyne staffs, all of whom came to the rescue with relevant information and data on short notice.

But the people who kept me going deserve more recognition than I can conjure up on paper: from my supportive colleagues at the high school, to my enduring office-mates and fellow graduate students (especially Roger, who has an undisputed knack of keeping alive my will to fight), to the graveyard shift at the computer center, to my forgiving typist, Colleen, and to Carol, who so quietly and efficiently attends to the affective domain of all our geophysical needs, to my pa-

tient family, to Exxon for allowing me free access to drafting and word processing facilities - to all of you I offer a simple, but truly sincere thanks.

This research was supported by the Advanced Research Projects Agency of the Department of Defense and was monitored by the Air Force Office of Scientific Research under Grant No. AFOSR-82-0054. Computing facilities were supplied by the Pennsylvania State University Computation Center.

LIST OF FIGURES

LIST OF TABLES

"You see, one thing is, I can live with doubt and uncertainty and not knowing. I think it's much more interesting to live not knowing than to have answers which might be wrong."

- Richard Feynman, 1983

CHAPTER 1

INTRODUCTION

The recent series of New Brunswick earthquakes, beginning with the January 9, 1982, mainshock (m_b = 5.7), has provided high quality data from which inferences on source mechanism and crustal structure may be drawn. Interest in these events has been particularly great due to the unusually large mainshock; most previous studies in eastern North America involve earthquakes of magnitudes less than 5 in ascertaining seismicity trends, stress patterns, and implications for regional tectonics, all important considerations in assessing seismic hazard. As of its occurrence, the mainshock was the largest event in eastern North America since the institution of the Global Digital Seismograph Network (GDSN), and, as such, it offers an unusual opportunity for analysis at both regional and teleseismic ranges. Resolution of source parameters for all the events from the available body wave data was complicated by ambiguities in depth determination resulting from depth phase identification and noisy teleseismic recordings of the aftershocks, conflicting evidence from locally monitored aftershock activity, and the suggestion of conjugate rupturing along intersecting fault limbs. Significantly different source parameters have been inferred for the mainshock by different investigators. There is even more uncertainty for the larger aftershocks, particularly with regard to focal depth. Long period and broad-band surface waves recorded at the State College, Pennsylvania (SCP) station of the Digital World-Wide Seismographic

System Network (DWWSSN) had very high signal-to-noise ratios. The fundamental mode Rayleigh and Love wave signals exhibited such classic dispersion features, along with a striking two-to-one Love-to-Rayleigh excitation that surface wave analysis seemed a viable alternate approach to acquire source information including depth of focus. The Lg contribution was also well-recorded for the mainshock and the larger aftershocks, so that source differences, reflected in the excitation of these higher order modes, could be investigated. This is of interest because m_{bLg} at SCP agrees closely with the magnitudes obtained from the total set of regional and teleseismic observations for these events.

Directions of the Present Study

Determination of focal depth using surface wave analysis, in particular, surface wave spectra and Love-to-Rayleigh spectral ratios, has been addressed by a number of investigators (Harkrider, 1970; Tsai and Aki, 1970a, 1970b; Canitez and Toksöz, 1971; Massé et.al.,1973; Turnbull, 1976; Mendiguren, 1977; Mitchell and Herrmann, 1979; Cybriwsky, 1979). Multi-station studies reveal that azimuthal variation in spectral amplitudes permits determination of source mechanism as well as depth. Single-station studies report precise results on focal depths when fault-plane solutions are well known. Although sensitive to the accuracy of all source parameters and models chosen for earth structure, precise focal depth determination via surface wave analysis is viable because the spectra are so strongly affected by depth of source. Attenuation, crustal thickness, spatial and temporal

behavior of the source are complicating factors which affect absolute amplitude spectra, but which do so to a far smaller extent than does depth (Tsai and Aki, 1970a) and which can be cancelled out when Love-to-Rayleigh amplitude ratios are used (Canitez and Toksöz, 1971). Given the shallow nature of the New Brunswick events, significant surface wave excitation was expected. The digital data at SCP - especially for the mainshock - quite obviously contained meaningful surface wave information, the usefulness of which compounded substantially with the number of modes that could be identified. It was hoped that a single-station, multi-mode surface wave analysis of the SCP data, incorporating source parameters available from existing body wave studies, would provide additional constraints on source mechanism, especially focal depth, for these New Brunswick events.

Spectral amplitude of surface wave modes observed at a recording station depend not only on the depth and focal mechanism of the earthquake source, but also on the elastic and anelastic properties of the crust and upper mantle between the source and the receiver and on the instrument response of the system recording the signal; these propagation and instrument effects must be removed from the observed signals before conclusions can be drawn about any single source parameter. This is far from a trivial operation, since different combinations of source and propagation effects can in some instances produce very different signals. The special advantage associated with surface waves is that, for a given path structure and receiving instrument, excitation of each of the various fundamental and higher modes of Love and Rayleigh waves is extremely sensitive to source parameters,

including strike, dip, rake and focal depth. In principle, each mode that can be resolved from the observed surface wave seismogram and compared by spectral amplitude, frequency by frequency, provides an independent piece of evidence with which to evaluate the source. In practice, this can be a challenging undertaking; however, relative modal excitation among events can be used more easily to characterize similarities and differences in the sources.

The New Brunswick earthquakes provided an unusual opportunity for surface wave analysis of source mechanism and depth, since the epicenters of the ten larger events recorded at SCP were all within a few tenths of a degree in latitude and longitude from one another. This ensured that the paths traveled from source to receiver were essentially identical and, thus, dispersion and attenuation effects were assured to be the same for each surface wave mode. Short, intermediate, and long period digital data at SCP were all used in the analysis. Since transfer functions for each instrument had been successfully developed to deconvolve amplitude and phase effects introduced by the recording instruments, the full spectral range recorded could be used to compare source excitation among the events.

The analysis and interpretation approach that was used is summarized as follows:

1. By applying multiple band-pass filters to the instrument-corrected data, group arrivals associated with the center frequency of each band-pass were identified and associated with individual modes, and group velocities were calculated from the arrival times of envelope peaks. Theoretical dispersion curves for crustal structures represent-

ing reasonable average paths between New Brunswick and SCP were compared with the band-pass dispersion results, and the best-fitting model was selected to represent the structure in subsequent calculations of theoretical seismograms. A source structure appropriate for the New Brunswick epicentral area was used to calculate the modal excitation for various source mechanisms and focal depths. In this case, the best-fitting path structure was also appropriate for the source structure, so the two were chosen to be the same.

2. Programs provided by D. Harkrider were adapted for use on the IBM 370/3081 at PSU (under the H-extended compiler option) to compute multi-mode Love and Rayleigh wave excitation and synthetic surface wave seismograms. After inputting eigenvalues of the preferred multilayer structure and assuming various source mechanisms obtained in previous studies of the New Brunswick events, amplitude spectra were generated for fundamental and higher order Love and Rayleigh modes for varying source depths. Comparison of the predicted excitations with the relative amplitudes of observed envelope peaks helped identify specific modes in the data. Since the mechanism for the January 11, 1982, aftershock was postulated to be different from the mainshock, synthetic spectra were generated using source parameters proposed by Wetmiller et.al. (1983) in an attempt to substantiate this mechanism and to use the predicted amplitude excitation to resolve the depth. With the evidence accumulated from analysis of the January sequence, application of the same technique to the data from the June 16, 1982, earthquake permitted inferences of its depth and source mechanism. Since it is located about 30 km west of the other events, and no earthquake activity has been

detected in the intervening region (Wetmiller et.al., 1982, 1983), its relationship to the others is of interest, particularly with regard to implications for further seismic activity in New Brunswick.

The objectives of this study have been: (a) to use multi-mode surface wave analysis to develop additional evidence for constraining focal depth and source mechanism for the New Brunswick events; (b) to delineate arrival times versus frequency for higher order modes from band-pass filter results, in hopes of providing more complete group velocity dispersion curves; (c) to determine the extent to which conventional single-station Lg magnitudes (m_{bLg}) give good estimates of source size when individual higher mode excitation varies significantly from event to event in the New Brunswick sequence; and (d) to characterize the substantial differences in path effects on Lg in eastern United States compared to the western United States.

CHAPTER 2

GEOLOGICAL BACKGROUND AND REGIONAL SEISMICITY

Introduction

> The present geological activity of the eastern United States does not offer the excitement of a lithospheric plate plunging under another along a Benioff plane or the rapid grinding of one plate against another along a system of transcurrent faults; nor is there active volcanism or continental rifting. No doubt, most of these processes were vigorously operative in the past. Today, we are left with a battered, contorted, and creaking remnant of the continental lithosphere that evolved over a long period of time and that somehow reflects these past processes. The challenge is to unravel the events and the influence of older fabric upon younger structure.
>
> - Diment et.al., 1966

Epicentral data for the New Brunswick events chosen for this study, as reported in the Preliminary Determination of Epicenters, are shown in Table 1. While this region is clearly not aseismic, it is unusual for events greater than magnitude 5 to occur there. Figure 1(a) presents a record of historical seismicity for eastern North America which can be expected to be subject to the usual population bias. Yang and Aggarwal (1981) have attempted to revise this record in their plots of epicentral locations of events of m_b greater than or equal to two for the period 1970 - 1979, as instrumentally recorded by the Northeastern Seismic Network [Figure 1(b)]. A more detailed picture of activity in the epicentral region has been presented by Wetmiller et.al. (1983), who illustrate the regional seismicity, distinguishing events of magnitudes less than 3 from four documented earthquakes of assigned magnitudes

between 4 and 5.5 (Figure 2). They report that, while it is likely the largest earthquake to occur in New Brunswick within historic times, the January 9 mainshock is not inconsistent with existing probabilistic ground motion maps of Canada derived for seismic risk purposes (referenced to Basham et.al., 1982). From these observations, it is evident that the remote New Brunswick area is considerably more seismically active than the historical data indicate; however, magnitudes on the order of m_b = 5 still are not common there.

Table 1

Earthquake Parameters of New Brunswick Mainshock and Four Principal Aftershocks

(As Reported in the PDE)

Date	Origin Time (h m s)	Latitude (Deg. N)	Longitude (Deg. W)	m_b
January 9, 1982	12:53:52	46.98	66.66	5.7
January 9, 1982	16:36:43	47.02	66.65	5.1
January 11, 1982	21:41:08	46.98	66.66	5.4
March 31, 1982*	21:02:20	47.00	66.60	5.0
June 16, 1982	11:42:30	46.97	66.99	4.7

* Not analyzed in the present study

Understanding the causes of large eastern North American earthquakes has been clouded by the fact that geologic and tectonic correlation with their hypocentral locations and focal mechanisms have in general been lacking (Herrmann, 1979; Fletcher et.al., 1978). Current hypotheses tend toward one of two extremes: a) fractures in previously unbroken rock, or b) slippage on major pre-existing faults (reported in Choy et.al., 1983). The first of these explanations has been linked tentatively with high stress drops that are important for consideration of strong ground motion; however, predicting future high stress-drop earthquake locations via traditional geologic methods would appear to be very difficult. The second should be intimately related to neotectonic fault patterns and contemporary crustal movements. Now that instrumental coverage of this area is so greatly improved, analysis of large-magnitude events such as the New Brunswick series, coupled with geological studies of their epicentral locations, including high-resolution seismic profiling, may make it possible to determine conclusively whether earthquake sources are associated with new or with pre-existing fault structures.

Geologic and Tectonic Setting

The New Brunswick earthquakes occurred within a granitic pluton of the Miramichi Anticlinorium (Figure 3) which is located within the Gander Zone, one of five major geologic provinces defined by sharp contrasts in the features of the late-Precambrian and early Paleozoic rocks across the Canadian Appalachians: in northwest to southeast progression, these are Humber, Dunnage, Gander, Avalon and Meguma zones (Williams, 1982; Bird and Dewey, 1970). In particular, the Dunnage,

Gander, and Avalon zones are likely extensions of the Connecticut-Valley Gaspé Synclinorium, the Bronson-Hill Anticlinorium, and the Merrimac Synclinorium, New England counterparts with somewhat different features (King, 1977; Taylor and Toksöz, 1979; Yang and Aggarwal, 1981). While their tectonic evolution is similar, these zones do not share the metamorphic and igneous character of the New England province nor the distinctive fold-fault features and longitudinal two-fold division so apparent in the trends of the U.S. Appalachians (Spencer, 1969).

In accord with plate tectonic theory, the current thinking on the evolution of the Northern Appalachians centers on the rifting and subsequent closing of a proto-Atlantic, Iapetus ocean during late-Precambrian through Paleozoic time, with the Taconic, Acadian, and Alleghenian orogenies all associated with various episodes in the closing process (Bird and Dewey, 1970; King, 1977; Rast and Stringer, 1974; Taylor and Toksöz, 1979, 1982; Williams, 1979, 1982). The Humber zone, with its Grenvillian basement, constituted the stable continental margin that was left behind as the Iapetus Ocean opened while the Dunnage and Gander zones comprised the oceanic region. The Avalon and Meguma zones may have been the eastward drifting continental mass (King, 1977), although the Precambrian and Paleozoic evolution of these zones is unclear and allows a wide range of explanations (Williams, 1982). As oceanic closing proceeded during early to mid-Ordovician through Permian time, Dunnage and Gander zones were juxtaposed with the Humber zone and with one another, producing at their boundaries the most dramatic impacts of the Taconic orogeny. Of particular interest were the steep faults with locally wide zones of ductile deformation produced in the Gander zone. In New England, the Bronson-Hill Anticlinorium experienced

considerable volcanic activity during this period, consistent with island-arc volcanism with subduction strongly suggested on an eastward-dipping Benioff zone. Similar trends in New Brunswick implied southeasterly subduction under the Gander zone (Bird and Dewey, 1970; Taylor and Toksöz, 1979, 1982; Williams, 1979, 1982).

After a period of relative quiescence during Silurian to early Devonian time, tectonic activity resumed with the Acadian orogeny; renewed volcanism, high-grade metamorphism in New England, intrusion of granitic plutons with accompanying large-scale recumbant folding in many cases, and deformation and development of large thrust belts were all featured, reaching peak activity in mid-Devonian time. The controlling features of this episode of major deformation remain enigmatic, but their impact affected the entire Canadian Appalachian sequence, including the western zones previously deformed in the Taconic orogeny (Williams, 1982). King (1977) asserts that almost all major granitic plutons were emplaced during this period of continental collision between North America and the Avalon block and that their features bear little similarity to modern island-arc counterparts, thus disfavoring a subduction mechanism for their origin (Williams, 1982). The subsequent Alleghenian orogeny was thought to be associated with the final continent-continent collision, but, since its impact was restricted to the Avalon-Meguma boundary, far eastward of the region of interest, it is not of immediate concern to this study.

Recent Seismic Activity and Associated Geologic Structures in the Study Area

To depict the epicentral region, Wetmiller et.al. (1983) show the aftershock activity from the January and March events superimposed upon a geologic map of the area (Figure 4). Although not included in this picture, location of the June event (Figure 3) supports the observation that all of the earthquakes occurred within a single massive granitic pluton of Devonian age, which has yet to reveal any indication of previous deformation. Preliminary geological mapping and gravity investigations have been carried out by Burke et.al. (1982), yielding some initial estimates on the size and extent of this pluton. They report that the area enclosing the epicenters of the mainshock and aftershocks is mainly underlain by granitic rock with small dioritic inliers, all part of the extensive 800 km^2 "North Pole pluton" which intruded deformed, Cambro-Ordovician metamorphic rocks. A large gravity low coincides with the position of the pluton, indicating a 100 - 200 kg/m^3 density contrast between the plutonic and surrounding metamorphic rocks. The low encompasses some smaller positive anomalies suggesting that the higher density diorite is more extensive at depth than is indicated in the surface exposures. These gravity anomalies, combined with the best available seismic evidence for depth of the earthquakes, indicate that the events were confined to the plutonic body, which is thus inferred to be more brittle and weaker than the surrounding metamorphic rocks when exposed to the same stress regime (Burke et.al., 1982).

The New Brunswick events occurred within an extensive granitic pluton and produced "the first observed earthquake-induced bedrock break

in eastern Canada, but the displacement [at the surface] was small (25 mm) and not obviously a primary movement." (p.2, Wetmiller et.al., 1983). Located on a pre-existing joint oriented parallel to the inferred rupture of the mainshock, the surface break occurred barely within a less-prominent joint system of steeply dipping joints (Burke et.al., 1982). If it could be established that there is a fundamental relationship among pre-existing fault structures, the prevailing joint system, and the earthquake rupture geometry (and associated stress orientation), it would certainly go a long way toward development of a coherent tectonic picture, but, so far, the available evidence has resisted such generalization. Additional field studies, including trenching in the epicentral area, are still in progress, so some definite conclusions regarding the influence of earlier episodes of deformation may become available when these investigations are completed.

CHAPTER 3

THEORY

The historical development of the theory for calculating surface wave dispersion and far-field time and frequency domain values for a variety of earthquake source types is traced very completely in Wang (1981) and Massé et.al. (1973). One of the central figures in this development is David G.Harkrider who developed the programs for modal excitation for earthquake and explosion sources in multilayered earth models and for generating the corresponding synthetic surface wave seismograms that were used in this study.

Following his conventional notation, as revised to include attenuation factors (Massé et.al., 1973), the far-field spectral amplitudes for Rayleigh (U_R) and Love (U_L) waves may be written as:

$$U_R(\omega) = S(\omega)\, k_R^m\, e^{-i(j+2m)\frac{\pi}{4}}\, \lambda_R^{\cdot}(\theta,h,\omega)\, \frac{E_R(\omega)\, e^{-ik_R r}}{r^{1/2}}\, e^{-\gamma_R(\omega) r}$$

$$U_L(\omega) = S(\omega) k_L^m\, e^{-i(j+2m)\frac{\pi}{4}} \chi_L(\theta,h,\omega)\, \frac{E_L(\omega)\, e^{-ik_L r}}{r^{1/2}}\, e^{-\gamma_L(\omega) r}$$

where $S(\omega)$ is the spectral source function, that is, the Fourier-transformed dislocation-time history (the same for Rayleigh and Love waves for non-propagating point sources); m=0 for a point force, m=1 for a couple

or double-couple source; k (as ω/C, angular frequency divided by phase velocity) is the Love or Rayleigh wave number; h is the source depth; θ is azimuth from the strike of the fault, as specified in Ben-Menahem and Harkrider (1964); r is the epicentral distance and $\gamma_R(\omega)$ and $\gamma_L(\omega)$ are the coefficients of anelastic attenuation which are frequency dependent. The factors E_R and E_L are defined separately for Love and Rayleigh waves as their amplitude response divided by the square root of their wave number, multiplied by ellipticity at the surface in the case of Rayleigh waves.

$$E_R = \epsilon_o A_R k_R^{-1/2} \qquad E_L = A_L k_L^{-1/2}$$

$$\epsilon_o = -\left[\frac{u_o^*}{w_o}\right]$$

The amplitude layer responses, A_R and A_L, are dependent on wave type, frequency, mode order, and the elastic properties of the multilayered medium through which the waves pass, and are independent of source type and depth. Harkrider's definitions for Love and Rayleigh amplitude response are based on Thomson-Haskell displacement-stress vector elements (Haskell, 1953), terms related to Thomson-Haskell displacement-stress matrices and their products, and the rate of change of the period equations, F_R and F_L, with respect to wave number as:

$$A_R = \frac{G^*N - L^*H}{\left(\frac{\partial F_R}{\partial k}\right)_\omega}$$

$$A_i = \frac{1}{\left[\frac{\dot{v}_{n-1}}{\dot{v}_o}\right]\left(\frac{\partial F_i}{\partial k}\right)_\omega}$$

Definition of the amplitude response functions in terms of depth integrals, which are proportional to the kinetic energy densities of their respective surface waves, provides an alternative method of calculation and a useful check on accuracy of the values determined by matrix methods. Both techniques are used in Harkrider's program. Numerical instabilities commonly appear in the Thomson-Haskell matrix technique as frequency or mode order is increased to the point that differences calculated between rapidly increasing exponential terms lose numerical significance as they become too small for the precision of the machine; these difficulties were overcome in the Harkrider program by incorporating the compound matrix formulations developed by Dunkin (1965) and Thrower(1965).

The complex, frequency-dependent radiation pattern, $\chi(\omega)$, is dependent on the source parameters: dip, δ, rake, λ, azimuth, θ, and depth (h) (see fault-plane geometry illustrated in Appendix 1) according to the relationships given in Table 2. A, B, C, G, V, and W, all frequency-dependent functions of source depth, are defined in terms of the displacement-stress vector elements (the quantities in brackets). These elements are determined by specifying the elastic parameters (compressional and shear wave velocities, densities, and layer thicknesses) for each layer of an assumed multilayered structure,

Table 2

RADIATION PATTERN COEFFICIENTS*

Coefficient	Point force	
	Love	Rayleigh
d_0	0	$\sin\lambda \sin\delta H'(h)$
d_1	$\cos\lambda I(h)$	$-\sin\lambda\cos\delta A(h)$
d_2	$-\sin\lambda\cos\delta I'(h)$	$-\cos\lambda A(h)$
d_3	0	0
d_4	0	0

Coefficient	Couple	
	Love	Rayleigh
d_0	$-\frac{1}{2}\cos\lambda \sin\delta I'(h)$	$\frac{1}{2}\sin\lambda \sin 2\delta B(h)$
d_1	$\cos\lambda\cos\delta G(h)$	$\sin\lambda[H(h)-\cos^2\delta C(h)]$
d_2	$-\sin\lambda\cos^2\delta G(h)$	$\cos\lambda\cos\delta[H(h)-C(h)]$
d_3	$\frac{1}{2}\sin\lambda \sin 2\delta I(h)$	$\frac{1}{2}\cos\lambda \sin\delta A(h)$
d_4	$\frac{1}{2}\cos\lambda \sin\delta I(h)$	$-\frac{1}{2}\sin\lambda \sin 2\delta A(h)$

Coefficient	Double-Couple	
	Love	Rayleigh
d_0	0	$\frac{1}{2}\sin\lambda \sin 2\delta B(h)$
d_1	$\cos\lambda\cos\delta G(h)$	$-\sin\lambda\cos 2\delta C(h)$
d_2	$-\sin\lambda\cos 2\delta G(h)$	$-\cos\lambda\cos\delta C(h)$
d_3	$\frac{1}{2}\sin\lambda \sin 2\delta I(h)$	$\cos\lambda \sin\delta A(h)$
d_4	$\cos\lambda \sin\delta I(h)$	$-\frac{1}{2}\sin\lambda \sin 2\delta A(h)$

(a)

$$\chi(\omega, h) = d_0 + i[d_1\sin(\theta) + d_2\cos(\theta)] + d_3\sin(2\theta) + d_4\cos(2\theta)$$

* The factors $H'(h)$, $A(h)$, $C(h)$, $B(h)$, $I'(h)$ and $G(h)$ in terms of the Thomson-Haskell displacement-stress vector elements (Haskell, 1953) are

$$H'(h) = [u_r(h)/u_0]$$

$$A(h) = -[u_\theta^\circ(h)/u_0]$$

$$C(h) = -\frac{1}{\mu_h}[\sigma_{rz}(h)/(\dot{u}_0/C_\beta)]$$

$$B(h) = -\left\{\left(3-4\frac{\beta_h^2}{\alpha_h^2}\right)[u_r^\circ(h)/u_0] + \frac{2}{\rho_h\alpha_h^2}[\sigma_{rr}^\circ(h)/(\dot{u}_0/C_\beta)]\right\}$$

$$V(h) = [v_r(h)/v_0]$$

and

$$G(h) = \frac{1}{\mu_E}[\sigma_{r\theta}^\circ(h)/(v_0/C_\beta)].$$

(b)

and demanding that the wave equation be satisfied under boundary conditions of zero stress at the free surface, zero displacement at (effectively) infinite depth, and continuity of stress and displacement at each layer interface within the medium.

The coefficients of anelastic attenuation, $\gamma_R(\omega)$ and $\gamma_L(\omega)$, are related to the specific quality factor, Q, as:

$$\gamma(\omega) = \frac{\omega}{2 Q_\beta U(\omega)}$$

where Q_β is mode- and frequency-dependent and $U(\omega)$ is the group velocity for the specified mode at the frequency ω. Although there is evidence suggesting that Q_β is not the same for Love and Rayleigh waves (Mitchell and Herrmann, 1979), there is some support for assuming that these differences can be ignored (Tsai and Aki, 1970a), at least for low frequencies. In this study, where the propagation path is relatively short (1130 km) and identical from event to event, it has been assumed that γ_R and γ_L are not significantly different throughout the period range over which the spectral ratio is calculated.

Since U_R and U_L are dependent on, and particularly sensitive to, source finiteness effects, errors in assumed time and space histories for the source mechanism will affect predicted results for these absolute spectral amplitudes adversely. However, assuming the source factors to be approximately the same for both Love and Rayleigh waves (Massé, Lambert, and Harkrider, 19), forming the amplitude ratio cancels their influence completely. Taken in combination with the additional simplifications introduced through cancellation of common distance and attenuation terms, this

advantage strongly suggests the merit of using Love-to-Rayleigh spectral ratios in the evaluation of source parameters, particularly depth. The L/R spectral ratio is very sensitive to focal depth (Ben-Menahem and Harkrider, 1964; Canitez and Toksöz, 1971; Cybriwsky, 1979; Harkrider, 1970; Massé et.al., 1973; Tsai and Aki, 1970a; Turnbull, 1976; and many other recent studies of specific earthquakes).

The flow of the numerical procedures used to calculate theoretical spectral amplitudes is detailed in Appendix 1; a summary of the steps is, however, appropriate here. A routine (RLSCFRQ), which scans frequency/phase-velocity space for appropriate roots in frequency and phase velocity by mode, greatly facilitates the more accurate root-finding process in the Love and Rayleigh eigenvalue-generating programs. These programs (LOVIT.UP) and (RAYLIT.UPEC) then calculate, for each mode specified, the disperion and depth-independent quantities for given input frequencies as well as displacement-stress values for the midpoint depth of each layer. In finding the roots of the period equation, $F(\omega, C, \text{layer parameters}) = 0$, the Love wave program uses the Thomson-Haskell formulation of F_L while the Rayleigh wave program uses the compound layer matrix formulation of F_R. Once bracketed to the desired accuracy for the given frequency, successive roots (resulting from perturbing phase velocity slightly) are used to calculate the group velocity, U, the kinetic energy density and the amplitude response of the medium, as well as the surface ellipticity in the case of the Rayleigh program. The group velocities and amplitude responses are computed by the two different techniques referred to earlier, using both partial derivative and energy integral formulations (Harkrider, 1970). Output of these programs, after minor

formatting adjustments, are then used as input to the source depth program (EQTR.ZBIG) where source type and associated source parameters are selected, and spectral amplitudes or the seismograms themselves can be calculated (and plotted) for each mode, for a given receiver azimuth and depth, for any number of desired source depths. It is important to point out that, at present, the program assumes that the structures are the same at the source and over the propagation path to the receiver. Modification of the program to accommodate excitation calculations at the source using one structure and propagation effects to the receiver using another structure is relatively straightforward. In this study, however, the chosen source structure fortuitously also adequately matched the observed path dispersion effects based on empirical band-pass group velocity determinations. Therefore, the synthetics generated here assume an average structure from New Brunswick to SCP that is the same as the source structure. Using various proposed source parameters obtained from the fault-plane solutions and moment tensor inversions of recent studies of the New Brunswick events, the main program was run to generate theoretical Rayleigh and Love mode spectra and spectral ratios for source depths ranging from 1 to 10 km. These were compared with the band-pass amplitude results in an attempt to identify a preferred depth for each of the events.

CHAPTER 4

DATA PROCESSING AND ANALYSIS

Acquisition of the Data

The original DWWSSN short, intermediate and long period seismograms for the four events described in Table 1 were subset from the SCP digital tapes; they are shown in Appendix 2. The long period data were continuously recorded at one sample per second. Short and intermediate period signals were triggered and sampled at twenty and ten samples per second, respectively. Only the vertical component is available for the short period; vertical and two horizontal components are available for intermediate and long period data, which, along with epicentral coordinate information, allow rotation to obtain radial and transverse components.

With reference to the seismograms in Appendix 2, it is evident that, at an epicentral distance of 1130 km (Δ = 10.2°), SCP recorded a short period signal for the mainshock that clipped for about fifty seconds while the intermediate period signal did not. Ratios of peak amplitudes measured on transverse and vertical components for both intermediate and long period records showed a high Love-to-Rayleigh excitation; the Love-to-Rayleigh ratio was nearly three on the intermediate period and approached two on the long period recordings. Classic dispersion features characterize the long period signals, suggestive of pure fundamental mode arrivals. Although substantially noisier, seismograms for the January 9 aftershock exhibit similar features, particularly in Love-to-Rayleigh excitation on intermediate and long period signals.

The January 11 aftershock displays considerably different waveform features on the long period components with a lower Love-to-Rayleigh ratio, suggestive of a different source mechanism than the mainshock. The earthquake which occurred on June 16, of substantially lower magnitude than the other events, has Love-to-Rayleigh ratios which agree more closely with the January 11 aftershock than with the other events.

Instrument Correction

In preparation for applying band-pass filters, the digital seismograms were transformed using the Cooley-Tukey (1965) algorithm for the Fast Fourier Transform (FFT), yielding the complex-valued frequency domain representation of the time domain seismograms. Choosing a power of two at least one greater than that associated with the number of data points sampled reduced cyclic convolution effects to a minimum when the filters were applied. Instrument correction was accomplished in the frequency domain by using the complex-valued transfer function, developed using poles and zeros given in the Directory of World Digital Seismic Stations for each of the SCP digital instruments. The transfer function was defined as:

$$T(S) = \frac{A\Phi \cdot DS \cdot (S - Z_1) \cdot (S - Z_2) \ldots\ldots (S - Z_m)}{(S - P_1) \cdot (S - P_2) \ldots\ldots (S - P_n)}$$

where $S = i\omega$

ω = angular frequency

$A\Phi$ = a scalar quantity - different for each instrument

DS = digital sensitivity expressed in counts per micron

m = the number of complex zeros

n = the number of complex poles

Table 3 gives the relevant constants for each instrument.

Deconvolution of the instrument response using this transfer function is, then, a straightforward complex division in the frequency domain. Dependent as it is on frequency, the function can accommodate any sampling interval required by the time window of the chosen seismogram. These corrections were applied to the SCP data in this study and can now be routinely applied to any acquired short, intermediate, and long period digital data as an option within the bandpass program.

Band-Pass Filtering

The band-pass method is a filtering procedure pioneered in its application to multi-mode surface wave analysis by Alexander (1963), further developed by Dziewonski et.al. (1969) and tested with regard to group velocity and amplitude determination by Herrmann (1973) and Mitchell (1973), among others. The method exploits the simple fact that energy associated with different surface wave modes comprising a dispersed wave train generally arrive at different times for each frequency; if only a single station (rather than an array) is available, the method fails when more than one mode arrives at the same time with the same frequency. In principle, by nulling out all but a very limited range of frequencies around a chosen, central value, the narrow band-pass filter gives the arrival time and spectral amplitude of each

Table 3

Complex Poles and Zeros of Transfer Functions
for SCP DWWSSN Instruments

	Short Period	Intermediate Period	Long Period
$A\Phi$	1.11×10^7	354.8	.02755
DS (counts/ micron)	1000	125	500
zeros	$Z_1 = Z_2 = Z_3 = Z_4 = Z_5 = 0$ for each instrument		
poles			
P_1	(-16.63, 0)	(-.377, .1827)	(-.377, .1827)
P_2	(-4.241, 6.432)	(-.377,-.1827)	(-.377,-.1827)
P_3	(-4.241,-6.432)	(-2.407, 5.804)	(-.654, 0)
P_4	(-8.415, .3575)	(-2.407,-5.804)	(-.2318, 0)
P_5	(-8.415,-.3575)	(-5.848, 2.366)	(-.2318, 0)
P_6	(-111.1, 111.1)	(-5.848,-2.366)	(-.2318, 0)
P_7	(-111.1,-111.1)	(-.02108, 0)	(-.3276, 0)
P_8	(-.04442, .04444)	(-.02108, 0)	(-.3276, 0)
P_9	(-.04442,-.04444)		(-.3276, 0)
P_{10}			(-.0214, 0)
P_{11}			(-.0214, 0)

individual signal comprising the seismogram at that frequency. It is especially useful for separating out the contributions of various surface wave modes, because modes of different frequency typically arrive simultaneously giving rise to the complex wave-forms associated with the Lg portion of most seismograms. Each envelope peak of the band-pass filtered signal corresponds to the group arrival time of a mode (the arrival time of the energy of each wave packet at that frequency) and the amplitude at each peak is proportional to the Fourier spectral amplitude of that arrival.

The uncertainty principle in quantum theory relates particle momentum and position through the Fourier Transform; resolution of one quantity is inversely related to resolution of the other. Similarly, there are time and frequency domain tradeoffs on resolution which must be considered in filter shape and design. Optimally, only a single frequency should be passed; however, inverse transformation of a spectrum windowed by such a narrow filter would produce a broad sinusoid in time, whose envelope peak would be difficult to pick with accuracy and whose interferences with the carrier of nearby arrivals could be easily mistaken for additional group arrivals. According to the frequency scaling property, broadening the frequency domain function narrows the corresponding time domain function in inverse proportion. By using a somewhat larger filter bandwidth and introducing a cosine taper to the filter in the frequency domain to minimize sidelobes, these spurious effects are reduced. Group arrivals are nearly invariant under changes in filter bandwidth. The filter that was used is defined as:

in shape:

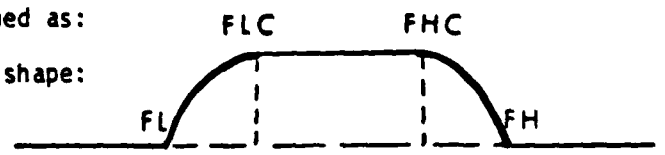

$$= \begin{cases} 1 \text{ from FLC to FHC, the bandwidth} \\ \cos\left|\dfrac{\pi\,(F - FLC)}{2\,(FLC - FL)}\right|, & FL < F < FLC \\ \cos\left|\dfrac{\pi\,(F - FHC)}{2\,(FHC - FH)}\right|, & FHC < F < FH \end{cases}$$

Any desired filter shape could have been used. For example, a Gaussian filter has the advantage of not having sidelobes, but it is susceptible to spectral leakage when the spectrum being filtered is highly colored as is typical of individual modal excitation spectra. The shape chosen with a cosine taper avoids this problem at the expense of small sidelobes and preserves the true signal energy between the taper points (FLC and FHC). It also allows assymmetrical filter shapes to be used (FL - FLC $\neq$ FHC - FH).

Application of the filter is accomplished conveniently by taking its product in the frequency domain with the real and imaginary spectral components of the transformed seismogram after instrument correction; it is a phaseless filter. A suite of these cosine-tapered, narrow band-pass filters was applied to the short, intermediate, and long period data, limiting the range of center frequencies to well within Nyquist[$1/(2\Delta t)$] where Δt is the sampling interval in time in each case. Using a computational trick consisting of nulling the negative frequency contributions and halving the spectral amplitude at DC and Nyquist frequencies, the inverse transform will be complex-valued (the analytic signal) where the real part is the filtered seismogram (times 0.5) and the imaginary part is its Hilbert transform (times 0.5). The envelope was calculated as the square root of the sum of the squares of the real and imaginary parts of the returned time series. Envelope peaks were identified, and

group velocities calculated very straightforwardly as the distance traveled divided by the travel time to each envelope peak.

For filters centered around lower frequencies, approaching zero Hz, narrowing the bandwidth of the filter becomes a necessity. Since the envelope amplitudes of the filtered signals are dependent on the bandwidth, indeed the filter shape in general, this effect had to be considered. Ideally, of course, it is desirable to always use the same filter bandwidth and shape. The narrow bandwidth required for low frequencies was inadequate for resolution of the various modal contributions at the higher frequencies. The compromise chosen was to use two filters with identical cosine tapers but with a bandwidth of .05 Hz for central frequencies greater than .1 Hz and a bandwidth of .005 Hz for those less than .1 Hz. Clearly, this bandwidth choice has a significant effect on the amplitude of the envelope, so comparison of absolute amplitudes was restricted to frequency ranges over which the filter shape was constant. Of course, effects of the filter shape can be cancelled completely by examining spectral ratios instead. Figure 5 illustrates probably the most extreme influence this effect can be expected to have on group velocity and amplitude values. Even with the dispersion apparent in the filtered signal of .05 Hz bandwidth, the group velocity is 3.37 km/sec, as compared with 3.27 km/sec for the filter of .005 Hz bandwidth. This suggests that the group velocity can be expected to be determined to within .1 km/sec, even with a factor of ten change in bandwidth. Amplitude scaling as illustrated by the peak amplitudes of the filtered signals is clearly a problem, however.

Another problem which affects both amplitude and group velocity results is spectral leakage due to radically varying spectral amplitudes

in the region of the central frequency. This can have an obvious effect on the amplitudes and will shift the peaks in the direction of high amplitude contributions, thereby affecting both the group velocity and amplitude calculations. The test for this effect is the instantaneous frequency of the band-pass filtered signal; it should be very close to the center frequency of the bandpass. Pre-whitening before filtering is expected to alleviate these leakage problems.

The results of applying the band-pass filters to the short, intermediate, and long period seismograms of Appendix 2 are compiled in Appendix 3. Figure 6 is an illustration of how dispersive effects can be observed as arrival times of the envelope peaks change for a given modal arrival. These results for the January 11 aftershock are remarkable in that a single mode seems to predominate throughout the suite of filters centering on frequencies ranging from 5 to 8.5 Hz. With Nyquist frequency at 10 Hz, it is surprising to see such clean evidence of energy from a single mode arriving at such high frequencies. Figure 7 is a sobering example of some of the difficulties to be faced in identifying different modes. Spurious peaks can be the result of truncation effects, interfering waveforms, or multipathed arrivals. Only the filtered signal centered at 5.5 Hz bears any resemblance to the clean modal arrivals of Figure 6. The result of applying a suite of filters to the vertical component, intermediate period signal of the January 9 mainshock is shown in Figure 8. A combination of simple dispersed fundamental mode arrivals at the lower frequencies and interfering waveforms of uncertain origin at higher frequencies illustrates the typical appearance of the filtered results.

Since the signals for all events traveled identical paths, disper-

sion is assured to be the same among events; amplitudes of the arrivals were expected to vary with modal excitation at the source and resultant variations in interfering waveforms. In an attempt to present the band-pass results in a way that might help isolate the modes, the amplitudes of each envelope peak on a single band-pass were normalized to the peak amplitude for that band-pass. A crude scale was then set to distinguish among these normalized amplitudes, symbols were assigned to correspond with these values, and composite plots of group velocity vs. frequency for all events, with relative amplitudes roughly indicated by the symbols, were drawn up separately for Love and Rayleigh waves. (See Figure 10 and its caption for more detail.)

The next step in sorting through this profusion of data consisted of assigning an average path structure and calculating theoretical dispersion curves for comparison with band-pass results.

Theoretical Path Dispersion - Choice of Average Path Structure

The search for a model to generate an appropriate theoretical dispersion curve representative of an average structure along the path from New Brunswick to SCP was confounded by the fact that most of the existing studies focused on geological provinces bordering on the desolate New Brunswick region, but not encompassing it. A comprehensive summary of eastern U.S. structures is presented by O'Neill (1983). Brune and Dorman (1963) used least-squares inversion of Love and Rayleigh phase velocities to determine their three-layered crust for the Canadian Shield. Dorman and Ewing (1962) refined the previous work of Oliver, Kovach, and Dorman (1960), using Rayleigh wave phase velocity

dispersion to deduce structure in the New York-Pennsylvania region that was consistent with the seismic refraction study performed by Katz (1955). Mitchell and Herrmann (1979) used single-station group velocities for earthquakes originating in the central U.S. with known fault plane solutions to invert for shear velocity structure in the Eastern United States. Recent work in New England by Curtin et.al. (1983) refined previous compressional and shear wave velocity structures by inverting short period data from quarry blasts and local earthquakes. Taylor and Toksöz of MIT have recently completed several studies of northeast United States structure. Their 1979 inversion of teleseismic P-wave travel time residuals recorded by the NE United States Seismic Network explored features of regional structures whose crustal portion was single-layered. In their 1982 paper, Taylor and Toksöz (1982a) summarized previous studies, keying velocity structures to their corresponding regions on a geologic map of the northeastern stretch of the Appalachian orogen. The most fruitful report for the present study proved to be their 1982 inter-station study of fundamental mode Rayleigh phase and group velocities of teleseismic events measured along great circle paths which sampled different regions in the Appalachians and the Grenville Province (Taylor and Toksöz, 1982b). Figure 9 illustrates the various paths studied. Their path A1 sampled structure parallel to the tectonic fabric of the Appalachians utilizing vertical component, long-period seismograph recordings from St. Johns, Newfoundland; Weston, Massachusetts; and Ogdensburg, New Jersey, of earthquakes originating in Sicily and Crete. The central New England Appalachians (Path A2) were sampled with events from the Kuriles and the mid-Atlantic Ridge as recorded at Montreal-Weston and Ottawa-Weston station pairs. Path G sampled the eastern

Grenville Province using events from South America and the Caribbean as recorded by the Ogdenburg-Ottawa, and Ogdenburg-Montreal station pairs. On the basis of the regions sampled, Paths A1 and Path G were selected along with Curtin's model as the starting structures. The layer parameters obtained for each proposed structure are given in Table 4.

Using Harkrider's scanning routine (RLSCFRQ) and the Rayleigh and Love eigenvalue generating programs (RAYLIT.UPEC and LOVIT.UP), theoretical fundamental mode dispersion curves were generated for the three trial structures and superimposed on the plots of group velocity vs. frequency which had been assembled for the January 9, 1982, mainshock. Agreement between the theoretical dispersion curve for Path G and the high amplitude group arrivals was remarkable, especially for the fundamental mode Love waves [Figures 10 (a) and (b)]. While the fit was not quite as good for the Rayleigh dispersion curve, it seemed to provide the best overall match between the band-pass data and the theoretical curves.

In an attempt to improve the fit of the theoretical dispersion curves with the result of the band-pass filtering, the Path G layer parameters were modified in keeping with the expected effects of changing crustal thickness and velocity contrast at the base of the crustal layer. Since separation in frequency between successive Airy phases is controlled by the velocity contrast at the base of the crustal layer (Alexander, 1963), the two effects could accommodated by simply reducing the shear wave velocity in layers three and four to 3.5 km/sec, thereby thickening the uniform layer to 35 km and increasing the velocity contrast from 3.8 to 4.5 km/sec to 3.5 to 4.5 km/sec at the base of the layer. Dispersion curves were gener-

Table 4

Taylor and Toksöz Proposed Structures

PATH A1

Layer	Thickness	Depth (km)	v_p	v_s	Density (g/cc)
1	10.	0.	6.0	3.4	2.7
2	10.	10.	6.2	3.5	2.75
3	10.	20.	7.0	4.0	3.0
4	10.	30.	7.0	4.0	3.0
5	20.	40.	8.1	4.6	3.3
6	20.	60.	8.1	4.5	3.3
7	20.	80.	8.2	4.5	3.3
8		100.	8.2	4.6	3.3

PATH G

1	5.	0.	6.0	3.5	2.7
2	10.	5.	6.0	3.5	2.7
3	10.	15.	6.6	3.8	2.8
4	10.	25.	6.8	3.8	2.85
5	20.	35.	8.1	4.5	3.3
6	20.	55.	8.1	4.5	3.3
7	20.	75.	8.2	4.7	3.3
8		95.	8.2	4.7	3.3

Curtin's Structure

Thickness (km)	v_p	v_s	Thickness (km)
8.8	6.00	3.51	11.3
11.3	6.35	3.86	7.2
19.8	6.95	4.04	19.9
	8.18	4.67	

ated for this modified structure and plotted in Figures 11 (a) and (b) as dotted lines in contrast with the solid line corresponding to the original model. Clearly, this modification overcompensated for the previously noted discrepancies in the Rayleigh dispersion fit; moreover, it worsened the fit for the Love wave dispersion. As a result, the original Path G model was retained as the preferred structure to represent the average path from New Brunswick to SCP for the remainder of the study.

While the fits are good in the long period range of the plots, it was not clear what was happening to the fundamental mode in the shorter periods, below ten seconds. Dispersion of short period fundamental mode surface waves is governed primarily by shallow structure and a low velocity sedimentary layer is assured to exist along at least some substantial portion of the path. Thus, it is likely that velocities at periods below 10 seconds are lower than the theoretical curves predict in Figures 10 and 11. Evidence of later, high amplitude arrivals (indicated by stars in the band-pass results) support this interpretation.

Higher order modes were expected in the period range below 10 seconds. In hopes of identifying these arrivals, theoretical dispersion curves were generated for the first four higher order modes. Figures 12 and 13 illustrate the predicted dispersion curves for the Path G structure, carried to the highest frequency for which stable calculations were possible. Group velocities from the bandpass results for the mainshock were plotted for comparison. Appendix IV shows these same dispersion curves superimposed on the band-pass results for each individual event as well as on the

composite plots of all the data. Although individual mode arrivals can't be identified, the overall theoretical patterns are consistent with the band-pass results.

Theoretical Amplitude Spectra

In order to generate theoretical spectral amplitudes for a number of modes at various depths, a structure at the source had to be specified and a source mechanism chosen. Since Harkrider's program to generate synthetic seismograms, EQTR.ZBIG, was set up to utilize the same structure at the source as was assumed for the propagation path, the Path G structure was taken to also represent the structure at the source. This was not unreasonable in light of the P-wave velocity structures present for nearby regions in Taylor and Toksöz (1982a) and density values for typical crustal rocks in the epicentral region provided by Dainty et.al. (1966). Wetmiller et.al. (1983) used a constant velocity half-space in their hypocentral location calculations with P and S velocities of 6.20 and 3.57 km/sec. Some limited refraction data in the area suggest a significantly lower P velocity near the surface (reported by Wetmiller et.al. (1983) to G. LeBlanc, personal communication), which places both values very much in line with the P and S velocities of the chosen Path G structure.

A number of investigators have proposed source mechanisms for the New Brunswick events based on a variety of methods of analysis. It is appropriate to sketch here the major conclusions of these studies since there is considerable variability among the mechanisms for these events, including the mainshock.

Well-defined P-wave pulse shapes were analyzed by Choy et.al.

(1983) to obtain source characteristics for the January 9, 1982, earthquake from broadband GDSN data. Moment tensor inversions of the long period P and SH waves provided largely corroborative evidence for their choice of focal parameters; some ambiguity was noted and attributed to differences in the data sets used in the two analyses and to the evident violation of a simple point source assumption for this event. Although acknowledging as significant the discrepancies in depth between their 9 km hypocenter location and the shallower (0-7 km) locally recorded aftershocks (Wetmiller et.al., 1982), Choy et.al. (1983) maintained that their interpretation favored the greater focal depth. Nabelek et.al. (1982) inverted short and long period body waveforms (P and SH) and amplitude spectra of vertical component Rayleigh waves to determine focal depth, source orientation and scalar seismic moment. Although consistent in type and orientation, their earthquake parameters fell outside the range of uncertainty of Choy's results and, in particular, indicated a hypocentral depth of 7 km. In a later report of this work, Nabelek and Toksöz (1983) reported revised source parameters more in line with Choy's, but maintained the shallower depth of 7 km.

It was clear that the teleseismically recorded aftershocks of January 9 and 11 had hypocenters which were significantly different from one another and from the mainshock (Choy et.al., 1983). As tempting as it was for simplicity to assume that these events occurred on a single plane with a similar mechanism, it was clear both from teleseismic data and the locally recorded aftershocks that this was not the case. If it could be inferred that the mainshock and the January 9 and 11 aftershocks occurred on a single plane, it would require assumption of a fault plane striking NNE and dipping steeply eastward. This orientation is

incompatible with nodal planes inferred from the broadband data (Choy et. al., 1983) and with direct evidence provided by aftershock patterns and by the north-trending, westward-dipping bedrock crack found in May, 1982, at the southern boundary of the January aftershock zone (Wetmiller et.al., 1982). Furthermore, it cannot account for the hypocentral depth of the March 31 aftershock, which is inferred to be less than 5 km (from Wetmiller et.al., 1983).

In probably the most comprehensive analysis of the New Brunswick events to date, Wetmiller, et.al. (1983) present body and surface wave evidence in support of their choice of focal mechanism for the mainshock and a detailed accounting of the spatial distribution and composite mechanisms of the aftershocks as determined from three field surveys conducted in January, April, and June, 1982, following the largest events. Their source parameters differ from those of Choy et.al. (1983) in dip and rake and they account for a discrepancy (in dip, at least) as being due to interpretation of a double event where movement progressed up a steepening fault plane. Aftershock activity convincingly supports conjugate rupturing on intersecting fault planes of steepening dip toward the surface. They propose that the January 9 and March 31 aftershocks occurred on the eastern limb and the January 11 aftershock on the western limb. Figure 14 illustrates the described fault orientation. Hasegawa (1983) used well-defined short-period P-wave first motions and analysis of fundamental mode Love and Rayleigh surface waves to determine P-nodal solutions for the mainshock consistent with those based on the aftershock activity and encompassing the previously reported results based on moment tensor inversions. He reported that study was continuing on the comparatively sparse and indistinct P-wave first motions and sur-

face wave records of the larger aftershocks with the specific objective of establishing their differences in source mechanism as compared with the January 9 mainshock. Thus, despite the abundance of data, there remain substantial disagreements with regard to the fault mechanism and focal depth of the mainshock and all of the large aftershocks. Focal depths for the aftershocks have not been determined based on recordings at teleseismic distances.

The relevant source parameters for the individual proposed mechanisms are summarized in Table 5. Using the values of strike, dip, and rake reported in these studies, theoretical surface wave modal excitations were calculated assuming the azimuth appropriate for propagation to SCP. Absolute spectral amplitudes were calculated for fundamental and four higher order modes and corresponding Love-to-Rayleigh ratios were formed for assumed depths from 1-10 km. Individual plots by depth of these theoretical spectra for each of the source mechanisms in Table 5 are included in Appendix 5; Love-to-Rayleigh fundamental mode spectral ratios for each depth are shown in Figures 15 - 18. The test of whether surface wave data from a single station could corroborate a preferred mechanism rested in the degree of fit between the theoretical spectra and the results of the band-pass filtering.

Table 5

	Strike	Dip (NW)	Rake	Depth
Mainshock				
Choy et.al.	195° (318°)*	65°	70°	9.0 ± 1.3 km (from depth phases)
Nabelek et.al.	3°(183°) (306°)*	34°	95°	7 km
Nabelek and Toksöz (in preparation)	175 ± 5° (298°)*	55 ± 2°	87 ± 10°	7 ± 1 km
Wetmiller et.al.	195° (318°)*	50°	120°	7 km (from aftershock and SW analysis)
January 11 Aftershock				
		SE		
Wetmiller et.al.	332° (95°)*	48°	59°	6 - 7 km

* These are the "azimuths from the hanging wall," as required by Harkrider's convention. See Appendix 1 for details.

CHAPTER 5

INTERPRETATION OF RESULTS

Comparison of theoretical dispersion curves and empirical band-pass filter results (Figures 12 and 13 and Appendix 4) permitted ready identification of the long period, fundamental mode Rayleigh and Love waves. Thus, conclusions regarding source mechanism and depth were based entirely on their Love-to-Rayleigh amplitude ratios. Although the presence of higher modes was supported by the data, accurate identification of individual modes was out of the question, eliminating these as sources of independent evidence for detailed analysis of the differences among events. Some interesting observations were gleaned from the high frequency, Lg arrivals, however: some consistent with higher mode excitation, some providing useful m_{bLg} estimates. These are presented as empirical evidence, worthy of further attention in subsequent investigations.

Fundamental Mode Analysis for Depth and Source Mechanism

In comparing theoretical Love wave spectra (Appendix 5, Figures A5-1a through 20a) for different mechanisms, it becomes immediately apparent that the excitations are almost identical for the fundamental mode. The Nabelek and Choy mechanisms (Table 5) show nearly identical features for

Nabelek and Choy mechanisms (Table 5) show nearly identical features for fundamental mode Rayleigh waves; where differences occur, they reflect similar shape but higher amplitude trends for the Nabelek mechanism (compare Figures A5-1b through 5b with A5-6b through 10b). As depth increases, the discrepancies in amplitude decrease and are more restricted to increasingly longer periods. Wetmiller et.al.'s January 9 mechanism yields Rayleigh wave amplitude spectra which differ substantially from the Choy spectra for shallow source depths (compare Figures A5-1b through 5b with A5 -11b through 15b). Remarkable agreement is evident in the short period range of the spectrum as depth increases, while very different amplitudes are seen for periods greater than 10 seconds for all depths. Wetmiller et.al.'s January 11 mechanism is substantially different in Rayleigh excitation at all depths (See Figures A5-16b through 20b), with a prominent spectral hole which moves to longer periods with increasing focal depth.

From these observations, it was clear that the spectral differences that were most likely to be diagnostic of source mechanism and depth were the Love-to-Rayleigh ratios for periods greater than 10 seconds. This was especially appealing in light of the fact that long period Rayleigh and Love fundamental modes can be unambiguously identified and that all band-pass filters in this period range were the same. Theoretical Love-to-Rayleigh spectral ratios were then formed for fundamental mode periods greater than ten seconds, superimposing ratios for all depths on a single plot for each mechanism. These results are displayed in Figures 15 to 18. The differences in the values of Love-to-Rayleigh ratios between the Nabelek and Choy mechanisms (Figures 15 and 16) are immediately apparent when viewed in

this way, though peak amplitudes with depth occur at almost identical frequencies for the two mechanisms. Wetmiller et.al's January 9 and January 11 proposed mechanisms exhibit distinctive features in their spectral ratios (see Figures 17 and 18).

Love and Rayleigh fundamental mode arrivals were selected from the band-pass filter results (on transverse and vertical components, respectively). Love-to-Rayleigh amplitude ratios were computed and plotted, by event, on the same amplitude vs. period scales as used for the theoretical spectral ratios. The mainshock amplitude ratios exhibit a smooth relationship in period, most consistent with Choy's mechanism. Superimposing the data points on the theoretical curves shows spectral ratios consistent with depths ranging from 5 - 8 km, tending toward 6 km at periods greater than 20 seconds and toward 8 km for shorter periods (Figure 19). Equally convincing are the results for the January 11 aftershock (Figure 20) which show evidence of a distinct peak in the spectral ratio entirely consistent with Wetmiller et.al.'s January 11 mechanism, with all the data points lying very close to the curve corresponding to 6 km depth. Again, there is a tendency for the short period data points to indicate a slightly greater depth.

The results for the January 9 aftershock (Figure 21), assuming the same mechanism as the mainshock, showed a great deal of scatter but, in general, had higher magnitude Love-to-Rayleigh ratios than those for the mainshock at periods less than 20 seconds, with an indication of a peak ratio located between 15 and 20 seconds period, that is, at a lower period than that of the mainshock. This is consistent with trends associated with shallower depths on the theoretical Love-to-Rayleigh

curves; a shallower depth than the mainshock is thus suggested for this event. However, the numerical values of the ratio are inconsistent with either Choy's or Nabelek's mechanisms.

In an attempt to modify source parameters to improve the fit for this event, it might seem that Love-to-Rayleigh ratios would be more sensitive to changes in strike than either dip or rake. However, evaluation of the rate of change of the Love and Rayleigh radiation pattern functions with each parameter, over ranges encompassing all the proposed mechanisms, indicated that the ratio is in fact most sensitive to dip. Since the strike of the fault plane seems so much better constrained for this event than either dip or rake, it made sense to vary these in seeking a better match between the data and the synthetic spectra.

Taking into account the differences in dip and rake among the proposed mechanisms, additional synthetic spectra were generated for variations of dip and rake on Choy's original model: rake values of 70°, 90° and 110° were assumed with dip values of 65° and 55° respectively. The effects of these changes in dip and rake can be seen in Figure 22. As rake is increased, the curves tend to flatten, with peak ratio values occurring at longer periods, both of which trends are inconsistent with the data. As dip is decreased, the ratios take on much higher values, peaking at lower periods than those for corresponding rakes and the larger dip value. The same trend to peak at somewhat longer periods with increasing rake is observed with the shallower dip. Of particular interest is comparison of the Choy mechanism ($\theta = 318°$, $\delta = 65°$, $\lambda = 70°$) (Figures 15 and 19), the modified Choy mechanism ($\theta = 318°$, $\delta = 55°$, $\lambda = 90°$) (Figure 22b) and the Nabelek mechanism ($\theta = 306°$, $\delta = 34°$, $\lambda = 95°$) (Figure 16). The three sets of curves show similar

trends, though the amplitude ratio dependence on decreasing dip and increasing rake is not apparent. The closest match of the data for the January 9 aftershock corresponds to the modified Choy mechanism - dip of 55° and rake of 90° (Figure 23); this result suggests that a shallow depth on the order of 3 km might be more consistent with the overall fit, though scatter in the data precludes identification of the period associated with the peak in the Love-to-Rayleigh ratios.

Considering the dip and rake trends indicated by these tests, increasing the dip and decreasing the strike beyond the ranges tested might produce a similar effect, though this is only conjecture. It is, however, the only way to proceed if the fault plane is indeed dipping more steeply near the surface as Wetmiller et.al. (1983) propose. The data seem to indicate a shallower depth; beyond that, little surface wave evidence is available to constrain the mechanism for this event.

Long period data for the June 16 aftershock is sparse due to many problems inherent in the data. While any interpretation suffers because of these difficulties, the fact that the observed broad-band Love-to-Rayleigh ratios are very high prompted a comparison of the shorter period band-pass results with the theoretical spectra for Wetmiller et.al.'s January 11 mechanism (Figure 24). Apart from the two spurious points in the long period range, the data seem to point to a deeper event, on the order of 8 km depth. No interpretation beyond this was attempted for this event.

None of the fundamental mode data show patterns typical of Wetmiller's mechanism for the mainshock.

Both the theoretical and observational results discussed here show that the fundamental mode surface waves in the period range of 10 to

50 seconds can be used to infer differences in source mechanism for shallow (less than 10 km) crustal earthquakes. In particular, depth differences on the order of one kilometer appear to be distinguishable with high-quality fundamental mode data. This may be significant for improving depth determinations from regional network recordings where accurate epicenter location and focal mechanism determination typically can be made, but source depth is uncertain.

Other Evidence for Focal Depth

The usual problems inherent in using body wave observations to determine focal depth for shallow earthquakes were encountered here. Examination of the GDSN short period waveforms for these four events revealed few easily identified pP arrivals. Probably the clearest indication of a useful depth phase appears on the short period vertical signal for the mainshock as recorded at station GRFO (Germany) (see Figure 25a). Assuming Choy's mechanism as the preferred focal mechanism for this event, (Figure 26), the P arrival at GRFO ($\Delta = 47°$ in a northeasterly direction from the source, with take-off angle of 26.5°) plots well within the compressional quadrant, while pP falls near a node. Thus, the distinct arrival following the emergent P is identified as sP. Measurement of the P-sP delay time and assuming P and S velocities consistent with assumed source structure yield a depth for this event of 9 km. This is consistent with Choy et.al.'s (1983) analysis of the sP arrival at TOL (Spain), for which they also calculate a focal depth of 9 km for the mainshock. Two other stations, BOCO (Colombia) and ZOBO (Bolivia) ($\Delta = 45°$ and 65°, respectively, just west of due south of the

source) would be expected to show strong pP arrivals for the mainshock and all the aftershocks; while very clearly present in the waveform, a distinct onset of a pP could not be identified for the mainshock. The January 9 aftershock showed an excellent depth phase at BOCO (Figure 25b); this is identified as pP since the mechanism is generally the same as the mainshock. The measured P-pP delay time of 2.7 seconds translated to a depth of 7.5 km for this event. The signal recorded at ZOBO for the January 11 aftershock (Figure 25c) illustrated the more typical arrival observed for all the events; further phase identification and depth calculations were not attempted in this study. Choy et.al. (1983) inferred a pP arrival and a corresponding focal depth of 6 km for the January 11 aftershock from the ZOBO velocity record, assuming that the mechanism for the event was not significantly different from that of the mainshock. Depths determined from these teleseismic depth phases give focal depths, in most cases, at least 2 km deeper than those inferred from surface wave analysis and local aftershock observations. Only the aftershock on January 11 gives exact agreement on the result.

Additional depth information was provided by the near-source monitoring of aftershock activity as reported in Wetmiller et.al.(1983). Figure 27 provides a multi-dimensional view of epicentral and hypocentral locations of the aftershocks, revealing that this activity is restricted to depths less than 7.5 km. These data suggest shallower depths than those indicated by body wave analyses. However, since the monitoring system was not installed until January 10, much important information on the aftershock activity that immediately followed the mainshock and first large aftershock is missing. This evidence, nonetheless, indicates

that the mainshock rupture began at depth and propagated upward.

Summary of Results on Depth Determination

The depths for the mainshock and January 9 aftershock obtained in this study using fundamental mode surface waves appear to be somewhat shallower than depths inferred from body wave depth phases observed at teleseismic distances and are more consistent with the depths suggested by the locally monitored aftershock activity. Assuming that all three types of observations are reliable in determining depth, and recalling the shape of the curve of the Love-to-Rayleigh ratio for the mainshock data, the apparent inconsistencies might be accounted for by assuming the upward propagating fault rupture suggested by Choy et.al. (1983). The high frequency body wave first arrivals would reflect the point of initiation of the rupture while the longer period body and surface wave arrivals would reflect an average depth over which the fault moved. This is also consistent with the trend in Love-to-Rayleigh ratios to give greater depths at shorter periods observed in the band-pass ratios for the mainshock and January 11 aftershock. Furthermore, it logically follows that the aftershocks would be largely restricted to depths shallower than the initial rupture if it indeed propagated upward toward the surface. To test the idea of an upward propagating rupture for the mainshock, theoretical spectral amplitudes for different combinations of depths were summed separately for Love and Rayleigh contributions and the ratios calculated and plotted for comparison with the same data analyzed in Figure 19. Results of preliminary testing are presented in Figure 28. The trend for Love-to-Rayleigh ratios to peak at shorter periods for

shallower depth ranges is clear in Figure 28a; the higher ratio values associated with deeper events is illustrated in Figure 28b. After a number of attempts at fitting the data to a combination of various depth contributions, the best match resulted from summing the spectra for depths of 4, 5, and 8 km, as shown in Figure 29. With the initial rupture set at 8 km, Choy's body wave depth determination of 9 km is more acceptable in light of this surface wave evidence. Focal depth for the January 11 aftershock is consistently determined at 6 km by all three methods; while the evidence is scanty for the June 16 event, a depth on the order of 7 - 8 km is indicated by both surface wave and local aftershock results. Table 6 provides a concise summary of depths determined by the various methods.

Table 6

Summary of Depths Determined by Various Methods

Event	Body Wave Evidence	Aftershock Evidence	Surface Wave Evidence of Present Study
1/9/82 mainshock	9 km	7 km	7 $\pm$ 1.5 km
1/9/82 aftershock	7.5 km	7 km	3 - 5 $\pm$ 2 km
1/11/82 aftershock	6 km	6 - 7 km	6 $\pm$ 1 km
6/16/82	-	7 km	8 $\pm$ 2 km

Lg Arrivals and m_{bLg} Estimates

Since higher order modes were not resolvable in the data, comparison with theoretical spectra was unfounded. However, three-dimensional plots of peak amplitudes vs. frequency in the higher frequency range associated with Lg arrivals did indicate some consistency with values predicted theoretically. This evidence is discussed in greater detail in Appendix 6.

Some additional observations were made in the short period region of the spectra by considering the relative peak amplitudes of the original waveforms on the short and intermediate period vertical signals and the band-pass traces and relating these to the published magnitudes of the events. Table 7 is a compilation of the available magnitude data for these events.

Table 7

Month/Day/Event	m_b	m_{bLg}*	M_s*	m_{bLg}**	M_s***
1/9 mainshock	5.7	5.8	5.2	5.9	4.9
1/9 aftershock	5.1	5.3	3.9	5.2	3.6
1/11 aftershock	5.4	5.5	4.5	5.5	4.25
6/16 aftershock	4.7	4.6	-	4.3	-

* Reported in Wetmiller et.al. (1983). m_{bLg} values are from the Canadian Network; M_s are from NEIS

** As measured from the digital records at SCP. m_{bLg} for the clipped mainshock signal was calculated from a short period record simulated from the intermediate period record

*** As measured from the photographic records at SCP

Nuttli's formula (taken from von Seggern and Alexander, 1982) for determining Lg magnitude very specifically requires measurements of sustained, high amplitude, vertical component arrivals of one second period; these tend to be the highest amplitude arrivals on the short and intermediate period signals.

$$m_{bLg} = .30 + 1.66[\log(\Delta^{\circ})] + \log(A/T)$$

Since the distance, Δ , is the same for these events, the change in m_{bLg} between events is due entirely to amplitude differences of the one-second arrivals. Specifically,

$$\Delta\ m_{bLg} = (m_{bLg})_2 - (m_{bLg})_1$$

$$\Delta\ m_{bLg} = \log\ (A_2/T) - \log\ (A_1/T)$$

$$\Delta\ m_{bLg} = \log\ (A_2/A_1)$$

Table 8 shows m_b values predicted from a reference m_{bLg} (the January 11 aftershock in the case of short period data and the January 9 mainshock in the case of the intermediate period data). Evidently, the ensemble of higher mode, Lg arrivals, propagating along this path in the northeastern United States, effectively transmits this information on source strength. If Lg can be shown to be the reliable measure of magnitude that is suggested, the results in Table 9 indicate that the magnitude for the aftershock on June 16 should be revised downward to a value closer to 4.3.

It is also interesting to notice the trends in amplitude ratios obtained from the peak arrivals at each central frequency on the band-pass

Table 8

Short Period (All events compared to 1/11 aftershock because of clipping for the mainshock):

	Ratio of Peak Signal Amplitudes Z - Component	Associated Δm_{bLg} = log (Ratio)	Adjusted m_b by Δm_{bLg}	Reported m_b
1/11 to 1/9 aftershocks	1.9	.29	5.1	5.1
1/11 to 1/11	1.0	0.00	5.4	5.4
1/11 to 6/16 aftershocks	10.5	1.02	4.4	4.7

Intermediate Period (All events compared with 1/9 mainshock)

1/9 main to 1/9 aftershock	8.2	.9	4.8	5.1
1/9 main to 1/11 aftershock	1.9	.3	5.4	5.4
1/9 main to 6/16 aftershock	32.5	1.5	4.2	4.7

filters where all ratios are comparisons with the associated mainshock peak (see Table 9). The expected differences due to variations in excitation at the source caused by the different source mechanisms are apparent, but it is also of interest to note the frequencies at which the ratios are consistent with the differences in the magnitudes of the events. Except for the January 11 aftershock, that information is clearly present in the frequencies around 1 Hz.

In spite of the noted differences, which can no doubt be attributed

Central Frequency (Hz)	Central Period (Sec)	1/9 Main to 1/9 After Ratio		1/9 Main to 1/11 After Ratio		1/9 Main to 6/16 After Ratio	
		IPZ	SPZ	IPZ	SPZ	IPZ	SPZ
Peak Signal Ratio		8.2		1.9		32.5	
.12	8.3	23.6		6.2			
.15	6.7	8.8		2.7			
.20	5.0	11.2	10.6	3.3	2.7		44.3
.25	4.0	19.5		2.8			
.30	3.3	10.2	10.1	2.0	2.0		68.1
.40	2.5	7.0	6.9	1.8	2.3		30.6
.50	2.0	6.8	5.0	2.1	1.6		15.8
.60	1.7	13.8	11.1	2.8	2.4		43.8
.70	1.4	14.3	12.5	6.8	5.7		71.4
.80	1.25	5.8	5.0	3.2	2.8		33.1
.90	1.1	2.8		1.2			
1.00	1.0	4.7	4.2	1.2	1.1		16.5
1.50	.7	2.1	2.2	.6	.6		10.0
2.00	.5	1.7	1.8	1.1	1.1		17.8
2.50	.4	3.9	3.2	1.2	.9		17.4
3.0	.33		5.2		2.5		31.4
3.5	.28		11.9		1.9		32.0
4.0	.25		14.6		2.1		40.4
4.5	.22		33.0		3.8		52.0
5.0	.20		26.7		5.3		40.0
5.5	.18		57.4		2.0		19.1
6.0	.17		74.0		1.8		92.5
6.5	.15		76.0		4.2		57.0
7.0	.14		46.8		4.4		70.2
7.5	.13		59.0		2.1		70.8
8.0	.125		50.6		1.9		50.6
8.5	.118		33.5		2.9		22.3
expected ratio, consistent with relative m_b		4.0		2.0		10.0	

Table 9

to variations in modal excitation at the source, visual inspection of the higher mode contributions to the theoretical Rayleigh amplitude spectra (Figures A5-1b through 20b) show a consistent maximum level of excitation for the modes, taken together, regardless of depth in the "granitic layer" for the different mechanisms. This conforms to the expectation that, for a given mechanism, the same fraction of the total source energy remains trapped as surface wave energy in the same constant velocity layer. Therefore, magnitudes determined by peak amplitudes of the recorded signal, representing the ensemble of Lg modes, should give accurate measures of the strength of the source for shallow earthquakes. m_{bLg} estimates from network averages and from the single-station SCP agree closely with one another and with teleseismic magnitude estimates.

CHAPTER 6

CONCLUSIONS AND DIRECTIONS FOR FURTHER STUDY

Single-station surface wave data from the 1982 New Brunswick sequence of earthquakes were used to help determine the preferred focal mechanisms including focal depths for the four events studied. By applying band-pass filters over the complete frequency range provided by the DWWSSN short, intermediate, and long period digital data recorded at SCP, group velocities and amplitudes were empirically determined for fundamental and higher mode arrivals. Theoretical Rayleigh and Love dispersion curves were generated for an assumed path structure which adequately fit the observed data. Synthetic Love and Rayleigh amplitude spectra and spectral ratios were calculated for various source mechanisms proposed by other investigators and compared to the data derived from the band-pass filters. Evaluation of source mechanism and depth determination were based on fundamental mode data of periods 10 seconds and greater and supported by qualitative behavior of the higher mode excitation.

Fundamental mode Love and Rayleigh ratios corroborated Choy et.al.'s (1983) choice of source parameters for the mainshock: fault plane striking at 195°, dip of 65° to the northwest, and a rake of 70°. The preferred average depth was found to be 7 km as opposed to the 9 km value calculated on the basis of depth phases observed at teleseismic distances. The surface wave results for this event can also be interpreted as indicative of rupture which propagates updip. For the January 9 aftershock, a mechanism similar to that of the mainshock is supported and a shallower

depth is indicated by the shift in the peak Love-to-Rayleigh ratio to shorter periods. The January 11 aftershock is well described by Wetmiller et.al.'s (1983) mechanism which indicates thrusting on a plane conjugate to the fault plane of the mainshock, with strike of 332°, dip 48° to the southeast, and a rake of 59°. Surface wave Love-to-Rayleigh ratios and body wave depth phase identification both support a 6 km depth for this event. Although subject to uncertainty because of significant long period noise and delayed triggering of the intermediate period recording system, analysis of the June 16 event reveals similarities in mechanism to the January 11 aftershock, with surface wave evidence supporting a deeper focus, on the order of 8 km depth. The chosen mechanism for the mainshock and the first aftershock is not entirely consistent with the prevailing ENE maximum compressive stress characteristic of most areas in eastern North America, although the inferred mechanisms for the January 11 and June 16 events are.

Conclusive identification of individual higher order Love and Rayleigh modes in the short period range that encompass the Lg arrivals was not possible. However, it was apparent from comparisons of the theoretical spectra and three-dimensional views of the band-pass results that differences in source excitation were well preserved for these waves even after traveling the 1130 km path to SCP. This is further support of the observation that crustal structure in the eastern United States provides a more uniform wave guide for Lg propagation than it does in the western United States (von Seggern and Alexander, 1982), where source information (other than magnitude) is unrecognizable after only a few hundreds of kilometers of propagation from the source. Furthermore, m_{bLg} calculations based on the ensemble

of Lg modes constituting the highest amplitude arrivals on the short period and intermediate period records proved remarkably consistent with m_b as a measure of source strength. This proved to be the case even though the amount of excitation of individual modes varied from frequency to frequency.

Constraint of source parameters with surface wave observations can be optimized by using data from many stations with good azimuthal coverage of the event. Turnbull (1976) was able to demonstrate that only six stations were needed to fit observed Love and Rayleigh amplitude spectra via an iterative, least-squares regression to well-constrained values of dip, slip, strike of the fault plane, and moment. The present study has shown that, in the case where good body wave evidence gives a reasonably accurate starting mechanism and where path and source structure can also be assumed with confidence, surface wave analysis at a single station can provide accurate estimates of focal depth and further constraints on mechanism, particularly in the case of shallow earthquakes. Resolution of the individual higher modes is still highly desirable, not only for constraining the source mechanism, but also for inverting for path structure, one of the more interesting possible extensions of this study. How this can best be accomplished is not immediately apparent; however, the theoretical dispersion curves in Appendix 3 suggest that one possible approach is to band-pass filter windows of the original time signal that are limited by the cut-off frequencies of successive modes. The short period records for the mainshock and the January 11 aftershock show clear evidence for the presence of a dispersing higher order mode, almost certainly the first higher mode. Although this method will encounter difficulties in the frequency ranges where

the different dispersion curves overlap, with many modes arriving at the same time, successful identification of just one higher order mode would be useful for both source and structure studies.

REFERENCES

Adams, J., and R.J. Wetmiller, Conjugate thrust faulting during the Miramichi, New Brunswick, earthquake sequence of 1982: Its geometry, geological control, surface expression, and mechanism, Earthquake Notes, 54, 84, 1983.

Aki, K. and P. Richards, Quantitative seismology theory and methods, W.H. Freeman, San Francisco, Calif., 1980.

Alexander, S.S., Surface wave propagation in the western United States, Ph.D. thesis, California Institute of Technology, Pasadena, 1963.

Basham, P.W., D.H. Weichert, F.M. Anglin and M.J. Berry, New probabilistic strong seismic ground motion maps of Canada: A compilation of earthquake source zones, methods and results, Earth Physics Branch Open File Report, 82-84, 1982.

Ben-Menahem, A. and D.G. Harkrider, Radiation patterns of seismic surface waves from buried dipolar point sources in a flat stratified earth, JGR, 69, 2605-2620, 1964.

Bhattacharya, S.N., Higher order accuracy in multiple filter technique, BSSA, 73, 1395-1406, 1983.

Brune, J. and J. Dorman, Seismic waves and earth structure in the Canadian Shield, BSSA, 53, 167-210, 1963.

Burke, K.B.S., J.J. Chandra, and L. Fyffe, Geological and gravity investigations in the epicentral region of the 1982 Miramichi earthquakes, New Brunswick, Canada, Earthquake Notes, 53, 15, 1982.

Canitez, N. and M.N. Toksöz, Focal mechanism and source depth of earthquakes from body and surface wave data, BSSA, 61, 1369-1379, 1971.

Cheng, C.C. and B.J. Mitchell, Crustal Q structure in the United States from multi-mode surface waves, BSSA, 71, 161-181, 1977.

Choy, G.L., J. Boatwright, J.W. Dewey, and S.A. Sipkin, A teleseismic analysis of the New Brunswick earthquake of January 9, 1982, JGR, 88, 2199-2212, 1983.

Cybriwsky, Z., Spectral excitation of Lg within the south-central Appalachian region, M.S. thesis, the Pennsylvania State University, University Park, 1979.

Harkrider, D.G., Surface waves in multilayered elastic media, Part II: Higher mode spectra and spectral ratios from point sources in plane layered earth models, BSSA, 60, 1937-1987, 1970.

Hasegawa, H.S., Surface wave analysis of the magnitude 5.7 Miramichi, New Brunswick, earthquake of 09 January, 1982, Earthquake Notes, 84, 1983.

Haskell, N.A., Dispersion of surface waves on multilayered media, BSSA, 43, 17-34, 1953.

Haskell, N.A., Radiation pattern of Rayleigh waves from a fault of arbitrary dip and direction of motion in a homogeneous medium, BSSA, 53, 619-642, 1963.

Herrmann, R.B., Some aspects of band-pass filtering of surface waves, BSSA, 63, 663-671, 1973.

Herrmann, R.B., Surface wave focal mechanisms for eastern North American earthquakes with tectonic implications, JGR, 84, 3543-3552, 1979.

King, Philip B., The Evolution of North America, Princeton University Press, Princeton, New Jersey, 1977.

Knopoff, L., F. Schwab, and E. Kausel, Interpretation of Lg, Geophys. J., 33, 389-404, 1973.

Massé, R.P., D.G. Lambert, and D.G. Harkrider, Precision of the determination of focal depth from the spectral ratio of Love/Rayleigh surface waves, BSSA, 63, 59-100, 1973.

Mitchell, B.J., and R.B. Herrmann, Shear velocity structure in the eastern United States from the inversion of surface-wave group and phase velocities, BSSA, 69, 1133-1148, 1979.

Nabelek, J., G. Suarez, and M.N. Toksöz, Source parameters of the New Brunswick earthquake of January 9, 1982, from inversion of teleseismic body and surface waves, Earthquake Notes, 53, 28, 1982.

Dainty, A.M., C.E. Keen, M.J. Keen, and J.E. Blanchard, Review of geophysical evidence on crust and upper-mantle structure on the eastern seaboard of Canada, in The Earth Beneath the Continents, J.S. Steinhart, T.J. Smith, eds., AGU Geophysical Monograph 10, Washington, D.C., 349-369, 1966.

Diment, W.H., C.W. Stover and M.F. Kane, The central New Brunswick earthquake sequence of 1982: History, distribution of intensity and tectonic environment, Earthquake Notes, 53, 17, 1982.

Diment, W.H., T.C. Urban, and F.A. Revetta, Some geophysical anomalies of the eastern United States, in The Nature of the Solid Earth, ed., E. Robutson, McGraw-Hill, New York, 544-574, 1972.

Dorman, J., and M. Ewing, Numerical inversion of seismic surface wave dispersion data and crust-mantle structure in the New York-Pennsylvania area, JGR, 67, 5227-5241, 1962.

Dwyer, J.J., Robert B. Herrmann, and Otto W. Nuttli, Spatial attenuation of the Lg wave in the central United States, BSSA, 73, 781-796, 1983.

Dziewonski, A.M., S. Bloch, and M. Landisman, A technique for analysis of transient seismic signals, BSSA, 59, 427-444, 1969.

Dziewonski, A.M., and A.L. Hales, Numerical analysis of dispersed seismic waves in Methods in Computational Physics, Vol. 11, Academic Press, New York, 1972.

Ebel, J.E. and Vudler, Foreshocks and aftershocks of the New Brunswick earthquake of January 9, 1982, Earthquake Notes, 53, 16, 1982.

Fletcher, J.B., M.L. Sbar, and L.R. Sykes, Seismic trends and travel-time residuals in eastern North America and their tectonic implications, Geol. Soc. of Am. Bull., 89, 1656-1676, 1978.

Ganse, R. and C.R. Hutt, Directory of World Digital Seismic Stations, Report SE-32, World Data Center A for Solid Earth Geophysics, U.S. Dept. of Commerce, Boulder, Colorado, 1982.

Harkrider, D.G., and D.L. Anderson, Computation of surface-wave dispersion for multilayered earth models, JGR, 71, 2967-2980, 1962.

Harkrider, D.G., Surface waves in multilayered elastic media, I: Rayleigh and Love waves from buried sources in a multilayered elastic half-space, BSSA, 54, 627-679, 1964.

Press, F., D. Harkrider, and C.A. Seafeldt, A fast, convenient program for computation of surface-wave dispersion curves in multilayered media, BSSA, 51, 495-502, 1961.

Rast, N. and P. Stringer, Recent advances and the interpretation of geological structure of New Brunswick, Geoscience, Canada, 1, 15-25, 1974.

Schwab, F. and L. Knopoff, Fast surface wave and free mode computations in Methods in Computational Physics, Vol. 11, Academic Press, New York, 87-180, 1972.

Schwab, F. and L. Knopoff, Surface wave dispersion computations, BSSA, 60, 321-344, 1970.

Takeuchi, H. and M. Saito, Seismic surface waves, in Methods in Computational Physics, Vol. 11, Academic Press, New York, 217-295, 1972.

Taylor, S.R. and M.N. Toksöz, Crust and upper mantle velocity structure in the Appalachian orogenic belt: Implications for tectonic evolution, Geol. Soc. of Amer. Bull., 93, 315-329, 1982a.

Taylor, S.R., and M.N. Toksöz, Structure in the northeastern United States from inversion of Rayleigh wave phase and group velocities, Earthquake Notes, 53, 1982b.

Taylor, S.R., and M.N. Toksöz, Three-dimensional crust and upper mantle structure of the north-eastern United States, JGR, 84, 7627-7644, 1979.

Thrower, E.N., The computation of dispersion curves on layered media, J. Sound Vib., 14-30, 1965.

Tsai, Y.B., and K. Aki, Precise focal depth determination from amplitude spectra of surface waves, JGR, 75, 5729-5743, 1970a.

Tsai, Y.B., and K. Aki, Source mechanism of the Truckee, California, earthquake of September 12, 1966, BSSA, 60, 1199-1208, 1970b.

Turnbull, L.S., Jr., Determination of seismic source parameters using far-field surface wave spectra, Ph.D., thesis, the Pennsylvania State University, University Park, 1976.

von Seggern, D. and S.S. Alexander, Investigation of source, path, and receiver effects for Lg waves from Nevada test site explosions and eastern North America earthquakes.

Wang, C.Y., Wave theory for seismogram synthesis, Ph.D. thesis, Saint Louis University, Saint Louis, 1981.

Watson, T.H., A note on fast computation of Rayleigh wave dispersion in the multilayered elastic half-space, BSSA, 60, 161-166, 1970.

Wetmiller, R.J., J. Adams, F.M. Anglin, H.S. Hasegawa, A.E. Stevens, Aftershock sequences of the 1982 Miramichi, New Brunswick, earthquakes, preprint, 1983.

Wetmiller, R.J., J. Adams, A.E. Stevens, F.M. Anglin, H.S. Hasegawa, and J. Berube, Aftershock sequences for the New Brunswick earthquakes of January 9 and 11, March 31 and June 16, 1982, Earthquake Notes, 53, 41, 1982.

Williams, H., Geology of the Canadian Appalachians, Perspectives in Regional Geological Synthesis, GSA, D-NAG publication 1, 57-66, 1982.

Williams, H., Appalachian orogen in Canada, Canadian Journal of Earth Sciences, 16, 792-807, 1979.

Yang, J.P., and Y.P. Aggarwal, Seismotectonics of northeastern United States and adjacent Canada, JGR, 86, 4981-4998, 1981.

FIGURE CAPTIONS

Figure 1 (a) Earthquake locations in northeast United States and conterminous Canada, 1534-1959. Epicentral region and SCP location are indicated with stars (from Yang and Aggarwal, 1981; after Smith, 1962, 1966).

1 (b) Epicenters of earthquakes with $m_b \geq 2$ in northeast United States and adjacent Canada as recorded by the Northeastern Seismic Network for the period 1970-1979 (after Yang and Aggarwal, 1981).

Figure 2 Seismicity of the New Brunswick study area prior to the 1982 sequence. No particular trend to the activity is indicated, although two events with magnitude > 3 did occur within the period 1970-1981. Uncertainty in epicenter location is not less than 10 km. Note the starred locations of the January and March, 1982, sequence as well as the separate June 16, 1982, event (after Wetmiller et. al., 1983).

Figure 3 Geology of the New Brunswick study area. Note that all the events of the earthquake sequence occur within a granitic intrusion of the Miramichi Anticlinorium which has not yet revealed any evidence of previous deformation. Existing, mapped faults were apparently not involved in the 1982 earthquake activity (after Wetmiller et.al., 1983).

Figure 4 Aftershock activity of the epicentral region superimposed on local geology. Although not shown on the map, the epicenter of the June 16 event is located within this same granitic pluton (after Wetmiller et.al., 1983).

Figure 5 Effect of bandwidth on peak amplitude and arrival time. The differences in group velocity determinations due to the factor of ten bandwidth difference amount to only .1 km/sec. The effects on peak amplitudes are substantial; however, working with spectral ratios will cancel these amplitude effects.

Figure 6 Observed signal and suite of band-pass filters for central frequencies ranging from 5 Hz to 8.5 Hz applied to the short period data for the January 11 aftershock.

Figure 7 Observed signal and suite of band-pass filters for central frequencies ranging from 5 Hz to 8.5 Hz applied to the short period data for the June 16 event.

Figure 8 Observed signal and suite of filters for central frequencies ranging from .05 Hz to .25 Hz applied to the intermediate period, vertical component data for the January 9 mainshock.

Figure 9 Great circle paths and stations used to determine two of the velocity models selected as possible path and source structure. Path A1 extends from OGD through WES to STJ (Ogdensburg, N.J.; Weston, Mass.; St. Johns, Newfoundland). Path G represents structure between OGD and MNT (Montreal) and OGD and OTT (Ottawa) and is the model selected to represent path and source structure in this study. Approximate epicenter and station locations are indicated (after Taylor and Toksöz, 1982b).

Figure 10 Fundamental mode Love (a) and Rayleigh (b) group velocity dispersion curves for the three structure models tested. plotted with data points representing group velociities associated with each peak on the band-pass filters. Of the three, Path G dispersion fits the data points best. On this and all subsequent dispersion plots, the symbols used to represent the peaks were assigned by amplitude. The amplitudes of each enveloped peak were normalized to the peak amplitude for that band-pass and then assigned a symbol according to the following scheme:

10 - the point having the peak amplitude for the given central frequency

9 - those point(s) representing peaks along the filtered signal with amplitude(s) 80-99% of maximum for that trace

8 - those point(s) representing peaks along the filtered signal with amplitude(s) 60-79% of maximum for that trace

7 - those point(s) representing peaks along the filtered signal with amplitudes less than 59% of maximum for that trace.

Figure 11 Fundamental mode Love (a) and Rayleigh (b) group velocity dispersion curves for Path G and modified Path G structures, plotted with data points representing group velocities associated with each peak on the band-pass filters. Modifying the Path G model was accomplished by changing the 3.8 km/sec shear velocity layers to 3.5 km/sec in order to effectively thicken the granitic layer and sharpen the velocity contrast at its base. The expected effects on the theoretical dispersion are evident; however, the original Path G structure provides a better overall fit to the data, so it was retained for the duration of the study.

Figure 12 Theoretical dispersion predicted by the Path G velocity model for fundamental and first four higher mode Love waves for the period range .2 - 80 sec. The theoretical curves are superimposed on the transverse component, band-pass amplitude results for the January 9, 1982, mainshock. Fundamental mode is the solid line; successively higher order modes are dashed lines of decreasing dash-length.

Figure 13 Theoretical dispersion predicted by the Path G velocity model for fundamental and first four higher mode Rayleigh waves for the period range .2 - 100 sec. The theoretical curves are superimposed on the vertical component, band-pass amplitude results for the January 9, 1982, mainshock. Fundamental mode is the solid line; successively higher order modes are dashed lines of decreasing dash-length.

Figure 14 Conjugate fault planes proposed for the New Brunswick earthquakes (from Wetmiller et.al., 1983).

Figure 15 Fundamental mode synthetic Love-to-Rayleigh spectral amplitude ratios for depths ranging from 1 - 10 km for the Choy mechanism: $\theta = 195°$, $\delta = 65°$, $\lambda = 70°$. The legend for depth is given in kilometers.

Figure 16 Fundamental mode synthetic Love-to-Rayleigh spectral amplitude ratios for depths ranging from 1 - 10 km for the Nabelek mechanism: $\theta = 3°(183°)$, $\delta = 34°$, $\lambda = 95°$. The legend for depth is given in kilometers.

Figure 17 Fundamental mode synthetic Love-to-Rayleigh spectral amplitude ratios for depths ranging from 1 - 10 km for the Wetmiller et.al. mechanism as proposed for the January 9, 1982, mainshock: $\theta = 195°$, $\delta = 50°$, $\lambda = 120°$. The legend for depth is given in kilometers.

Figure 18 Fundamental mode synthetic Love-to-Rayleigh spectral amplitude ratios for depths ranging from 1 - 10 km for the Wetmiller et.al. mechanism as proposed for the January 11, 1982, aftershock: $\theta = 332°$, $\delta = 48°$, $\lambda = 59°$. The legend for depth is given in kilometers.

Figure 19 Observed ratios, calculated from the band-pass results for the January 9, 1982 mainshock, superimposed on the theoretical fundamental mode Love-to-Rayleigh curves (by depth) for the Choy et.al.(1983) mechanism. A depth range of 4 - 8 km is indicated by these points. In this and all subsequent figures, stars indicate ratios obtained by selecting fundamental mode arrivals from the dispersion curves, finding their asso-

amplitudes on the transverse and vertical components and calculating their ratios. For band-passes with central frequencies in the plotted period range, the arrival corresponding to the peak amplitude is assured to be the fundamental mode, so peak amplitude ratios were calculated for each transverse-to-vertical pair available. This did not contribute much new information for the mainshock, but helped provide additional data points for the aftershocks, where even fundamental mode identification was difficult.

Figure 20 — Observed ratios, calculated from the band-pass results for the January 11, 1982, aftershock, superimposed on the theoretical Love-to-Rayleigh curves (by depth) for the Wetmiller et.al. (1983) January 11 mechanism. Although constrained by a single value near the peak, the data points are consistent with the theoretical curve for the 6 km depth.

Figure 21 — Observed ratios, calculated from the band-pass results for the January 9, 1982, aftershock, superimposed on the theoretical Love-to-Rayleigh curves (by depth) for the Choy et.al. (1983) mechanism. Although not really consistent with the theoretical curves for this model, the trend to peak at shorter period, corresponding to shallower depth than the mainshock, is evident.

Figure 22 — Comparison of synthetic Love-to-Rayleigh spectral amplitude ratios for modified Choy mechanisms for depths ranging from 4 - 9 km. In all cases, $\theta = 195°$; (a) $\delta = 55°$, $\lambda = 70°$; (b) $\delta = 55°$, $\lambda = 90°$; (c) $\delta = 55°$, $\lambda = 110°$; (d) $\delta = 65°$, $\lambda = 70°$; (e) $\delta = 65°$, $\lambda = 90°$; (f) $\delta = 65°$, $\lambda = 110°$.

Figure 23 — Band-pass results for the January 9, 1982, aftershock superimposed on the synthetic Love-to-Rayleigh ratios (by depth) for the modified Choy mechanism ($\theta = 195°$, $\delta = 55°$, $\lambda = 90°$) for depths from 4 to 9 km. Although the data are scattered and fall beyond the depth ranges covered by the theoretical curves, a depth less than 4 km is indicated.

Figure 24 — Band-pass results for the June 16, 1982, aftershock superimposed on the synthetic Love-to-Rayleigh ratios (by depth) for the Wetmiller et.al.(1983) January 11, 1982, mechanism. The values suggest a range of possible focal depths of 7 - 9 km.

Figure 25 — GDSN first-motion data for the January 9, 1982, New Brunswick mainshock, recorded at GRFO; for the January 9, 1982, aftershock, recorded at BOCO; and for the January 11, 1982, aftershock recorded at ZOBO.

Figure 26 — Choy et.al. (1983) preferred focal mechanism (solid line), $\theta = 195°$, $\delta = 65°$, $\lambda = 70°$. Triangles are takeoff angles of P and pP; squares are sP takeoff angles. All takeoff angles are plotted on a lower hemisphere plot (after Choy et.al., 1983).

Figure 27 — Composite distribution of January and April aftershocks from the local surveys (after Wetmiller et.al., 1983)

Figure 28 — Love-to-Rayleigh spectral amplitude ratios plotted for a variety of depth ranges, compared with data for the January 9 mainshock. Spectral contributions for different depth ranges are calculated for Love and Rayleigh amplitudes and ratios plotted.

(a) Depth ranges include: 2, 3, 4 km; 5, 6, 7, km; 8, 9, 10 km.

(b) Depth range shown: 7, 8 km.

Figure 29 — Best-fitting Love-to-Rayleigh spectral amplitude ratios for the January 9 mainshock. Spectral contributions for 4, 5, and 8 km depths are calculated for Love and Rayleigh amplitudes and ratios plotted.

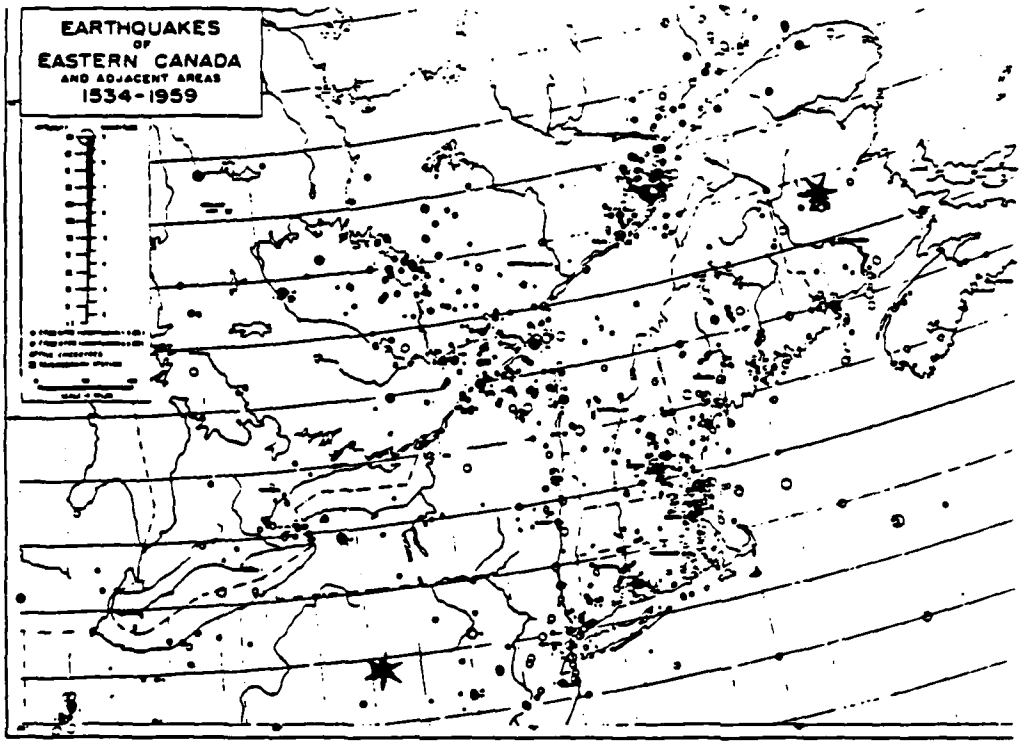

Figure 1(a)

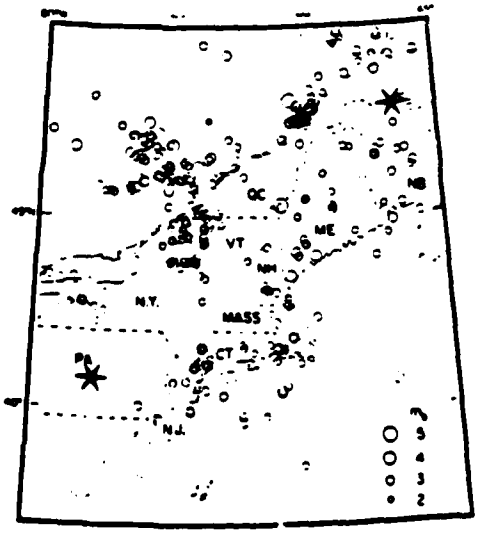

Figure 1(b)

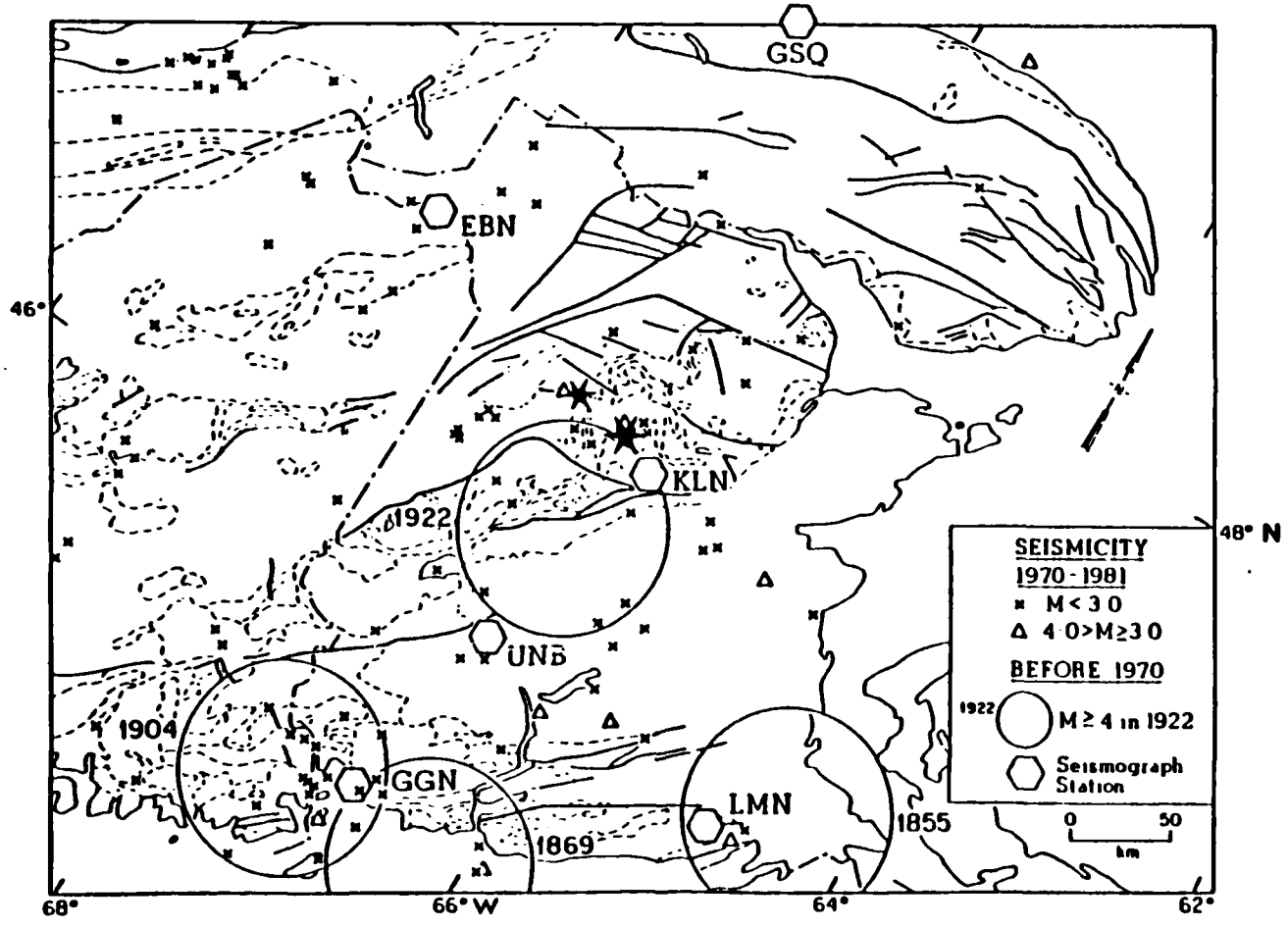
GSQ
EBN
KLN
UNB
GGN
LMN
1922
1904
1869
1855
46°
48° N
68°
66° W
64°
62°
SEISMICITY
1970-1981
M < 3.0
4.0 > M ≥ 3.0
BEFORE 1970
1922 M ≥ 4 in 1922
Seismograph Station
0 50
km

Figure 2

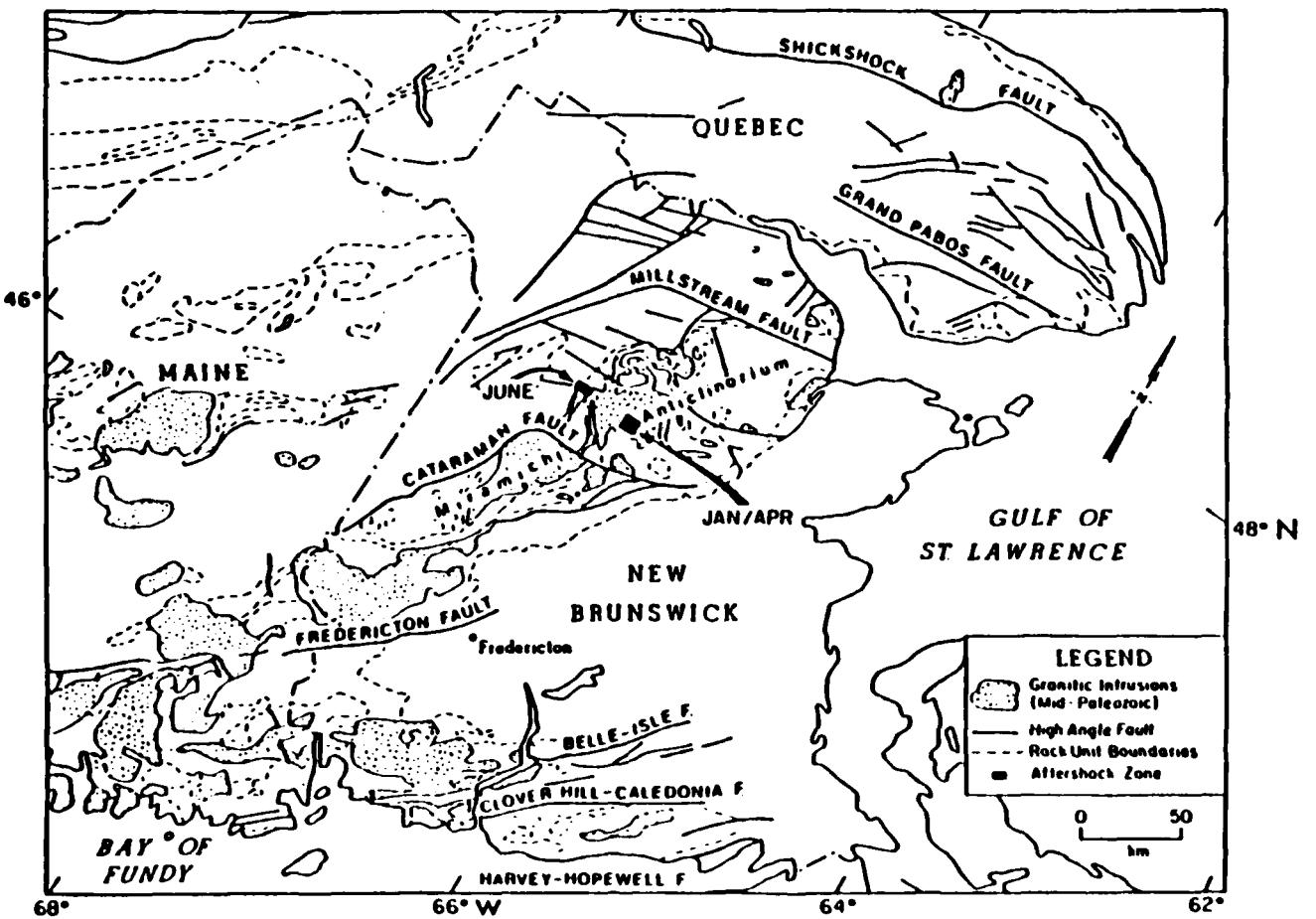
SHICKSHOCK FAULT
QUEBEC
GRAND PABOS FAULT
MILLSTREAM FAULT
46°
MAINE
JUNE
Ammelinopsis
CATARAMAN FAULT
Miramichi
JAN/APR
GULF OF
ST LAWRENCE
48° N
NEW
BRUNSWICK
FREDERICTON FAULT
Fredericton
LEGEND
Granitic Intrusions (Mid - Paleozoic)
High Angle Fault
Rock Unit Boundaries
Aftershock Zone
0
50
km
BELLE-ISLE F.
CLOVER HILL-CALEDONIA F
BAY OF
FUNDY
HARVEY-HOPEWELL F
68°
66° W
64°
62°

Figure 3

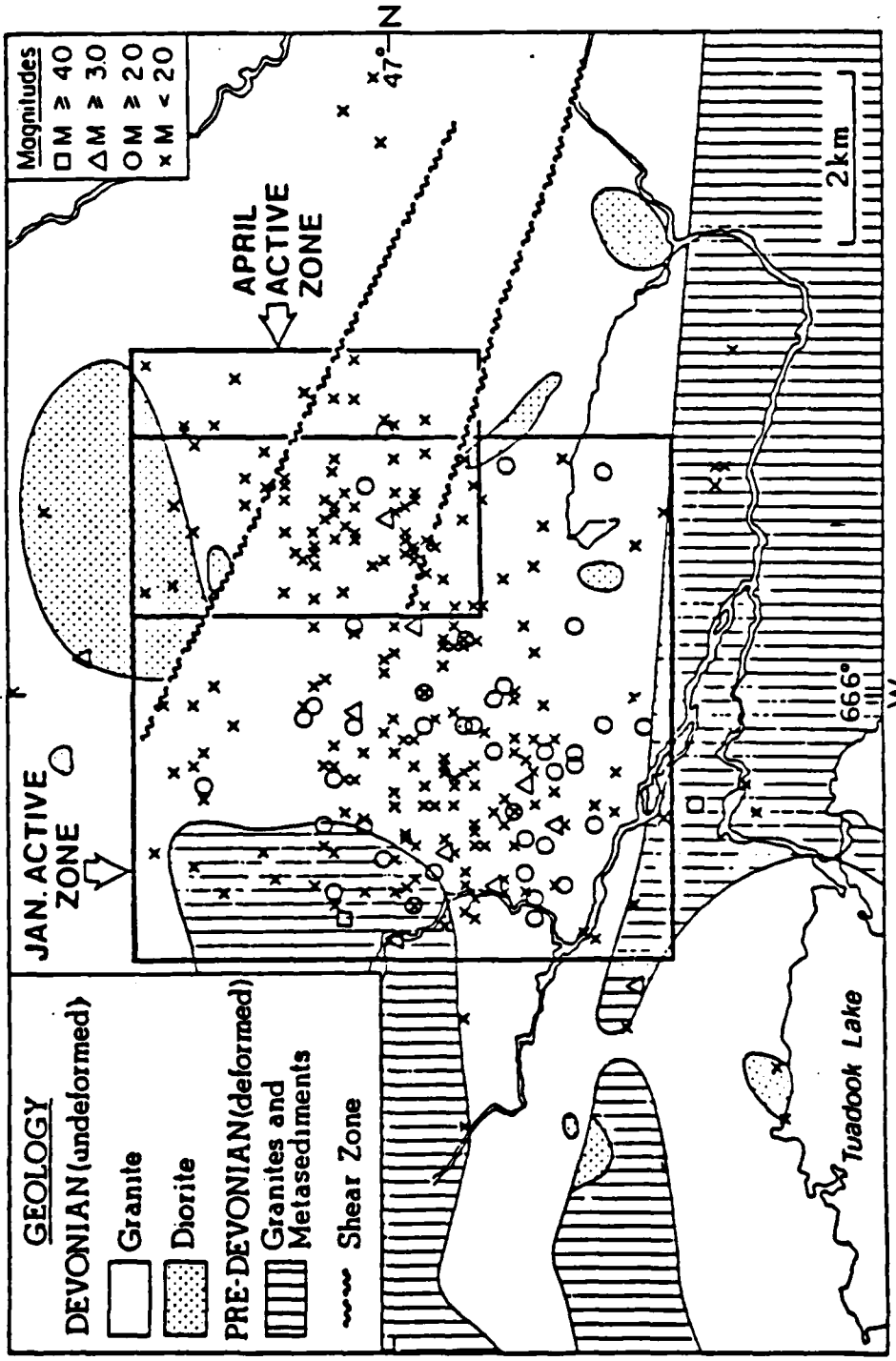
Magnitudes
□ M ≥ 4.0
△ M ≥ 3.0
○ M ≥ 2.0
× M < 2.0
APRIL ACTIVE ZONE
JAN. ACTIVE ZONE
47°
N
666°
W
2km
GEOLOGY
DEVONIAN (undeformed)
Granite
Diorite
PRE-DEVONIAN (deformed)
Granites and Metasediments
Shear Zone
Tuadook Lake

Figure 4

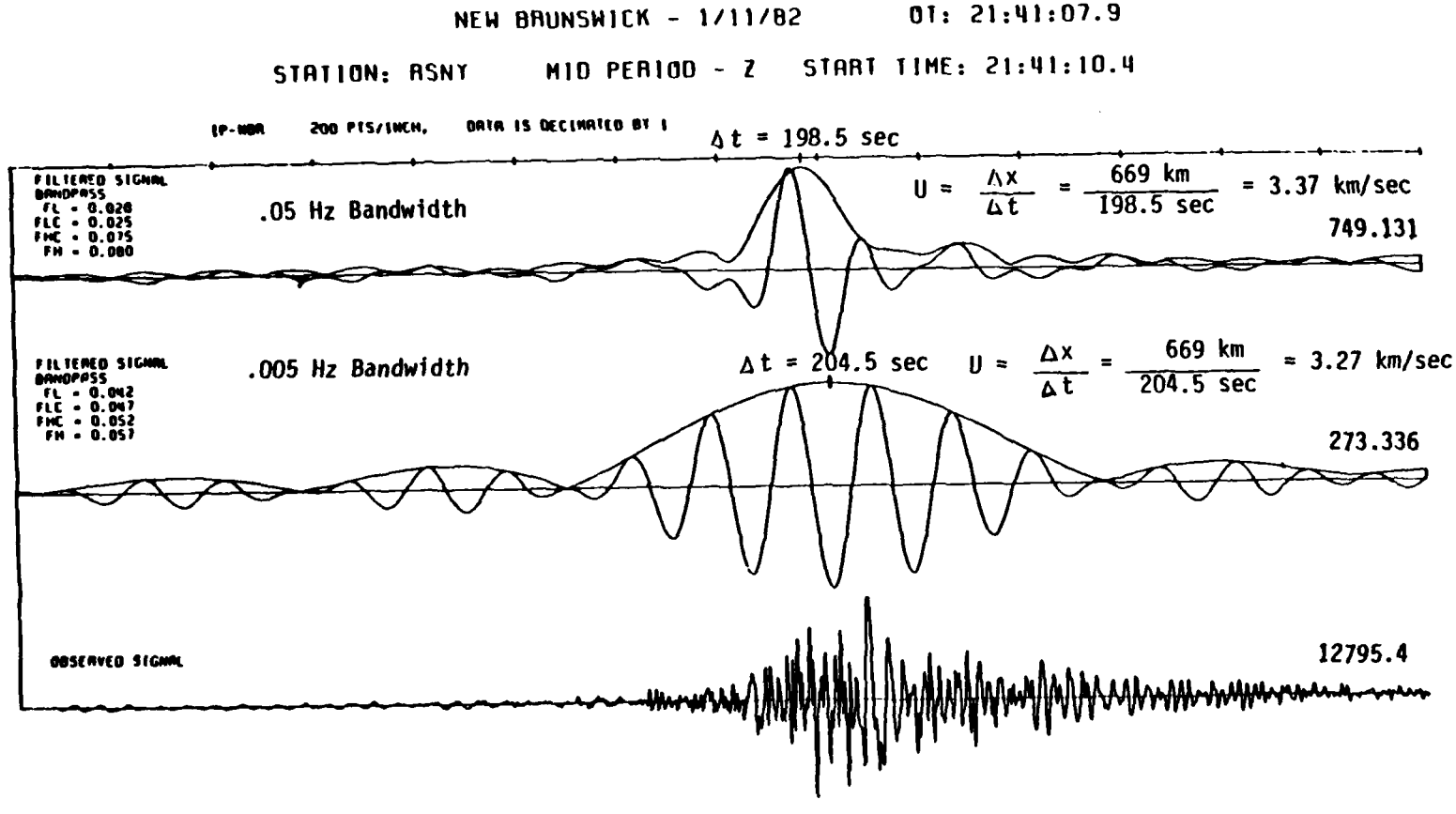
NEW BRUNSWICK - 1/11/82 OT: 21:41:07.9
STATION: RSNY MID PERIOD - Z START TIME: 21:41:10.4
LP-NOR 200 PTS/INCH. DATA IS DECIMATED BY 1
Δt = 198.5 sec
FILTERED SIGNAL BANDPASS FL = 0.028 FLC = 0.025 FHC = 0.075 FH = 0.080
.05 Hz Bandwidth
U = Δx/Δt = 669 km / 198.5 sec = 3.37 km/sec
749.131
FILTERED SIGNAL BANDPASS FL = 0.042 FLC = 0.047 FHC = 0.052 FH = 0.057
.005 Hz Bandwidth
Δt = 204.5 sec U = Δx/Δt = 669 km / 204.5 sec = 3.27 km/sec
273.336
OBSERVED SIGNAL
12795.4

Figure 5

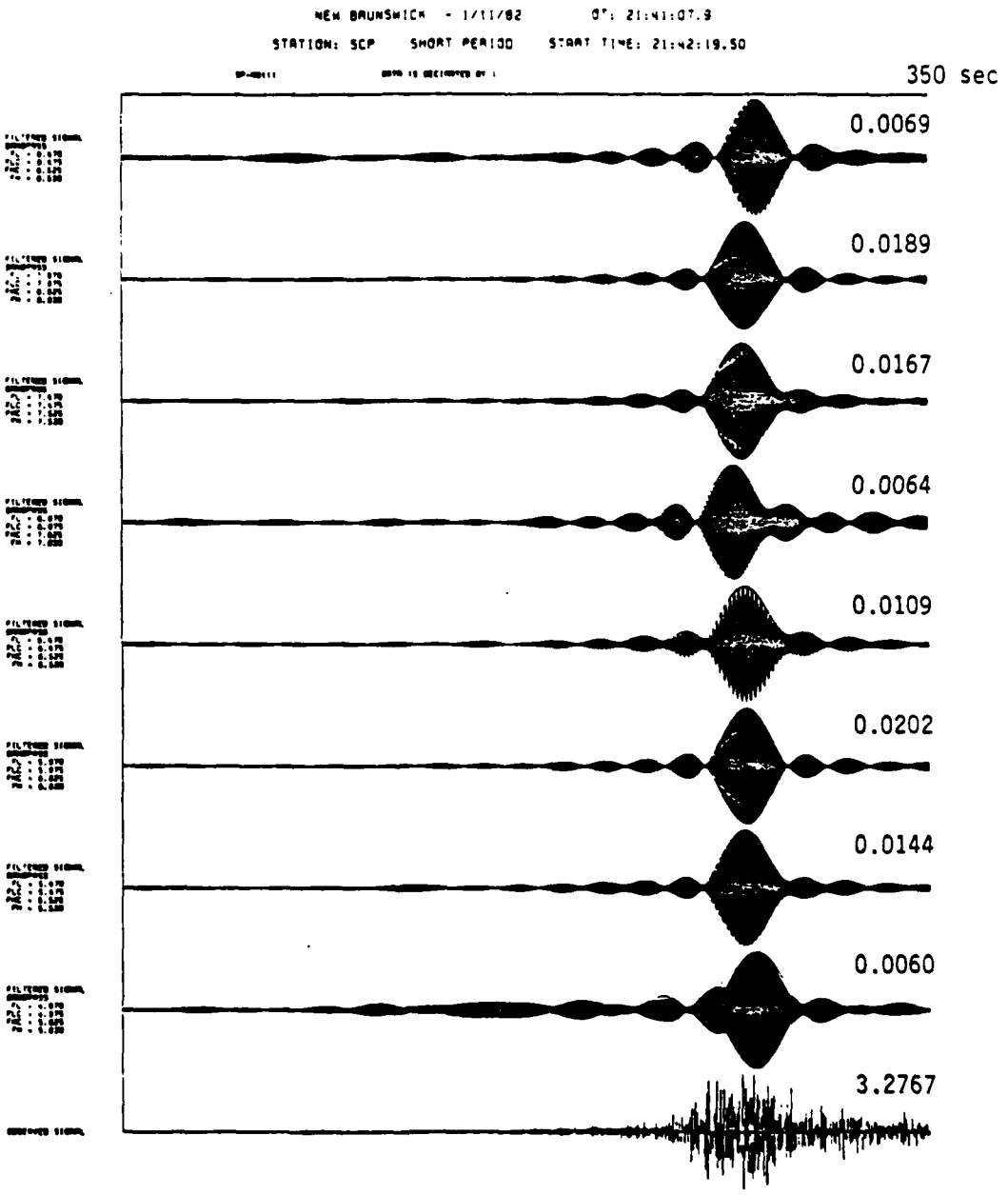
NEW BRUNSWICK - 1/11/82 0': 21:41:07.9
STATION: SCP SHORT PERIOD START TIME: 21:42:19.50
350 sec
0.0069
0.0189
0.0167
0.0064
0.0109
0.0202
0.0144
0.0060
3.2767

Figure 6

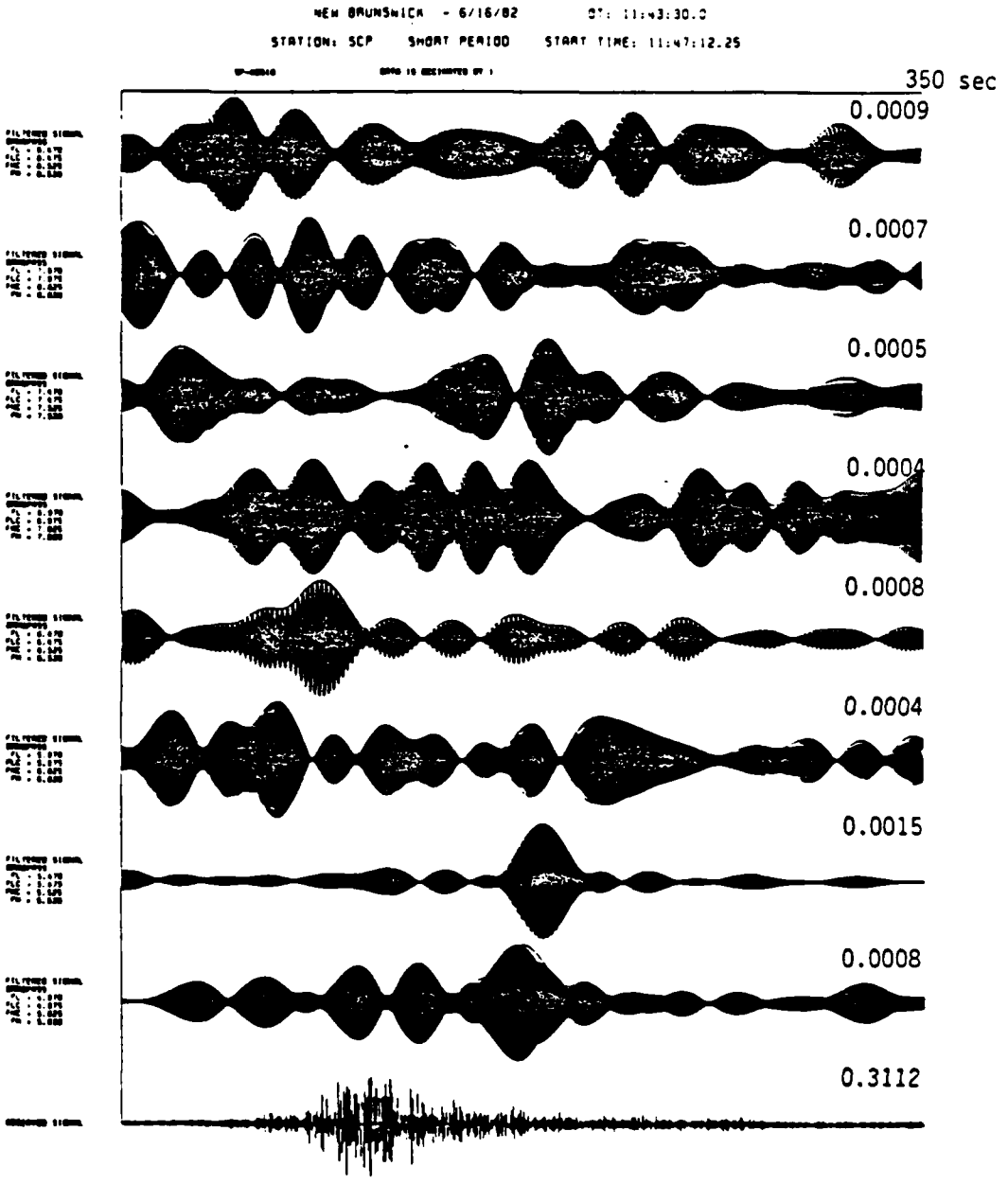
NEW BRUNSWICK - 6/16/82
STATION: SCP SHORT PERIOD START TIME: 11:47:12.25
350 sec
0.0009
0.0007
0.0005
0.0004
0.0008
0.0004
0.0015
0.0008
0.3112

Figure 7

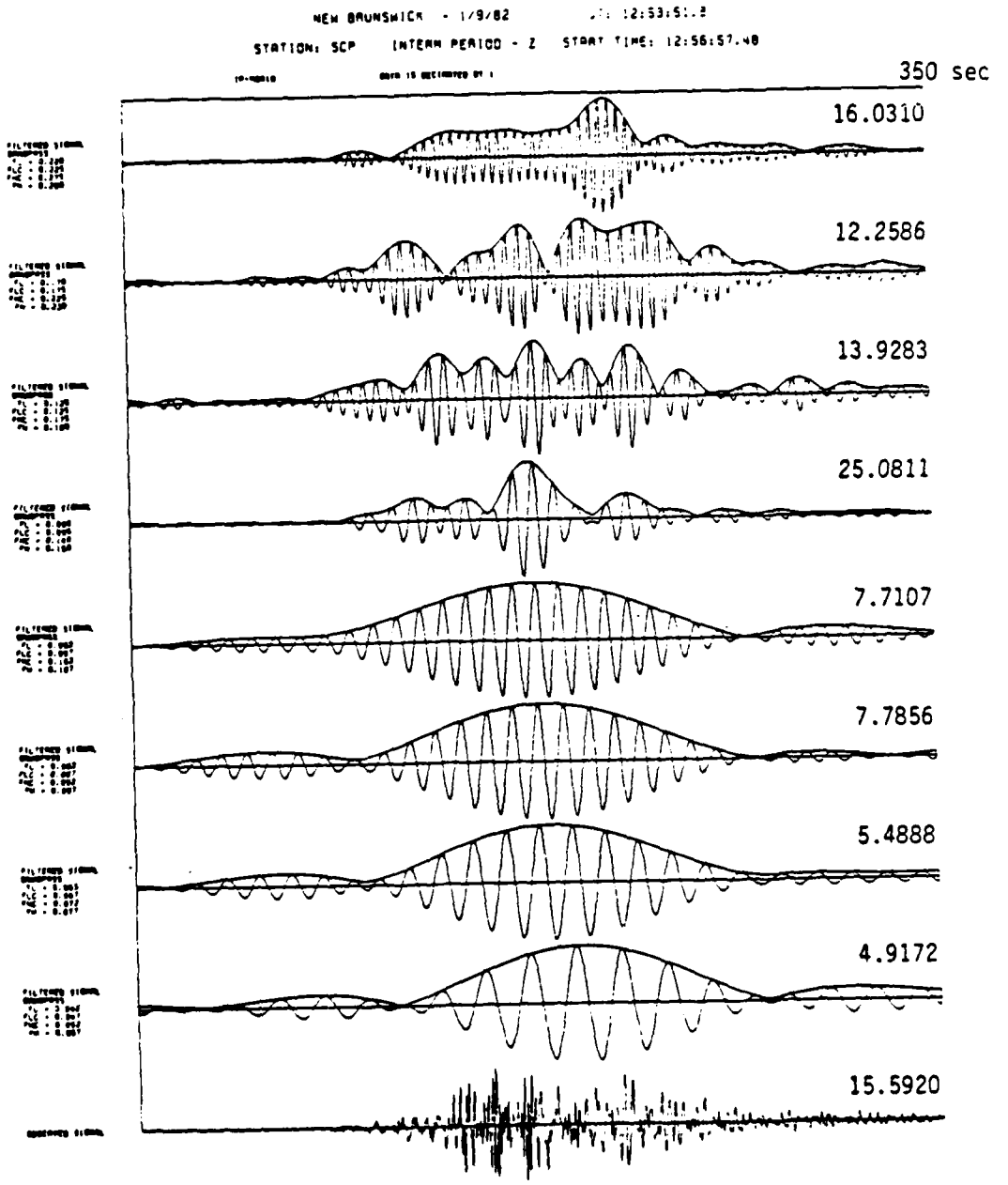
NEW BRUNSWICK - 1/9/82
STATION: SCP INTERM PERIOD - Z START TIME: 12:56:57.48
350 sec
16.0310
12.2586
13.9283
25.0811
7.7107
7.7856
5.4888
4.9172
15.5920

Figure 8

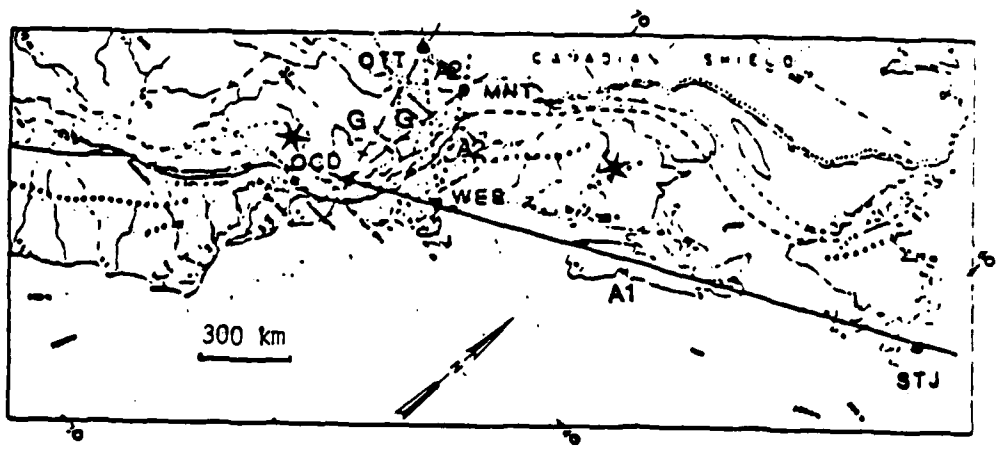

Figure 9

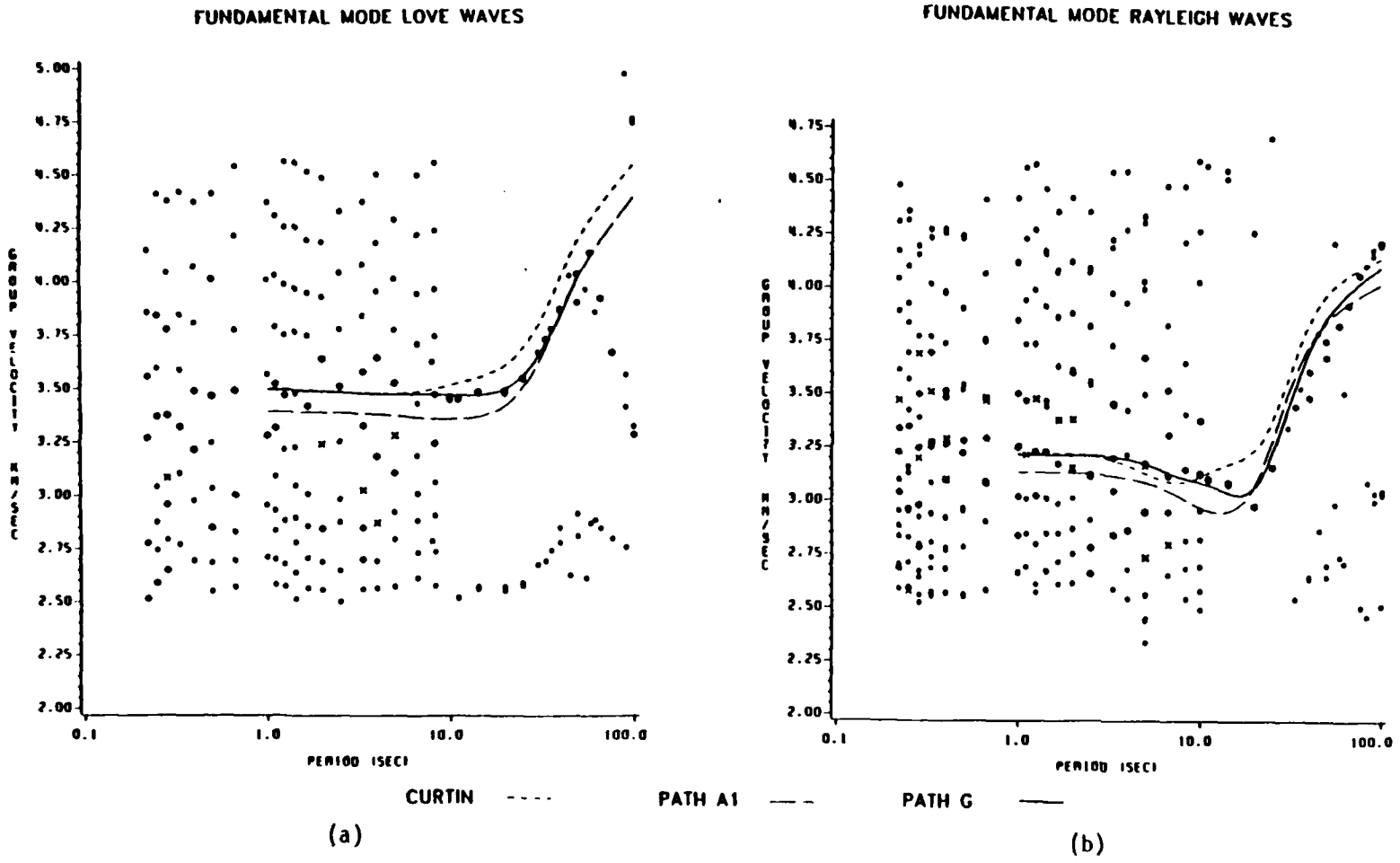
FUNDAMENTAL MODE LOVE WAVES
FUNDAMENTAL MODE RAYLEIGH WAVES
GROUP VELOCITY KM/SEC
PERIOD (SEC)
5.00
4.75
4.50
4.25
4.00
3.75
3.50
3.25
3.00
2.75
2.50
2.25
2.00
0.1
1.0
10.0
100.0
CURTIN
PATH A1
PATH G
(a)
(b)

Figure 10

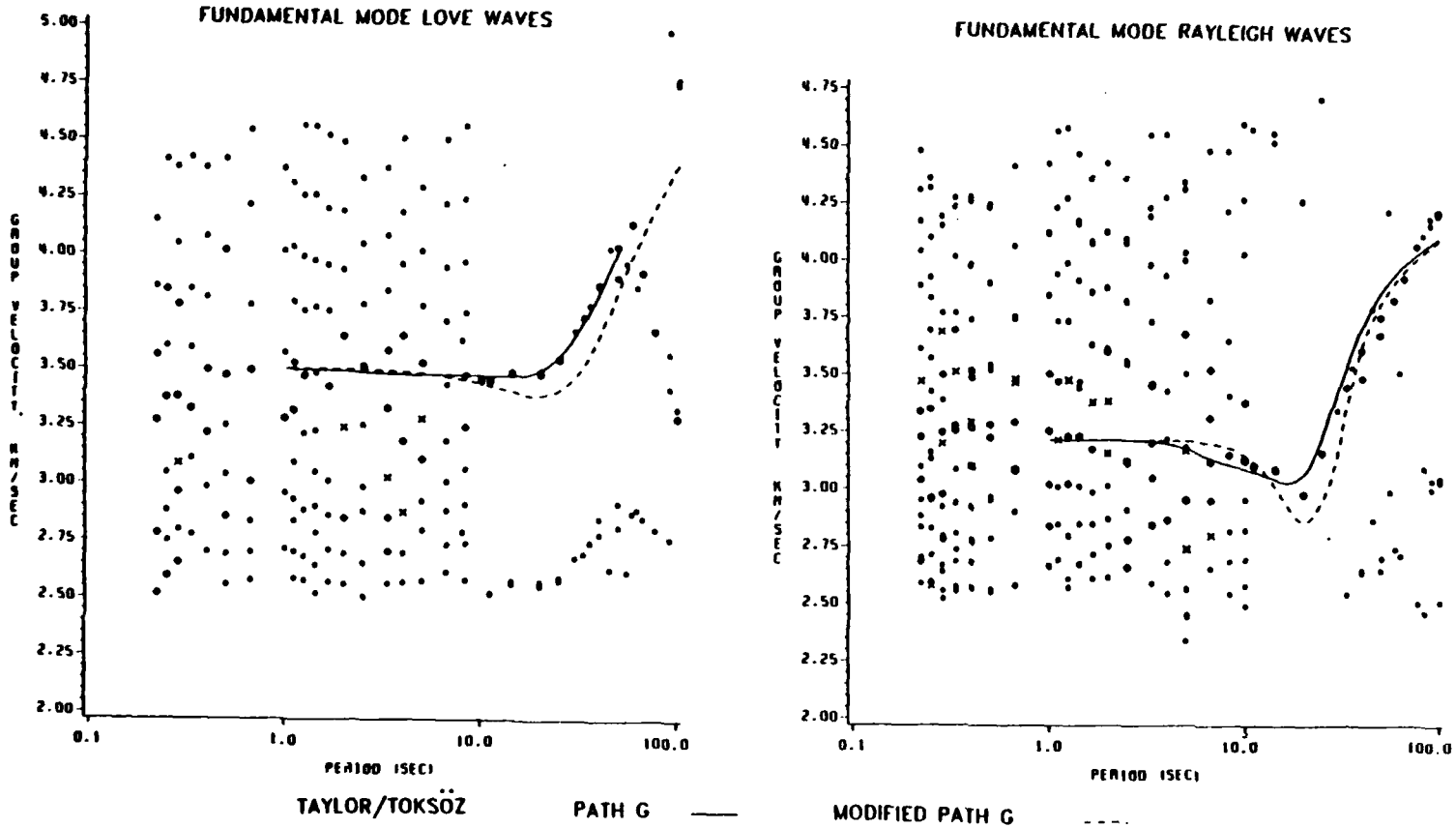
FUNDAMENTAL MODE LOVE WAVES
FUNDAMENTAL MODE RAYLEIGH WAVES
GROUP VELOCITY KM/SEC
PERIOD (SEC)
5.00
4.75
4.50
4.25
4.00
3.75
3.50
3.25
3.00
2.75
2.50
2.25
2.00
0.1
1.0
10.0
100.0
TAYLOR/TOKSÖZ
PATH G
MODIFIED PATH G
(a)
(b)

Figure 11

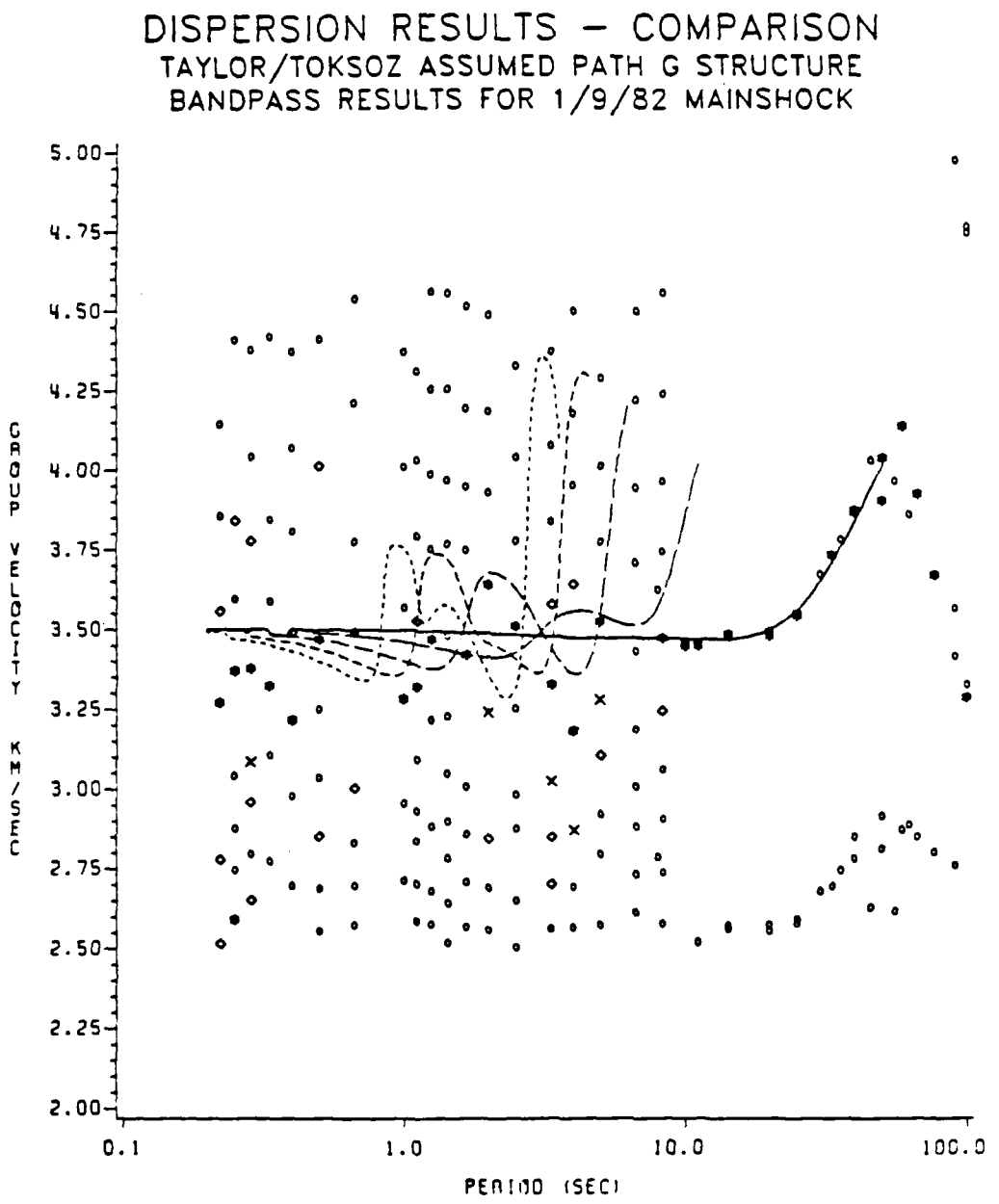
DISPERSION RESULTS – COMPARISON
TAYLOR/TOKSOZ ASSUMED PATH G STRUCTURE
BANDPASS RESULTS FOR 1/9/82 MAINSHOCK
GROUP VELOCITY KM/SEC
5.00
4.75
4.50
4.25
4.00
3.75
3.50
3.25
3.00
2.75
2.50
2.25
2.00
0.1
1.0
10.0
100.0
PERIOD (SEC)

Figure 12

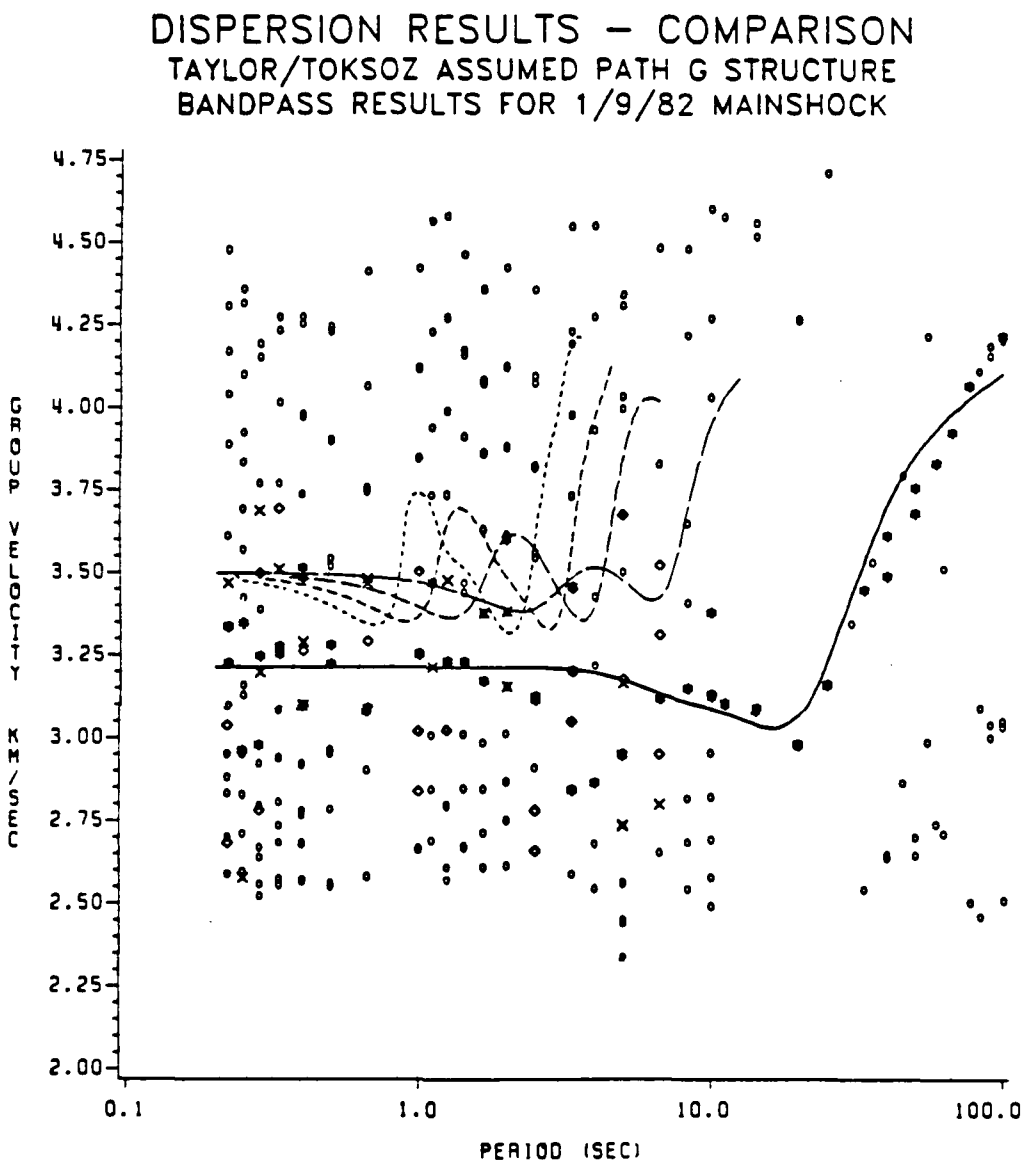
DISPERSION RESULTS – COMPARISON
TAYLOR/TOKSOZ ASSUMED PATH G STRUCTURE
BANDPASS RESULTS FOR 1/9/82 MAINSHOCK
GROUP VELOCITY KM/SEC
4.75
4.50
4.25
4.00
3.75
3.50
3.25
3.00
2.75
2.50
2.25
2.00
0.1
1.0
10.0
100.0
PERIOD (SEC)

Figure 13

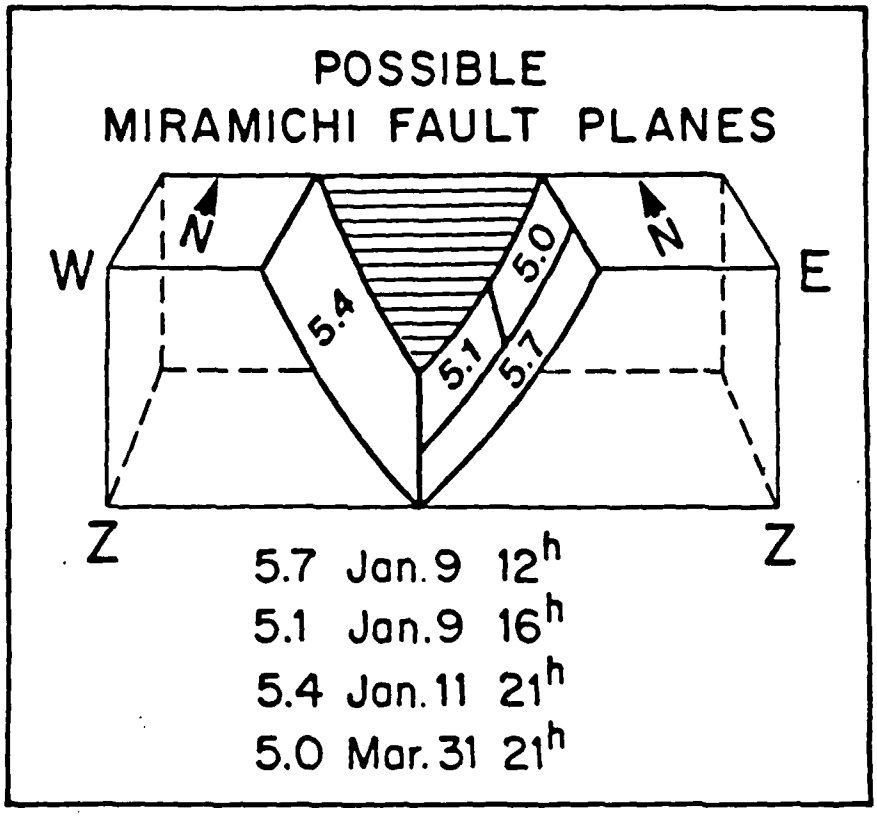
POSSIBLE
MIRAMICHI FAULT PLANES
W
N
N
E
5.4
5.1
5.7
5.0
Z
Z
5.7 Jan.9 12h
5.1 Jan.9 16h
5.4 Jan.11 21h
5.0 Mar.31 21h

Figure 14

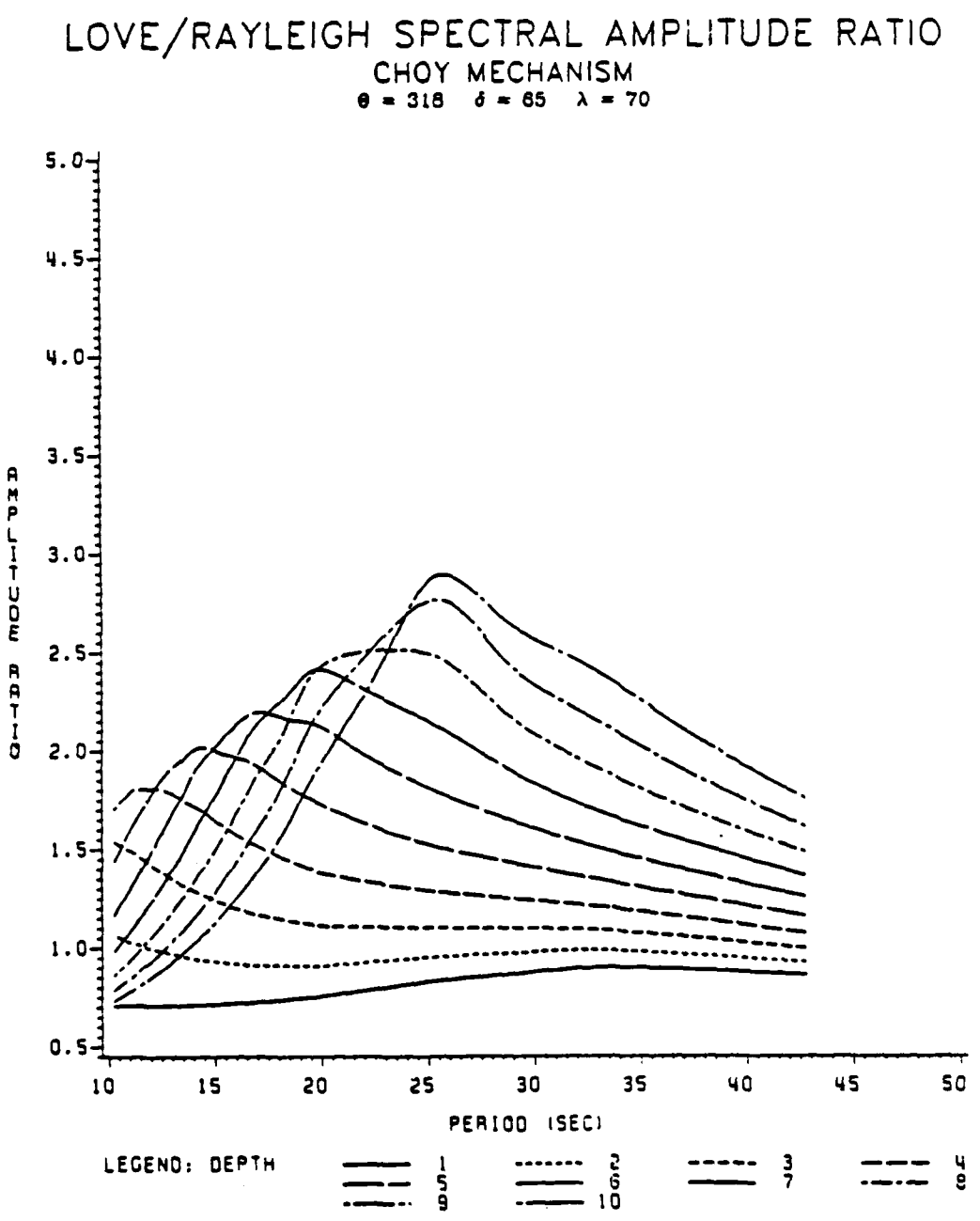
LOVE/RAYLEIGH SPECTRAL AMPLITUDE RATIO
CHOY MECHANISM
θ = 318 δ = 65 λ = 70
AMPLITUDE RATIO
5.0
4.5
4.0
3.5
3.0
2.5
2.0
1.5
1.0
0.5
10
15
20
25
30
35
40
45
50
PERIOD (SEC)
LEGEND: DEPTH
1
2
3
4
5
6
7
8
9
10

Figure 15

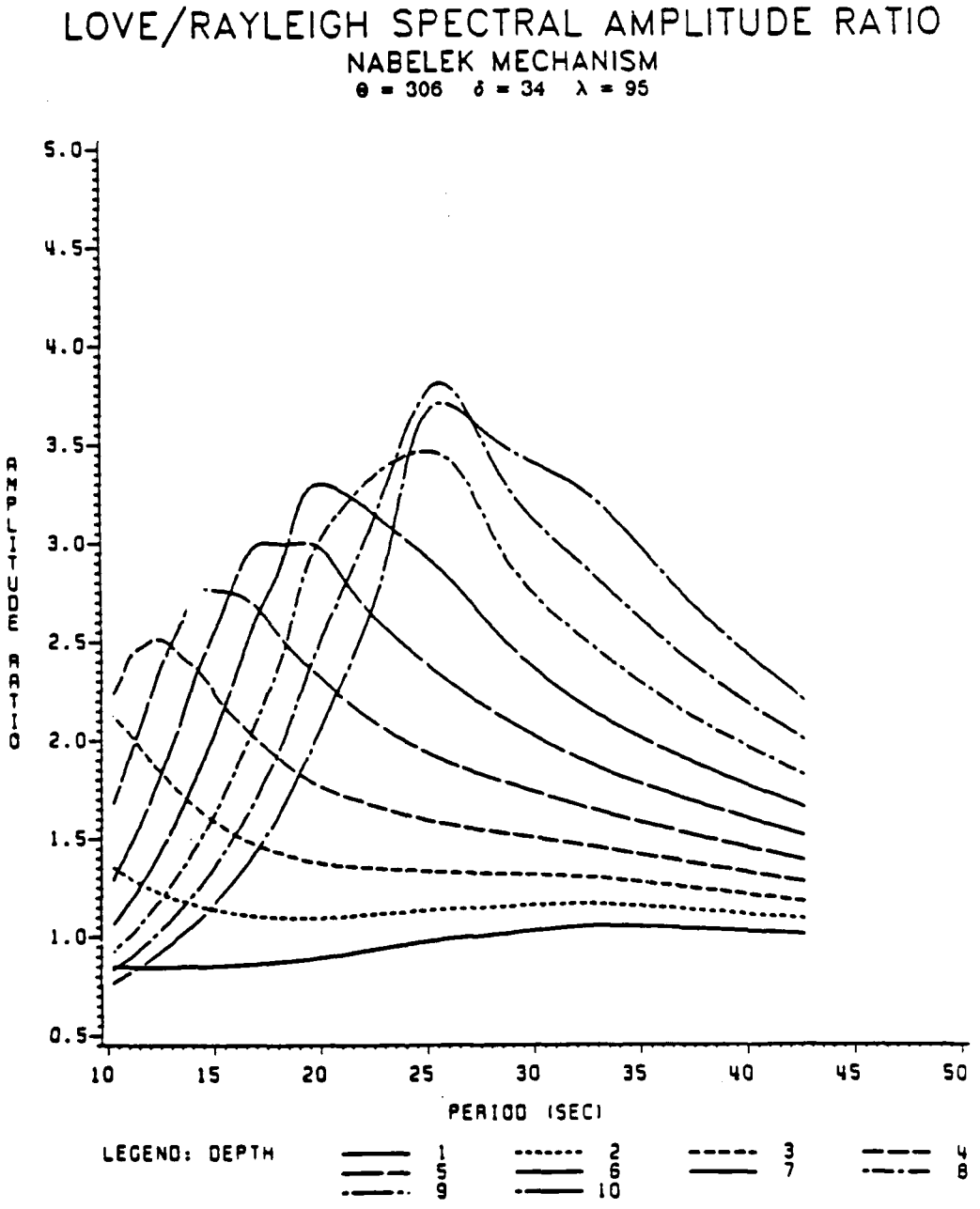
LOVE/RAYLEIGH SPECTRAL AMPLITUDE RATIO
NABELEK MECHANISM
θ = 306 δ = 34 λ = 95
AMPLITUDE RATIO
5.0
4.5
4.0
3.5
3.0
2.5
2.0
1.5
1.0
0.5
10
15
20
25
30
35
40
45
50
PERIOD (SEC)
LEGEND: DEPTH
1
2
3
4
5
6
7
8
9
10

Figure 16

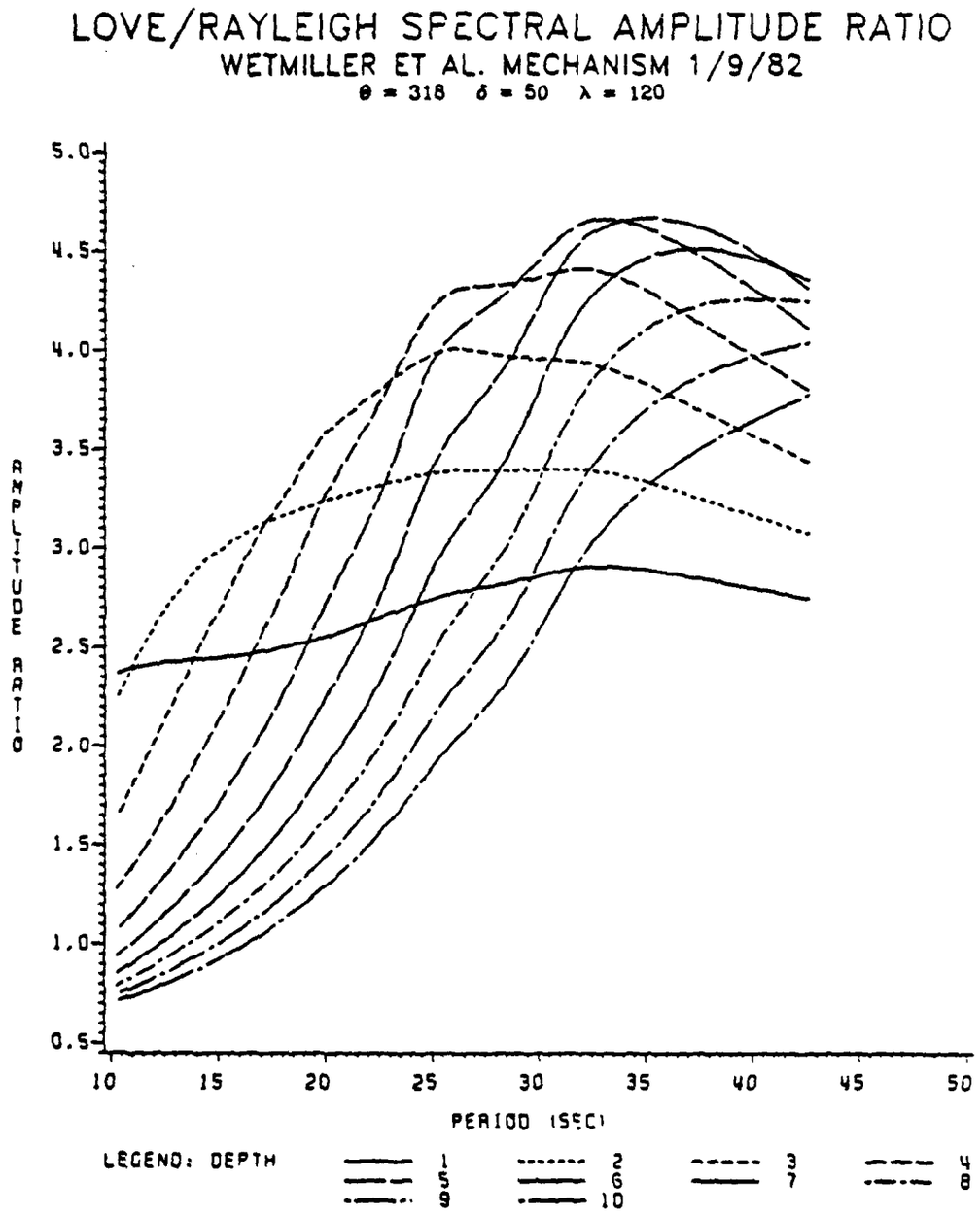
LOVE/RAYLEIGH SPECTRAL AMPLITUDE RATIO
WETMILLER ET AL. MECHANISM 1/9/82
θ = 318 δ = 50 λ = 120
AMPLITUDE RATIO
5.0
4.5
4.0
3.5
3.0
2.5
2.0
1.5
1.0
0.5
10
15
20
25
30
35
40
45
50
PERIOD (SEC)
LEGEND: DEPTH
1
2
3
4
5
6
7
8
9
10

Figure 17

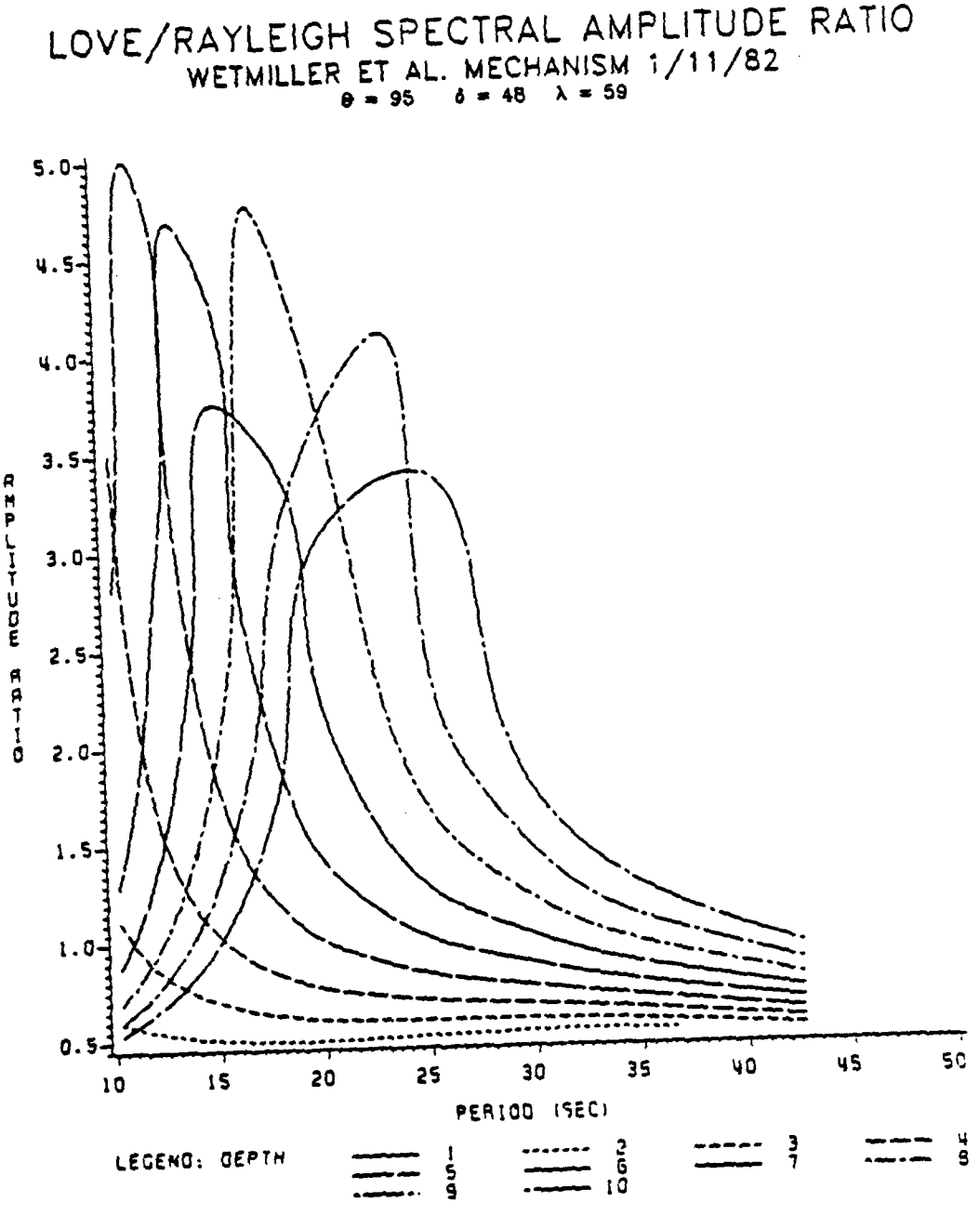
LOVE/RAYLEIGH SPECTRAL AMPLITUDE RATIO
WETMILLER ET AL. MECHANISM 1/11/82
θ = 95 δ = 48 λ = 59
AMPLITUDE RATIO
5.0
4.5
4.0
3.5
3.0
2.5
2.0
1.5
1.0
0.5
10
15
20
25
30
35
40
45
50
PERIOD (SEC)
LEGEND: DEPTH
1
2
3
4
5
6
7
8
9
10

Figure 18

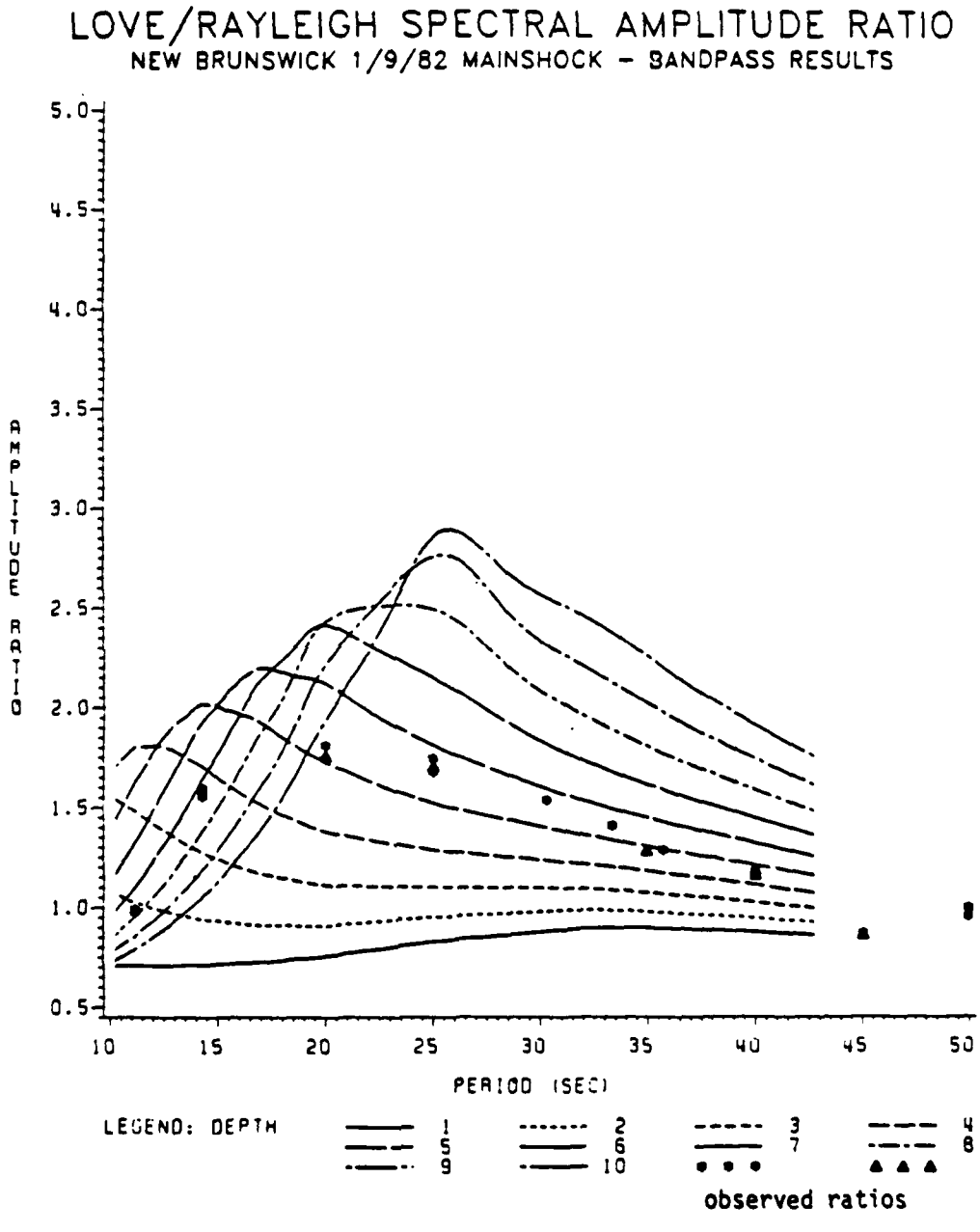
LOVE/RAYLEIGH SPECTRAL AMPLITUDE RATIO
NEW BRUNSWICK 1/9/82 MAINSHOCK - BANDPASS RESULTS
AMPLITUDE RATIO
5.0
4.5
4.0
3.5
3.0
2.5
2.0
1.5
1.0
0.5
10
15
20
25
30
35
40
45
50
PERIOD (SEC)
LEGEND: DEPTH
1
2
3
4
5
6
7
8
9
10
observed ratios

Figure 19

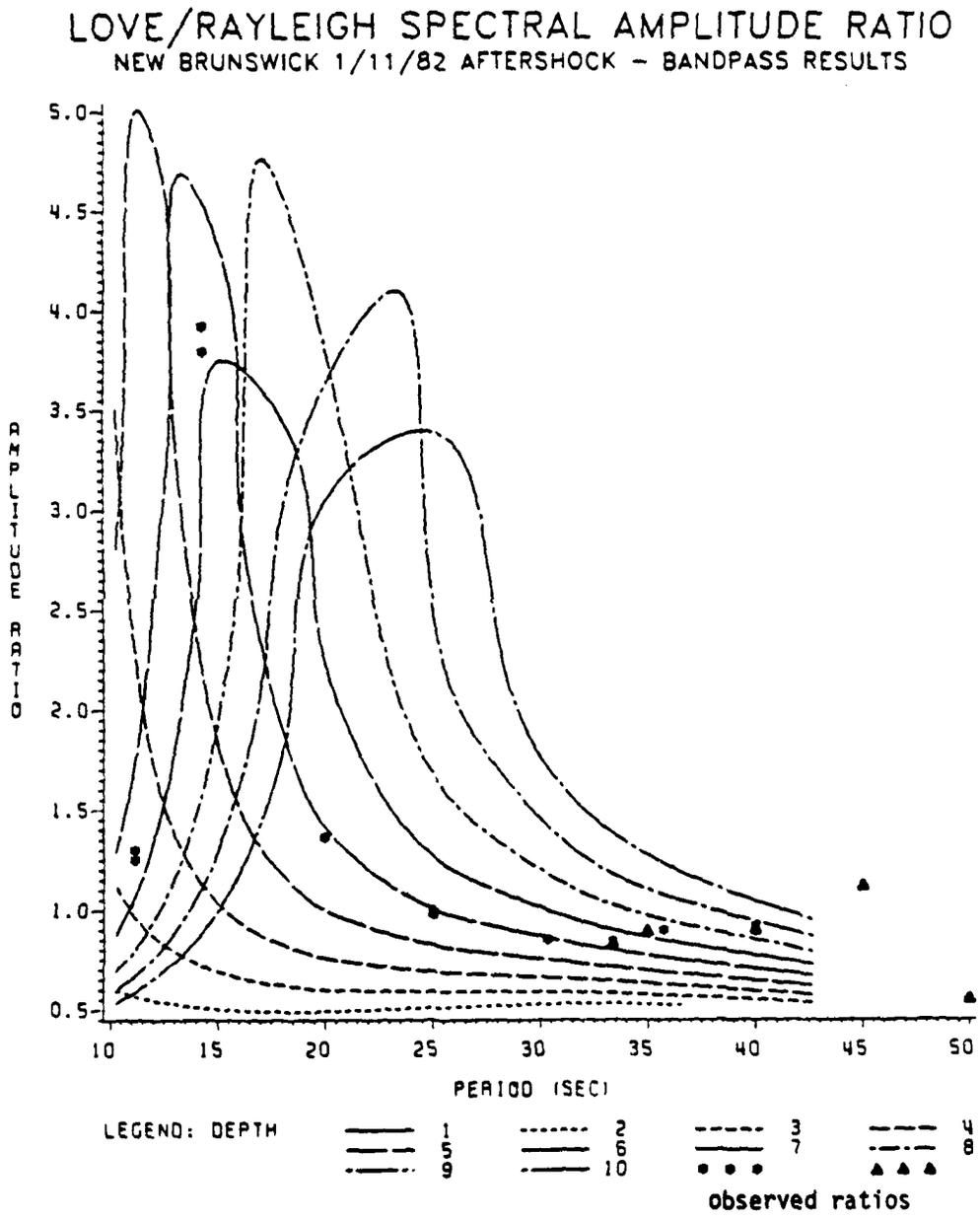
LOVE/RAYLEIGH SPECTRAL AMPLITUDE RATIO
NEW BRUNSWICK 1/11/82 AFTERSHOCK - BANDPASS RESULTS
AMPLITUDE RATIO
5.0
4.5
4.0
3.5
3.0
2.5
2.0
1.5
1.0
0.5
10
15
20
25
30
35
40
45
50
PERIOD (SEC)
LEGEND: DEPTH
1
2
3
4
5
6
7
8
9
10
observed ratios

Figure 20

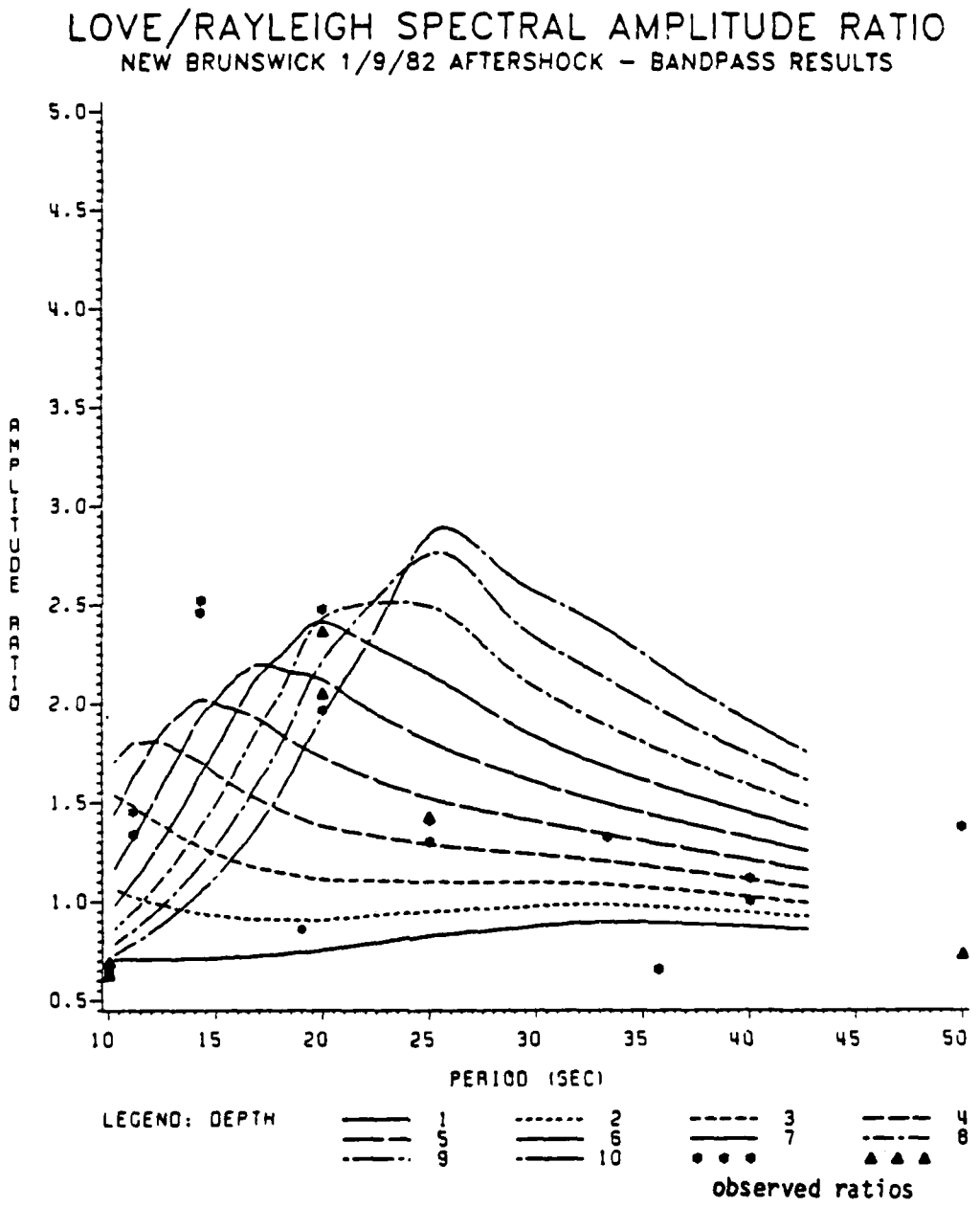
LOVE/RAYLEIGH SPECTRAL AMPLITUDE RATIO
NEW BRUNSWICK 1/9/82 AFTERSHOCK - BANDPASS RESULTS
AMPLITUDE RATIO
5.0
4.5
4.0
3.5
3.0
2.5
2.0
1.5
1.0
0.5
10
15
20
25
30
35
40
45
50
PERIOD (SEC)
LEGEND: DEPTH
1
2
3
4
5
6
7
8
9
10
observed ratios

Figure 21

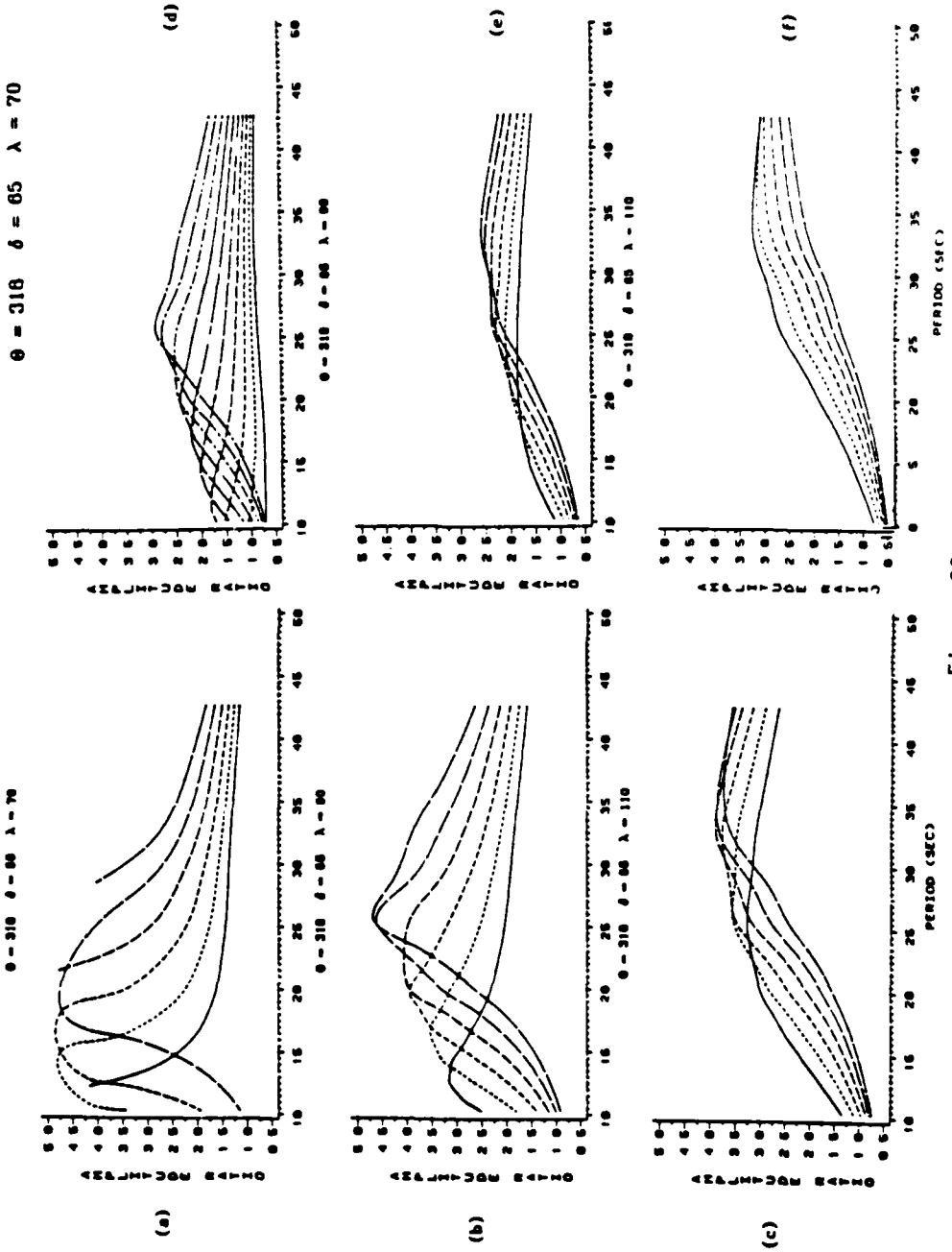

Figure 22

LOVE/RAYLEIGH SPECTRAL AMPLITUDE RATIO

CHOY MECHANISM – MODIFIED DIP AND RAKE

$\theta = 318 \quad \delta = 55 \quad \lambda = 90$

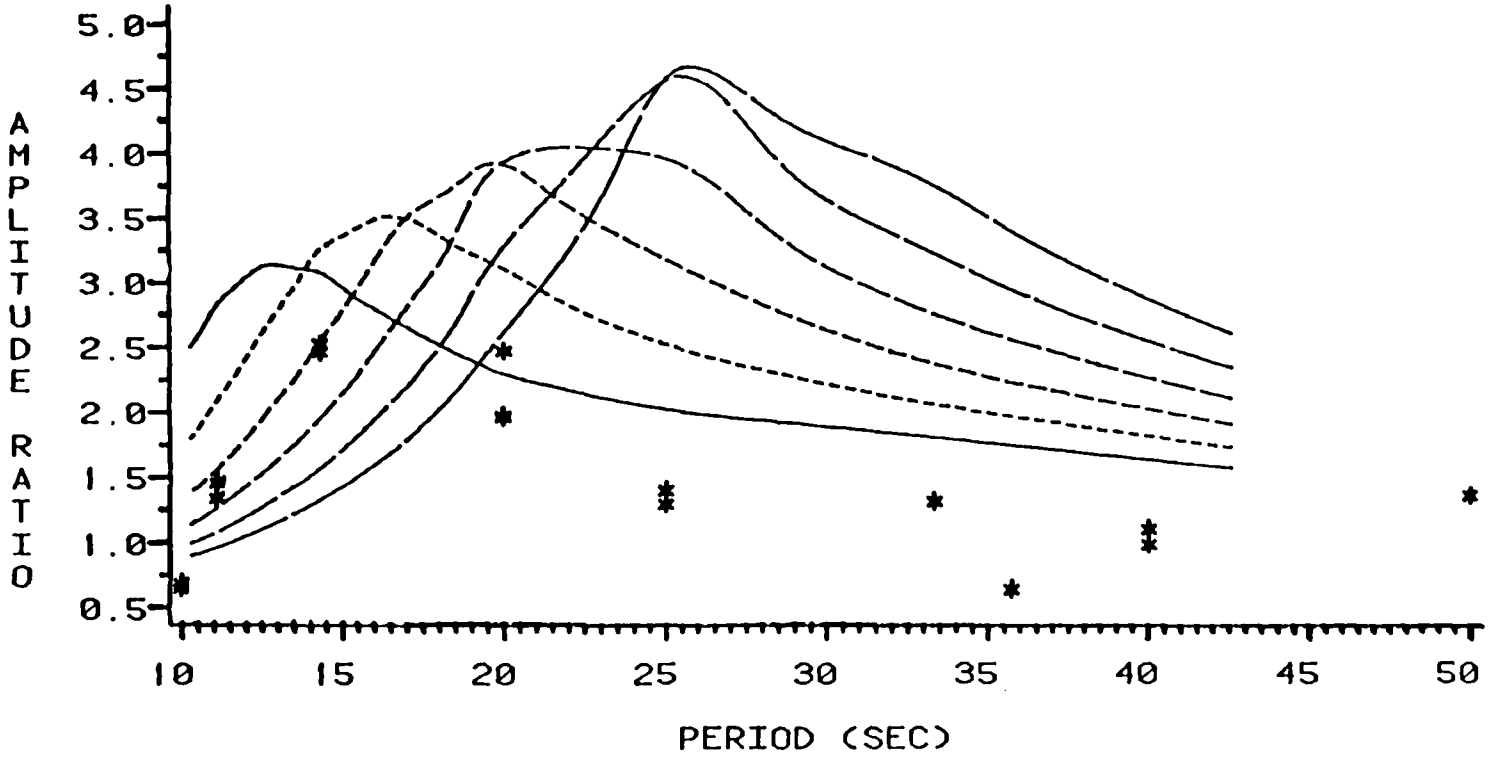

Figure 23

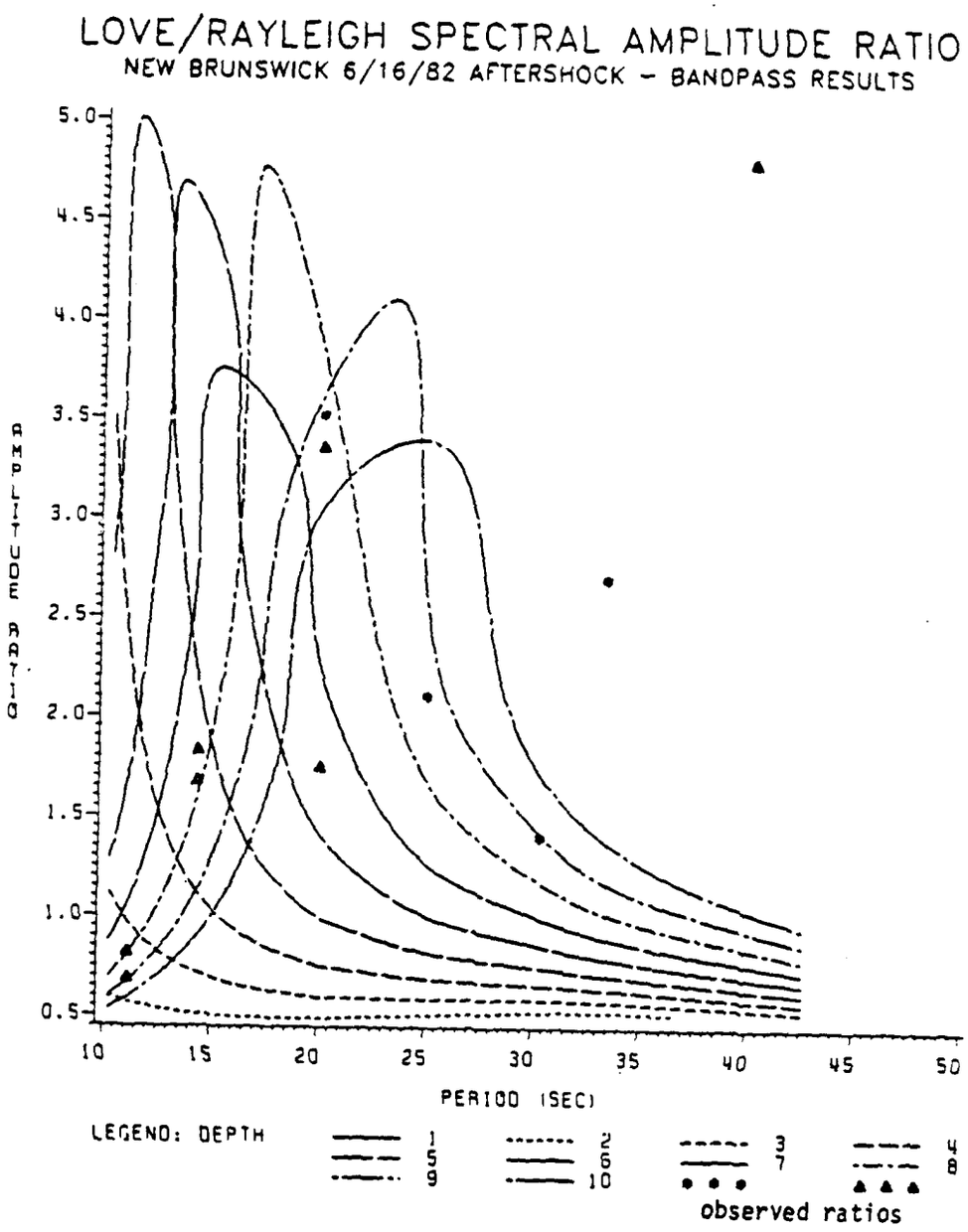
LOVE/RAYLEIGH SPECTRAL AMPLITUDE RATIO
NEW BRUNSWICK 6/16/82 AFTERSHOCK - BANDPASS RESULTS
5.0
4.5
4.0
3.5
3.0
2.5
2.0
1.5
1.0
0.5
10
15
20
25
30
35
40
45
50
PERIOD (SEC)
LEGEND: DEPTH
1
2
3
4
5
6
7
8
9
10
observed ratios

Figure 24

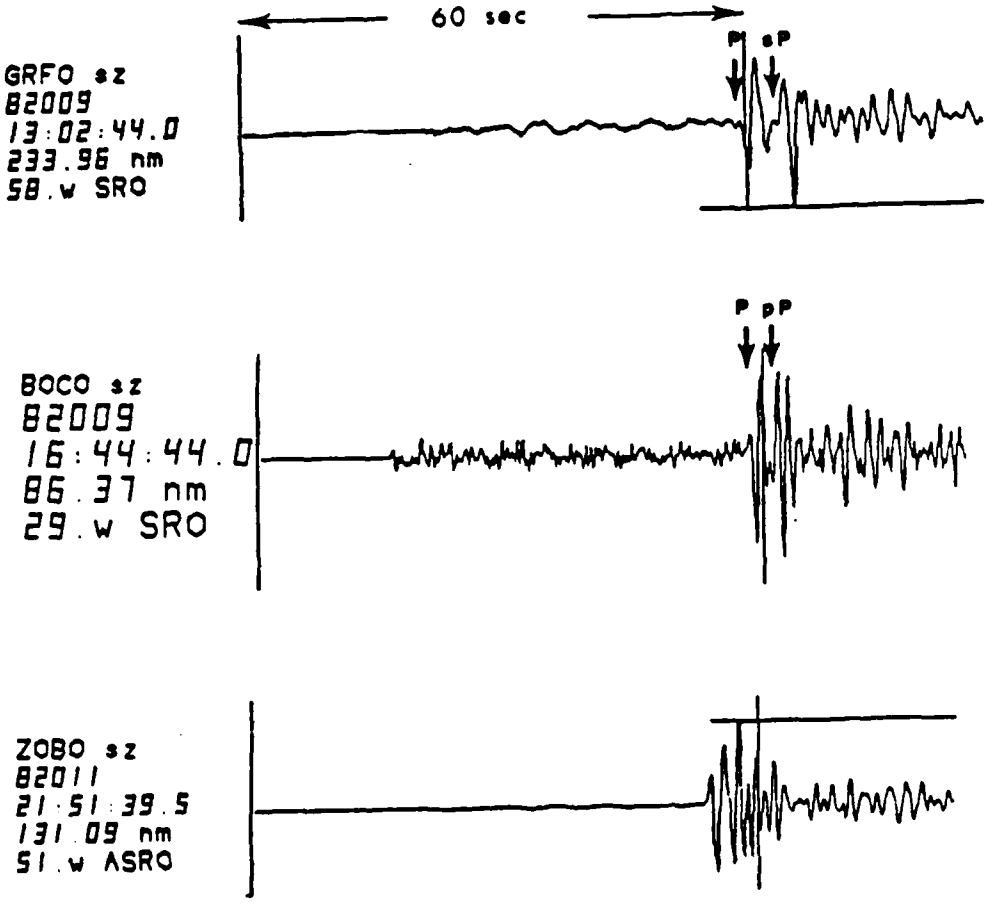
60 sec
GRFO sz
82009
13:02:44.0
233.96 nm
58.w SRO
P
sP
BOCO sz
82009
16:44:44.0
86.37 nm
29.w SRO
P pP
ZOBO sz
82011
21:51:39.5
131.09 nm
51.w ASRO

Figure 25

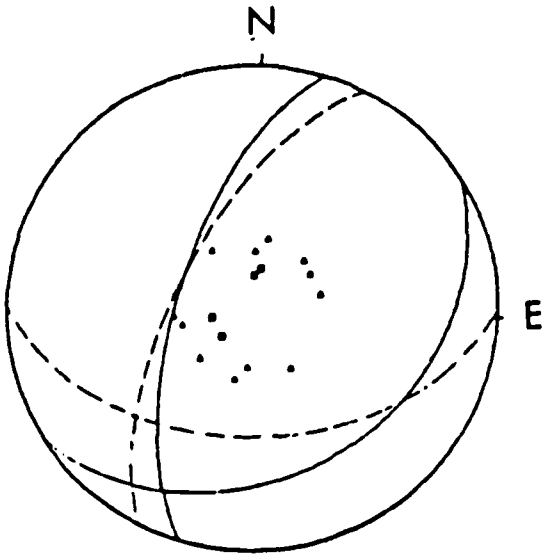

Figure 26

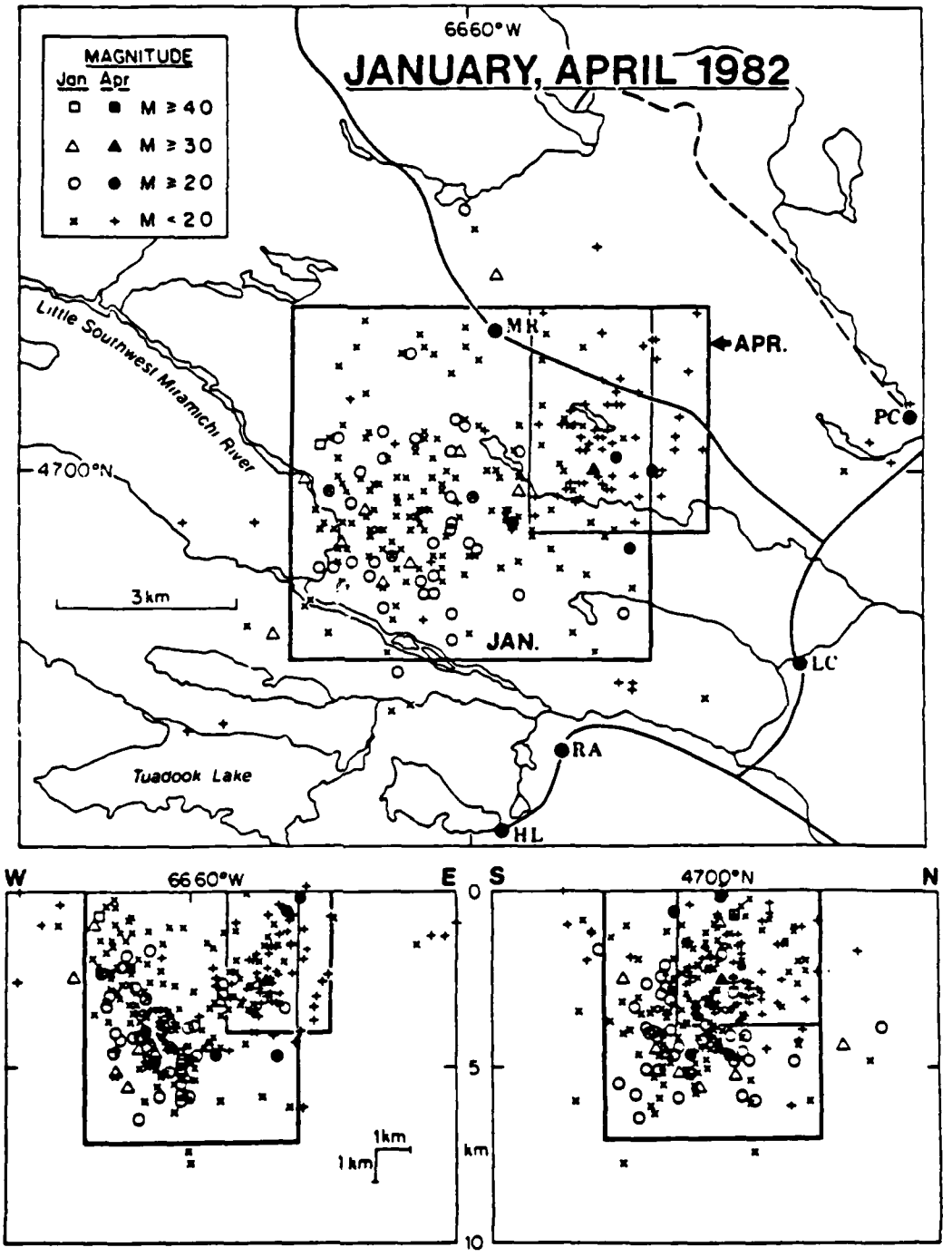
6660°W
JANUARY, APRIL 1982
MAGNITUDE
Jan Apr
M ≥ 40
M ≥ 30
M ≥ 20
M < 20
Little Southwest Miramichi River
MR
APR.
PC
4700°N
3km
JAN.
LC
RA
Tuadook Lake
HL
W
6660°W
E
S
4700°N
N
0
5
10
km
1km
1km

Figure 27

LOVE/RAYLEIGH SPECTRAL AMPLITUDE RATIO

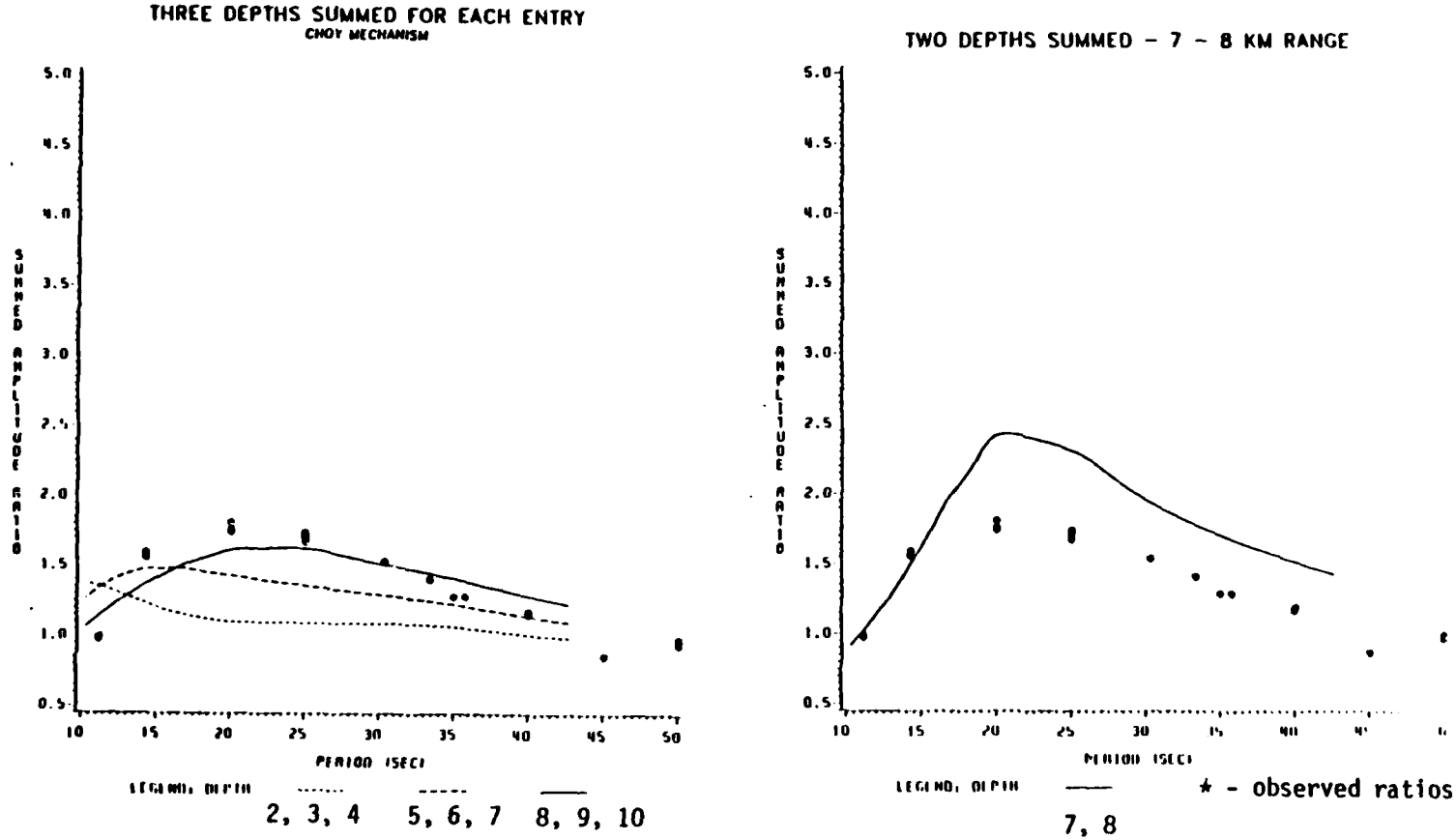

LEGEND INDICATES DEPTHS SUMMED TO FORM AMPLITUDE RATIOS

(a) (b)

Figure 28

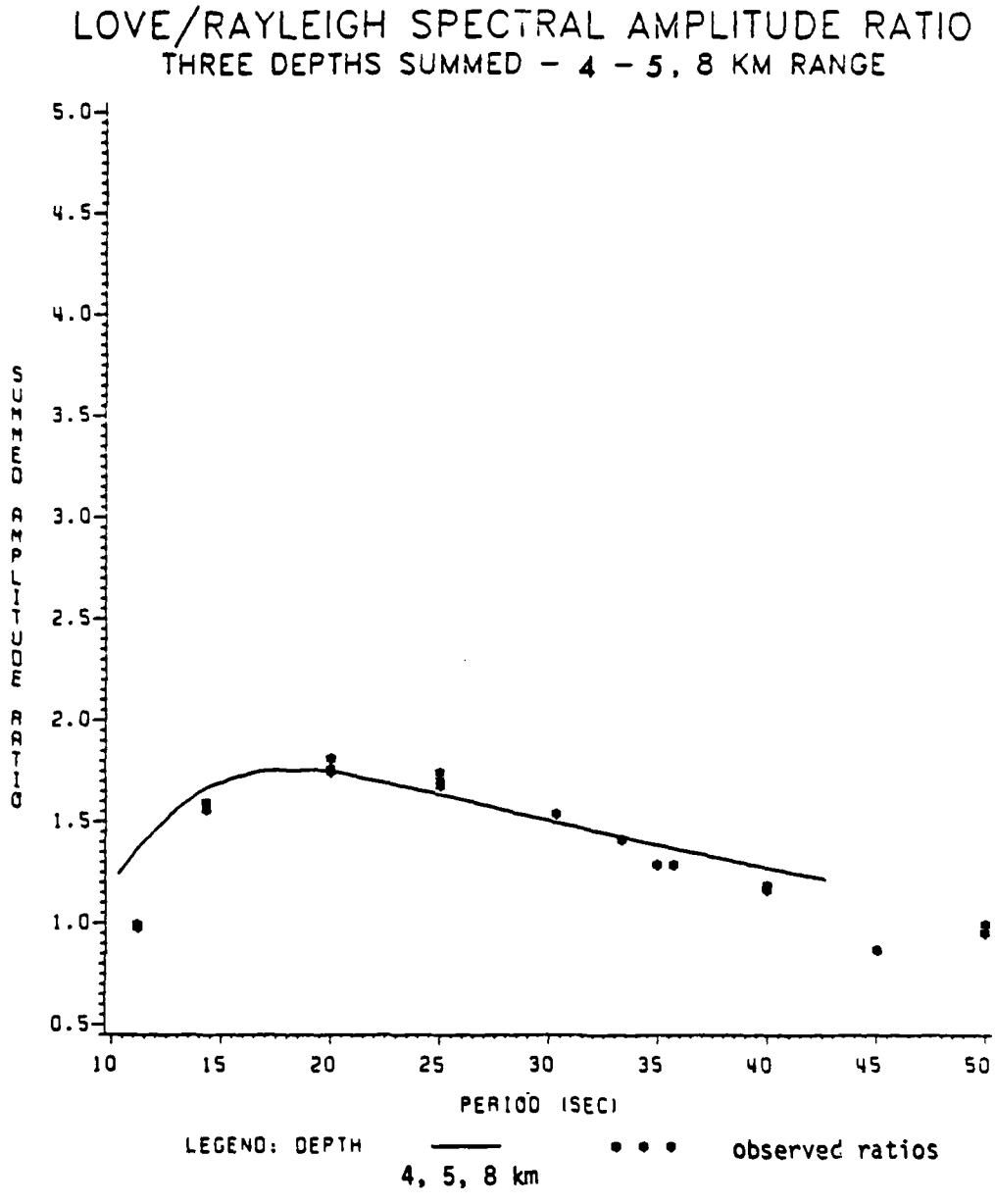

LEGEND INDICATES DEPTHS SUMMED TO FORM AMPLITUDE RATIOS

Figure 29

APPENDIX 1

Harkrider Program

Description

> The use of Harkrider's layered half-space dispersion program,... has been accomplished much like one would handle a folk tale - handed down from one graduate student to the next.
>
> - Turnbull (1976)

The purpose of this appendix is to facilitate future use of the Harkrider programs by describing specifically the steps to be followed in preparing the data and control parameters for input to the main program which generates the synthetic seismograms. The routines were written in single precision for use on the PRIME computer and sent to us in that form. The computations performed in this study were carried out on an IBM computer, so the programs were modified as needed in order to accommodate the different system requirements. The original programs and support libraries needed for execution on the PRIME have been stored in the first 17 files on tape HARK1 (standard labeled, 6250 bpi) which resides in the PSU IBM tape library (a listing of tape contents can be obtained quickly by running PSUDEBE on the tape). The modified versions for use on the IBM are contained in the last files on HARK1 and these are the versions which will be discussed here. It must be pointed out that the compiler used to execute the main program was an H-extended, translated version of VTPLOT, which modified VS Fortran as needed to process the data for plotting on the Versatec. After Fall semester, 1983, this compiler was no longer supported, so conversions will be necessary to ensure full compatibility with VS Fortran (if continued IBM use is anticipated).

The first step in preparing the data is to scan frequency/phase velocity space for approximate roots to the period equation. Input

parameters to SCAN are defined as they were used in this application; further work with the program may reveal subtleties in their meanings that were missed.

LMODET = NCASE = the number of modes to process

IDUM = 0

INST = 0 = presumed to be related to instrument correction, set equal to zero since the SCP data were already deconvolved for instrument response

IDENT = 80 characters available for commenting the trial run

N = the number of layers in the structure model

NW = 1 if there is no water layer included in the structure (0 if there is)

H, ALP, BET, RHO = layer parameters; thickness of layer, compressional velocity, shear velocity, and density should be indicated for each of the N layers

CL, CS, NPTC = largest, smallest and number of values of phase velocity to be scanned in the region of interest; in this case, the largest was just greater than the specified shear velocity in the half-space, the smallest was just less than the shear velocity in the uppermost layer; 100 was felt to be a reasonable number of values to search through (130 might have been simpler given the specified phase velocity range)

FL, FS, NPTT = largest, smallest and number of points to be scanned in frequency; our range was chosen as 1 - .01 Hz (1 sec - 100 sec period) on the basis of the range of values to be studied and with some attention to time cost

NMODES = the number of modes requested; for want of a better idea, the number of modes was held the same (NMODES = LMODET = NCASE). This can be sensibly varied in later steps; the reasons for retaining three different control parameters at this stage is unclear.

The program is set to scan for both Rayleigh and Love modes automatically, if two sets of the above input variables are specified. The original PRIME version (RLSCFRQ) allows for one or the other depending on the values specified for NLO and NRA.

Output of this scanning routine includes listings of input and computed layer parameters, a visualization of the sign of the period equation in frequency/phase velocity space (the roots are sought where the function has a zero value), and "INPUT FILES FOR LATER CALCULATIONS." The output of interest appears under this last heading where starting phase velocities and frequencies are indicated by mode. The first entry is for the fundamental mode; subsequent entries correspond to as many higher order modes as were requested. Since there were 100 frequency points to be tested in the case illustrated in Figure A1 - 1, the frequencies for the fundamental mode cover the full range: 100 frequency values spanning the range from .01 to 1 Hz, with a starting phase velocity value of 4.1982 km/sec. The first higher mode will have its first root at a frequency value of .08 Hz, with 93 roots extending out to 1 Hz, and the initial value for phase velocity should be set at 4.5429 km/sec. These are the starting values which must be used as input to the Love and Rayleigh eigenvalue-generating programs, which search the frequency/phase velocity space on a finer grid for more accurate values of the roots.

Input to RAYLIT.UPEC and LOVIT.UP, the programs for more precise determination of Rayleigh and Love eigenvalues, respectively, takes on the same form for both. LPAR is currently not used in any of the programs - its purpose is unknown.

NCASE = has been assumed to be the number of modes to process

NNN = setting this not equal to zero indicates that the same structure model will be applied for all NCASE

MPRNT = controls the amount of diagnostic output; if equal to 0, maximum output is listed; if equal to 1, only the layer parameters and dispersion calculations are listed

IDENT = again, 80 characters of identifying comment

N and NW = number of layers and water layer (0 or 1) (as specified in SCAN)

The following are specified first for the fundamental mode:

CI = starting phase velocity (value from SCAN)

DC = increment for phase velocity (.01 works well)

LC = number of frequencies to be calculated for this mode (100 in the case of the fundamental mode for this example; values for higher modes are the number of roots specified by SCAN)

LD = controls the root-searching process and is described within the program

NLAP = appears to control input, a choice of zero was consistent

NHS = 0

FK = starting frequency (specified in SCAN)

FKD = frequency decrement = -.01 Hz in this case

NLES = number of layers to ignore in the calculation. This is set at zero to begin, the program performs layer reduction as needed to eliminate instabilities as computation proceeds

LHF = 0

DKS = this specifies even/odd modes; the value should be set at +1.0 for fundamental mode, -1.0 for first higher mode, +1.0 for second higher mode, etc.

DELTA AND CPERT = parameters which control the perturbation in phase velocity and decide when the root has been achieved to sufficient accuracy; they are set within the program if not specified as input

Layer parameters must again be specified as they were for the scanning routine, followed by starting phase velocity and frequency values for as many higher order modes as desired, adhering to the same format as for the fundamental mode.

The output from RAYLIT.UPEC and LOVIT.UP can include as much detail

```
1*** INPUT FILES FOR LATER CALCULATIONS ***
                          6      1      1
SCAN FOR NEW BRUNSWICK STRUCTURE - PATHG - RAYLEIGH
                  N =      9              NN =      1
    4.19820       0.00556          6      5      1      0
   0.010050                        0      0
  1.0          <-starting frequency     ignore for fundamental mode
      5.0000       6.0000       3.5000       2.7000
     10.0000       6.0000       3.5000       2.7000
     10.0000       6.6000       3.8000       2.8000
     10.0000       6.8000       3.8000       2.8500
     10.0000       8.1000       4.5000       3.3000
     10.0000       8.1000       4.5000       3.3000
     20.0000       8.1000       4.5000       3.3000
     20.0000       8.2000       4.7000       3.3000
     20.0000       8.2000       4.7000       3.3000
      0.0100       4.1982       0.0200       4.0902       0.0300
      0.0400       3.7879       0.0500       3.6366       0.0600
    4.54291       0.00556         93      5      1      0
   0.080050                        0      0
 -1.0
```

Figure A1 - 1

as desired, controlled by the value specified for MPRNT. For example, to ensure that the correct mode has been found in the root-searching process, layer displacements can be checked in the detailed listing. The fundamental mode should show no zero crossings, while each successively higher order mode should show one additional zero crossing. The information needed for the main program (EQTR.ZBIG for the PRIME; HARKRUNR and HARKRUNL for the IBM), are the values (for each frequency specified) of the phase velocity, group velocity, medium amplitude response, ellipticity (in the case of Rayleigh waves) and an integer value indicating the number of layers used in the calculation. These can either be stored directly in a file or modified from the listed output for later use with EQTR.ZBIG.

Commenting for the main program is very complete, so far as it goes. The crucial input for the case of a double couple source rests with

eight lines of input parameters:

```
READ (     ) NSR

READ (     ) LMODO,NTYF,THETA,DELT,FLAM,LMODES

READ (     ) LRDP,LEXP,SP,SSV,SSH

READ (     ) DIST,TO,DT,LNT,LFFT,LINSY,LATN,LU

READ (     ) NDISL,STO,DT1,DT2,DT3

READ (     ) NSCALE,XSCALE,SCAF,LPLT,IBUG,LSAVE,LMOPLT

READ (     ) (DEPT(I), I= 1, NDEP)
```

These quantities are defined as follows:

NSR = 1 if only one source structure is to be considered

LMODO = 0 for the Love wave run; = 1 for the Rayleigh wave run

NTYF = 2, specifying the douple couple

THETA = station azimuth measured counter-clockwise ** from the strike of the hanging wall. This definition must be considered carefully, as it appears to be the reverse of current conventions. Theta and other parameters of the source geometry are illustrated in Figure A1 - 2.

DELT, FLAM = fault dip and rake as defined in Figure A1 - 2

LMODES = the number of modes to include in the synthetic calculation from the results of LOVIT.UP or RAYLIT.UPEC

LRDP = 4, indicating a double couple, in this case, with no explosion component; therefore, LEXP = 0, and SP, SSV and SSH automatically become 0

DIST = the distance frm source to receiver which may be specified in kilometers or degrees

TO,DT,LNT = starting time, time interval, and number of time points, respectively, with options given as to how they may be specified

LFFT = 1, calls for straight line interpolation FFT

** After subsequent work by later investigators revealed inconsistent results, it was discovered that this convention was reversed in final revisions of the program. Therefore, THETA should be measured clockwise from strike.

LINS = 0, indicates that instrument response will not be included in the calculation

LATN = 0, indicates that attenuation values will not be incorporated

(in the present study, it made sense to set LINS and LATN equal to 0 since amplitude spectra, rather than synthetic seismograms, were calculated for comparison with spectral values which had already been corrected for instrument response and for which attenuation was assumed constant. If, however, a synthetic seismogram were to be calculated for comparison with the original SCP record, these quantities would have to be specified.)

LU = 0, specifies that displacement is to be calculated at the surface

NDISL = 4, and STO = 0 calling for a step moment or dislocation with both moments set to 10^{25} dyne-cm

DT1, DT2, DT3 = all equal to zero because of the previous choice of step moment

NSCALE, XSCALE, SCAF = are all scaling calls for the seismogram plot They may be specified or default values are set.

LPLT = 0, calls for no plotting; if > 0, the numerical value gives the number of plots per page

IBUG = controls the amount of output to be listed

LSAVE = allows the time series to be saved in an external file

LMOPLT = 1, specifies that each individual modal contribution is to be plotted, as well as the accumulated time series. If equal to 0, only the final, accumulated time series is plotted.

NDEP = the number of source depths for which complete calculations are to be performed

LCHG = 0

DEPT(I), I = 1,NDEP = the values of depth to use in the calculations

Once all these source parameters have been processed, the structure parameters are called within SUBROUTINE LAYERS and calculation proceeds. It is a minor modification to obtain spectral amplitudes rather than the time series; just prior to the call to COOLB, the values can be retrieved.

With these hints about the flow of the program steps, accompanied by sample output listings for immediate reference, it should be a routine matter to get the Harkrider routines up and running and performing over the wide range of applications for which they are designed.

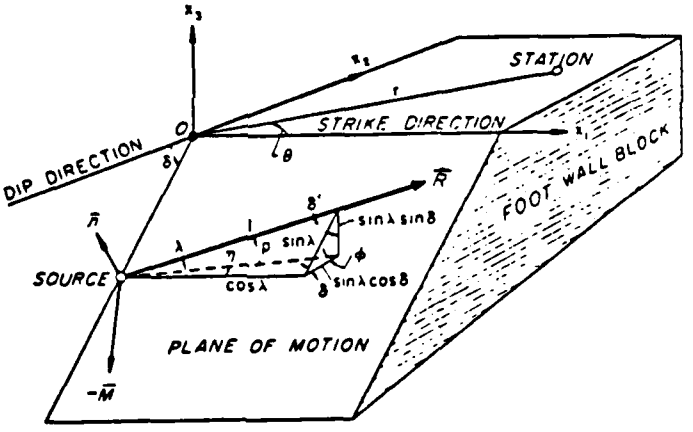

Figure A1 - 2

Geometry of source parameters and relative position of receiving station on the free surface (after Ben-Menahem and Harkrider, 1964)

APPENDIX 2

Original Digital Seismograms

at SCP

Figures A2 - 1 through A2 - 12 are the original digital seismograms as recorded at SCP. Short, intermediate, and long period data are displayed for each event along with information on origin time, epicentral location, magnitude, depth and record start time. Short period data are sampled at 20 samples per second; intermediate period at 10 samples per second; long period at 1 sample per second. The signal-to-noise ratio is good for both the January 9 mainshock and the January 11 aftershock (Figures A2-1 through A2-3 and A2-7 through A2-9). The long period signal for both the January 9 aftershock and the June 16 event (Figures A2-6 and A2-12) are barely discernible from the noise. Note that the intermediate period instrument did not begin recording data for the June 16 event (Figure A2 - 11) until well after the first arrival. This posed significant difficulty when the band-pass filters were applied to this data, resulting in very few usable group velocity data points.

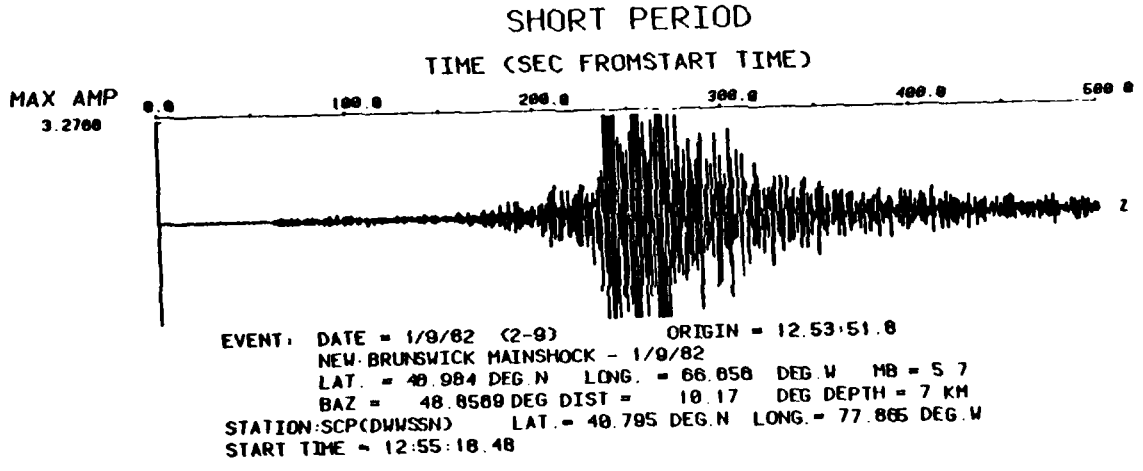
SHORT PERIOD
TIME (SEC FROMSTART TIME)
MAX AMP
3.2700
0.0
100.0
200.0
300.0
400.0
500.0
Z
EVENT: DATE = 1/9/82 (2-9) ORIGIN = 12:53:51.8
NEW BRUNSWICK MAINSHOCK - 1/9/82
LAT. = 48.984 DEG.N LONG. = 66.858 DEG.W MB = 5.7
BAZ = 48.8589 DEG DIST = 10.17 DEG DEPTH = 7 KM
STATION:SCP(DWWSSN) LAT.= 40.795 DEG.N LONG.= 77.865 DEG.W
START TIME = 12:55:18.48

Figure A2 - 1

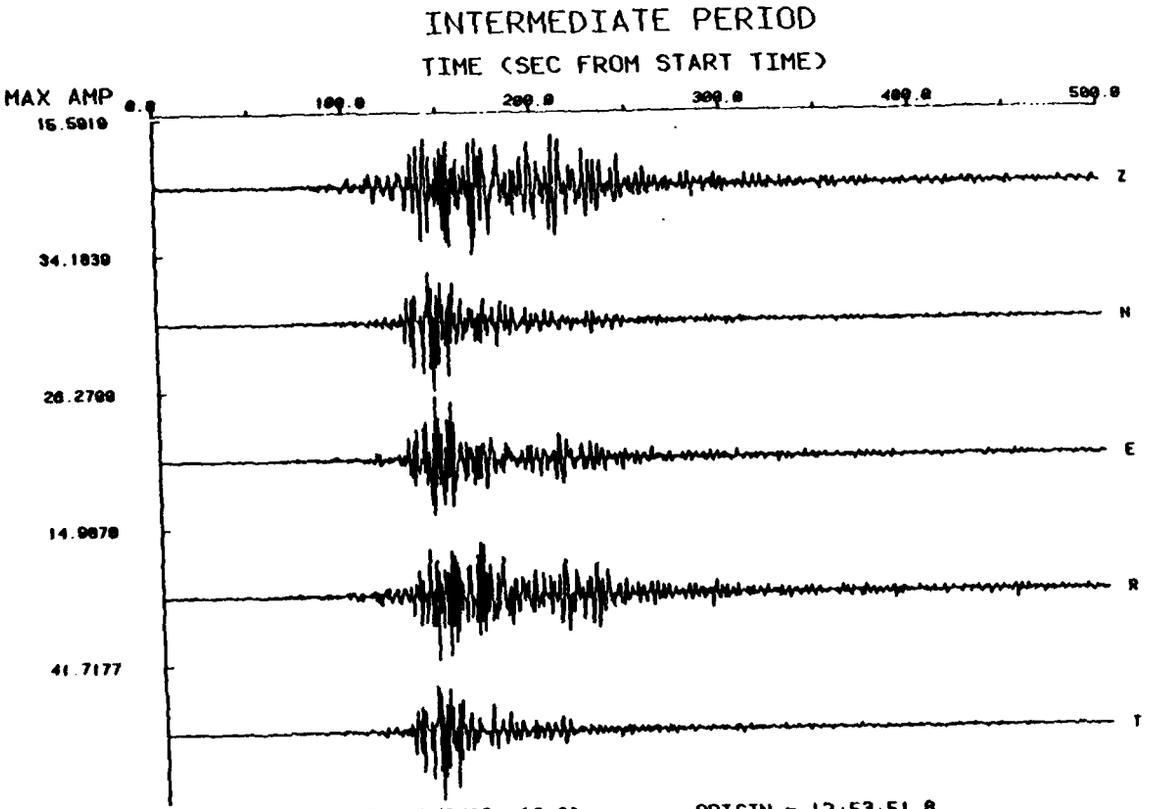
INTERMEDIATE PERIOD
TIME (SEC FROM START TIME)
MAX AMP
0.0
100.0
200.0
300.0
400.0
500.0
15.5919
34.1839
26.2709
14.9878
41.7177
Z
N
E
R
T
EVENT: DATE = 1/9/82 (2-9) ORIGIN = 12:53:51.8
NEW BRUNSWICK MAINSHOCK - 1/9/82
LAT. = 46.984 DEG.N LONG. = 66.656 DEG.W MB = 5.7
BAZ = 0.8527 DEG DIST = 10.17 DEG DEPTH = 7 KM
STATION: SCP(DWWSSN) LAT.= 40.795 DEG.N LONG.= 77.865 DEG.W
START TIME = 12:56:57.48

Figure A2 - 2

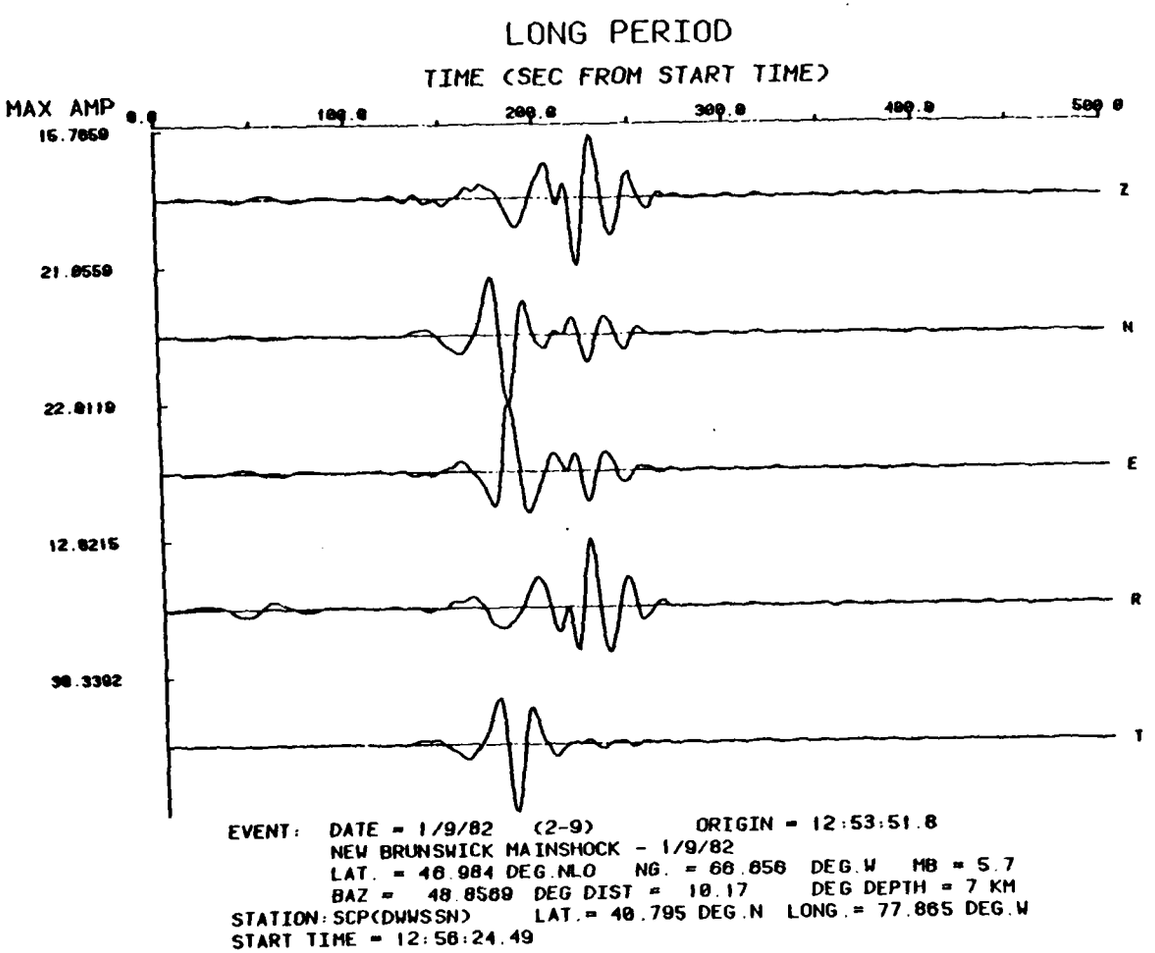
LONG PERIOD
TIME (SEC FROM START TIME)
MAX AMP
0.0
100.0
200.0
300.0
400.0
500.0
15.7659
Z
21.0559
N
22.8119
E
12.8215
R
30.3302
T
EVENT: DATE = 1/9/82 (2-9) ORIGIN = 12:53:51.8
NEW BRUNSWICK MAINSHOCK - 1/9/82
LAT. = 46.984 DEG.NLO NG. = 66.656 DEG.W MB = 5.7
BAZ = 48.8569 DEG DIST = 10.17 DEG DEPTH = 7 KM
STATION: SCP(DWWSSN) LAT.= 40.795 DEG.N LONG.= 77.865 DEG.W
START TIME = 12:56:24.49

Figure A2 - 3

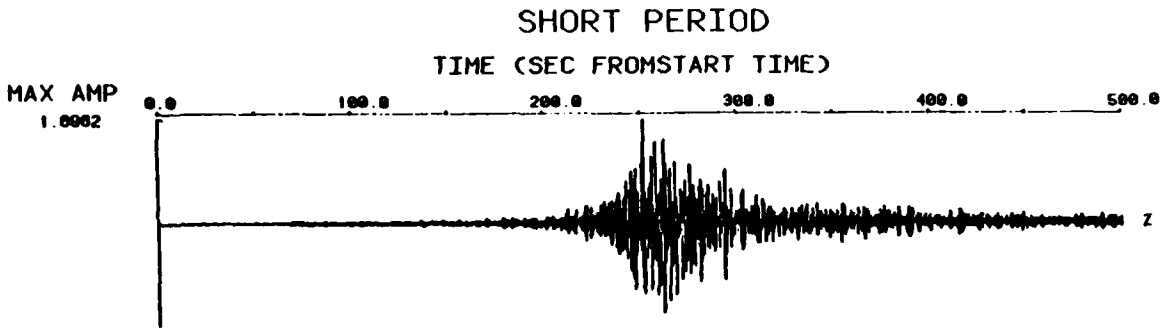

EVENT: DATE = 1/9/82 (2-9) ORIGIN = 16:36:43.6
NEW BRUNSWICK - AFTERSHOCK
LAT. = 48.98 DEG.N LONG. = 66.66 DEG.W MB = 5.0
BAZ = 48.8673 DEG DIST = 10.17 DEG DEPTH = 10
STATION:SCP(DWWSSN) LAT.= 40.795 DEG.N LONG.= 77.865 DEG.W
START TIME = 16:38:3.48

Figure A2 - 4

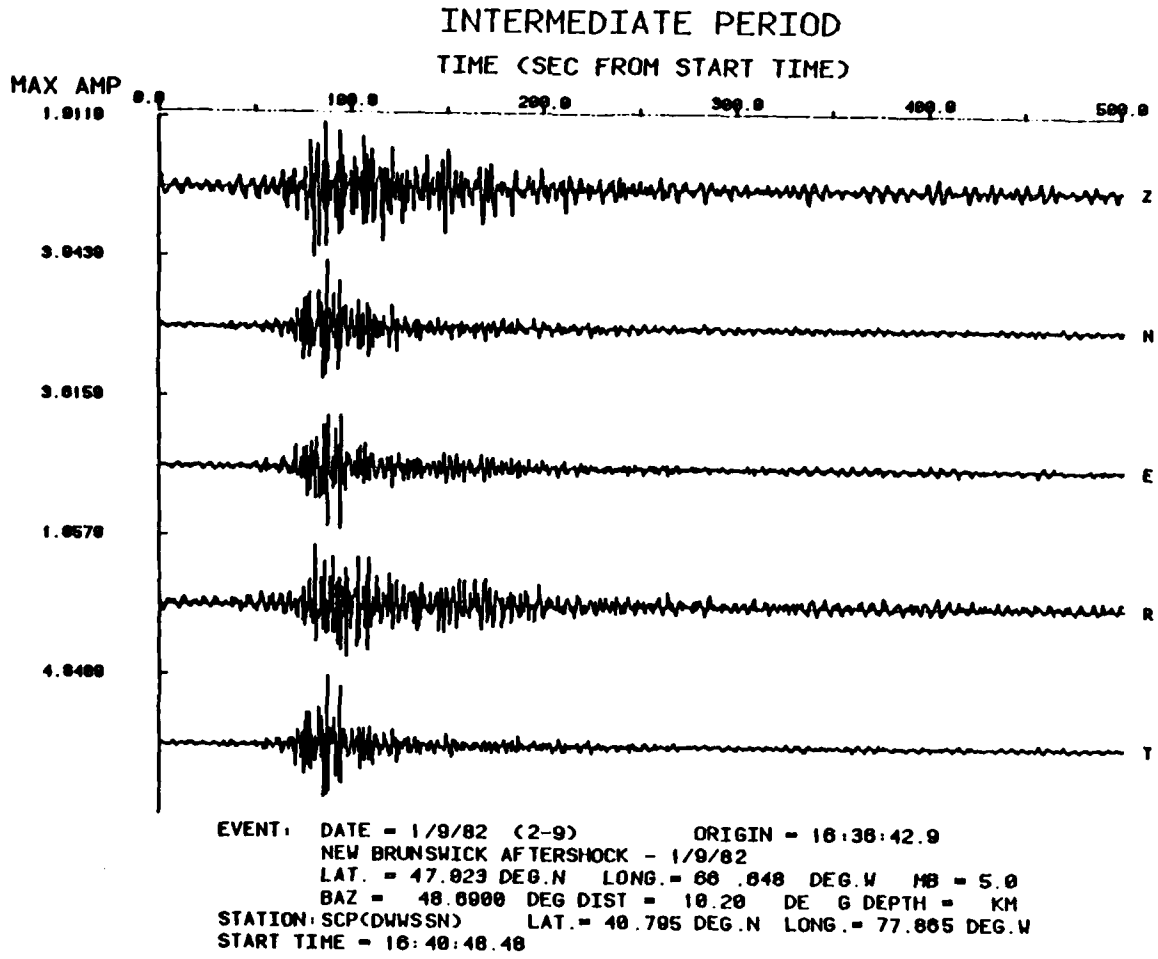
INTERMEDIATE PERIOD
TIME (SEC FROM START TIME)
MAX AMP
1.9119
3.8438
3.8158
1.8578
4.8488
0.0
100.0
200.0
300.0
400.0
500.0
Z
N
E
R
T
EVENT: DATE = 1/9/82 (2-9) ORIGIN = 16:38:42.9
NEW BRUNSWICK AFTERSHOCK - 1/9/82
LAT. = 47.023 DEG.N LONG.= 66 .648 DEG.W MB = 5.0
BAZ = 48.6900 DEG DIST = 10.20 DE G DEPTH = KM
STATION: SCP(DWWSSN) LAT.= 40.795 DEG.N LONG.= 77.865 DEG.W
START TIME = 16:40:48.48

Figure A2 - 5

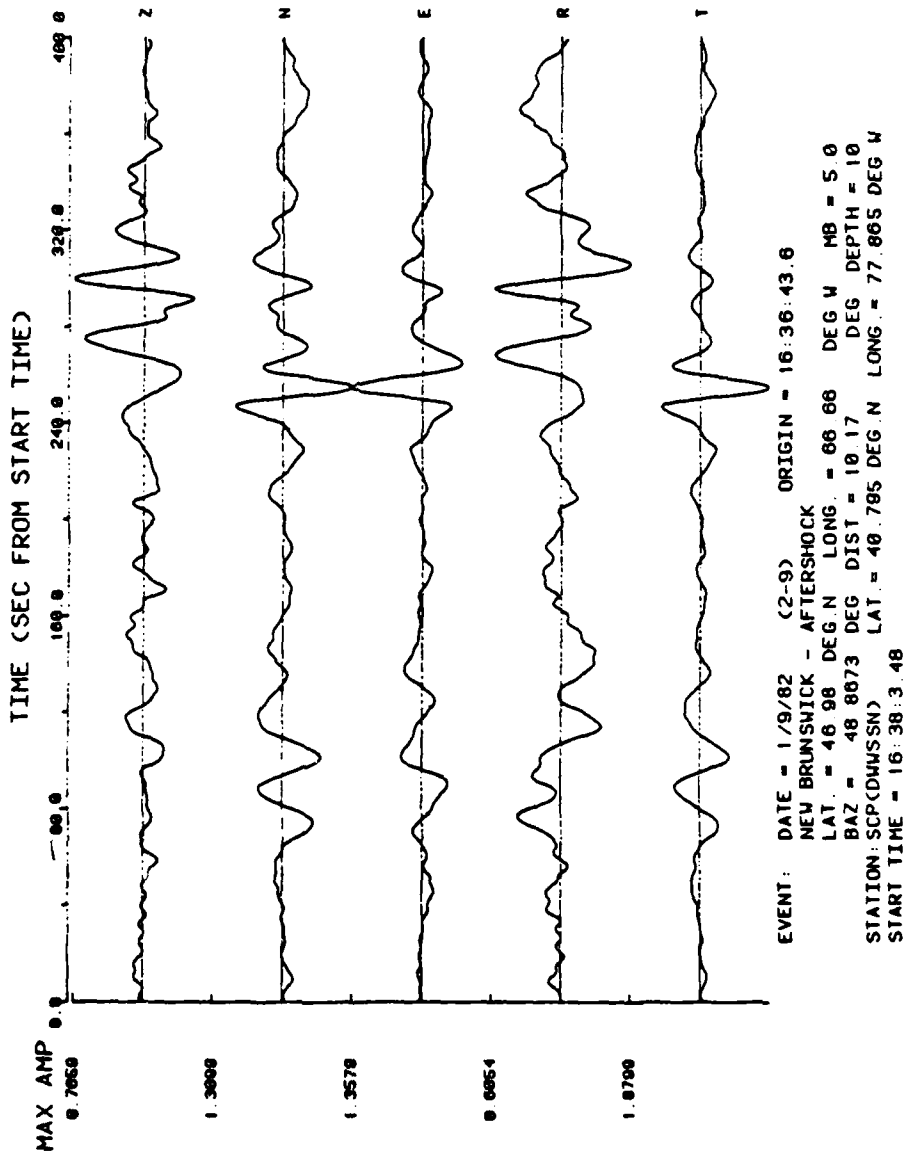
LONG PERIOD
TIME (SEC FROM START TIME)
MAX AMP
Z
N
E
R
T
EVENT: DATE = 1/9/82 (2-9) ORIGIN = 16:36:43.6
NEW BRUNSWICK - AFTERSHOCK
LAT. = 46.98 DEG.N LONG. = 66.66 DEG W MB = 5.0
BAZ = 48.8073 DEG DIST = 10.17 DEG DEPTH = 10
STATION: SCP(DWWSSN) LAT. = 40.795 DEG.N LONG. = 77.865 DEG W
START TIME = 16:38:3.48

Figure A2 - 6

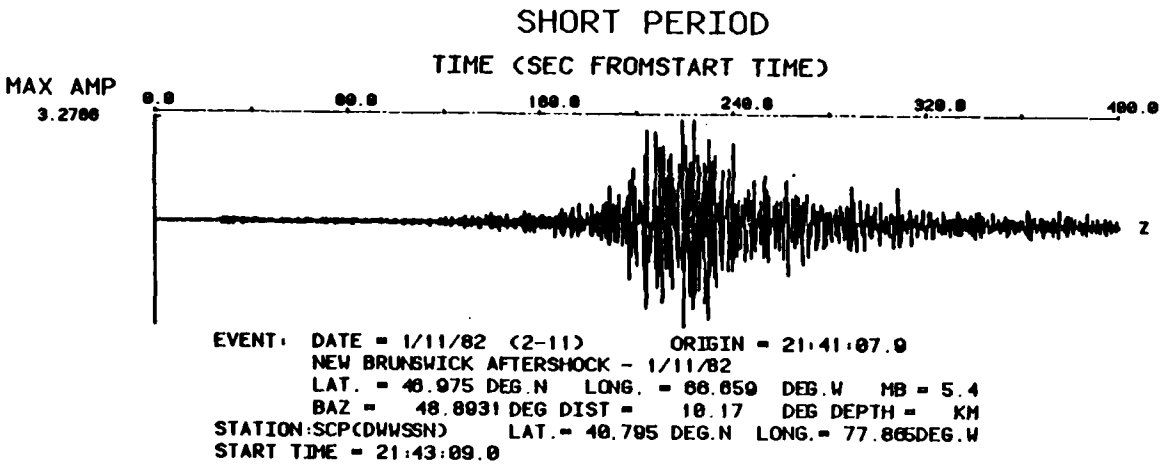
SHORT PERIOD
TIME (SEC FROMSTART TIME)
MAX AMP
3.2788
0.0
80.0
160.0
240.0
320.0
400.0
Z
EVENT: DATE = 1/11/82 (2-11) ORIGIN = 21:41:07.9
NEW BRUNSWICK AFTERSHOCK - 1/11/82
LAT. = 46.975 DEG.N LONG. = 66.659 DEG.W MB = 5.4
BAZ = 48.8931 DEG DIST = 10.17 DEG DEPTH = KM
STATION:SCP(DWWSSN) LAT.= 40.795 DEG.N LONG.= 77.865DEG.W
START TIME = 21:43:09.0

Figure A2 - 7

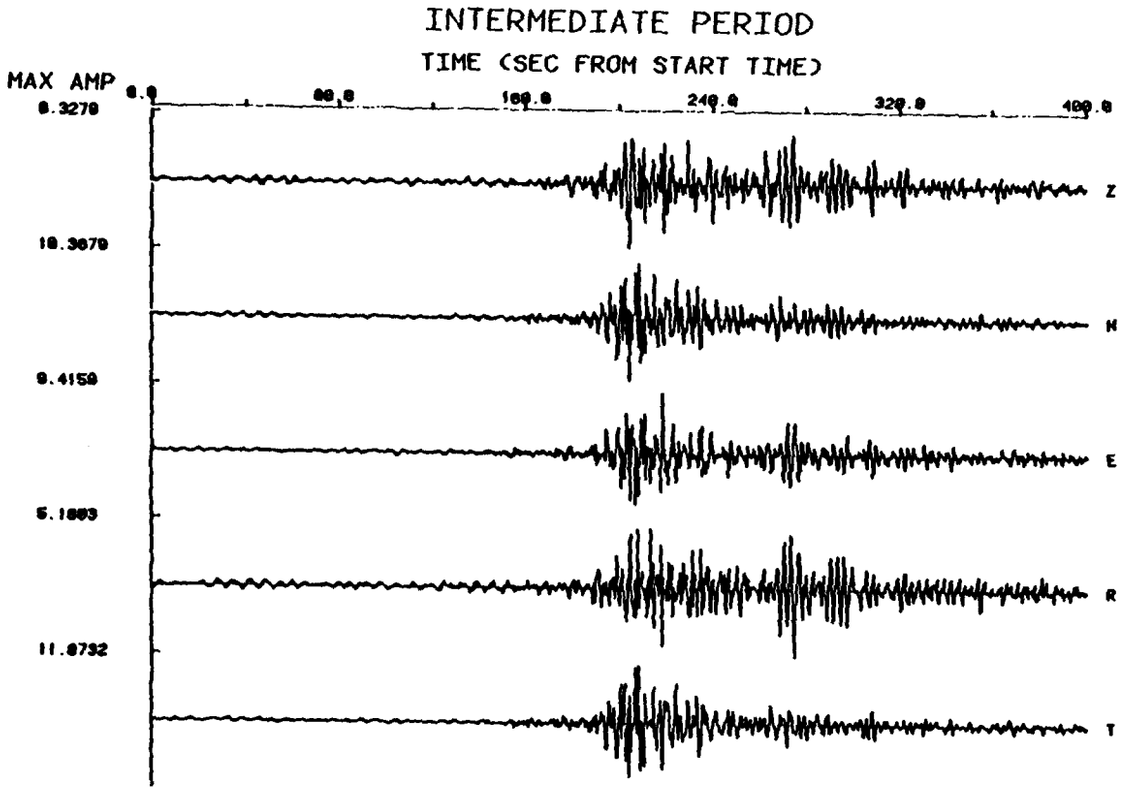
INTERMEDIATE PERIOD
TIME (SEC FROM START TIME)
MAX AMP
0.3270
80.0
160.0
240.0
320.0
400.0
10.3670
9.4150
5.1803
11.0732
Z
N
E
R
T
EVENT: DATE = 1/11/82 (2-11) ORI GIN = 21:41:07.9
NEW BRUNSWICK AFTERSHOCK - 1/11/82
LAT. = 46.975 DEG.N LONG. = 66.659 DEG.W MB = 5.4
BAZ = 46.8931 DEG DIST = 10.17 DEG DEPTH = KM
STATION: SCP(DWWSSN) LAT.= 40.795 DEG.N LONG.= 77.865 DEG.W
START TIME = 21:43 :09.0

Figure A2 - 8

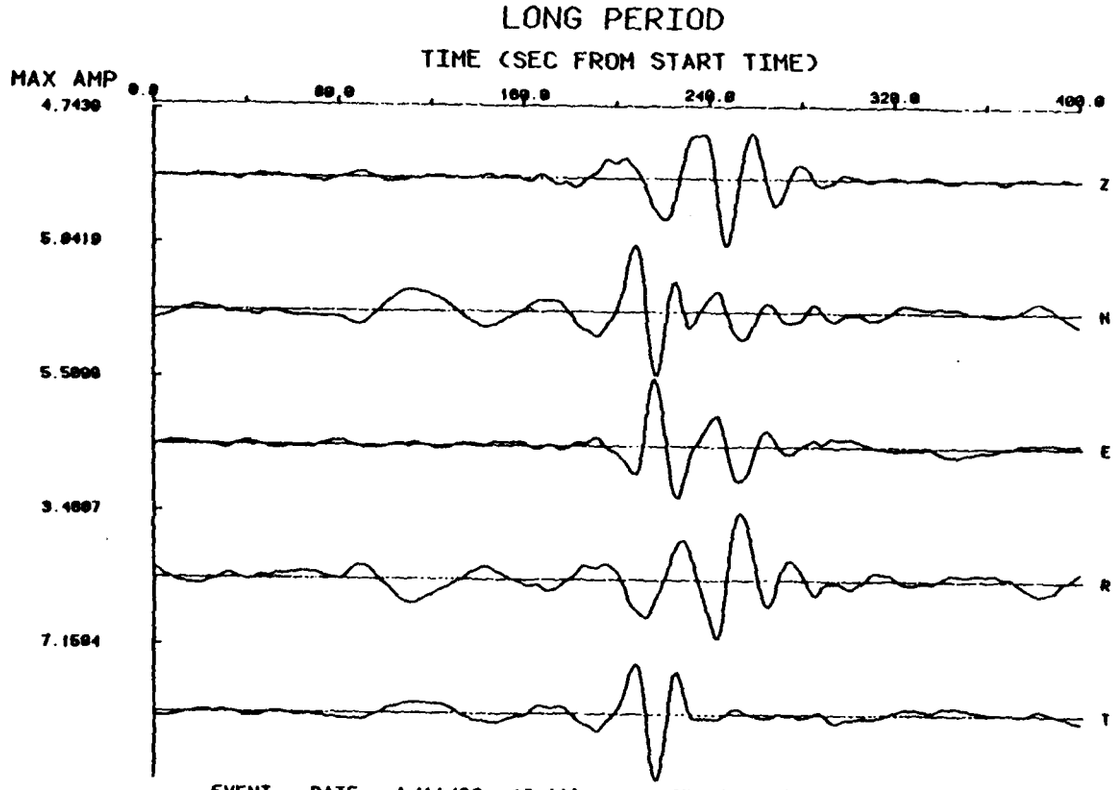
LONG PERIOD
TIME (SEC FROM START TIME)
MAX AMP
4.7430
5.0419
5.5000
3.4007
7.1584
0.0
80.0
160.0
240.0
320.0
400.0
Z
N
E
R
T
EVENT: DATE = 1/11/82 (2-11) ORIGIN = 21:41:07.9
NEWBRUN SWICK AFTERSHOCK - 1/11/82
LAT. = 48.975 DEG.N LONG. = 66.659 DEG.W MB = 5.4
BAZ = 48.6031 DEG DIST = 10.17 DEG DEPTH = KM
STATION: SCP(DWWSSN) LAT.= 40.705 DEG.N LONG.=77.86 5 DEG.W
START TIME = 21:43:09.0

Figure A2 - 9

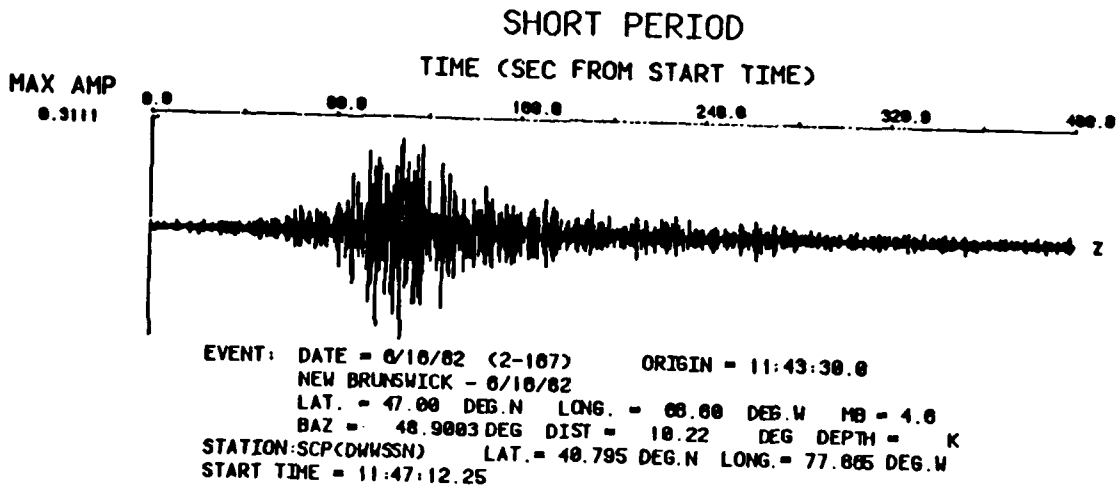
SHORT PERIOD
TIME (SEC FROM START TIME)
MAX AMP
0.9111
0.0
80.0
160.0
240.0
320.0
400.0
Z
EVENT: DATE = 6/16/82 (2-167) ORIGIN = 11:43:30.0
NEW BRUNSWICK - 6/16/82
LAT. = 47.00 DEG.N LONG. = 66.60 DEG.W MB = 4.6
BAZ = 48.9003 DEG DIST = 10.22 DEG DEPTH = K
STATION:SCP(DWWSSN) LAT.= 40.795 DEG.N LONG.= 77.865 DEG.W
START TIME = 11:47:12.25

Figure A2 - 10

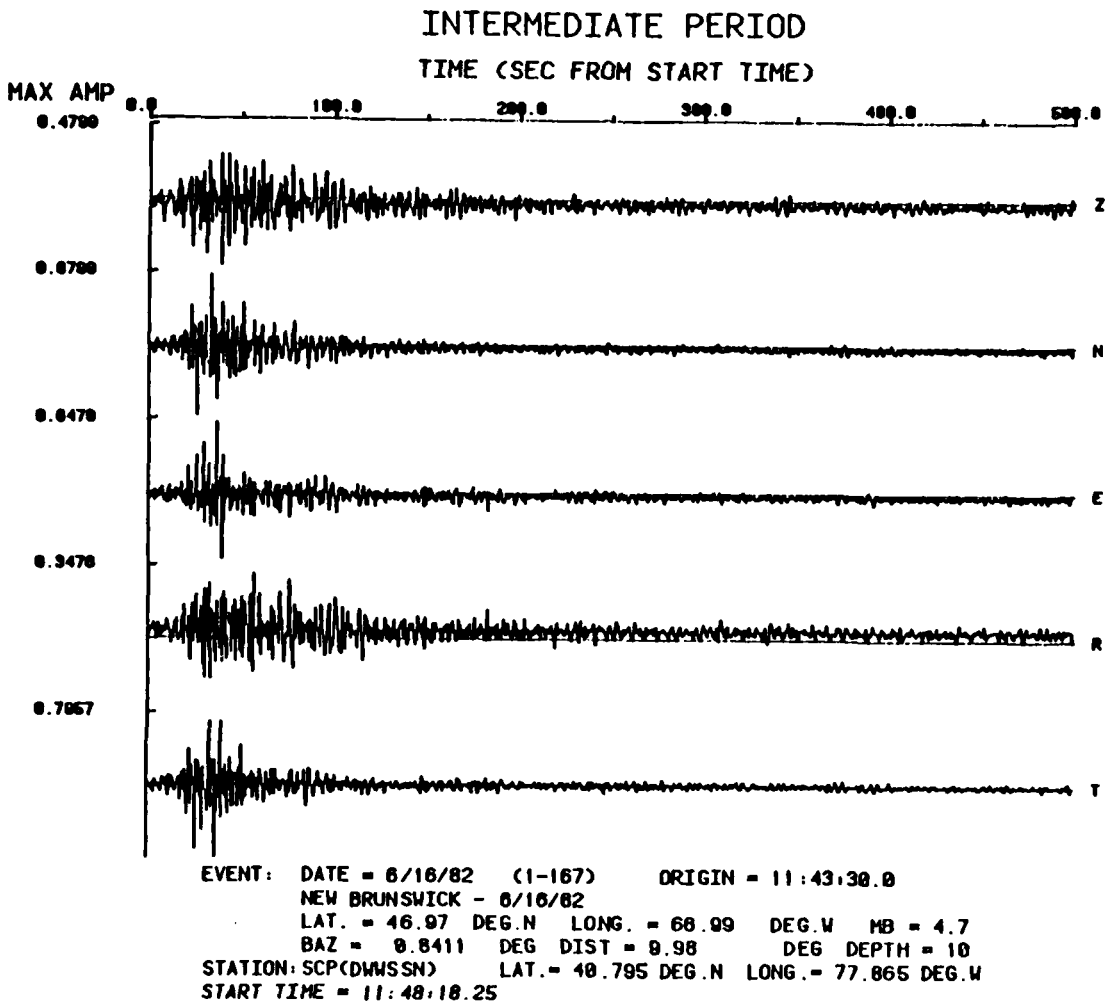
INTERMEDIATE PERIOD
TIME (SEC FROM START TIME)
MAX AMP
0.4700
0.0700
0.0470
0.3470
0.7057
0.0
100.0
200.0
300.0
400.0
500.0
Z
N
E
R
T
EVENT: DATE = 6/16/82 (1-167) ORIGIN = 11:43:30.0
NEW BRUNSWICK - 6/16/82
LAT. = 46.97 DEG.N LONG. = 66.99 DEG.W MB = 4.7
BAZ = 0.8411 DEG DIST = 9.98 DEG DEPTH = 10
STATION: SCP(DWWSSN) LAT.= 40.795 DEG.N LONG.= 77.865 DEG.W
START TIME = 11:48:18.25

Figure A2 - 11

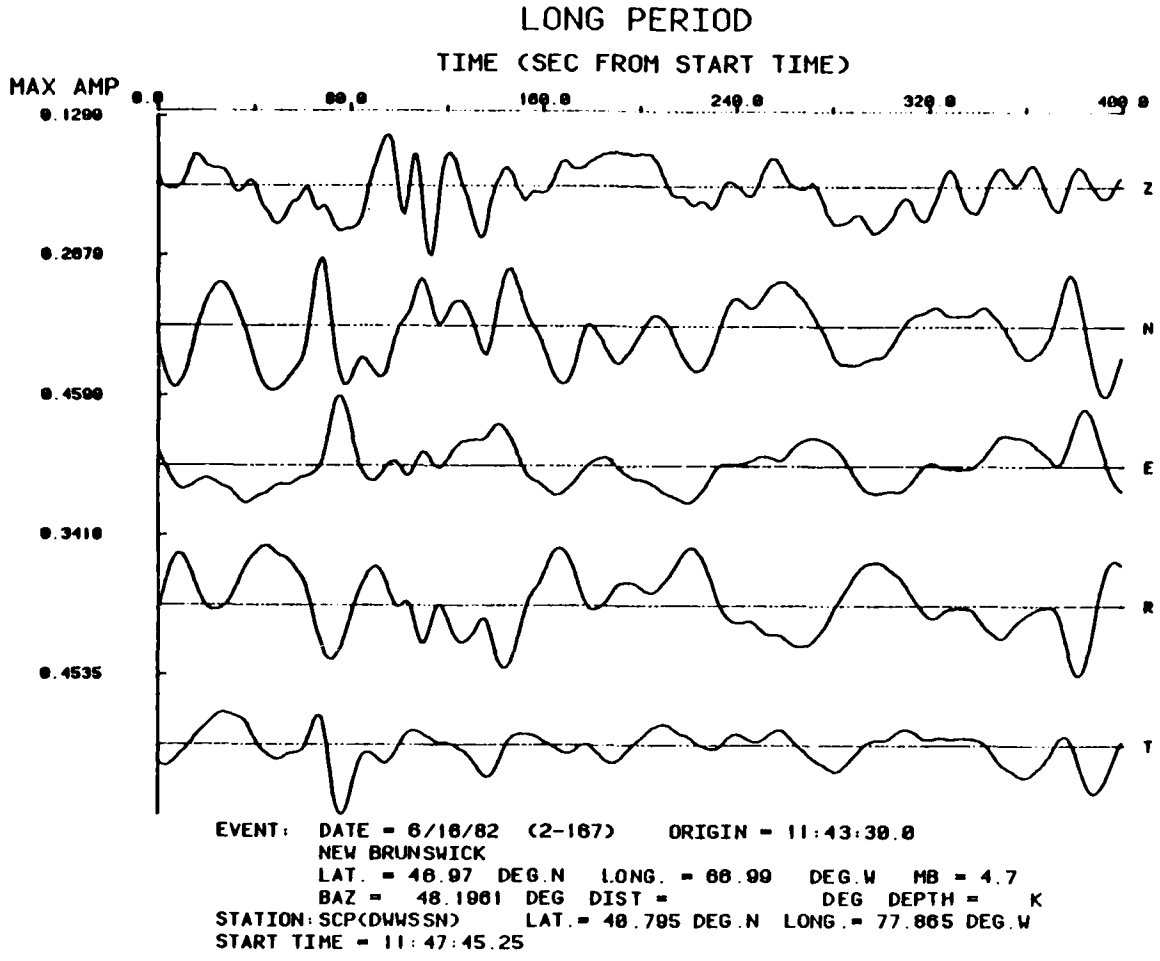
LONG PERIOD
TIME (SEC FROM START TIME)
MAX AMP
0.0
80.0
160.0
240.0
320.0
400.0
0.1200
0.2070
0.4500
0.3410
0.4535
Z
N
E
R
T
EVENT: DATE = 6/16/82 (2-167) ORIGIN = 11:43:30.0
NEW BRUNSWICK
LAT. = 46.97 DEG.N LONG. = 66.99 DEG.W MB = 4.7
BAZ = 48.1961 DEG DIST = DEG DEPTH = K
STATION: SCP(DWWSSN) LAT.= 40.795 DEG.N LONG.= 77.865 DEG.W
START TIME = 11:47:45.25

Figure A2 - 12

APPENDIX 3

Band-Pass Filtered Seismograms

From Mainshock

And Three Aftershocks

The figures in Appendix 3 include all bandpass filter results, as obtained from the short, intermediate, and long period data for the four events considered in this paper. Each figure includes the original seismogram (at the bottom of the page) and results of applying a suite of band-pass filters centered on selected frequencies. The time scale is 25 seconds per tick mark at the top of the figure. On the left, the filter parameters (lower cutoff, lower corner, upper corner, and upper cutoff frequencies as described in Chapter 4) are given for each band-pass and, on the right, are peak amplitudes, by trace, expressed in microns. Each trace is normalized to this peak amplitude. Filter parameters common to each suite are detailed on a separated page for clarity. In some cases, only the envelopes of the band-passes are displayed in an effort to bypass the significant cost of plotting the carrier signal.

Figures A3-1 through A3-12 include three suites of short period filters ordered by event date (January 9 mainshock, January 9 aftershock, January 11 aftershock, and June 16 event). Figures A3-13 through A3-42 are the results of applying four suites of intermediate period filters, again ordered by event date. Figures A3-43 through A3-54 present the long period results for all but the June 16 event where noise obscured the filtered signal completely. Short period filters were applied to the vertical component (SPZ) only; intermediate and long period filters were applied to both vertical and transverse components (IPZ, IPT, LPZ, LPT).

The filter parameters for Figures A3 - 1 through 4 are as indicated:

FL = 8.470	FLC = 8.475	FHC = 8.525	FH = 8.530
FL = 7.970	FLC = 7.975	FHC = 8.025	FH = 8.030
FL = 7.470	FLC = 7.475	FHC = 7.525	FH = 7.530
FL = 6.970	FLC = 6.975	FHC = 7.025	FH = 7.030
FL = 6.470	FLC = 6.475	FHC = 6.525	FH = 6.530
FL = 5.970	FLC = 5.975	FHC = 6.025	FH = 6.030
FL = 5.470	FLC = 5.475	FHC = 5.525	FH = 5.530
FL = 4.970	FLC = 4.975	FHC = 5.025	FH = 5.030

OBSERVED SIGNAL

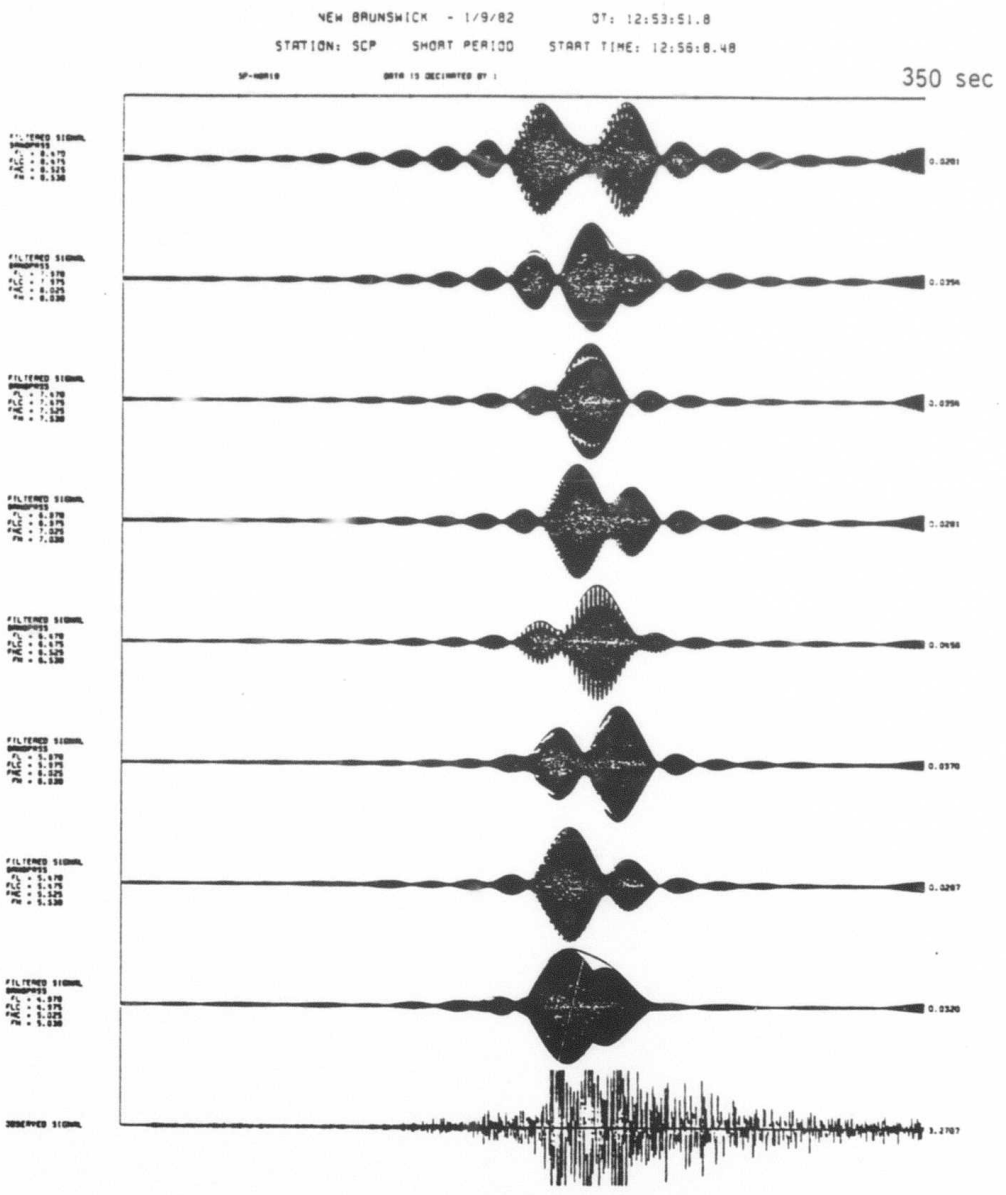
NEW BRUNSWICK - 1/9/82 OT: 12:53:51.8
STATION: SCP SHORT PERIOD START TIME: 12:56:8.48
350 sec
FILTERED SIGNAL
OBSERVED SIGNAL

Figure A3 - 1

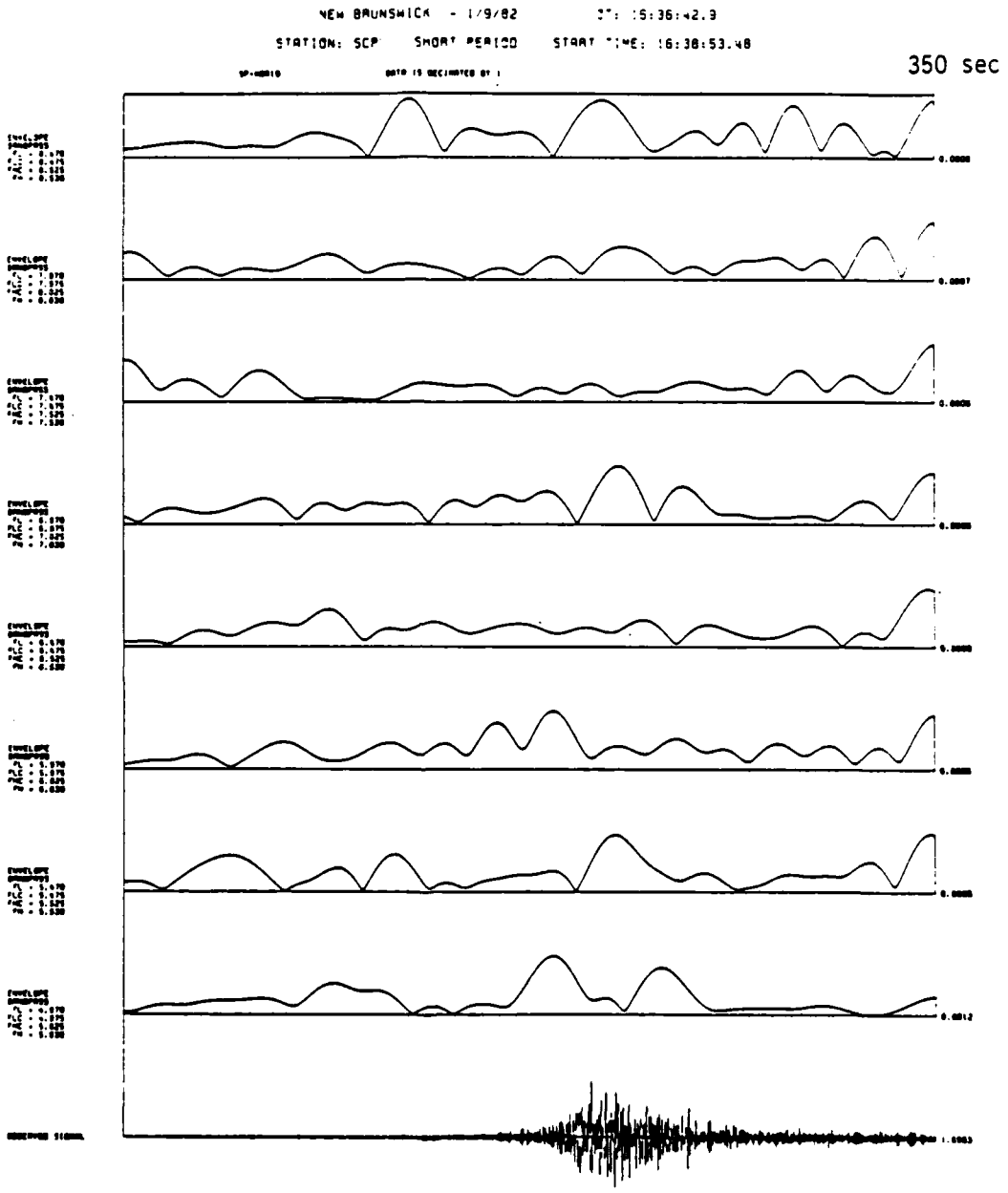

Figure A3 - 2

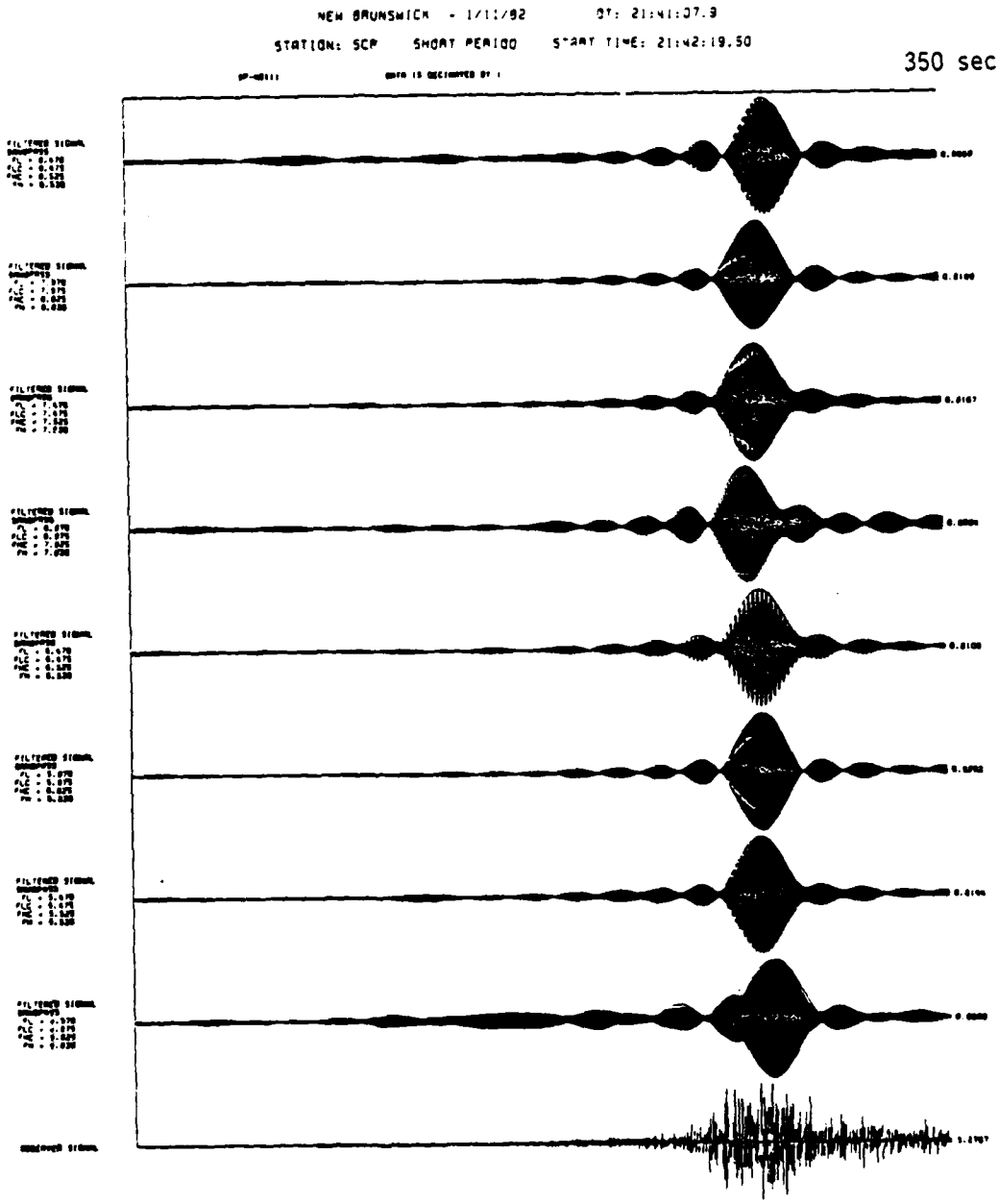

Figure A3 - 3

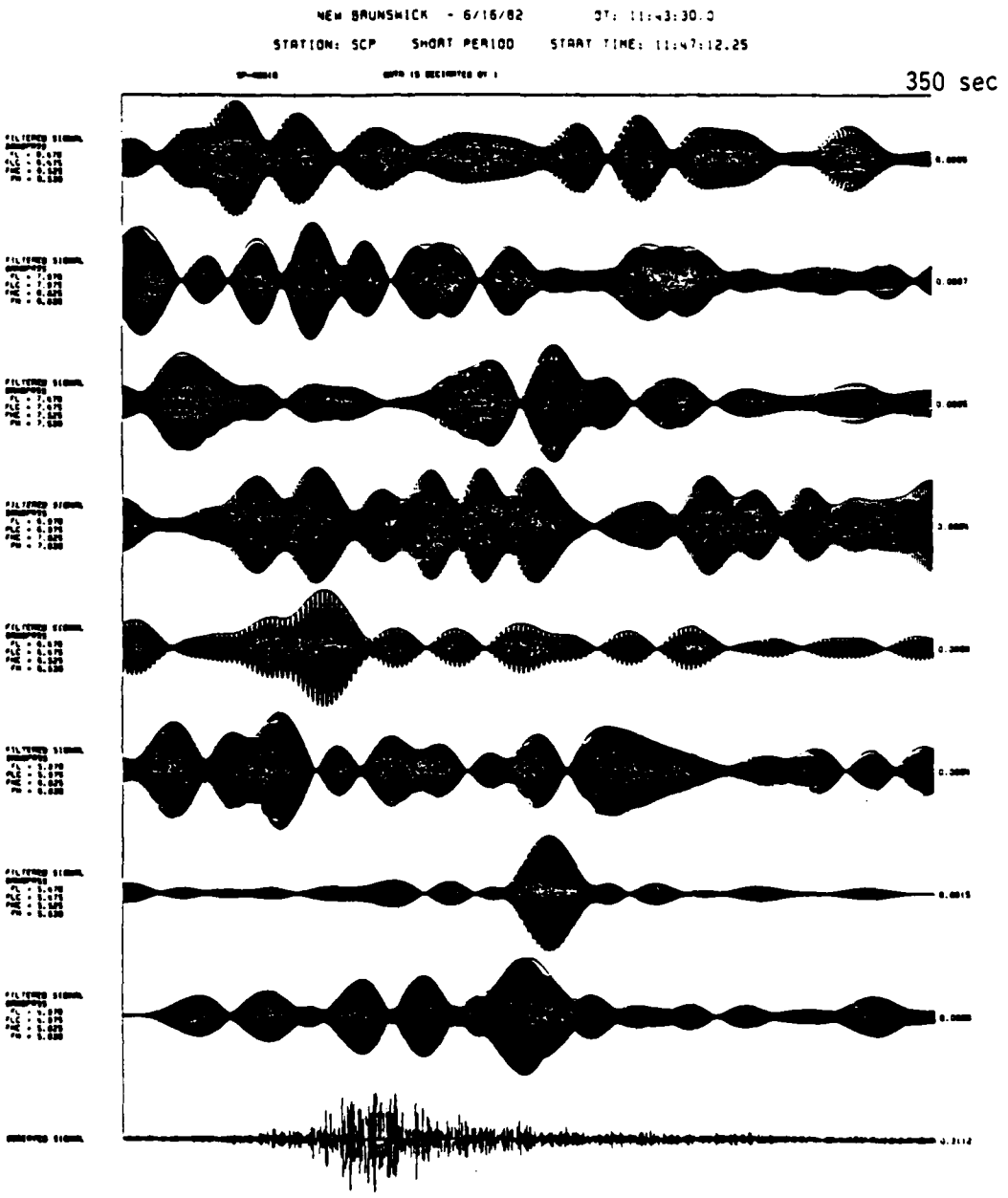
NEW BRUNSWICK - 6/16/82
STATION: SCP SHORT PERIOD START TIME: 11:47:12.25
350 sec

Figure A3 - 4

The filter parameters for Figures A3 - 5 through 8 are as indicated:

FL = 4.470	FLC = 4.475	FHC = 4.525	FH = 4.530
FL = 3.970	FLC = 3.975	FHC = 4.025	FH = 4.030
FL = 3.470	FLC = 3.475	FHC = 3.525	FH = 3.530
FL = 2.970	FLC = 2.975	FHC = 3.025	FH = 3.030
FL = 2.470	FLC = 2.475	FHC = 2.525	FH = 2.530
FL = 1.970	FLC = 1.975	FHC = 2.025	FH = 2.030
FL = 1.470	FLC = 1.475	FHC = 1.525	FH = 1.530
FL = 0.970	FLC = 0.975	FHC = 1.025	FH = 1.030

OBSERVED SIGNAL

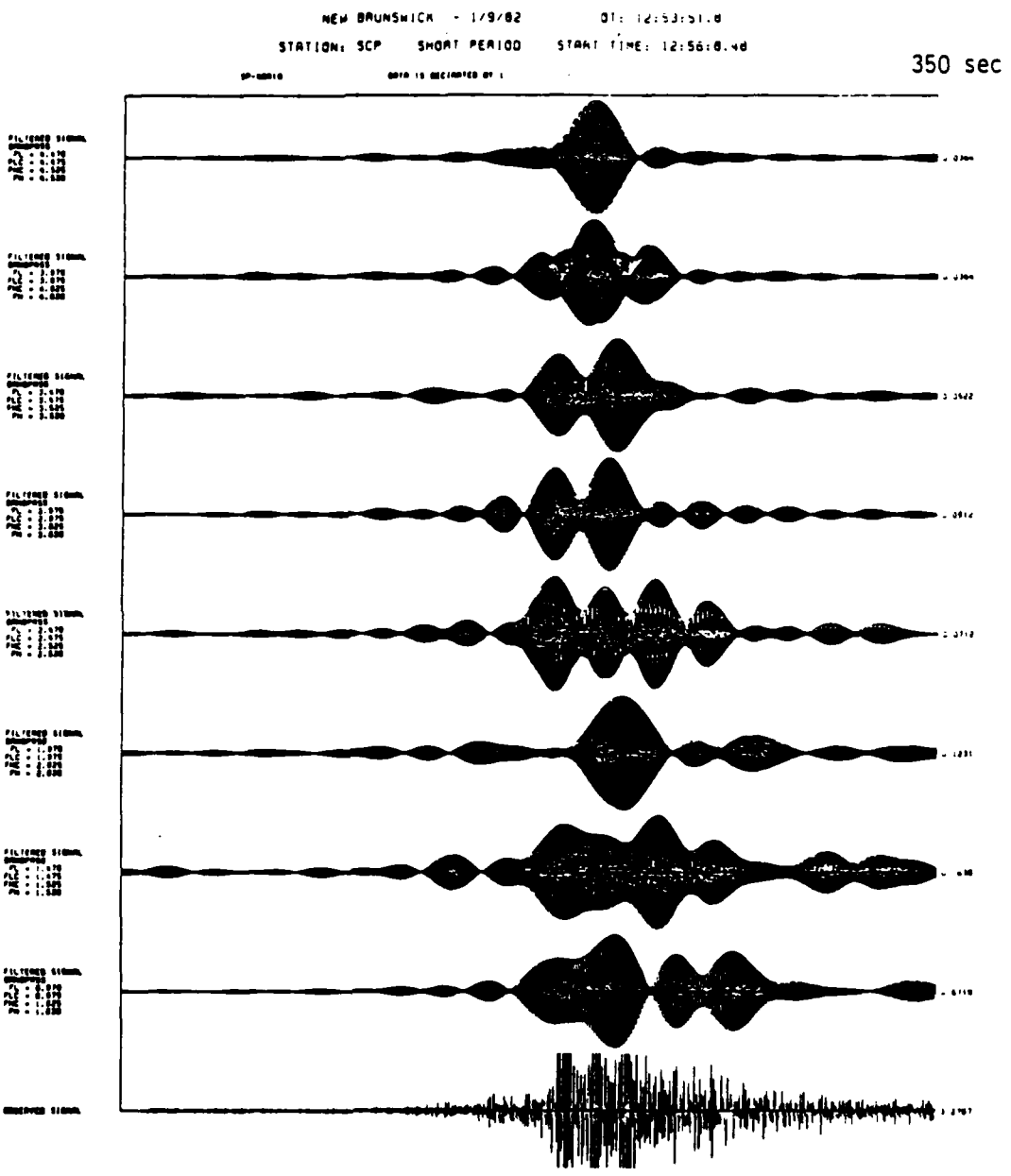
NEW BRUNSWICK - 1/9/82
STATION: SCP SHORT PERIOD START TIME: 12:56:8.48
350 sec

Figure A3 - 5

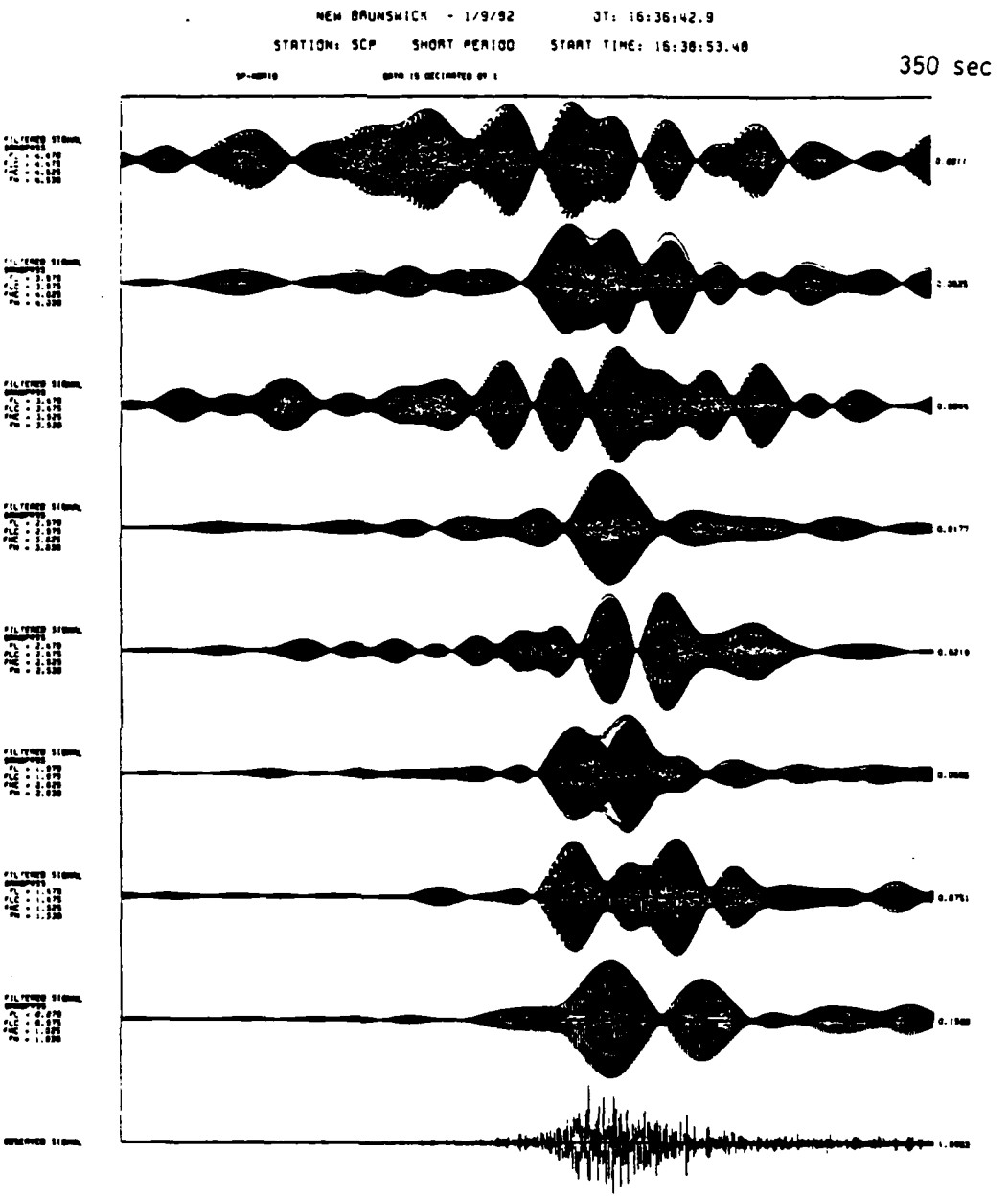
NEW BRUNSWICK - 1/9/92
OT: 16:36:42.9
STATION: SCP SHORT PERIOD START TIME: 16:38:53.48
350 sec

Figure A3 - 6

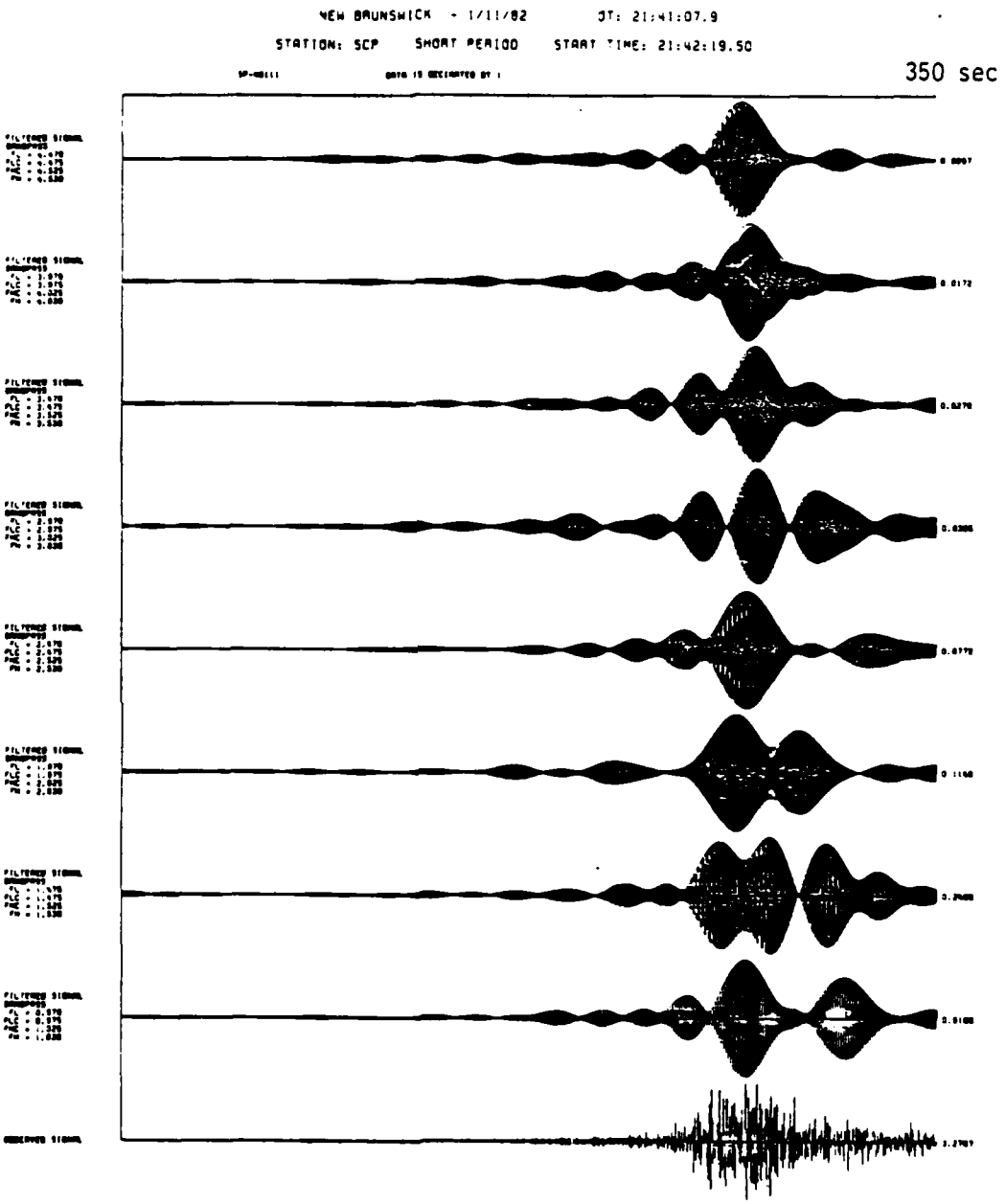
NEW BRUNSWICK - 1/11/82 OT: 21:41:07.9
STATION: SCP SHORT PERIOD START TIME: 21:42:19.50
350 sec

Figure A3 - 7

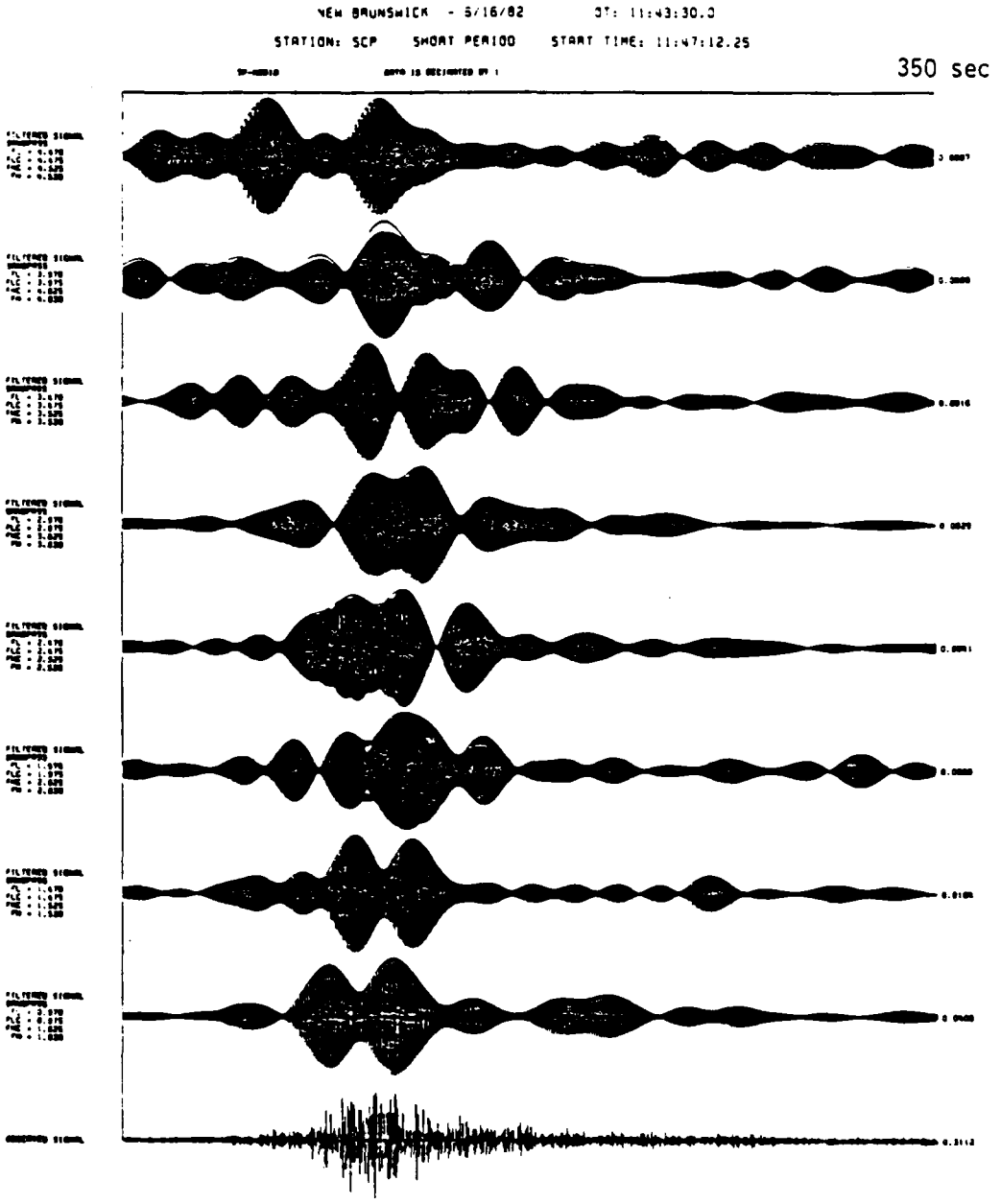
NEW BRUNSWICK - 5/16/82 OT: 11:43:30.0
STATION: SCP SHORT PERIOD START TIME: 11:47:12.25
350 sec

Figure A3 - 8

The filter parameters for Figures A3 - 9 through 12 are as indicated:

FL = 0.770	FLC = 0.775	FHC = 0.825	FH = 0.830
FL = 0.670	FLC = 0.675	FHC = 0.725	FH = 0.730
FL = 0.570	FLC = 0.575	FHC = 0.625	FH = 0.630
FL = 0.470	FLC = 0.475	FHC = 0.525	FH = 0.530
FL = 0.370	FLC = 0.375	FHC = 0.425	FH = 0.430
FL = 0.270	FLC = 0.375	FHC = 0.325	FH = 0.330
FL = 0.170	FLC = 0.175	FHC = 0.225	FH = 0.230
FL = 0.070	FLC = 0.075	FHC = 0.125	FH = 0.130

OBSERVED SIGNAL

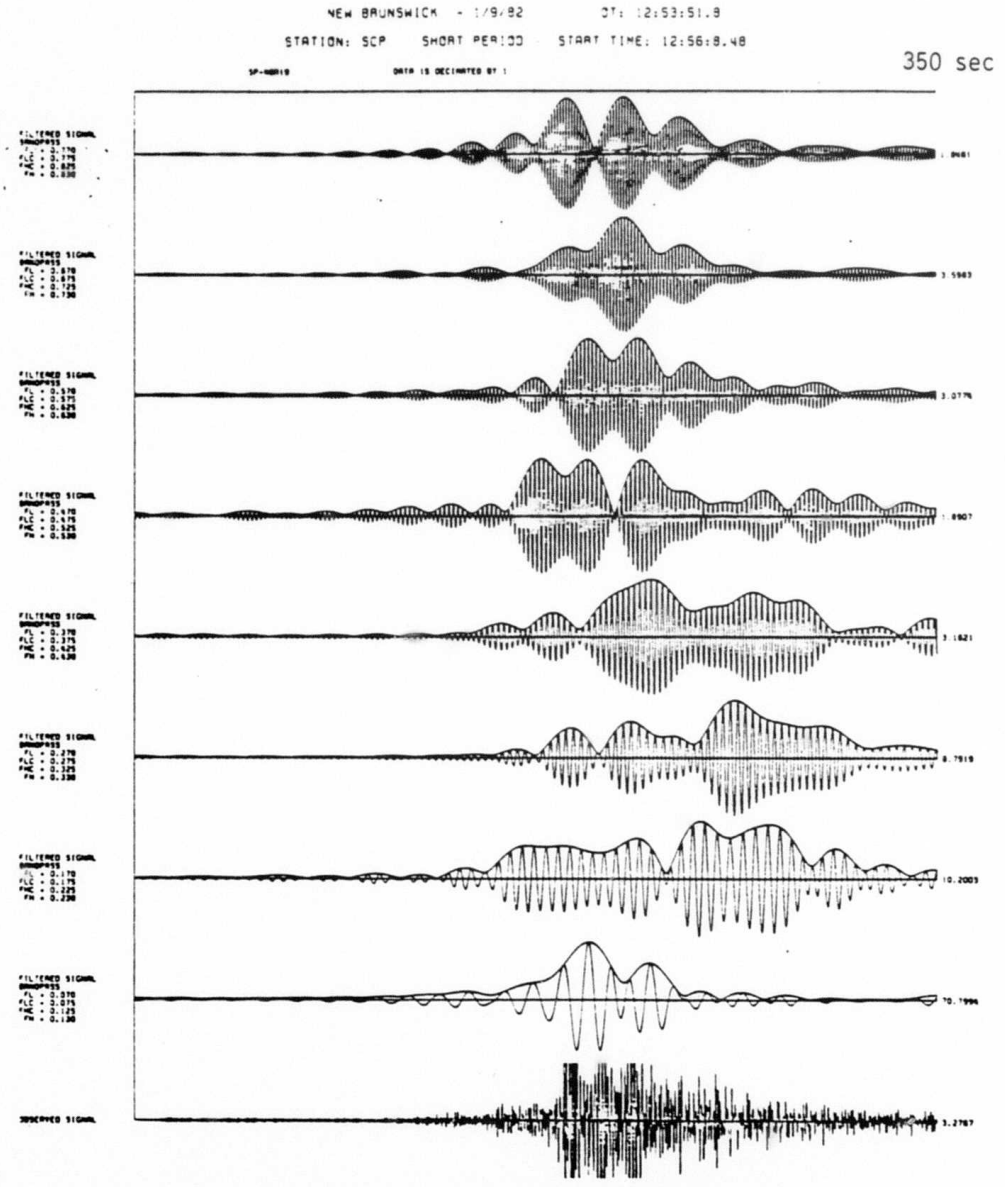
NEW BRUNSWICK - 1/9/82
STATION: SCP SHORT PERIOD START TIME: 12:56:8.48
350 sec

Figure A3 - 9

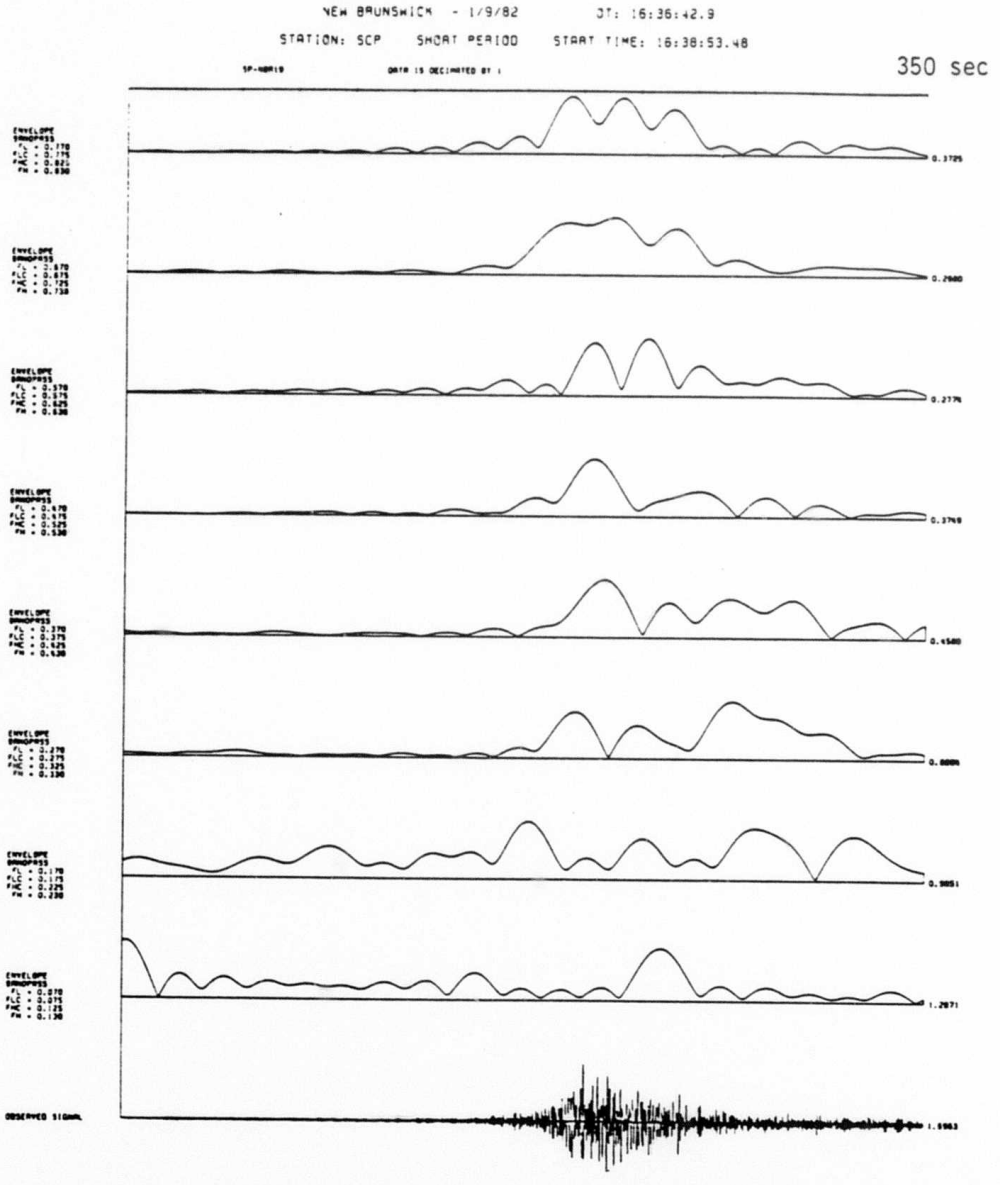
NEW BRUNSWICK - 1/9/82 OT: 16:36:42.9
STATION: SCP SHORT PERIOD START TIME: 16:38:53.48
350 sec

Figure A3 - 10

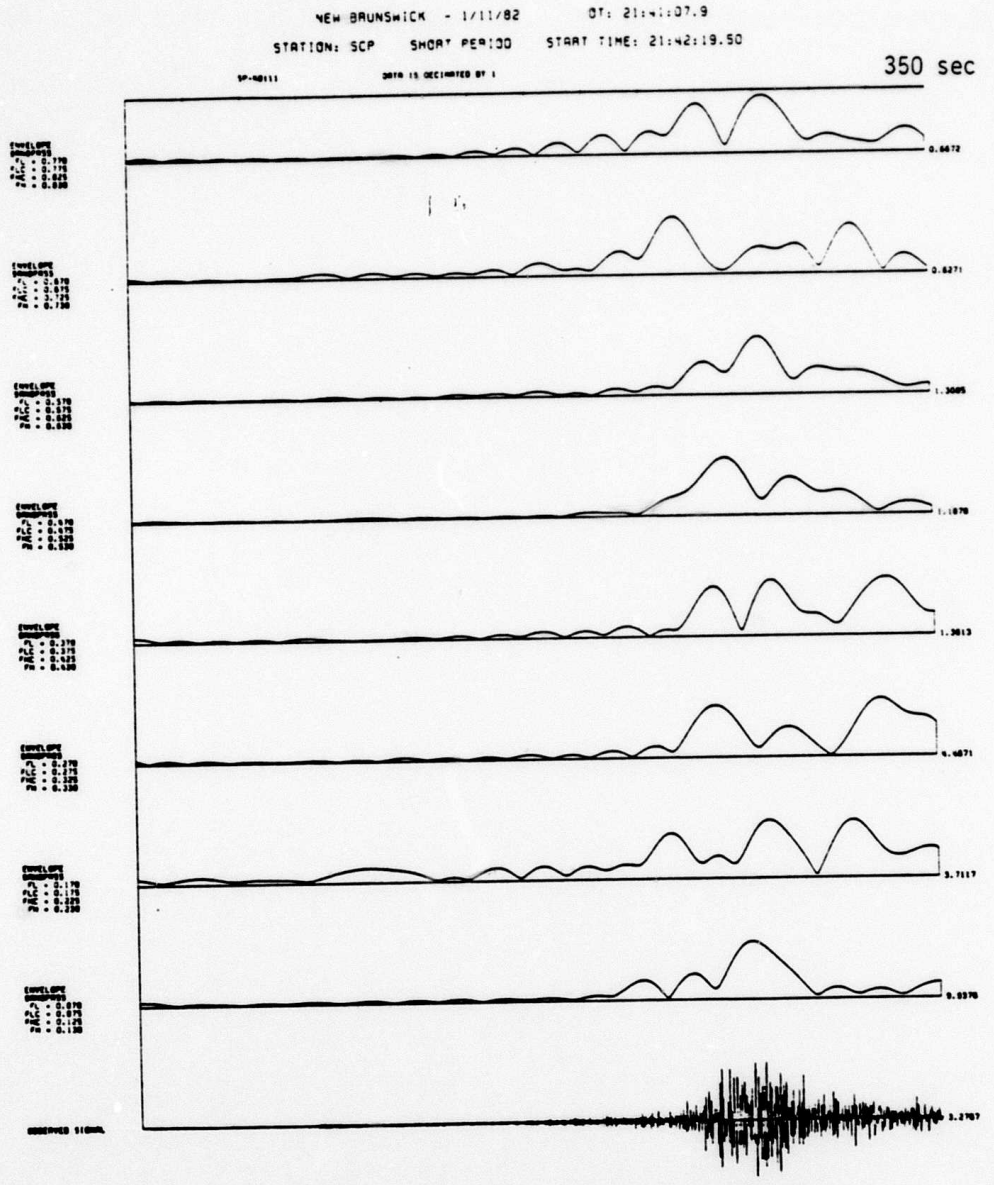
NEW BRUNSWICK - 1/11/82
STATION: SCP SHORT PERIOD START TIME: 21:42:19.50
350 sec

Figure A3 - 11

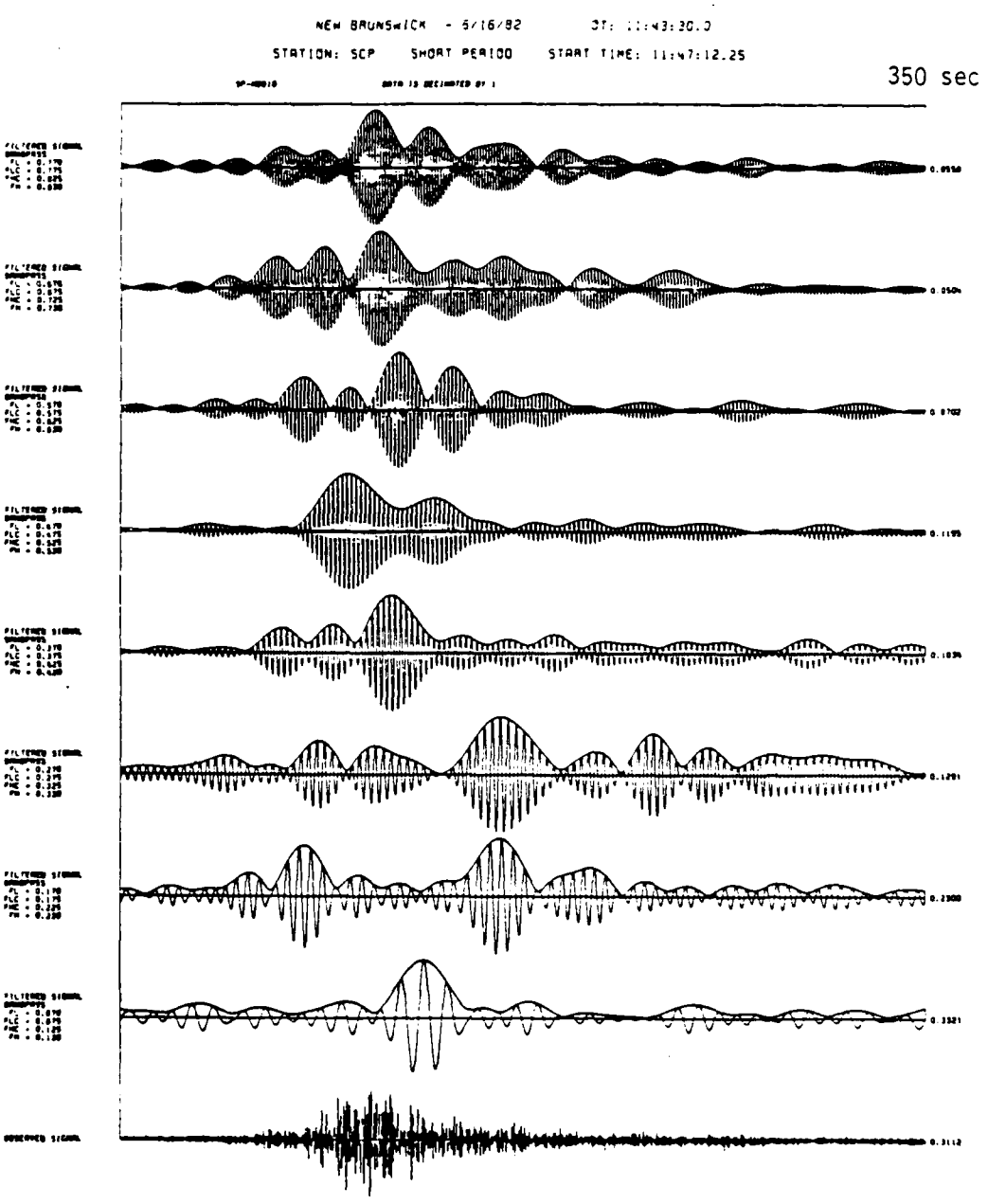
NEW BRUNSWICK - 5/16/82
STATION: SCP SHORT PERIOD START TIME: 11:47:12.25
350 sec

Figure A3 - 12

The filter parameters for Figures A3 - 13 through 20 are as indicated:

FL = 4.470	FLC = 4.475	FHC = 4.525	FH = 4.530
FL = 3.970	FLC = 3.975	FHC = 4.025	FH = 4.030
FL = 3.470	FLC = 3.475	FHC = 3.525	FH = 3.530
FL = 2.970	FLC = 2.975	FHC = 3.025	FH = 3.030
FL = 2.470	FLC = 2.475	FHC = 2.525	FH = 2.530
FL = 1.970	FLC = 1.975	FHC = 2.025	FH = 2.030
FL = 1.470	FLC = 1.475	FHC = 1.525	FH = 1.530
FL = 0.970	FLC = 0.975	FHC = 1.025	FH = 1.030

OBSERVED SIGNAL

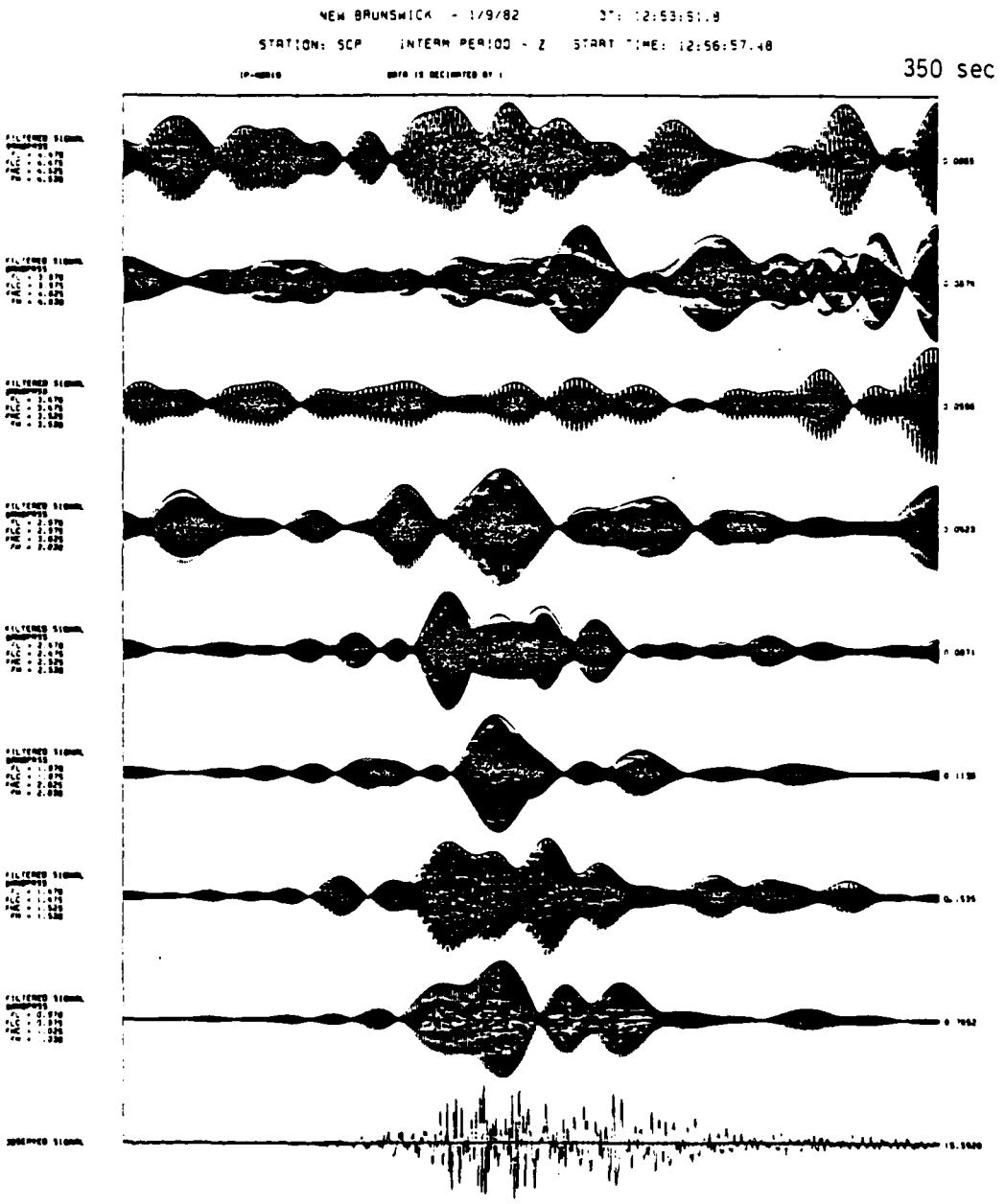

Figure A3 - 13

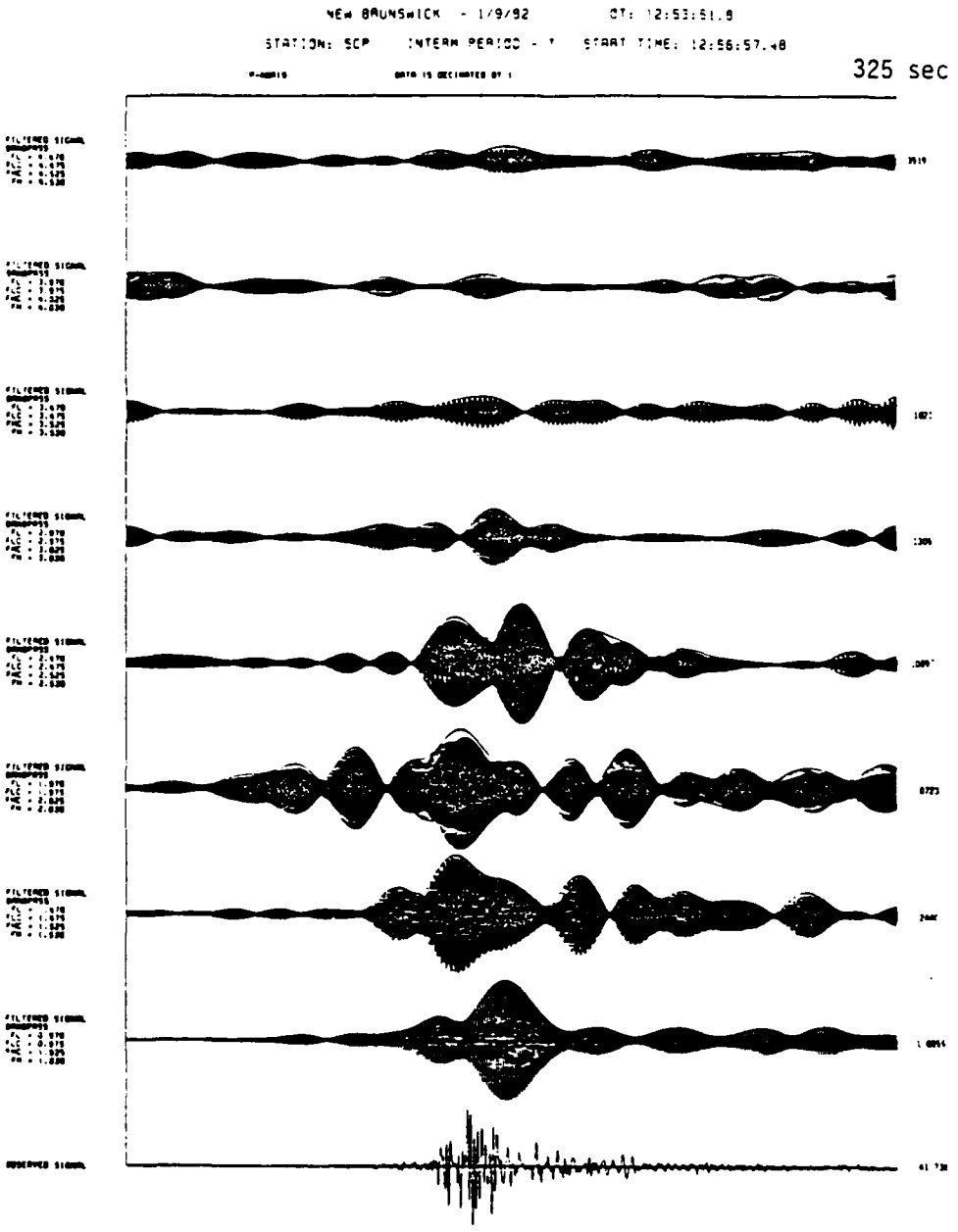
NEW BRUNSWICK - 1/9/92
STATION: SCP
INTERM PERIOD - 7
START TIME: 12:56:57.48
325 sec

Figure A3 - 14

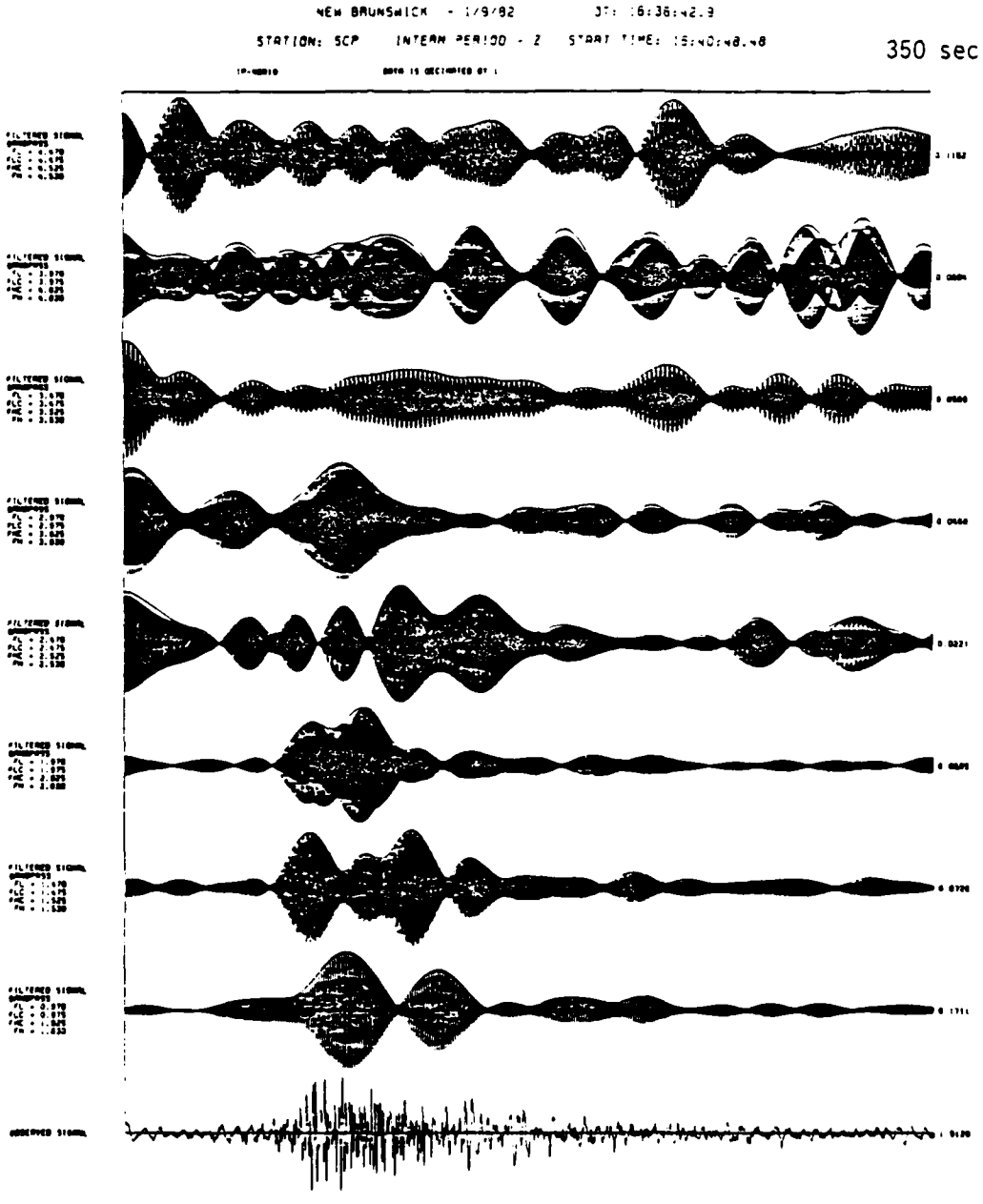

Figure A3 - 15

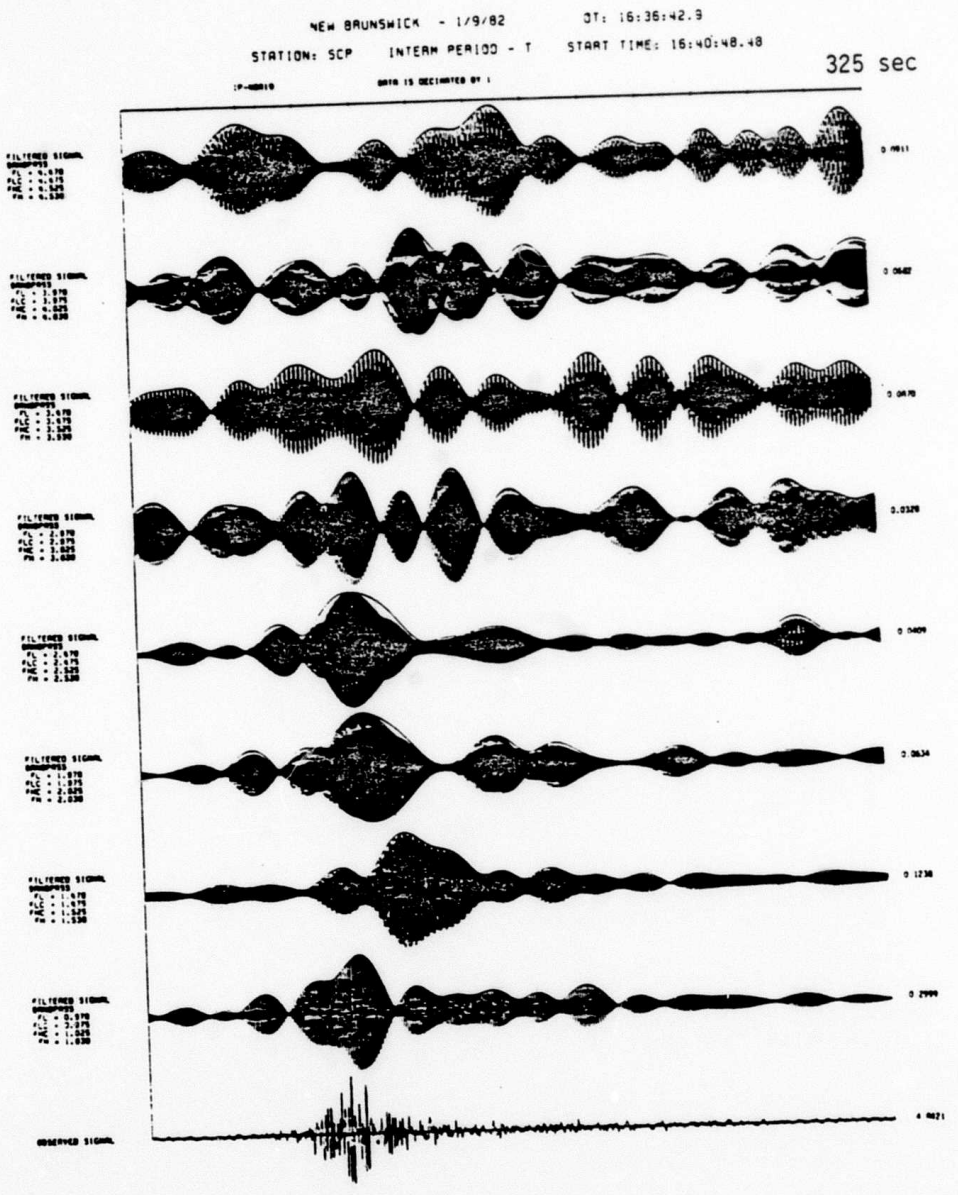
NEW BRUNSWICK - 1/9/82
OT: 16:36:42.9
STATION: SCP INTERN PERIOD - T START TIME: 16:40:48.48
325 sec
FILTERED SIGNAL
OBSERVED SIGNAL

Figure A3 - 16

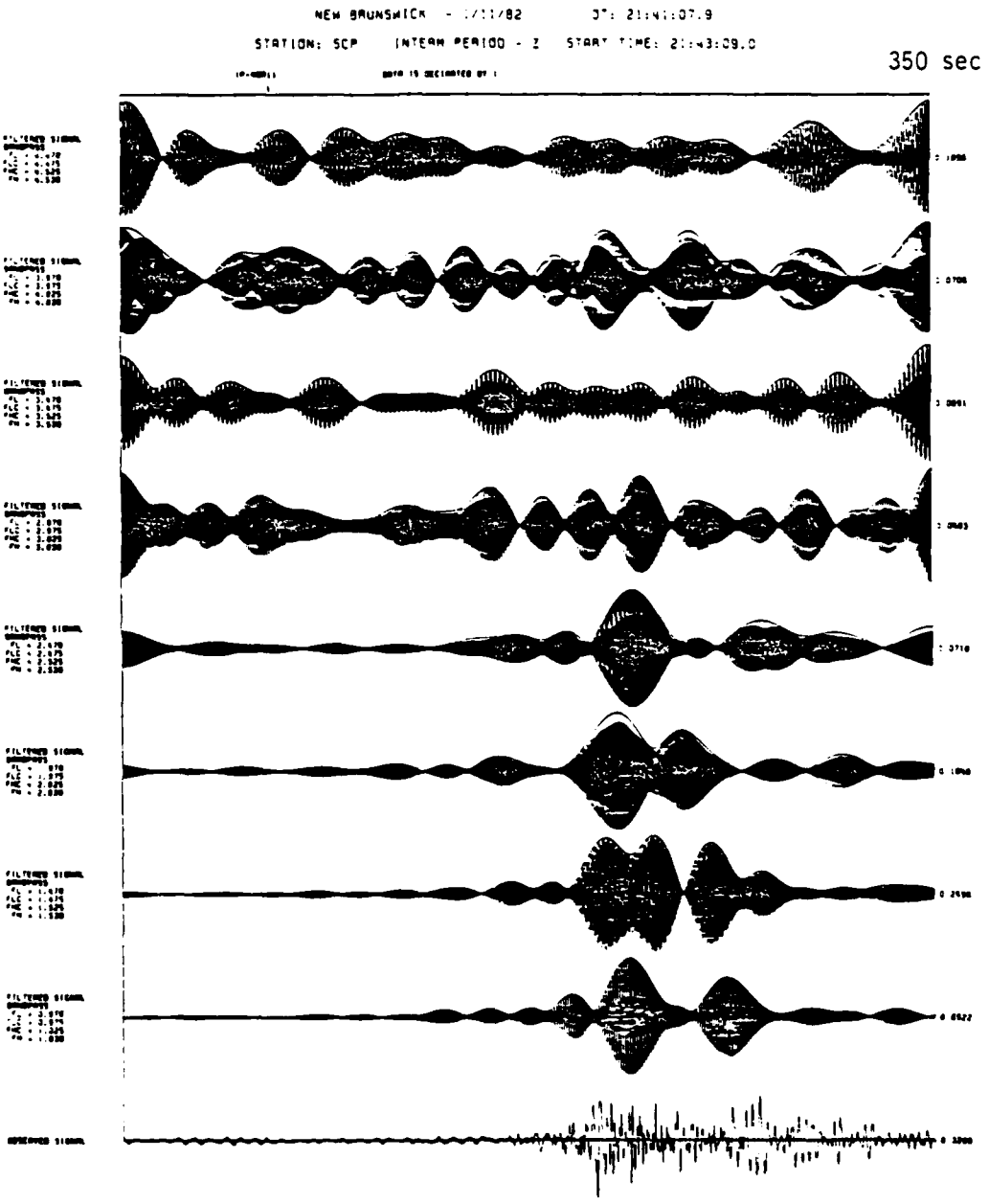
NEW BRUNSWICK - 7/11/82
STATION: SCP
INTERN PERIOD - Z
START TIME: 21:43:09.0
350 sec

Figure A3 - 17

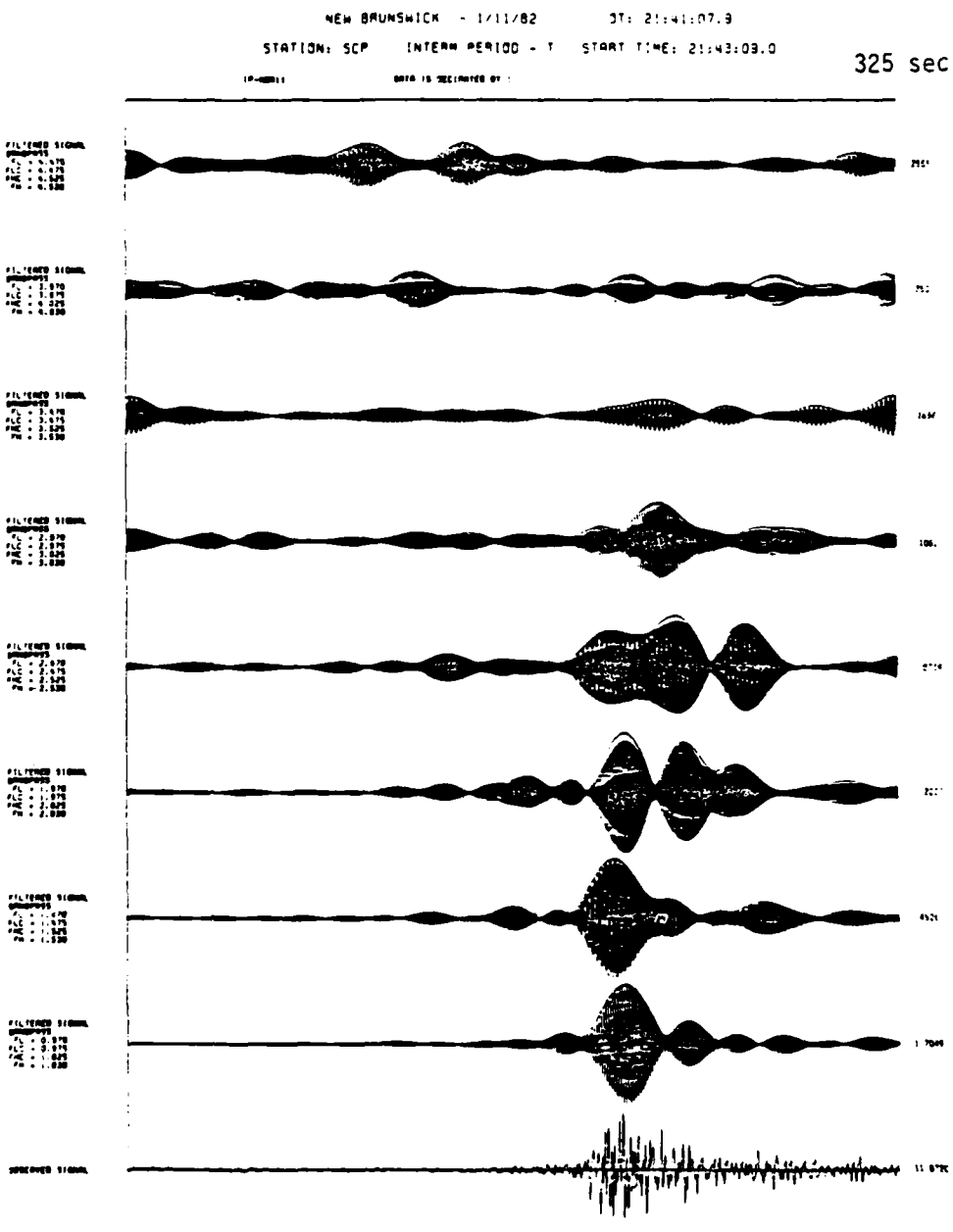
NEW BRUNSWICK - 1/11/82
ST: 21:41:07.9
STATION: SCP
INTERM PERIOD - T
START TIME: 21:43:09.0
325 sec

Figure A3 - 18

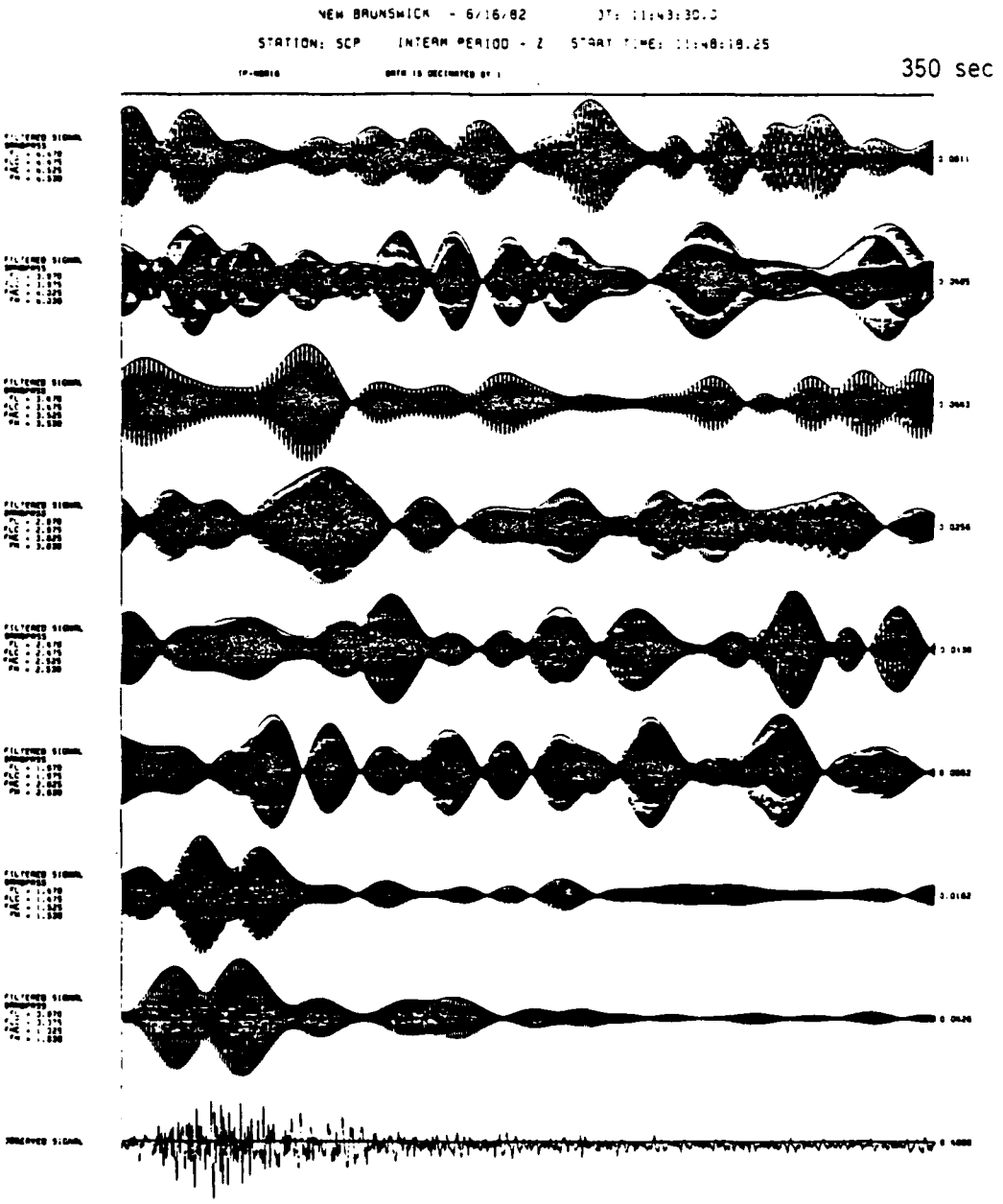

Figure A3 - 19

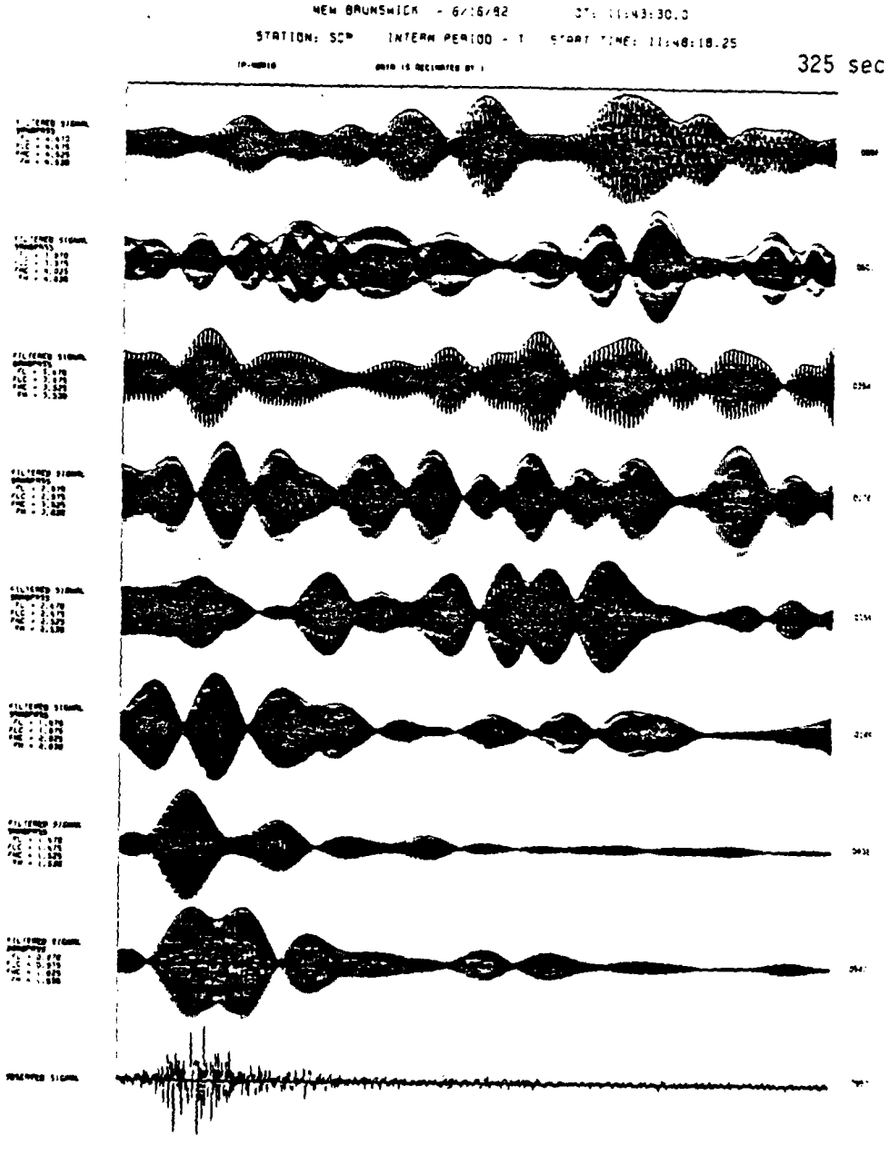

Figure A3 - 20

The filter parameters for Figures A3 - 21 through 28 are as indicated:

FL = 0.970	FLC = 0.975	FHC = 1.025	FH = 1.030
FL = 0.870	FLC = 0.875	FHC = 0.925	FH = 0.930
FL = 0.770	FLC = 0.775	FHC = 0.825	FH = 0.830
FL = 0.670	FLC = 0.675	FHC = 0.725	FH = 0.730
FL = 0.570	FLC = 0.575	FHC = 0.625	FH = 0.630
FL = 0.470	FLC = 0.475	FHC = 0.525	FH = 0.530
FL = 0.370	FLC = 0.375	FHC = 0.425	FH = 0.430
FL = 0.270	FLC = 0.275	FHC = 0.325	FH = 0.330

OBSERVED SIGNAL

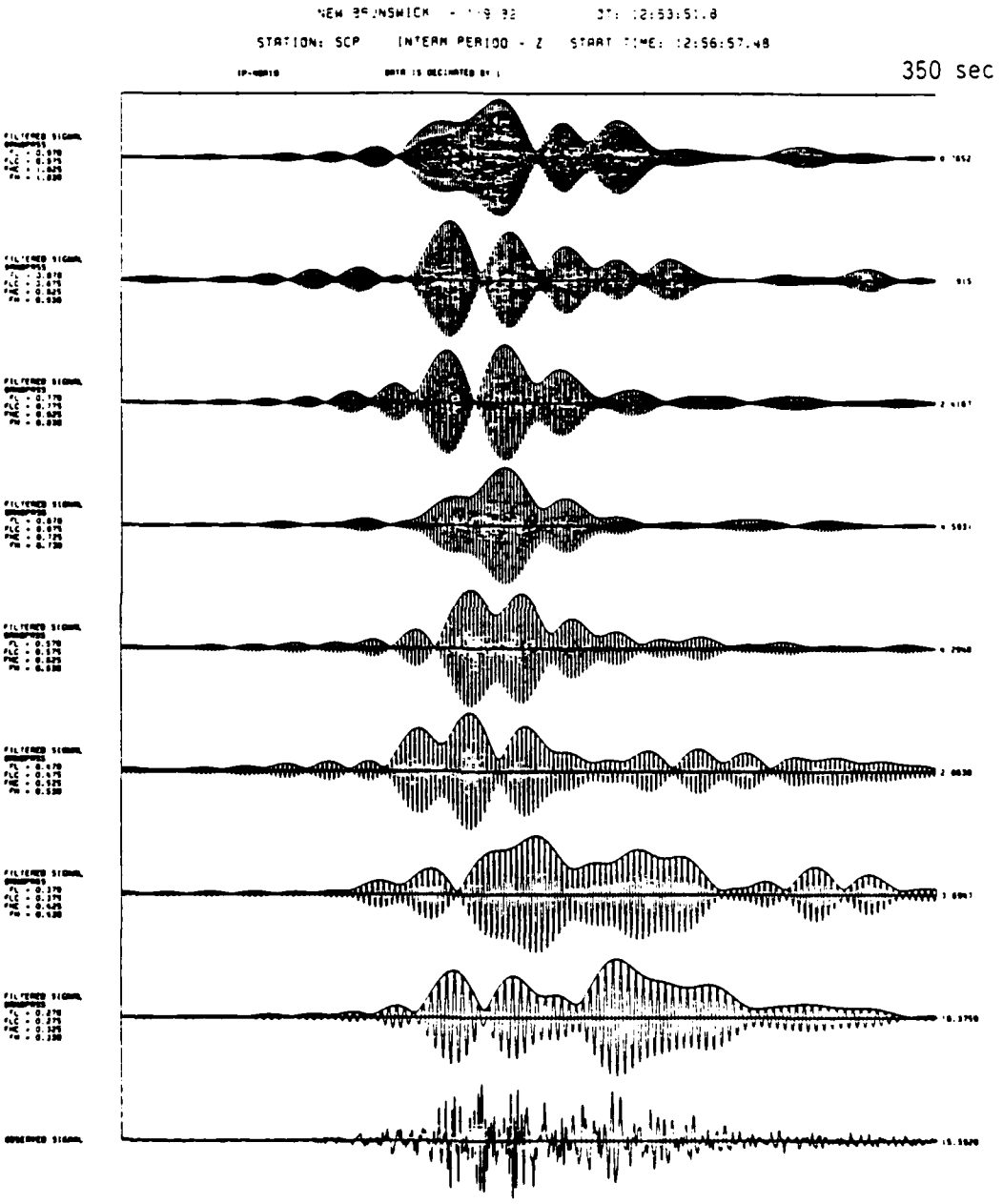

Figure A3 - 21

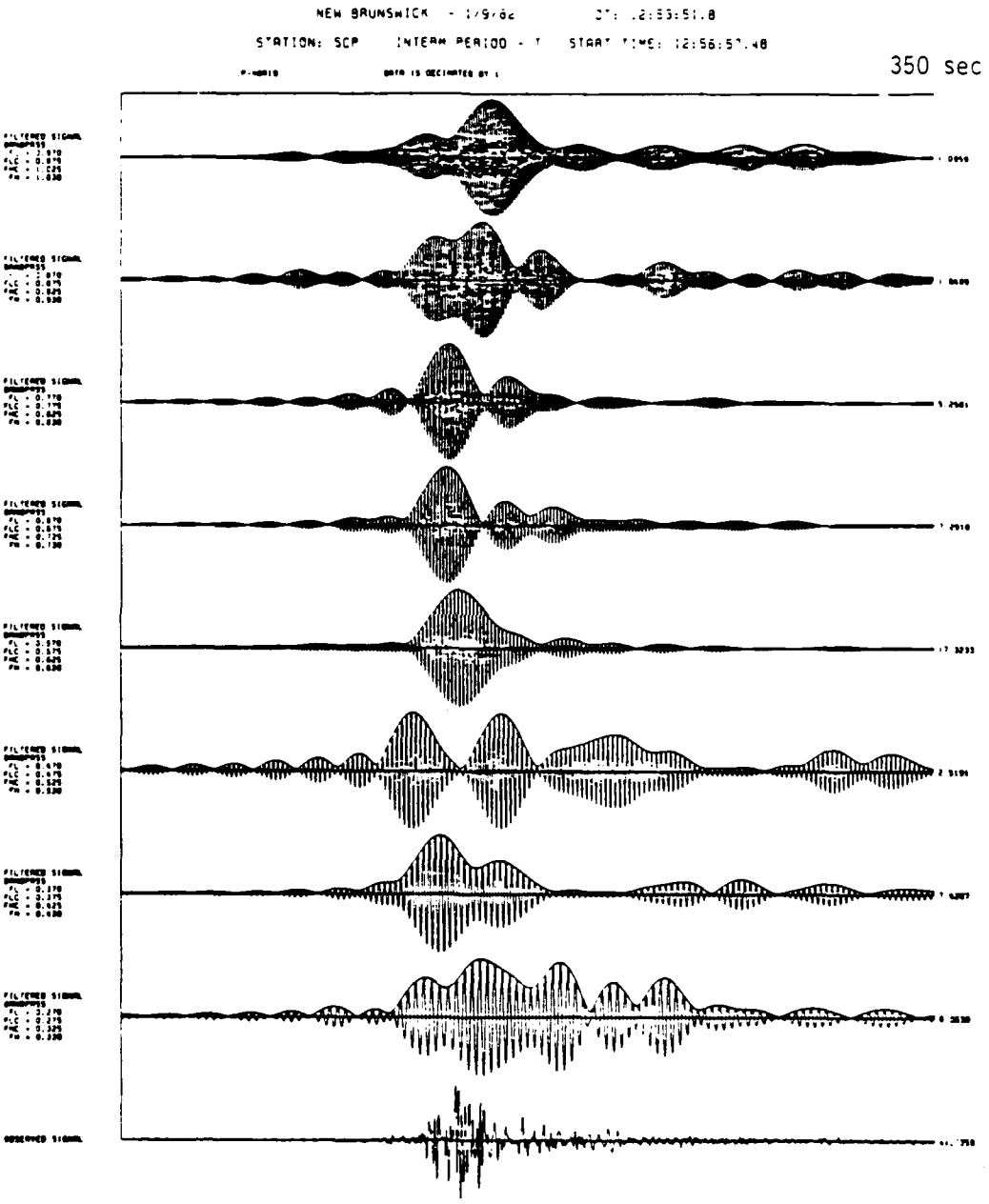

Figure A3 - 22

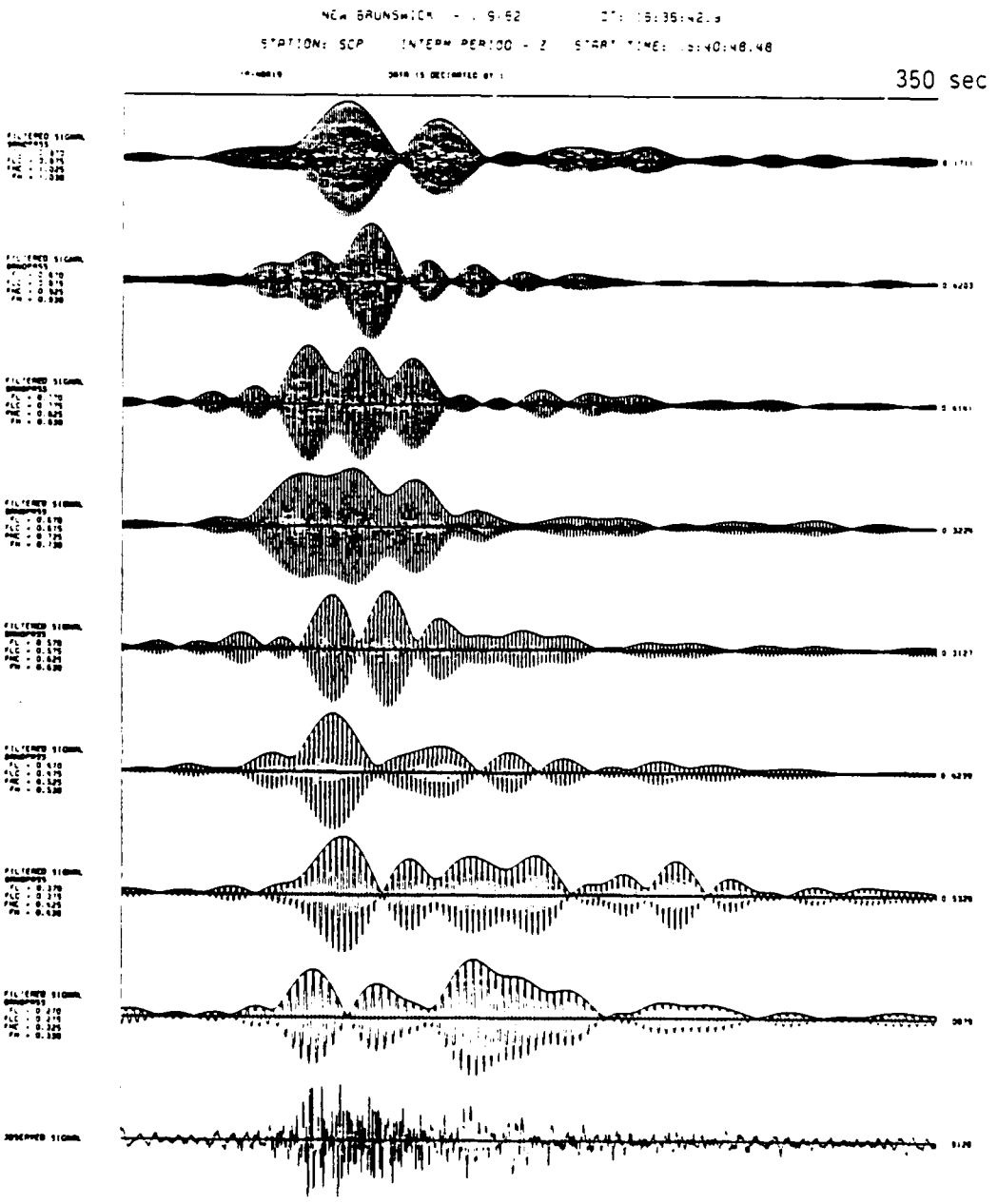

Figure A3 - 23

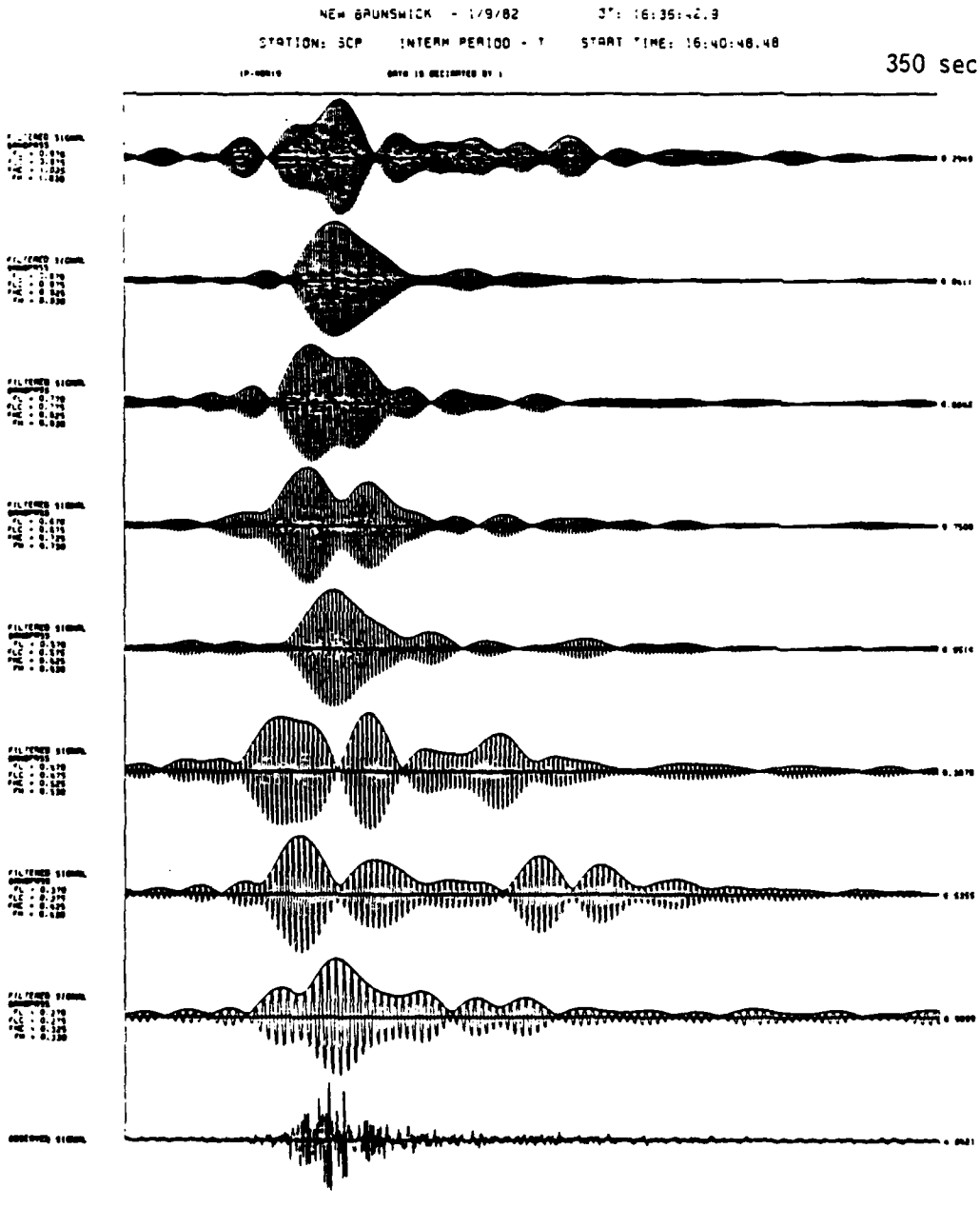
NEW BRUNSWICK - 1/9/82
STATION: SCP
INTERN PERIOD - 1
START TIME: 16:40:48.48
350 sec

Figure A3 - 24

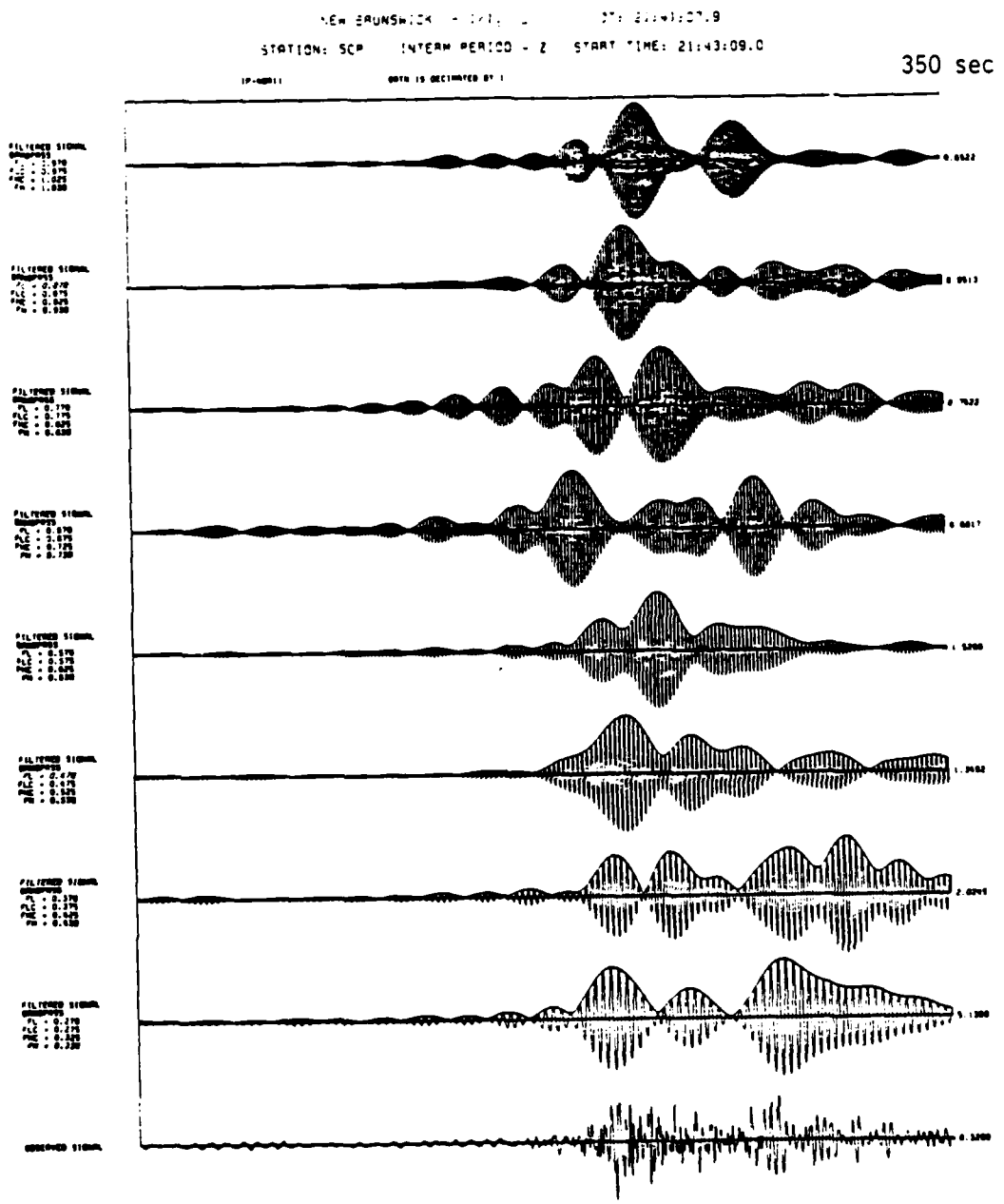

Figure A3 - 25

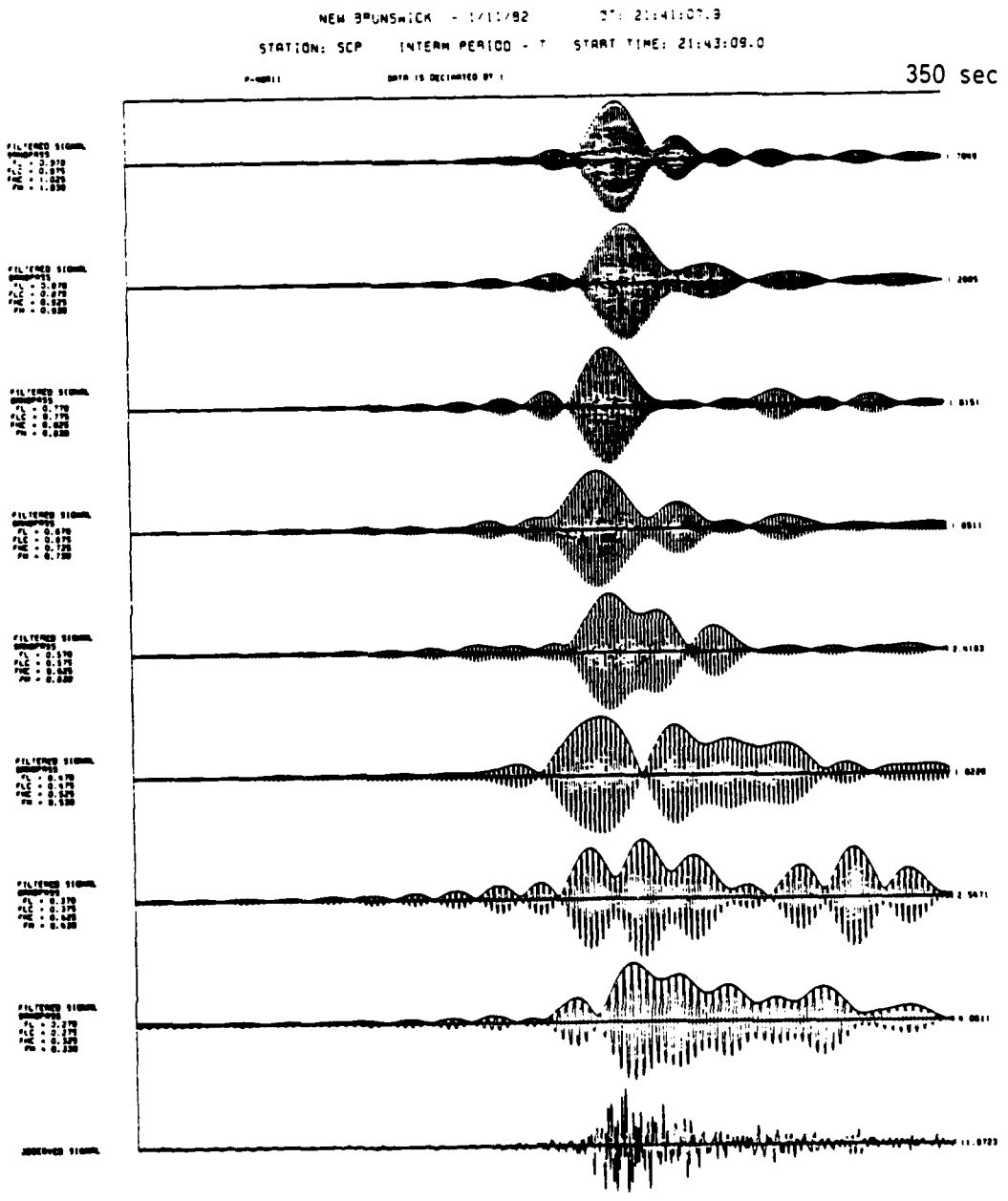
NEW BRUNSWICK - 1/11/92
STATION: SCP INTERM PERIOD - T START TIME: 21:43:09.0
350 sec

Figure A3 - 26

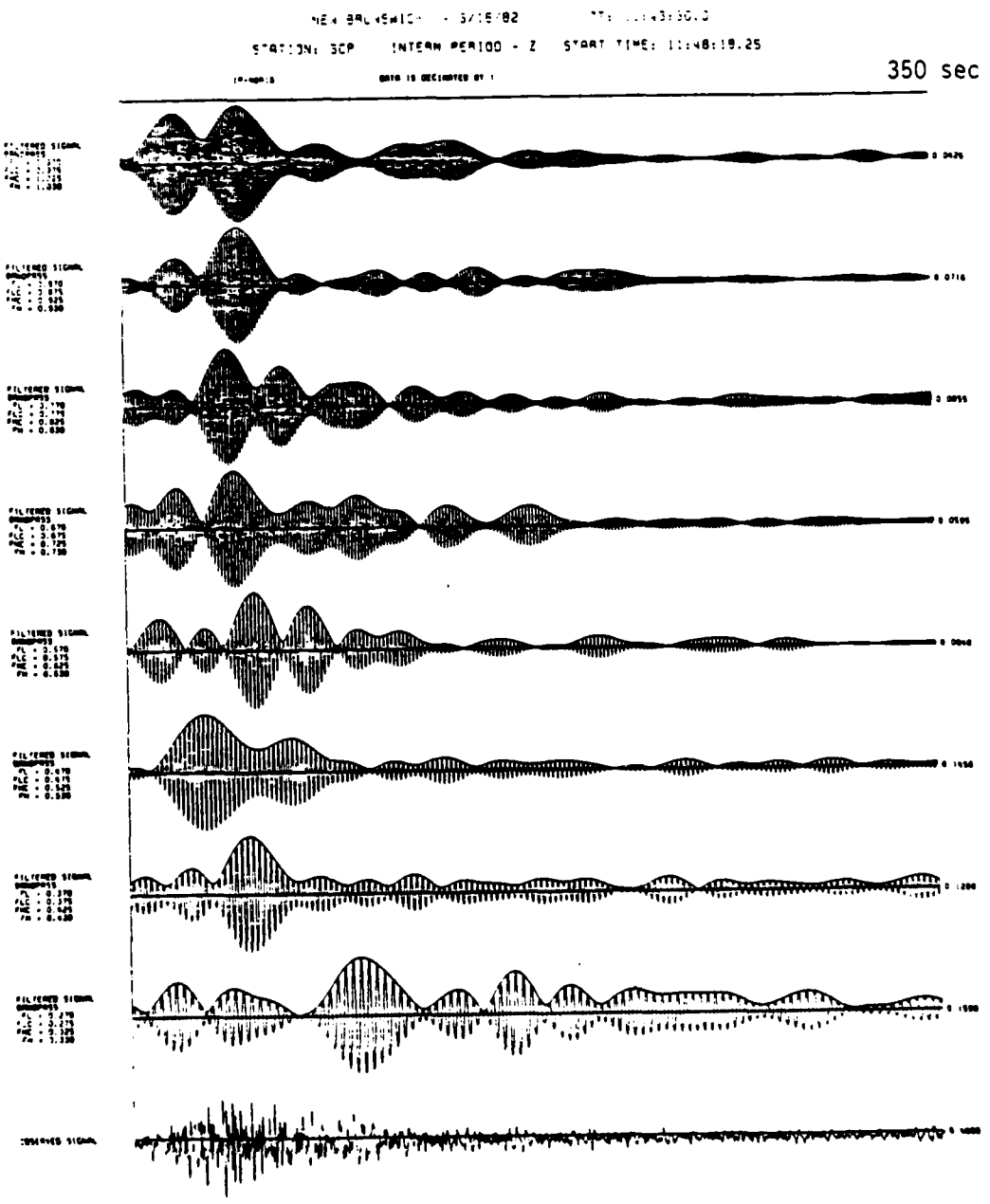

Figure A3 - 27

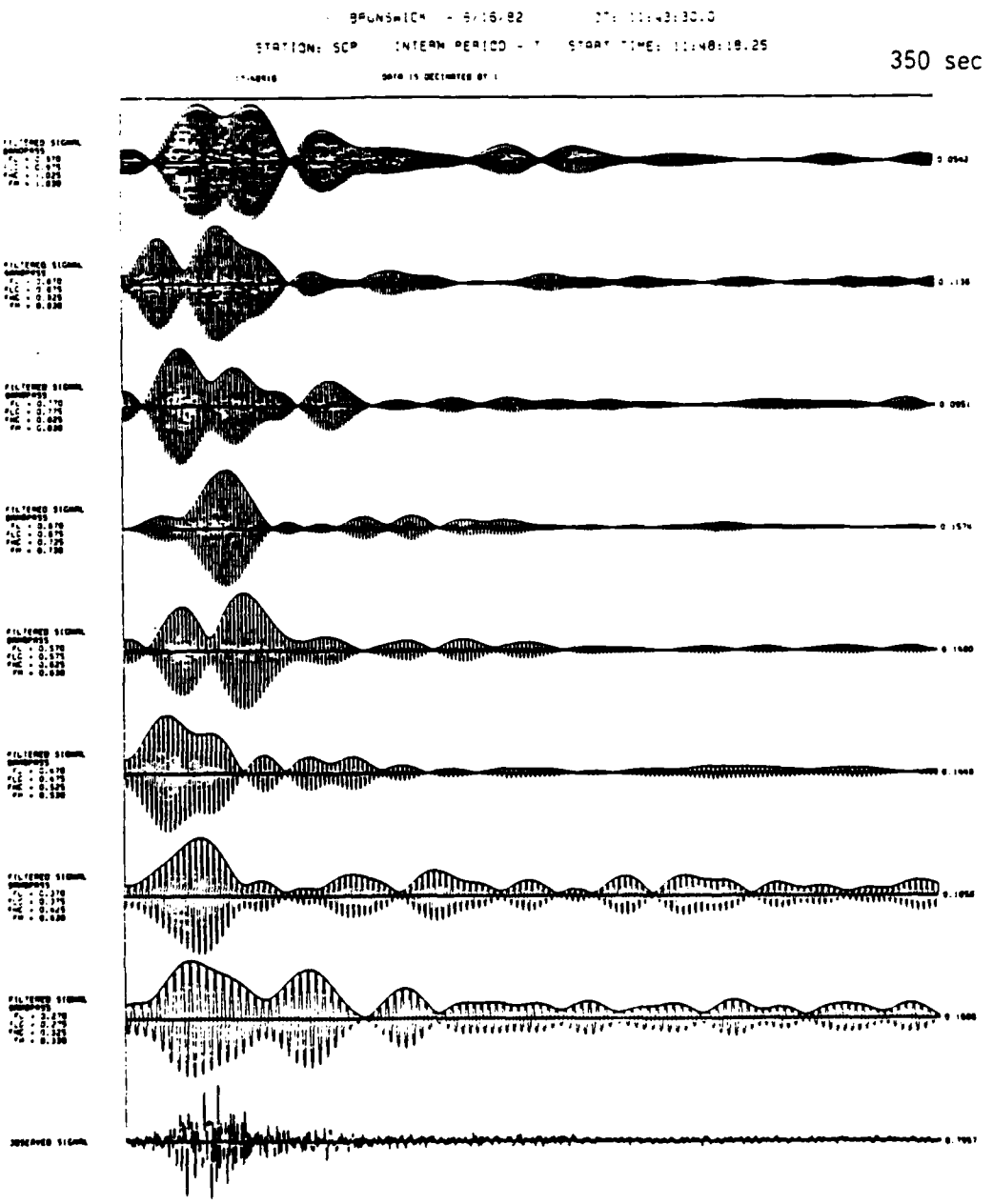

Figure A3 - 28

The filter parameters for Figures A3 - 29 through 36 are as indicated:

FL = 0.220	FLC = 0.225	FHC = 0.275	FH = 0.280
FL = 0.170	FLC = 0.175	FHC = 0.225	FH = 0.230
FL = 0.120	FLC = 0.125	FHC = 0.175	FH = 0.180
FL = 0.090	FLC = 0.095	FHC = 0.145	FH = 0.150
FL = 0.092	FLC = 0.097	FHC = 0.102	FH = 0.107
FL = 0.082	FLC = 0.087	FHC = 0.092	FH = 0.097
FL = 0.063	FLC = 0.067	FHC = 0.072	FH = 0.077
FL = 0.042	FLC = 0.047	FHC 0.052	FH = 0.057

OBSERVED SIGNAL

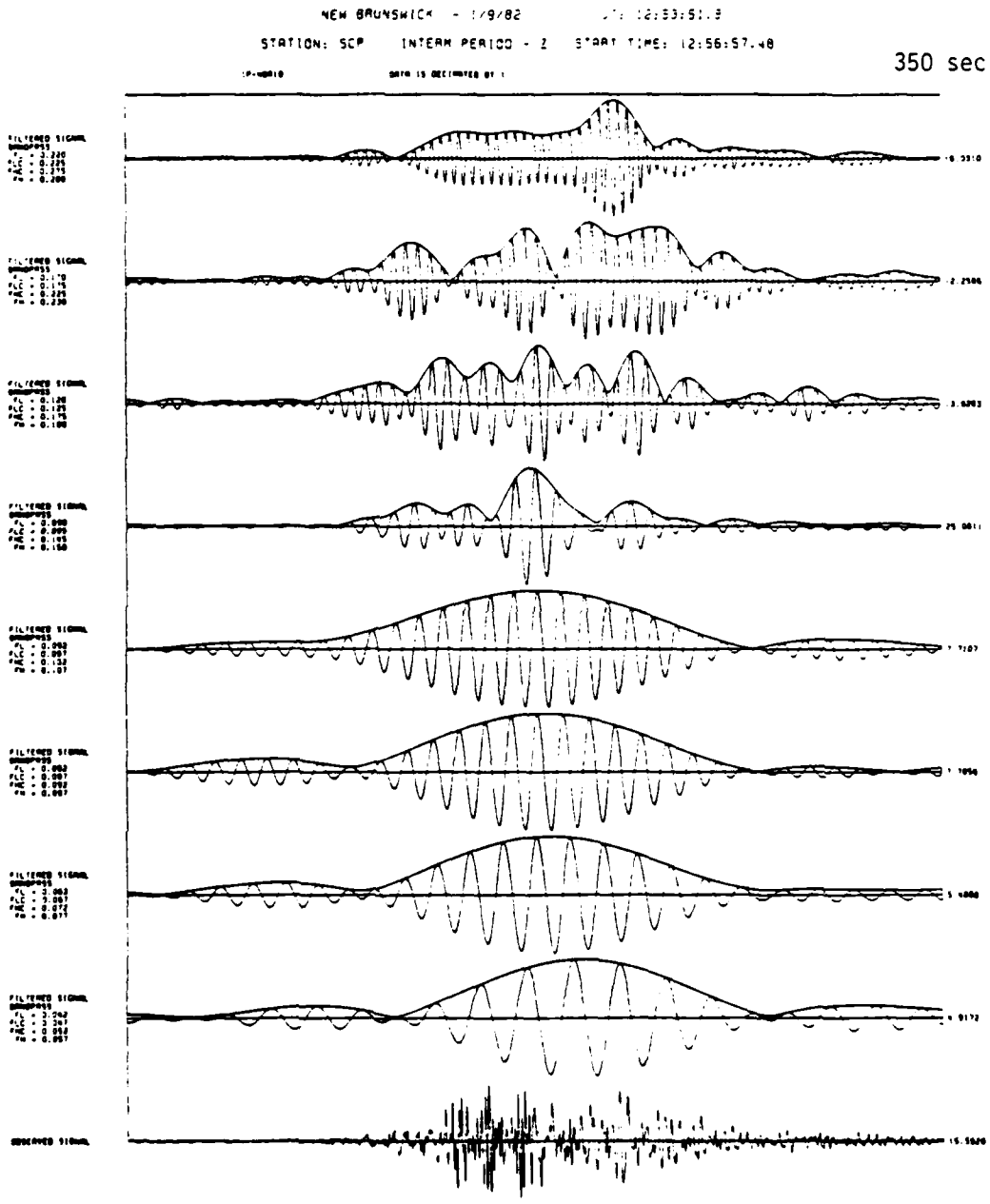

Figure A3 - 29

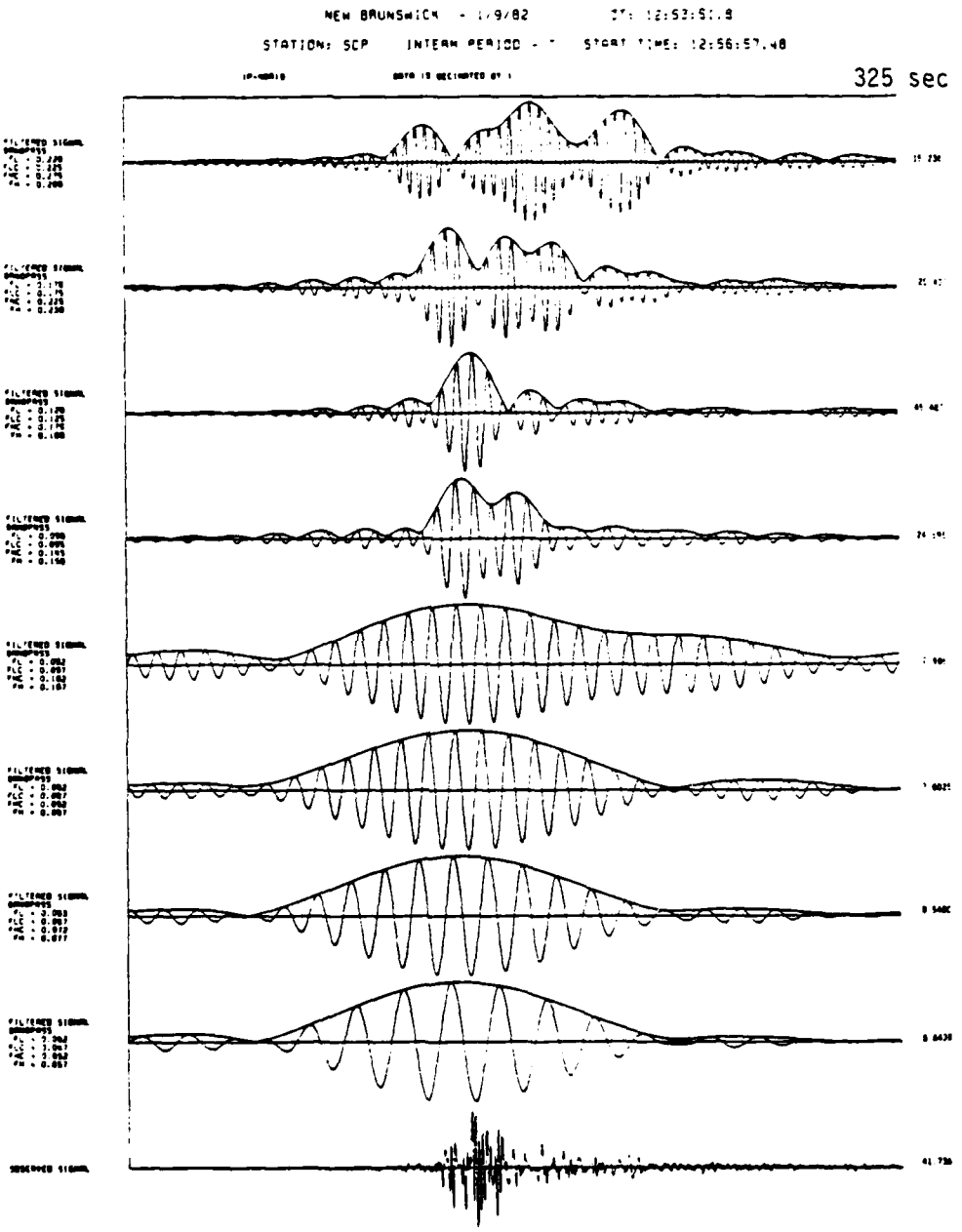

Figure A3 - 30

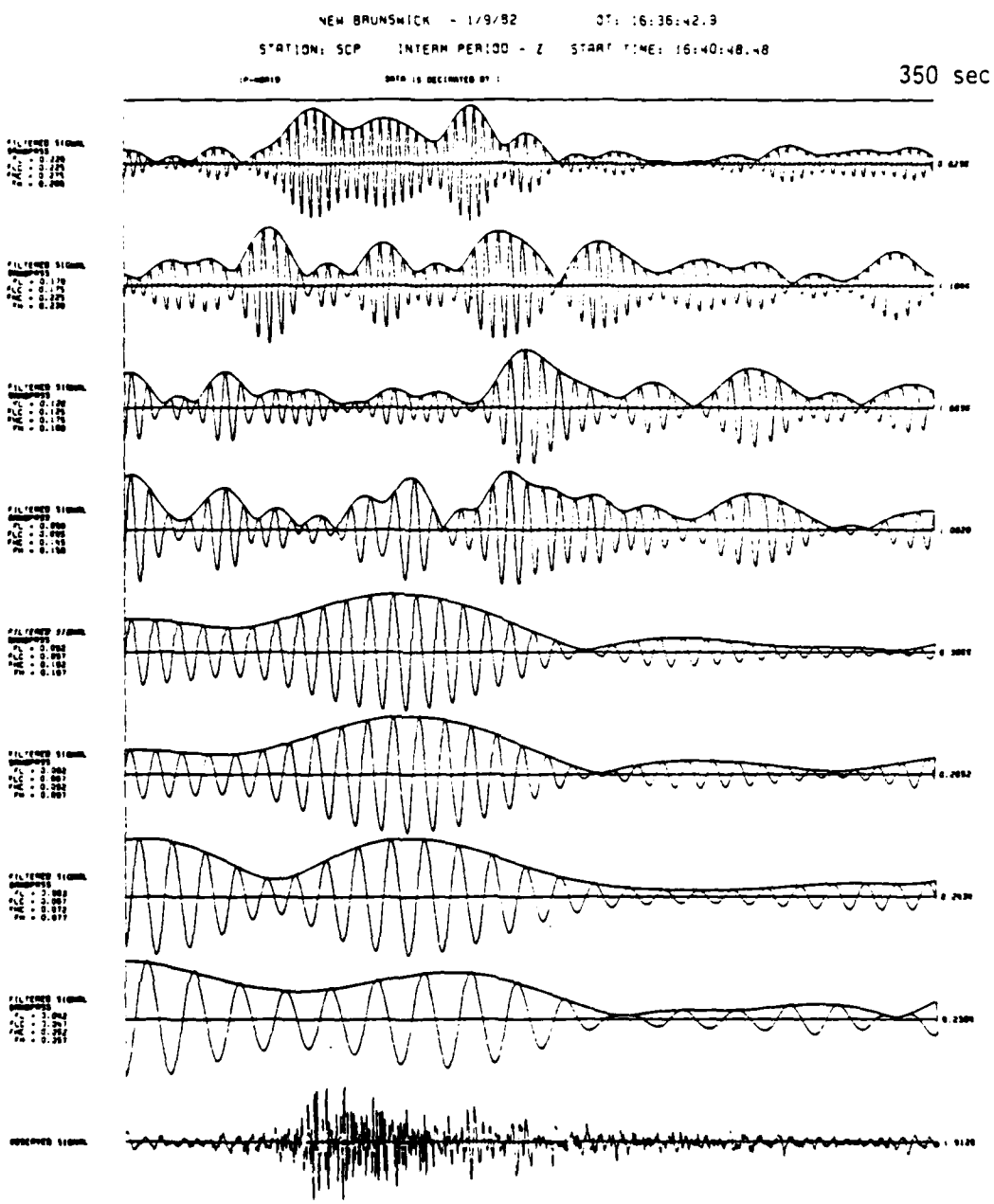

Figure A3 - 31

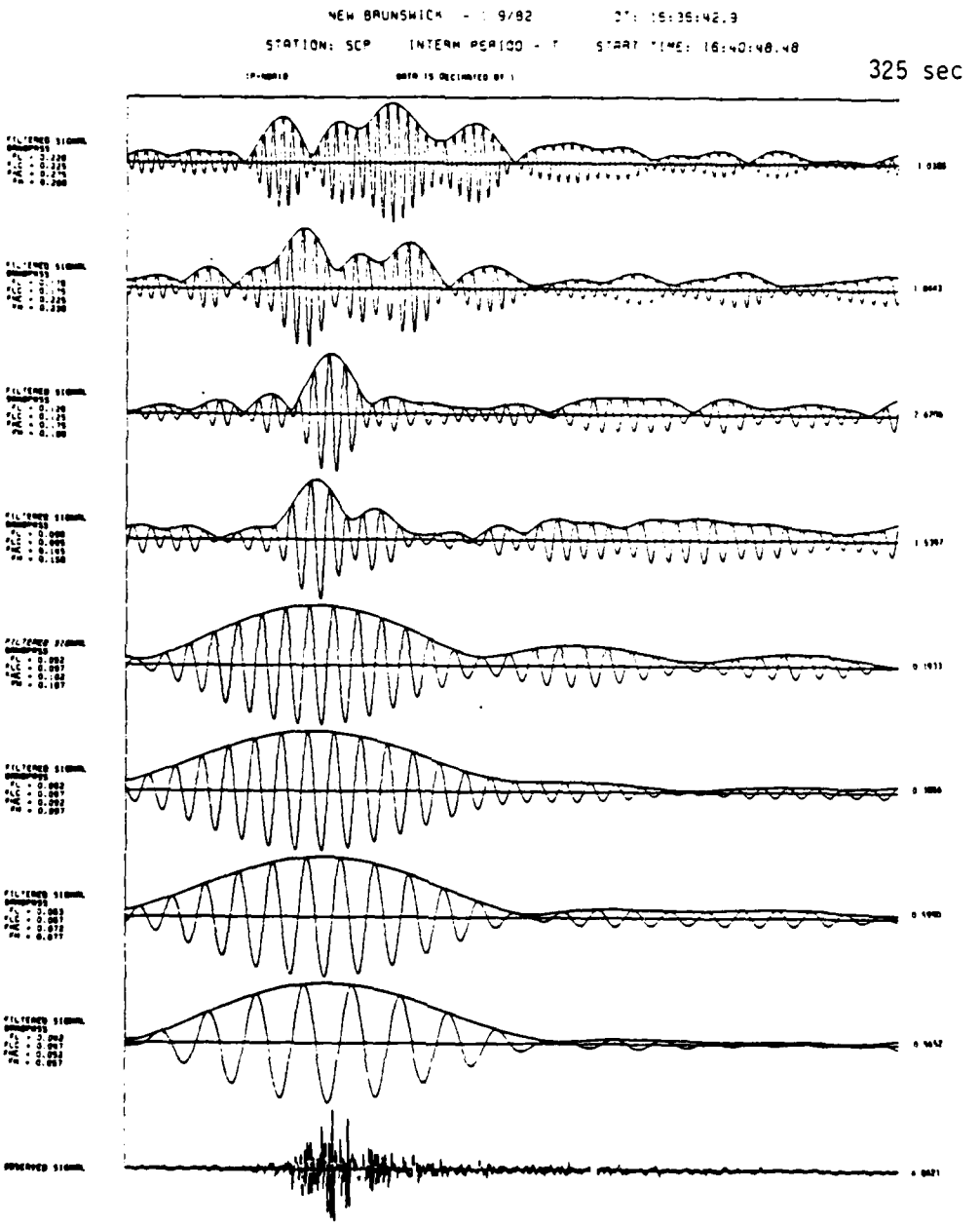

Figure A3 - 32

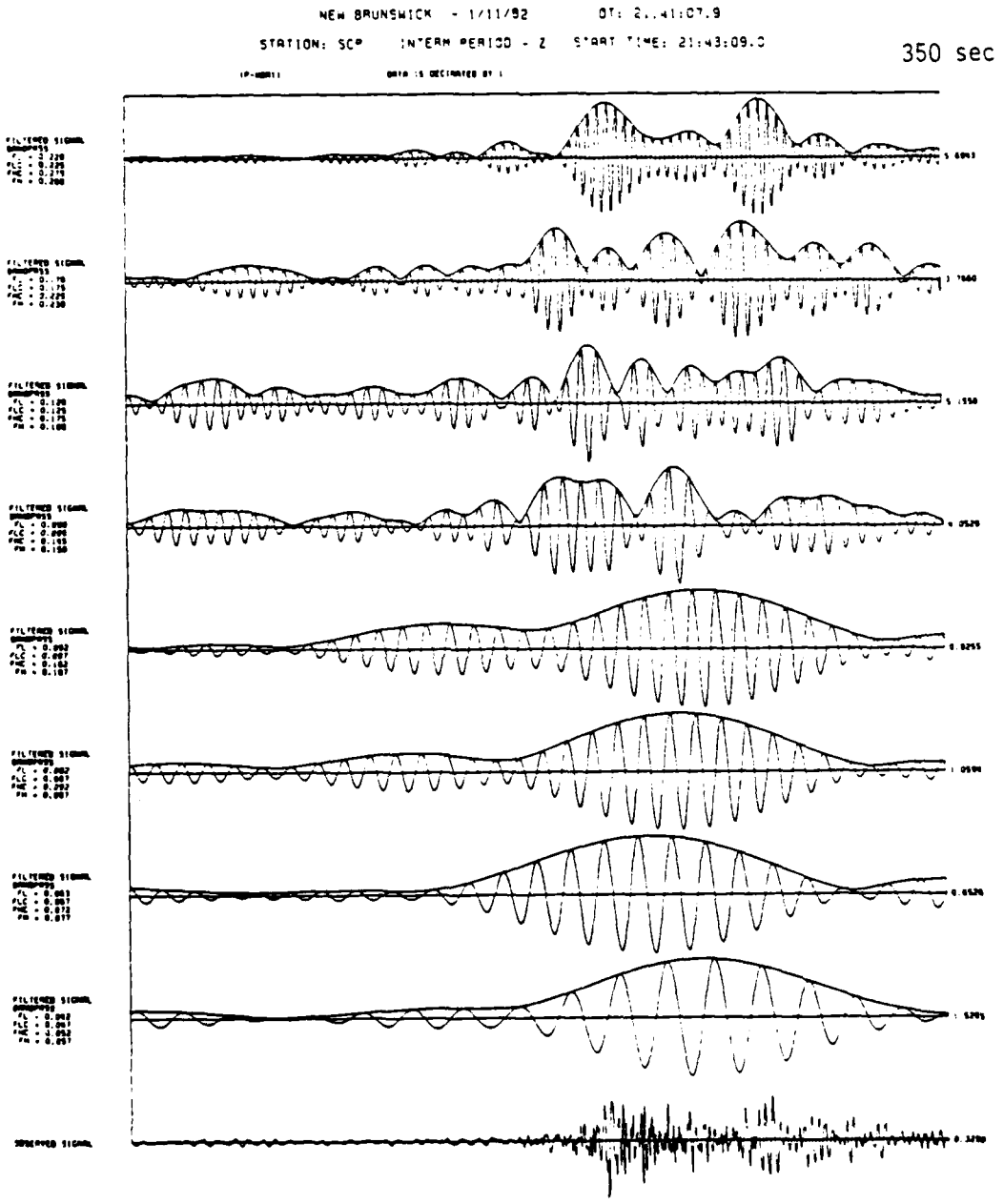

Figure A3 - 33

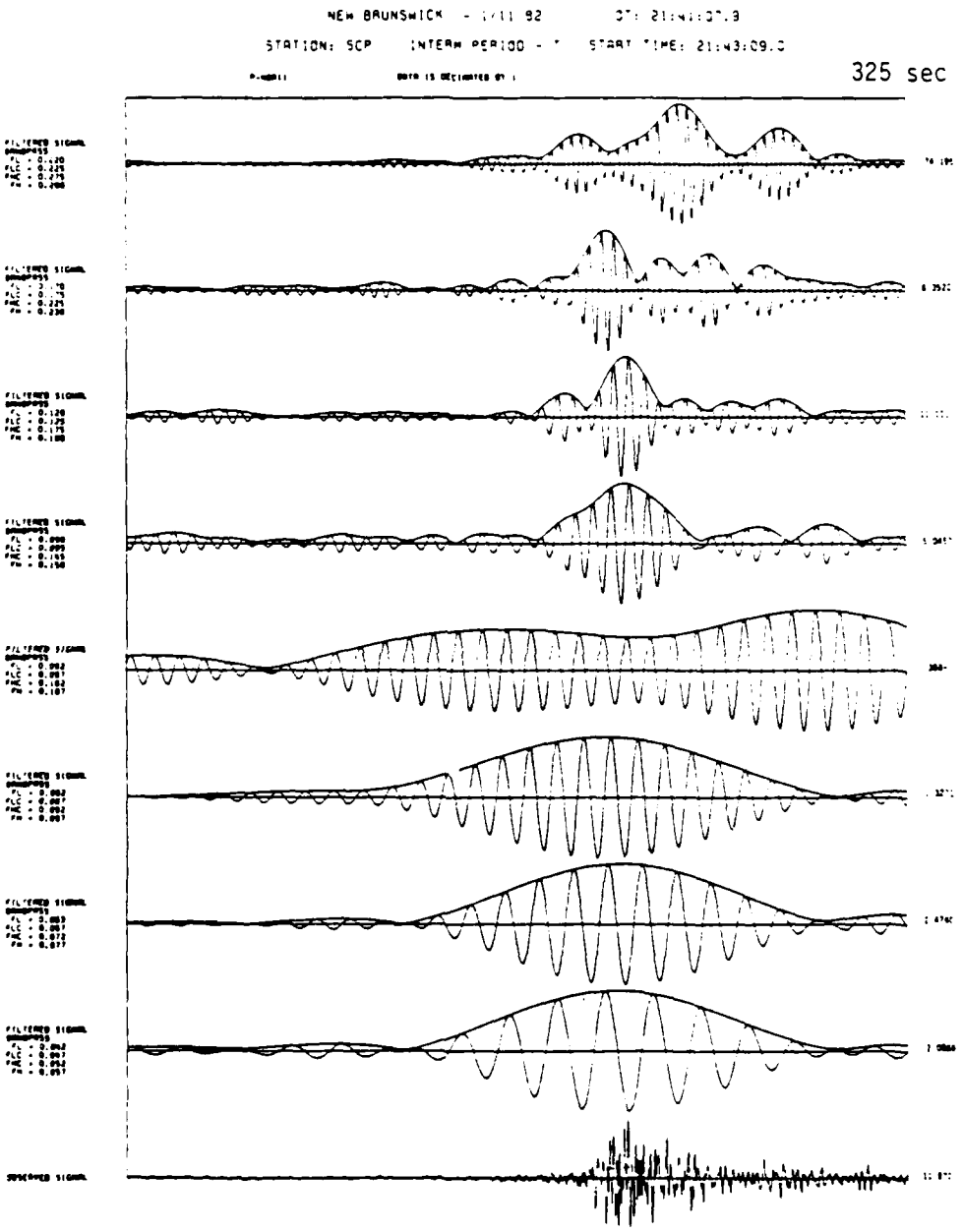

Figure A3 - 34

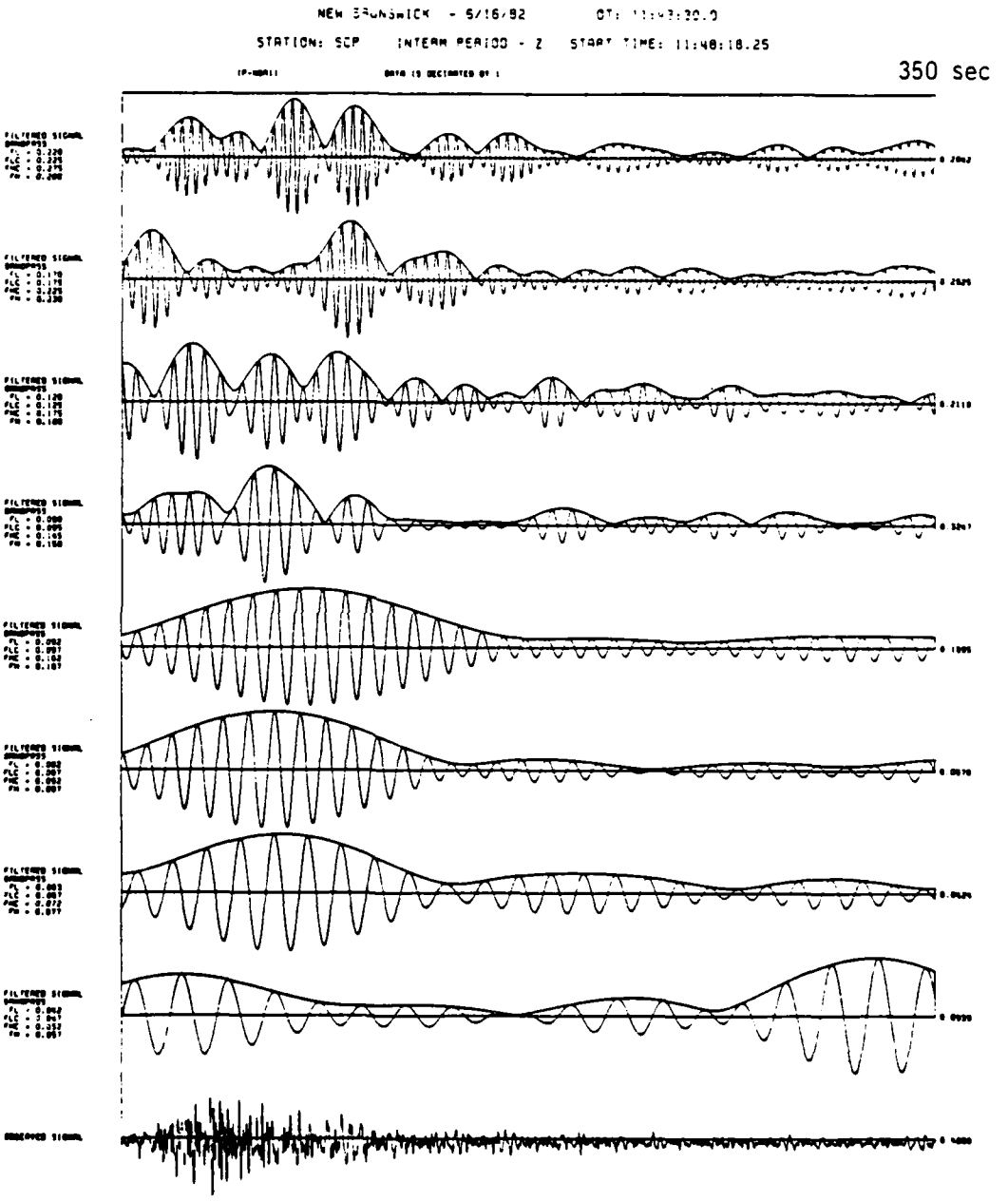
NEW BRUNSWICK - 5/16/82
STATION: SCP INTERM PERIOD - Z START TIME: 11:48:18.25
350 sec

Figure A3 - 35

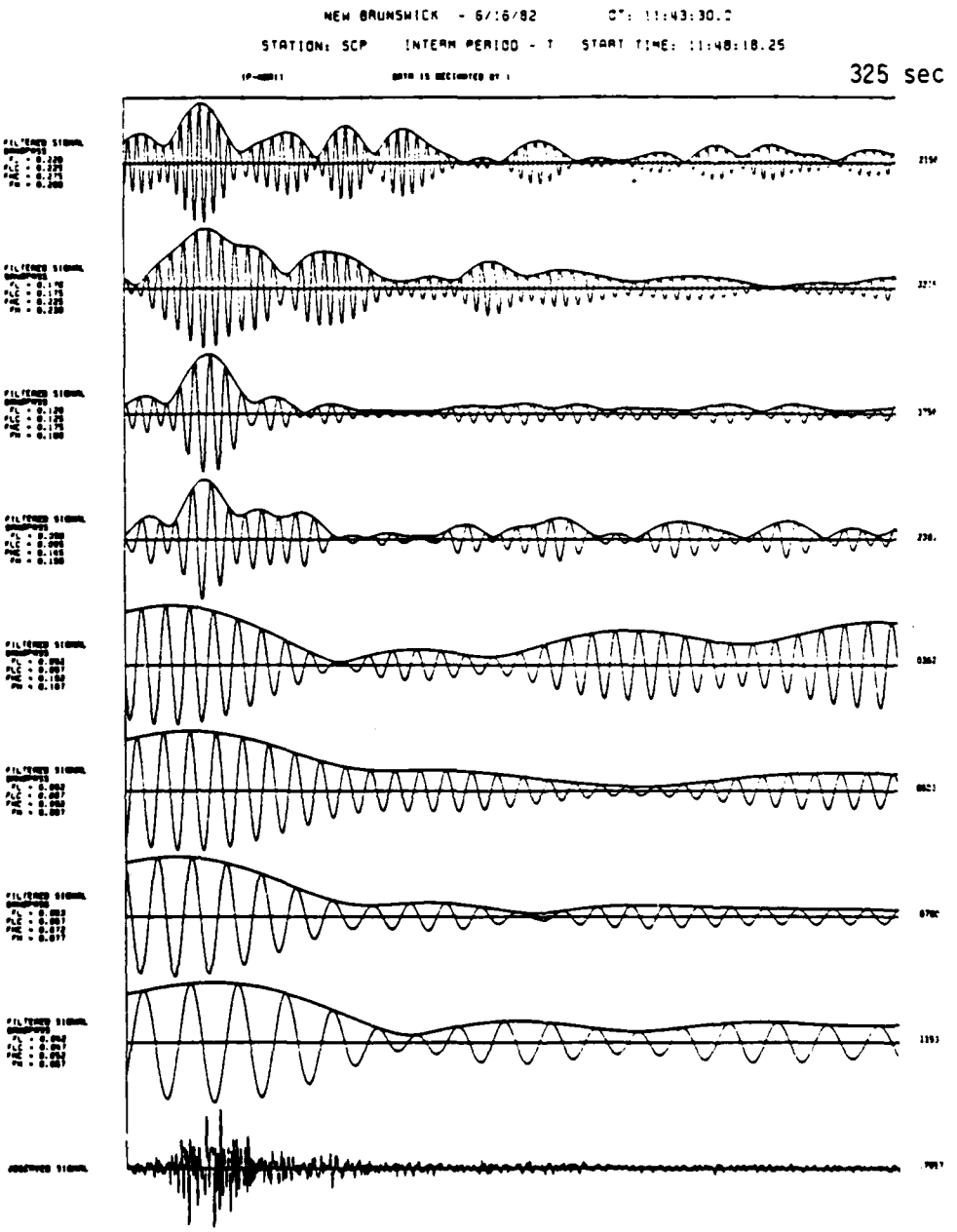
NEW BRUNSWICK - 6/16/82
STATION: SCP
INTERN PERIOD - T
START TIME: 11:48:18.25
325 sec

Figure A3 - 36

The filter parameters for Figures A3 - 37 through 42 are as indicated:

FL = 0.009	FLC = 0.014	FHC = 0.019	FH = 0.024
FL = 0.011	FLC = 0.016	FHC = 0.021	FH = 0.026
FL = 0.012	FLC = 0.017	FHC = 0.022	FH = 0.027
FL = 0.015	FLC = 0.020	FHC = 0.025	FH = 0.030
FL = 0.017	FLC = 0.022	FHC = 0.027	FH = 0.032
FL = 0.021	FLC = 0.026	FHC = 0.031	FH = 0.036
FL = 0.026	FLC = 0.031	FHC = 0.036	FH = 0.041
FL = 0.032	FLC = 0.037	FHC = 0.042	FH = 0.047

OBSERVED SIGNAL

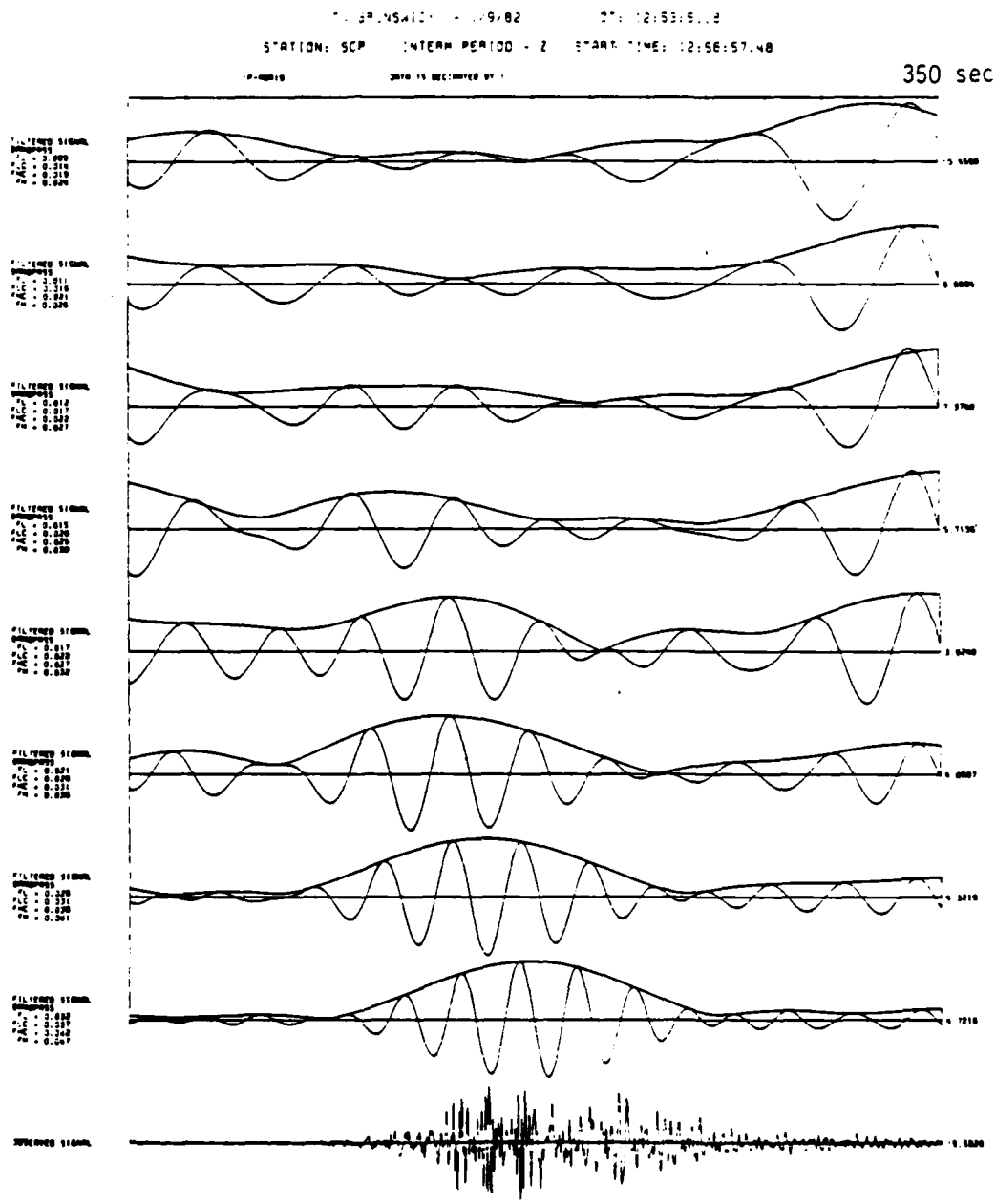

Figure A3 - 37

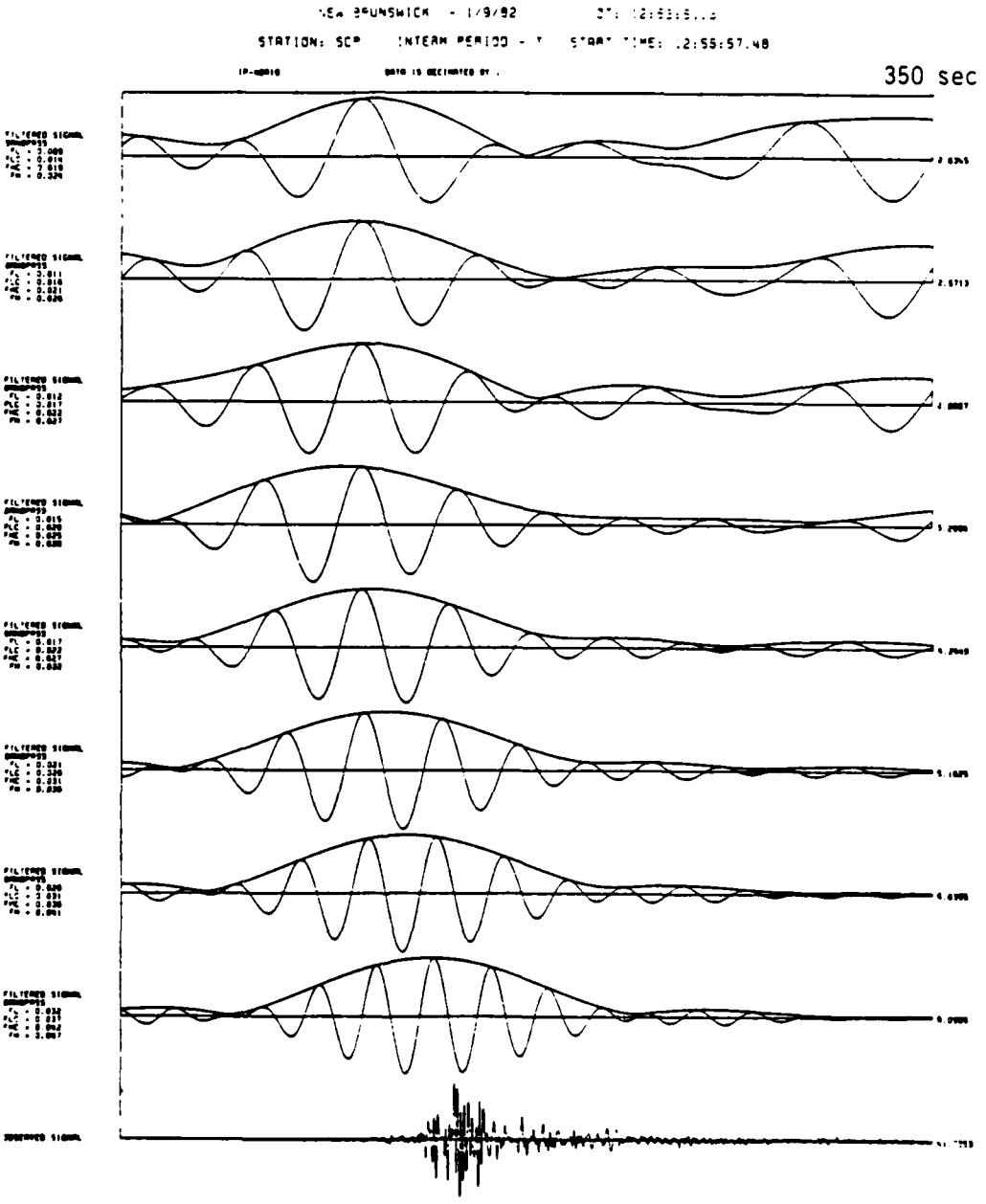

Figure A3 - 38

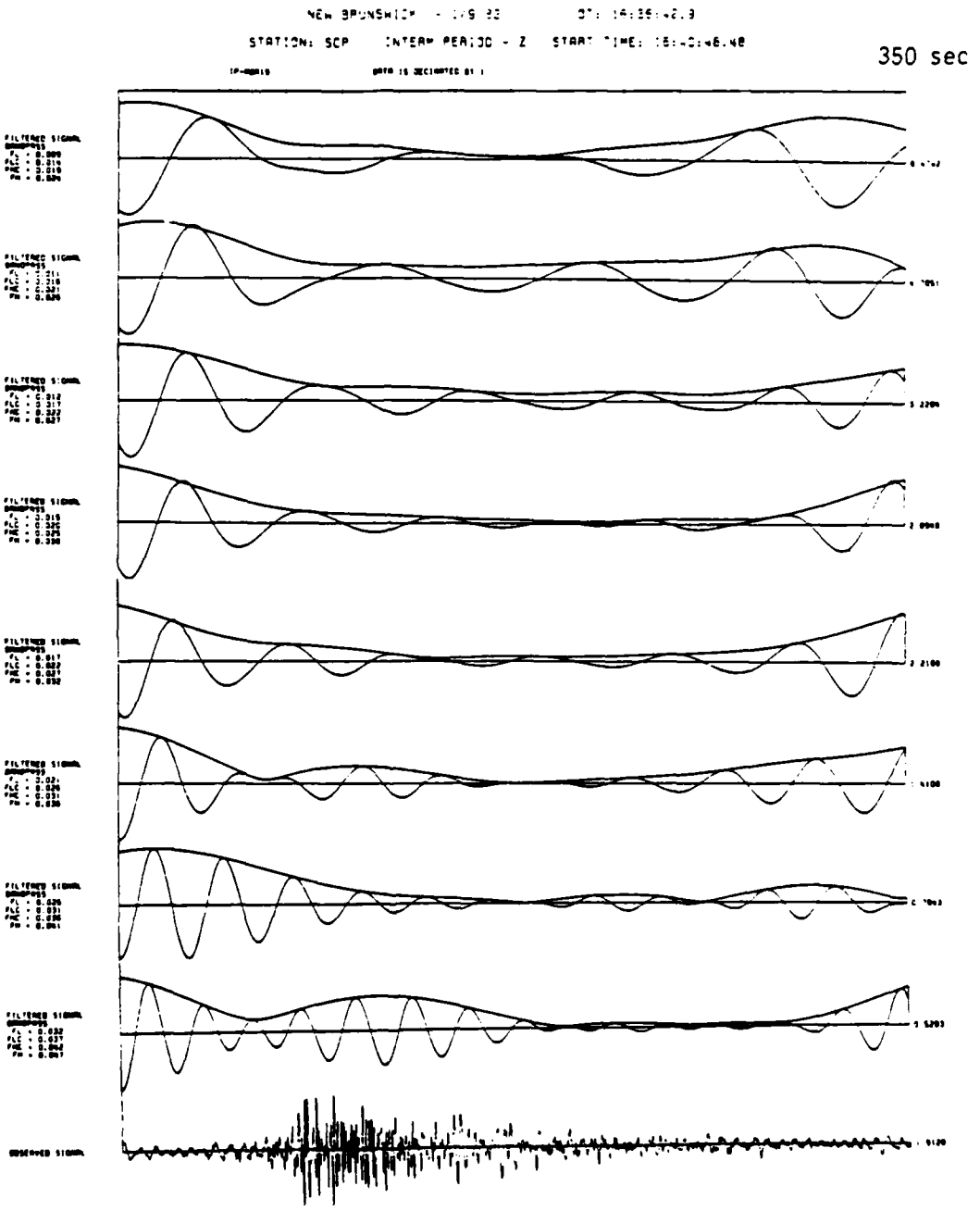

Figure A3 - 39

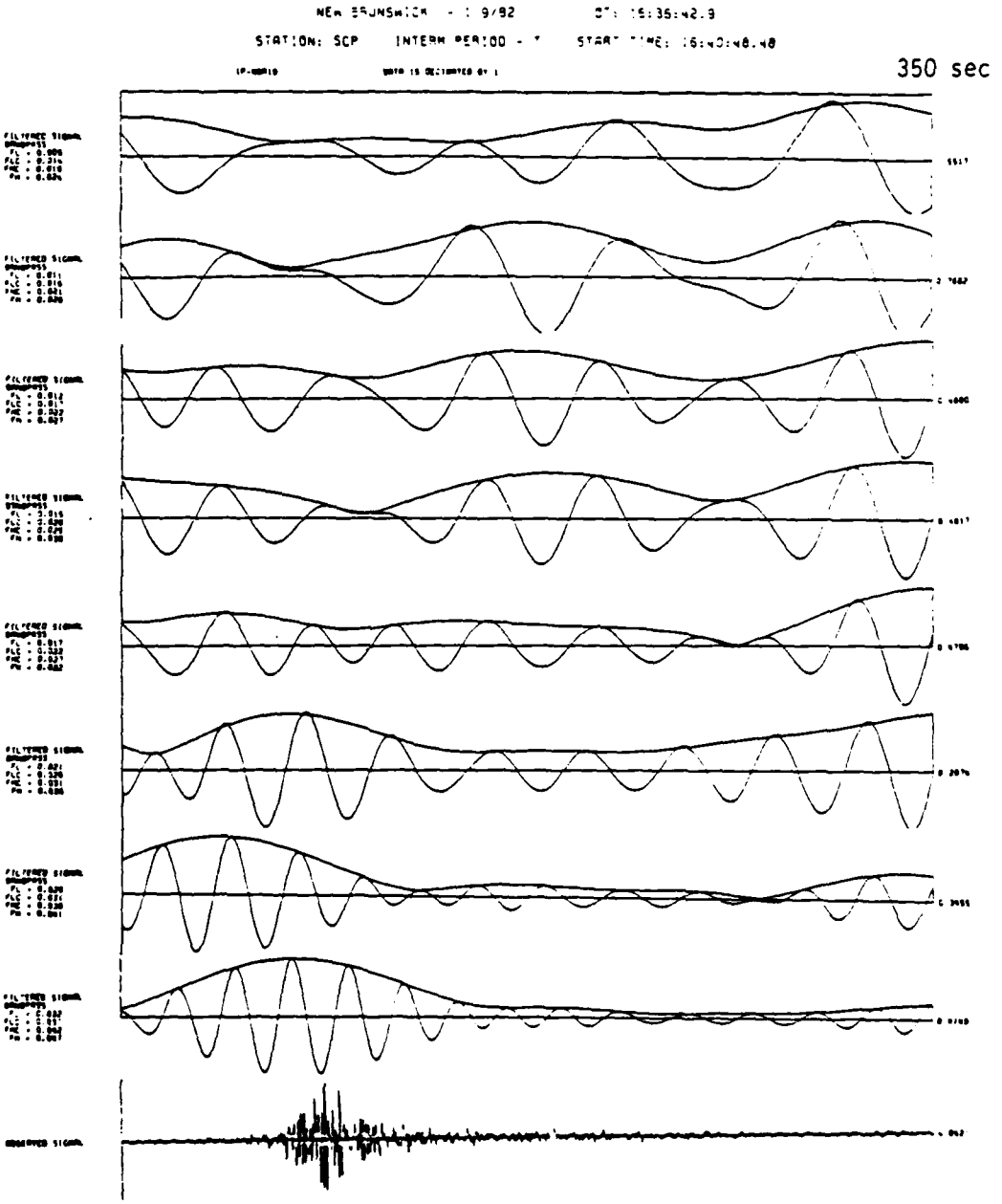

Figure A3 - 40

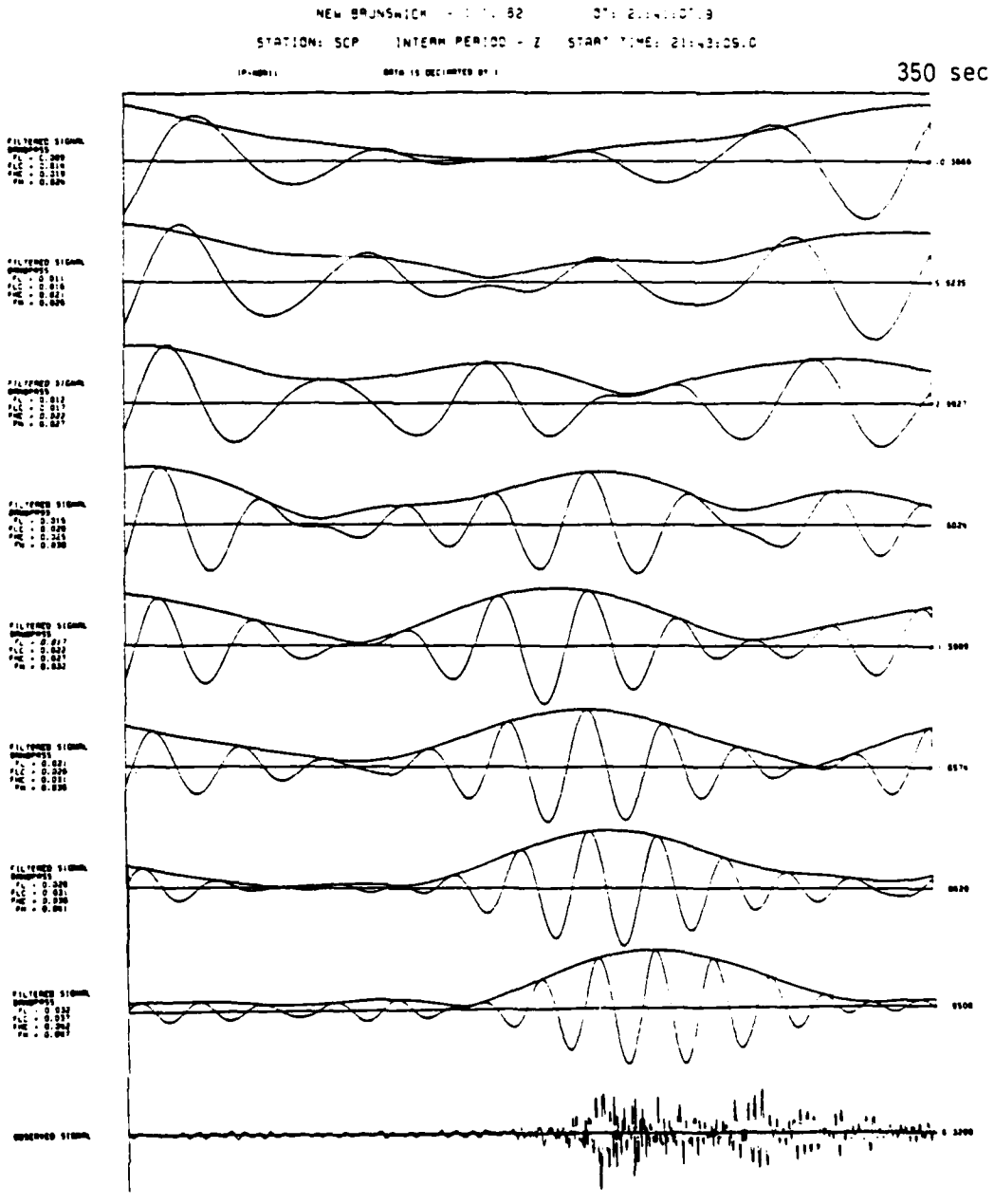

Figure A3 - 41

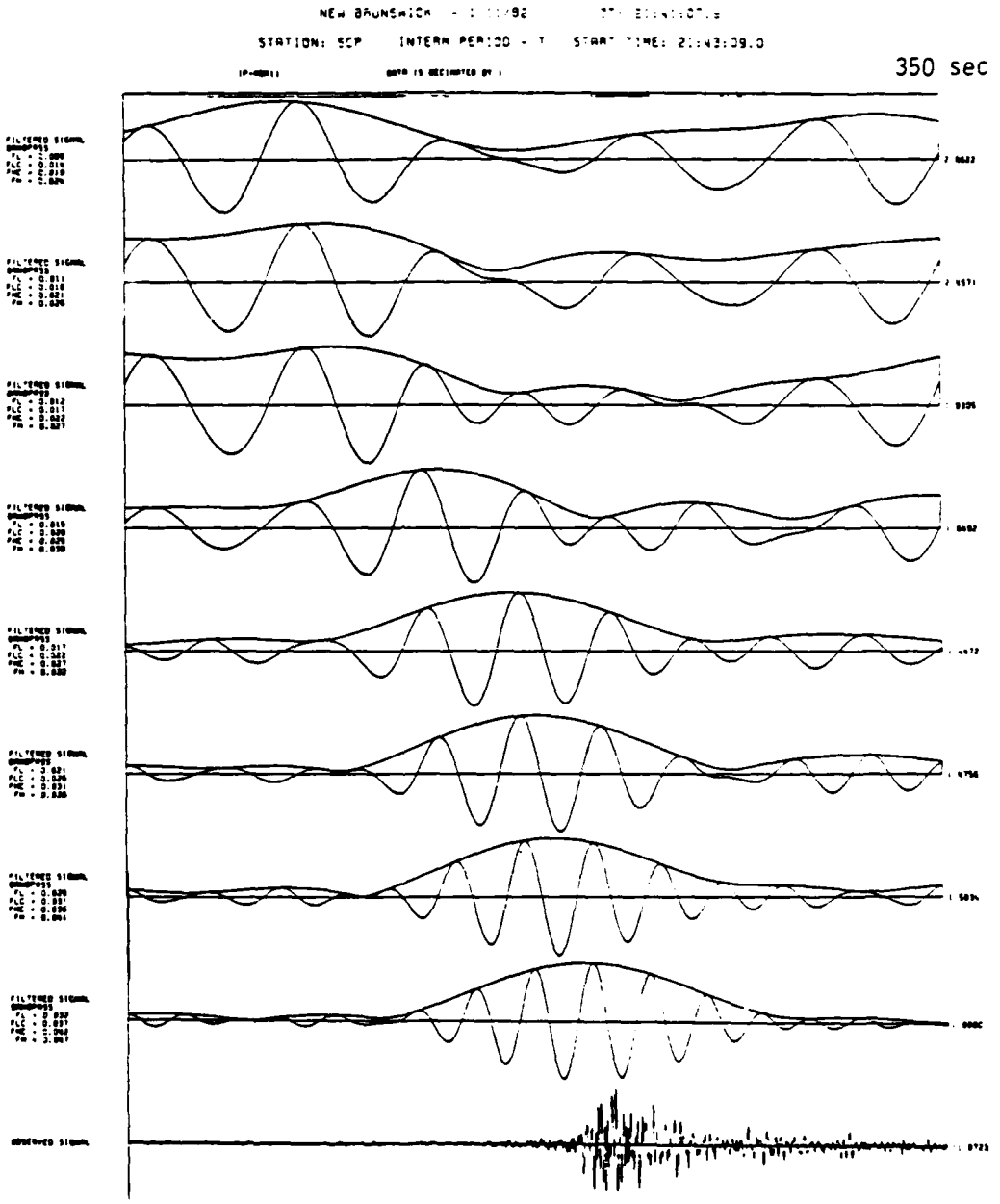

Figure A3 - 42

The filter parameters for Figures A3 - 43 through 48 are as indicated:

FL = 0.082	FLC = 0.087	FHC = 0.092	FH = 0.097
FL = 0.063	FLC = 0.067	FHC = 0.072	FH = 0.077
FL = 0.042	FLC = 0.047	FHC = 0.052	FH = 0.057
FL = 0.032	FLC = 0.037	FHC = 0.042	FH = 0.047
FL = 0.022	FLC = 0.027	FHC = 0.032	FH = 0.037
FL = 0.012	FLC = 0.017	FHC = 0.022	FH = 0.027
FL = 0.007	FLC = 0.012	FHC = 0.017	FH = 0.022
FL = 0.002	FLC = 0.007	FHC = 0.012	FH = 0.017

OBSERVED SIGNAL

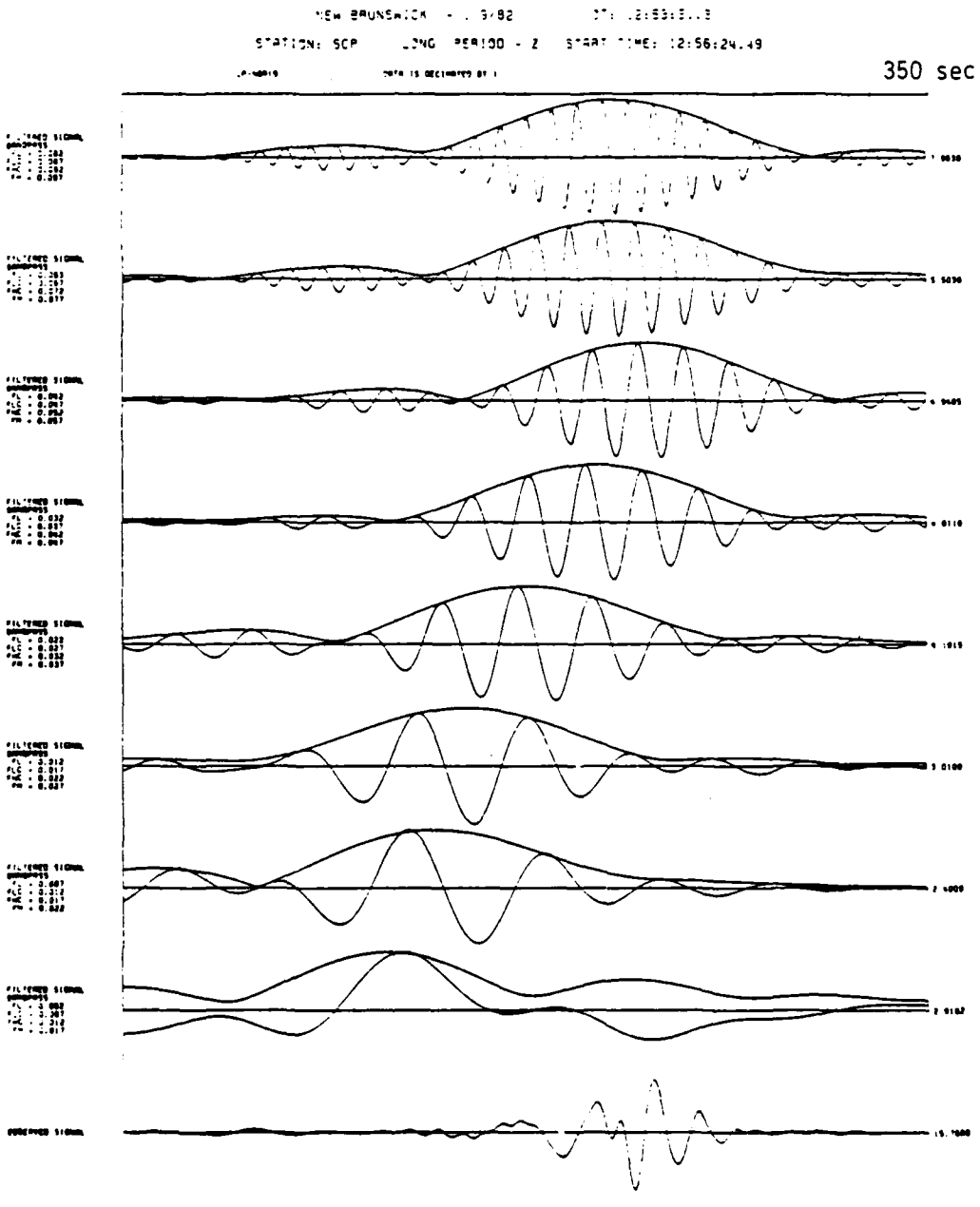

Figure A3 - 43

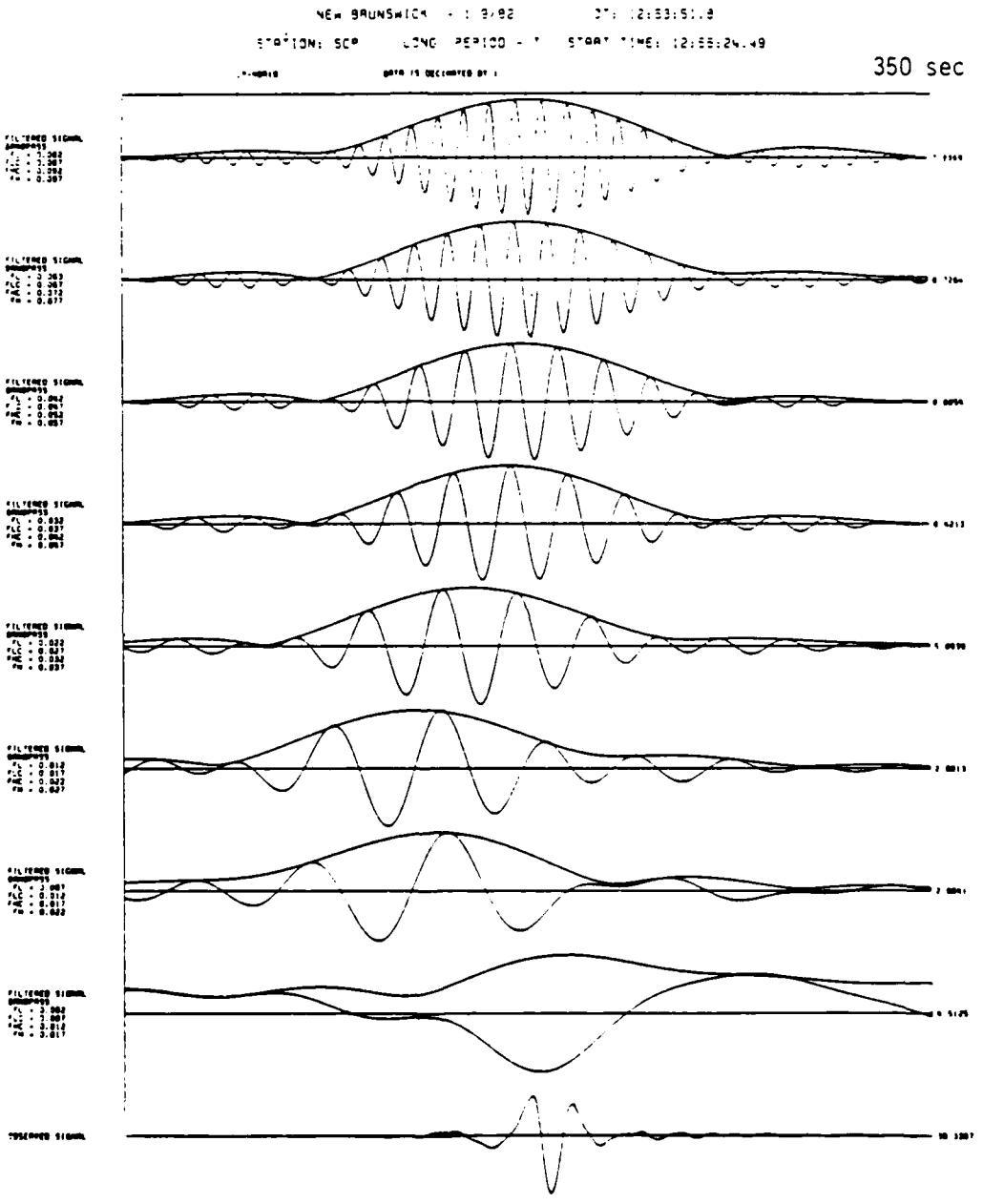

Figure A3 - 44

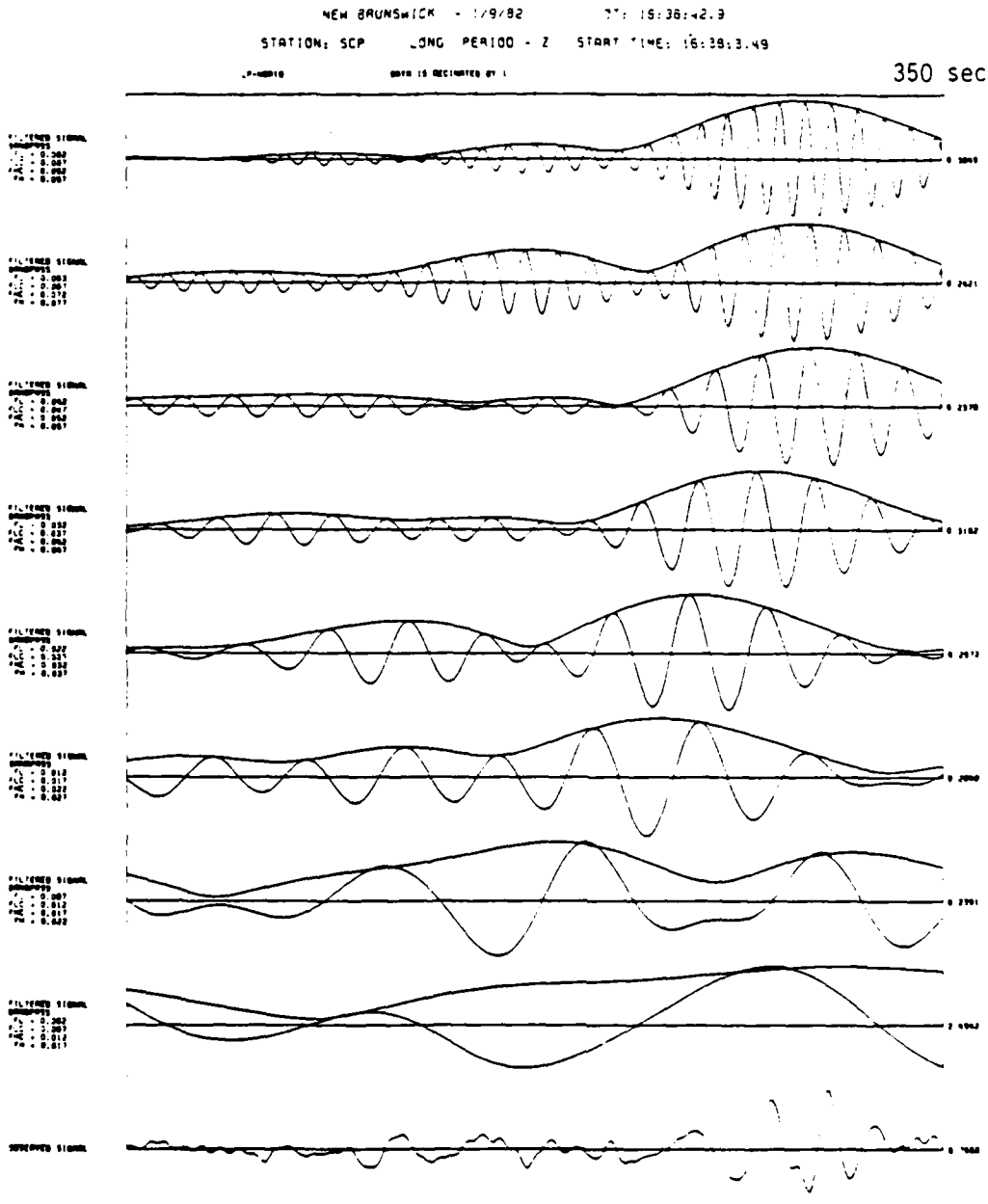
NEW BRUNSWICK - 1/9/82
STATION: SCP
LONG PERIOD - Z
START TIME: 16:38:3.49
350 sec

Figure A3 - 45

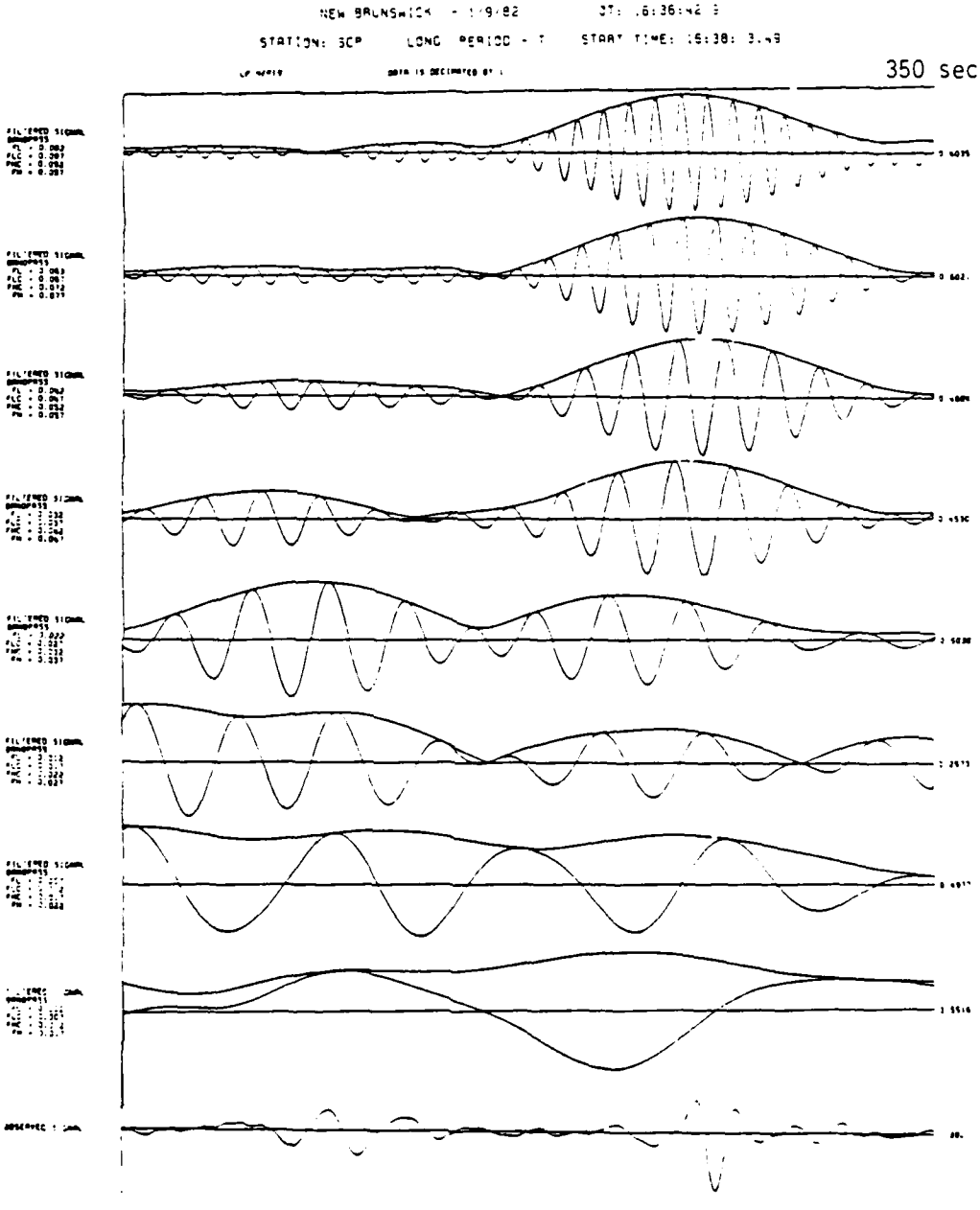

Figure A3 - 46

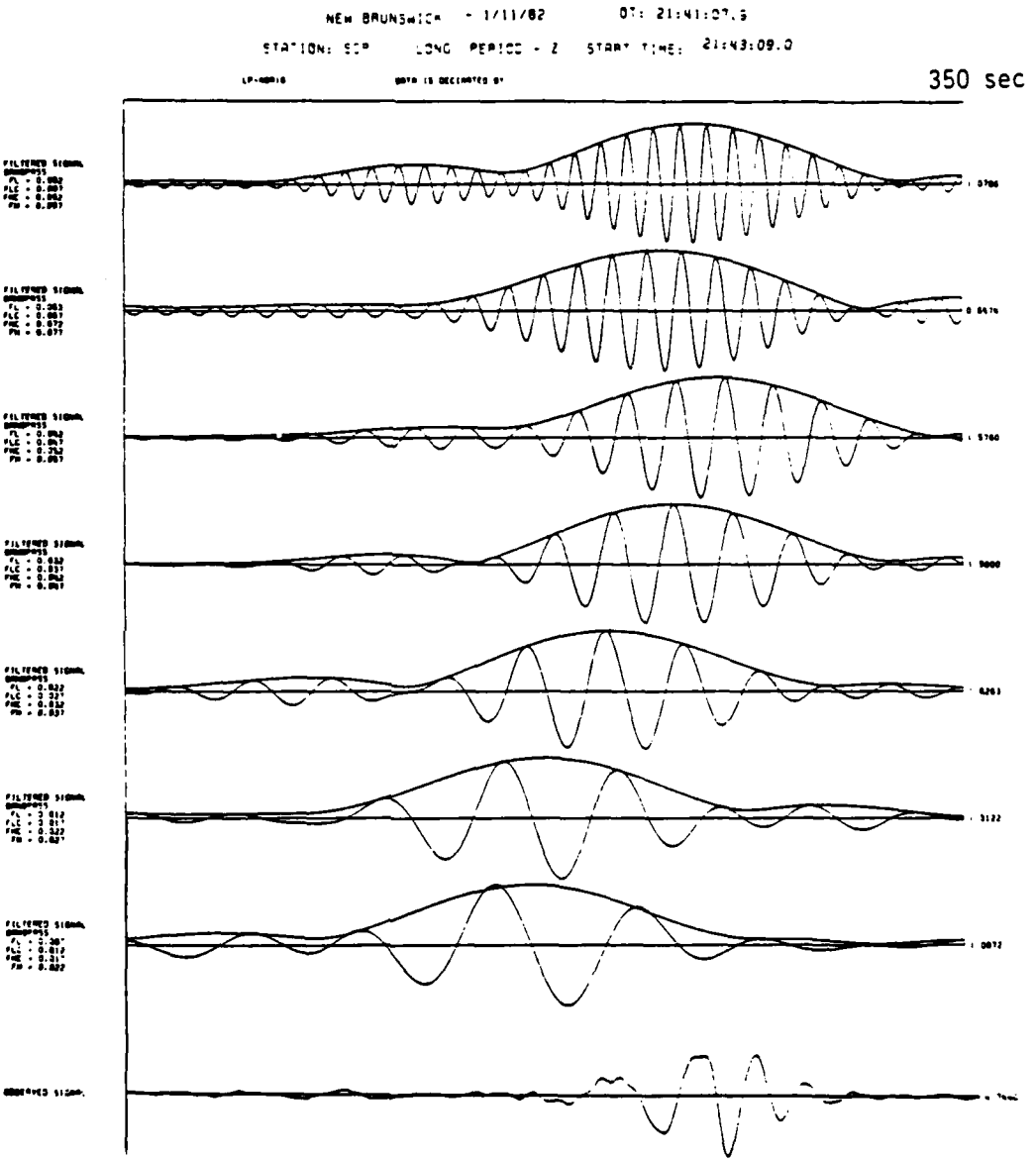
NEW BRUNSWICK - 1/11/82
STATION: SCP LONG PERIOD - Z START TIME: 21:43:09.0
350 sec

Figure A3 - 47

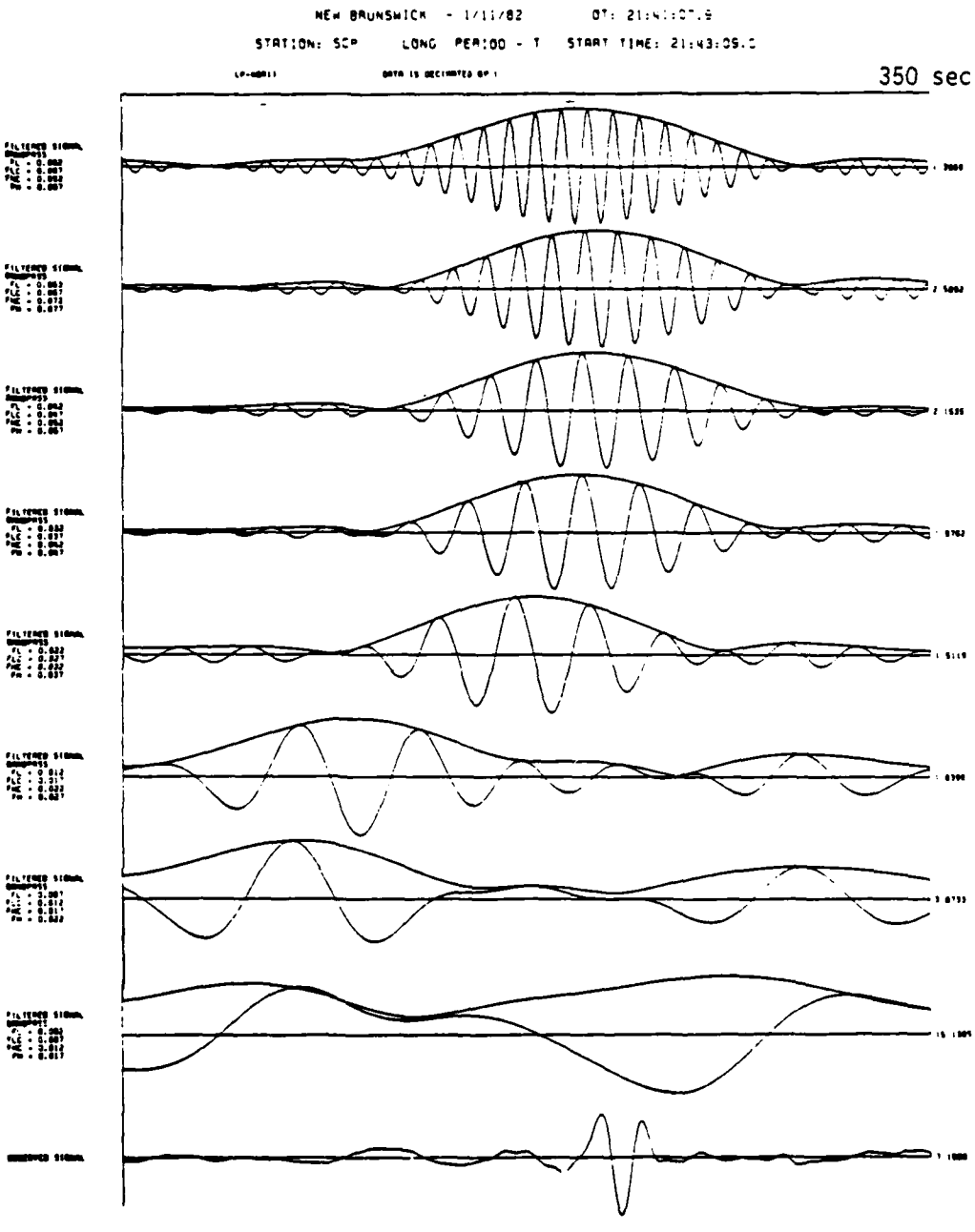
NEW BRUNSWICK - 1/11/82
STATION: SCP LONG PER:00 - T START TIME: 21:43:09.0
350 sec

Figure A3 - 48

The filter parameters for Figures A3 - 49 through 54 are as indicated:

FL = 0.003	FLC = 0.008	FHC = 0.013	FH = 0.018
FL = 0.004	FLC = 0.009	FHC = 0.014	FH = 0.019
FL = 0.004	FLC = 0.009	FHC = 0.014	FH = 0.019
FL = 0.005	FLC = 0.010	FHC = 0.015	FH = 0.020
FL = 0.005	FLC = 0.010	FHC = 0.015	FH = 0.020
FL = 0.009	FLC = 0.014	FHC = 0.019	FH = 0.024
FL = 0.017	FLC = 0.022	FHC = 0.027	FH = 0.032
FL = 0.092	FLC = 0.097	FHC = 0.102	FH = 0.107

OBSERVED SIGNAL

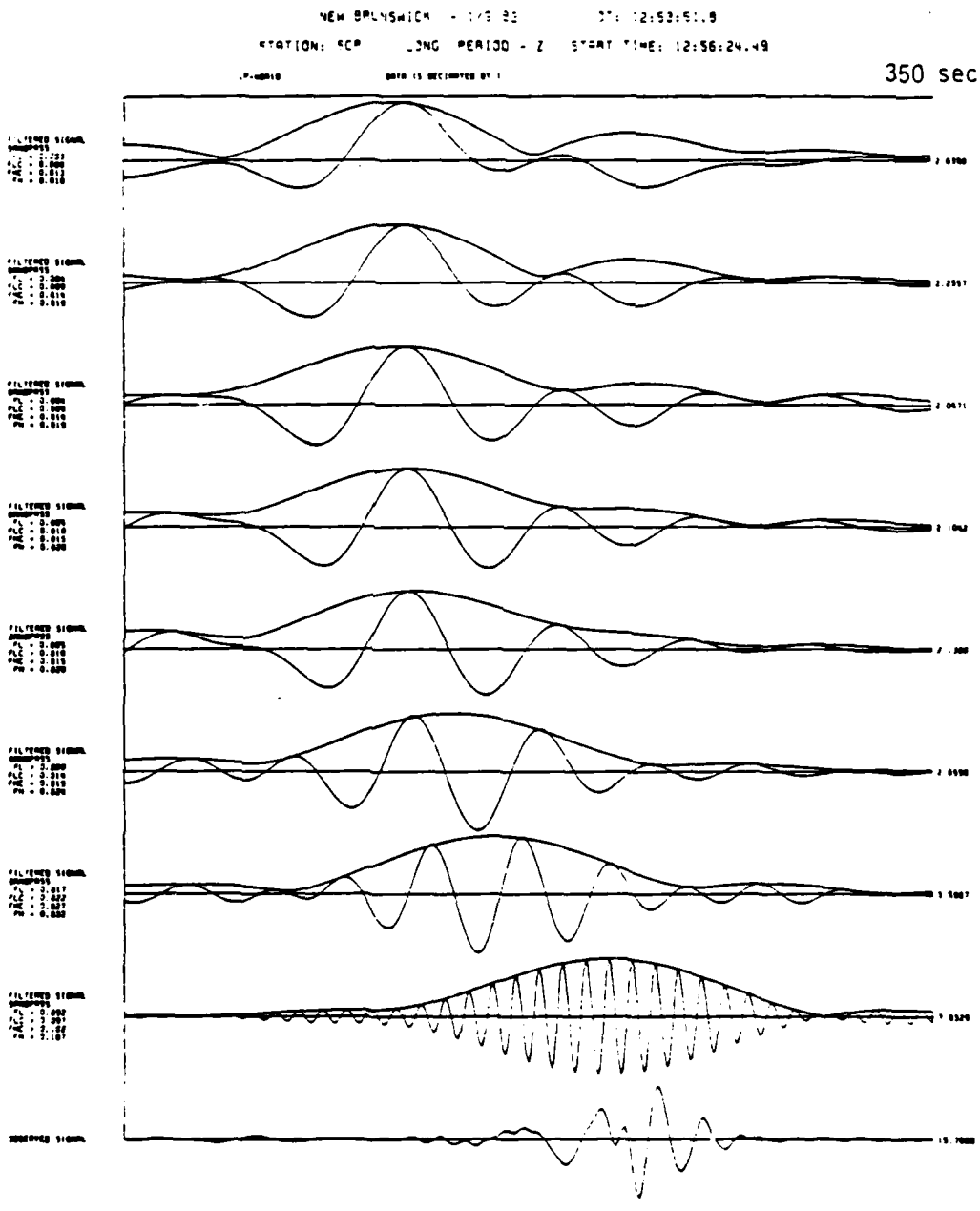

Figure A3 - 49

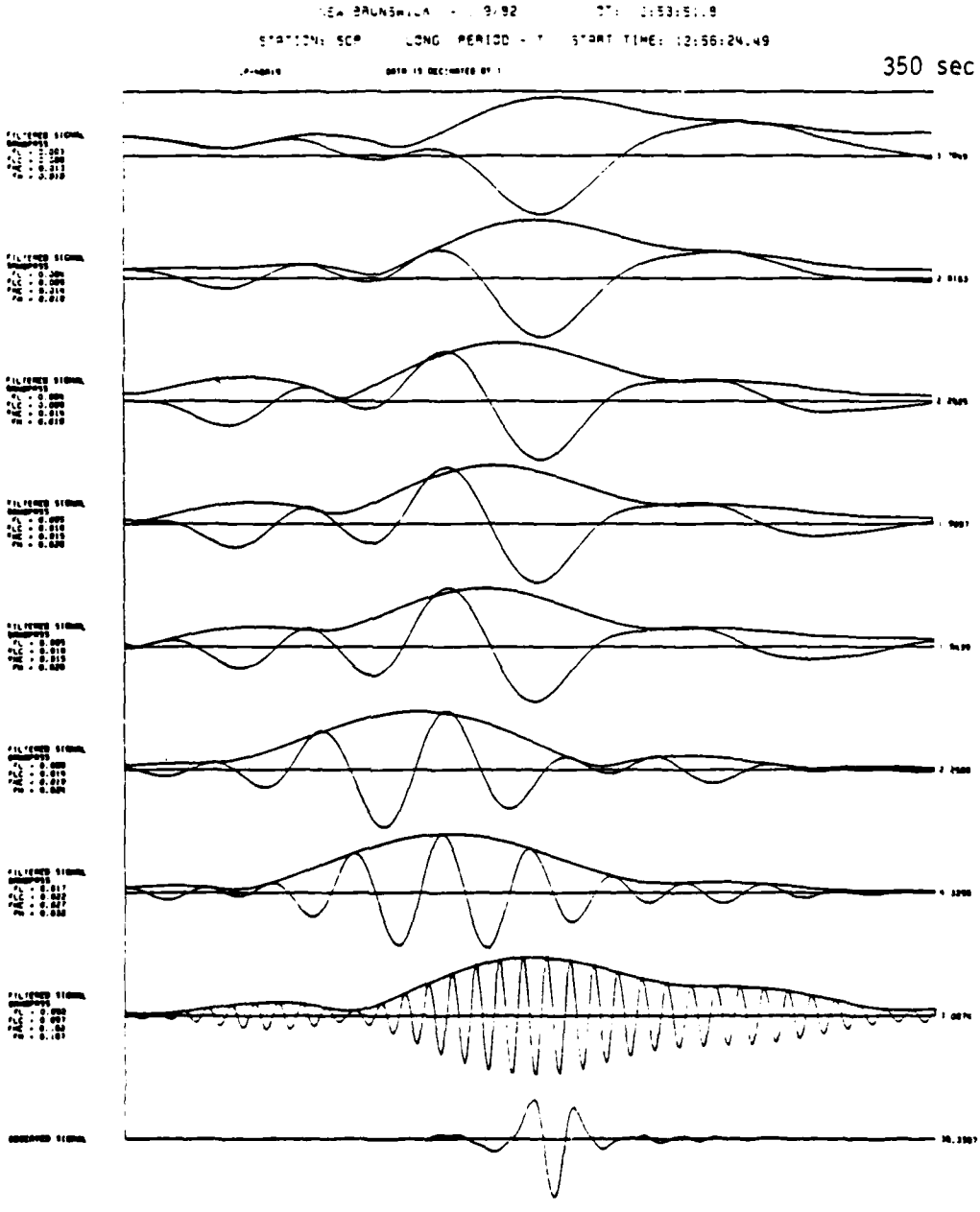

Figure A3 - 50

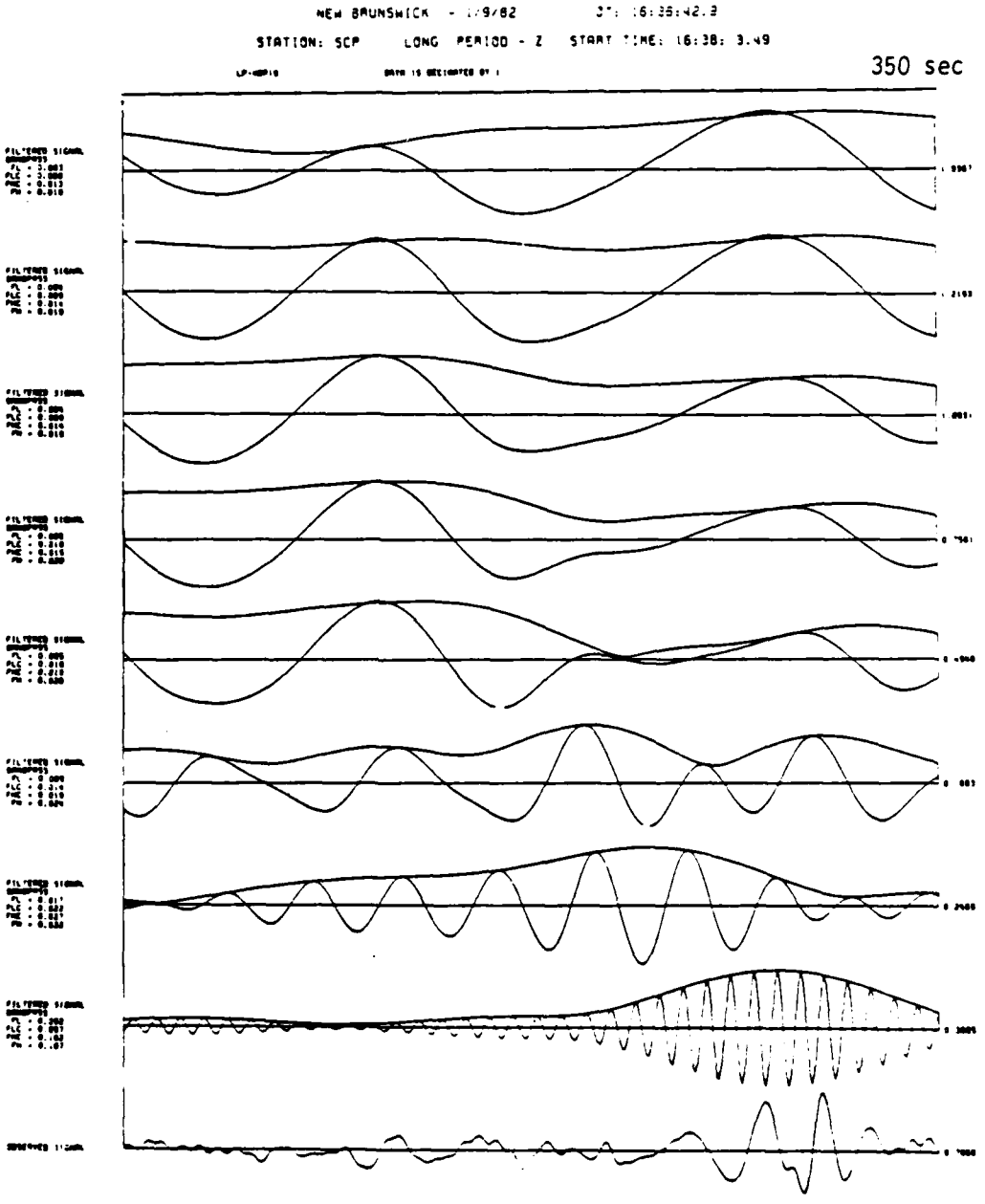

Figure A3 - 51

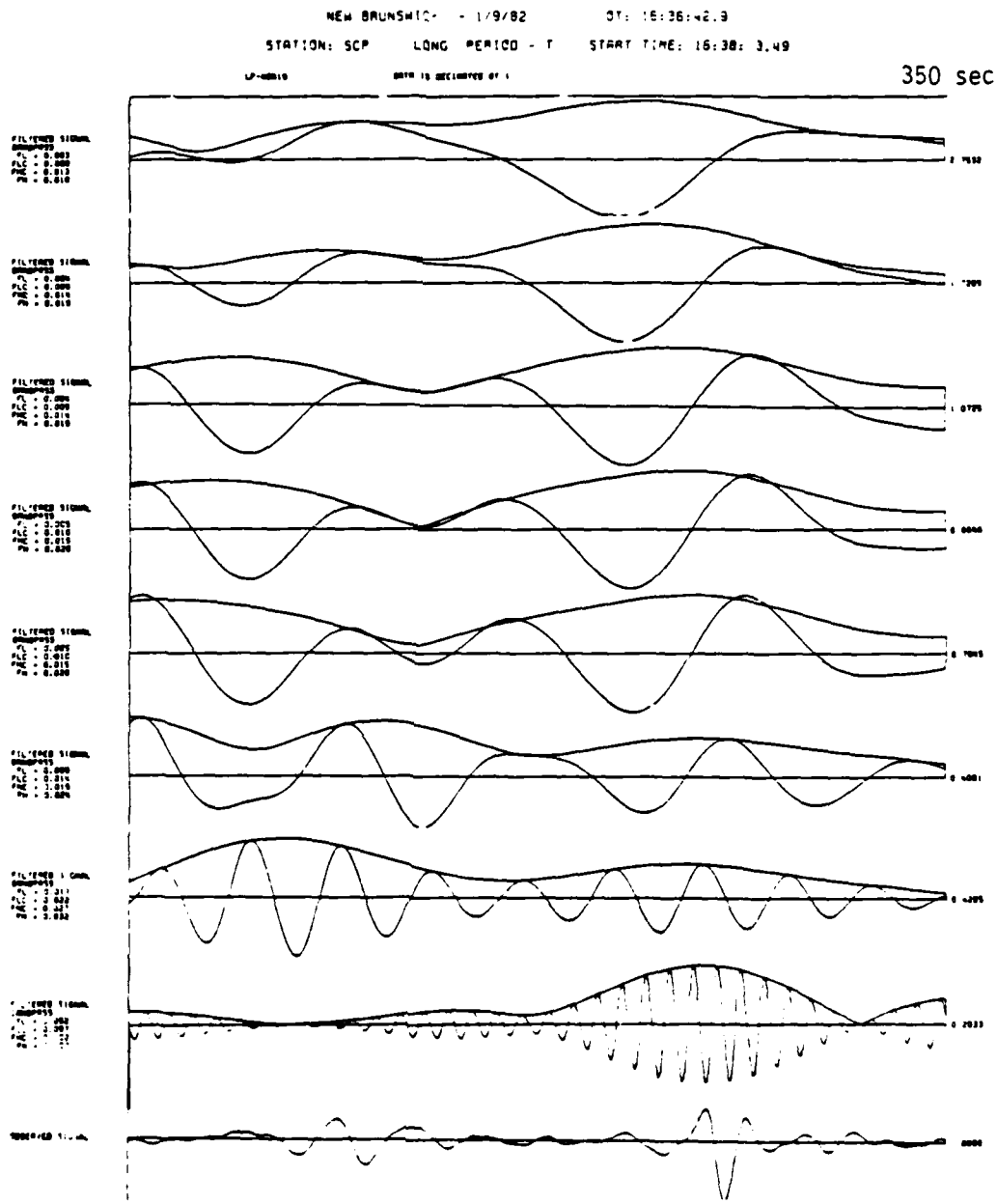
NEW BRUNSWIC- - 1/9/82 OT: 16:36:42.9
STATION: SCP LONG PERIOD - T START TIME: 16:38: 3.49
350 sec

Figure A3 - 52

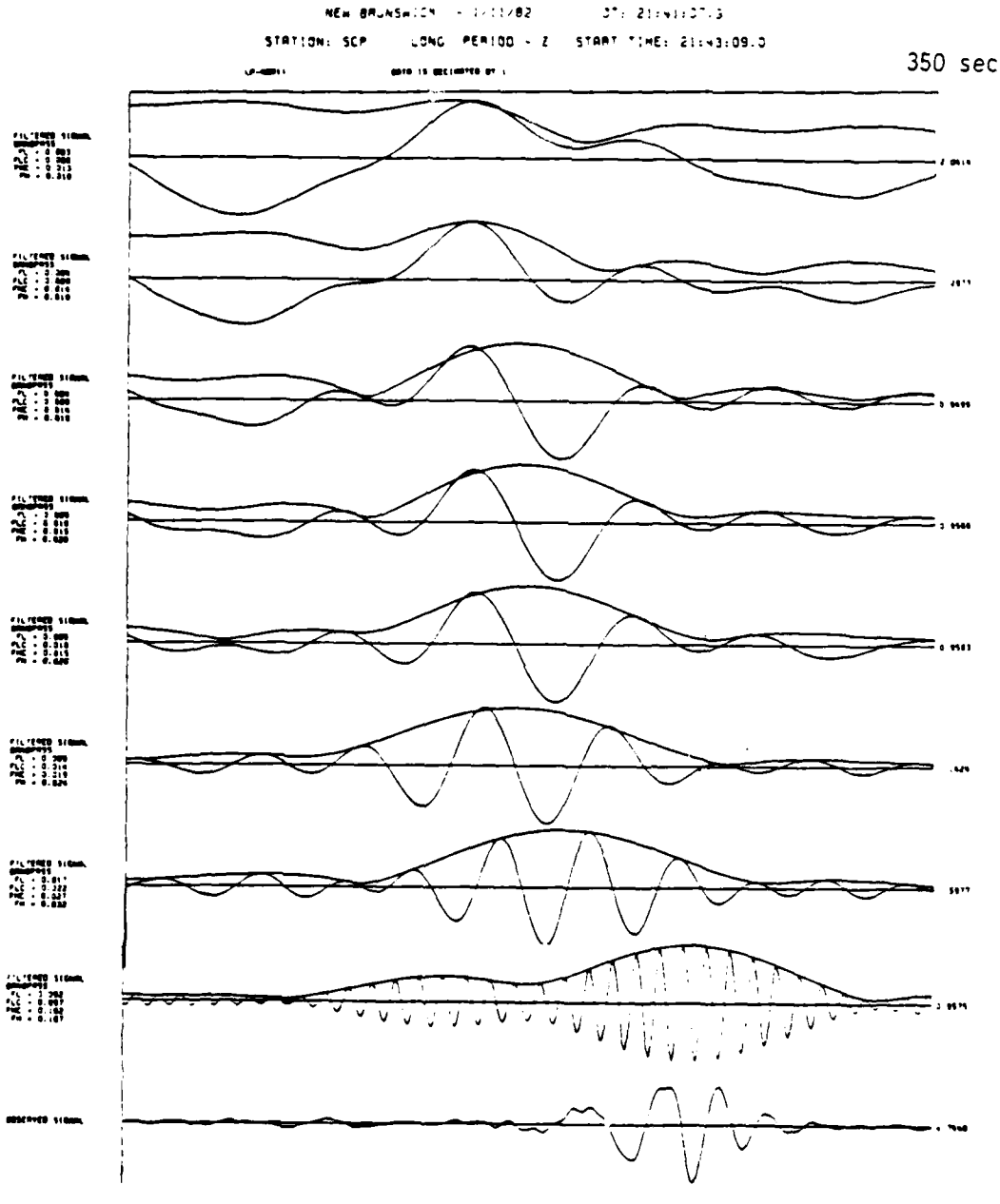

Figure A3 - 53

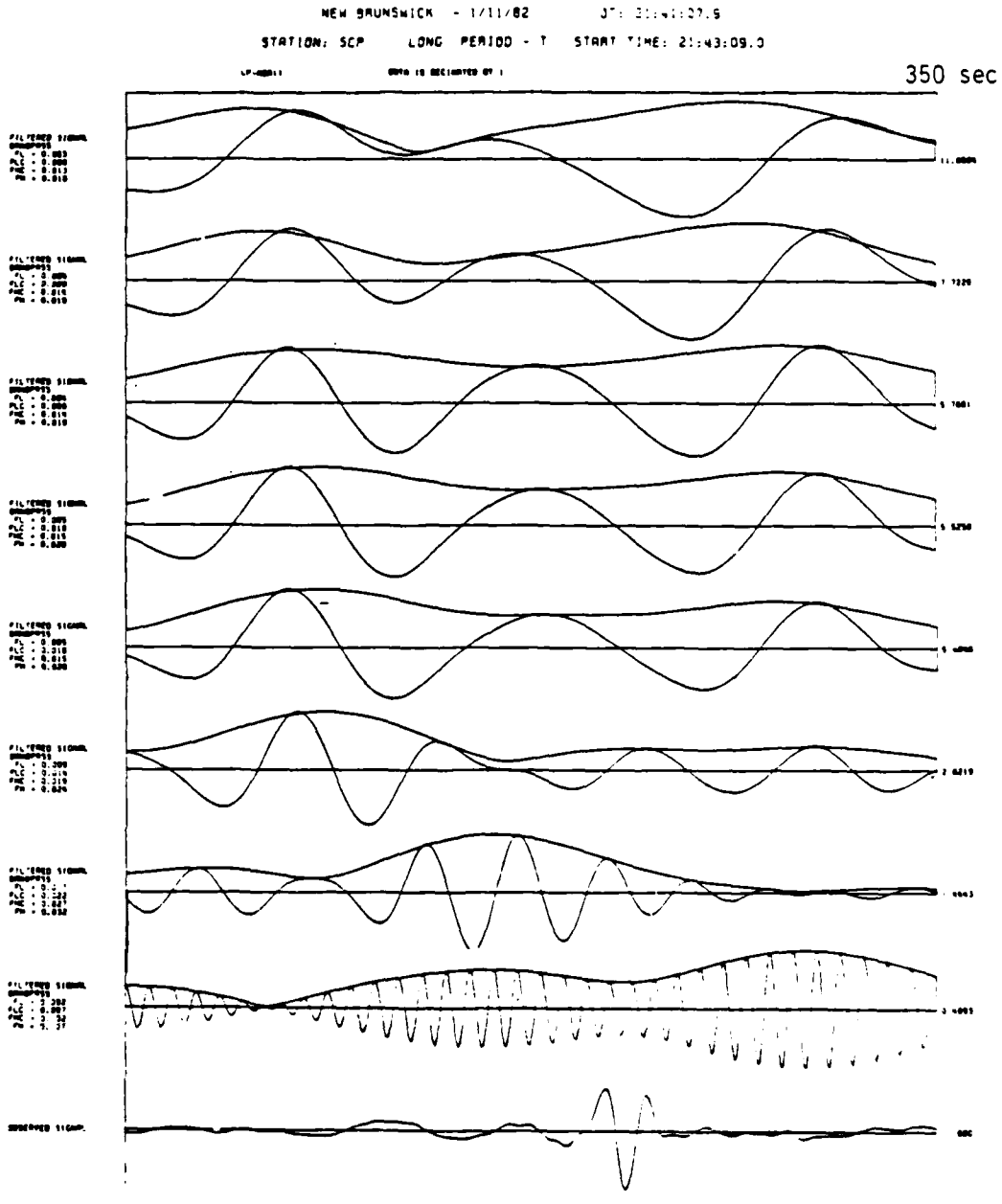
NEW BRUNSWICK - 1/11/82
STATION: SCP LONG PERIOD - T START TIME: 21:43:09.0
350 sec

Figure A3 - 54

APPENDIX 4

Theoretical Dispersion Curves and Band-Pass Dispersion Data

Appendix 4 presents a compilation of group velocity results for all events superimposed and each event separately, with overlying theoretical dispersion curves appropriate for the Love and Rayleigh modes. As in Figures 10-13, the different symbols correspond to values of peak amplitudes. Each peak amplitude is normalized to the maximum amplitude for the given band-pass and then assigned a symbol according to the following scheme:

10 - the point having the peak amplitude for the given central frequency

9 - those point(s) representing peaks along the filtered signal with amplitude(s) 80-99% of maximum for that trace

8 - those point(s) representing peaks along the filtered signal with amplitude(s) 60-79% of maximum for that trace

7 - those point(s) representing peaks along the filtered signal with amplitudes less than 59% of maximum for that trace

This scale made possible rapid identification of significant arrivals by visual inspection.

Figure A4-1 shows the results for the vertical component band-pass filters for all four events with theoretical Rayleigh dispersion superimposed; Figure A4-2 shows this same information separately for each event. Similarly,. Figure A4-3 shows the Love mode results for all events, while Figure A4-4 shows the results separately by event.

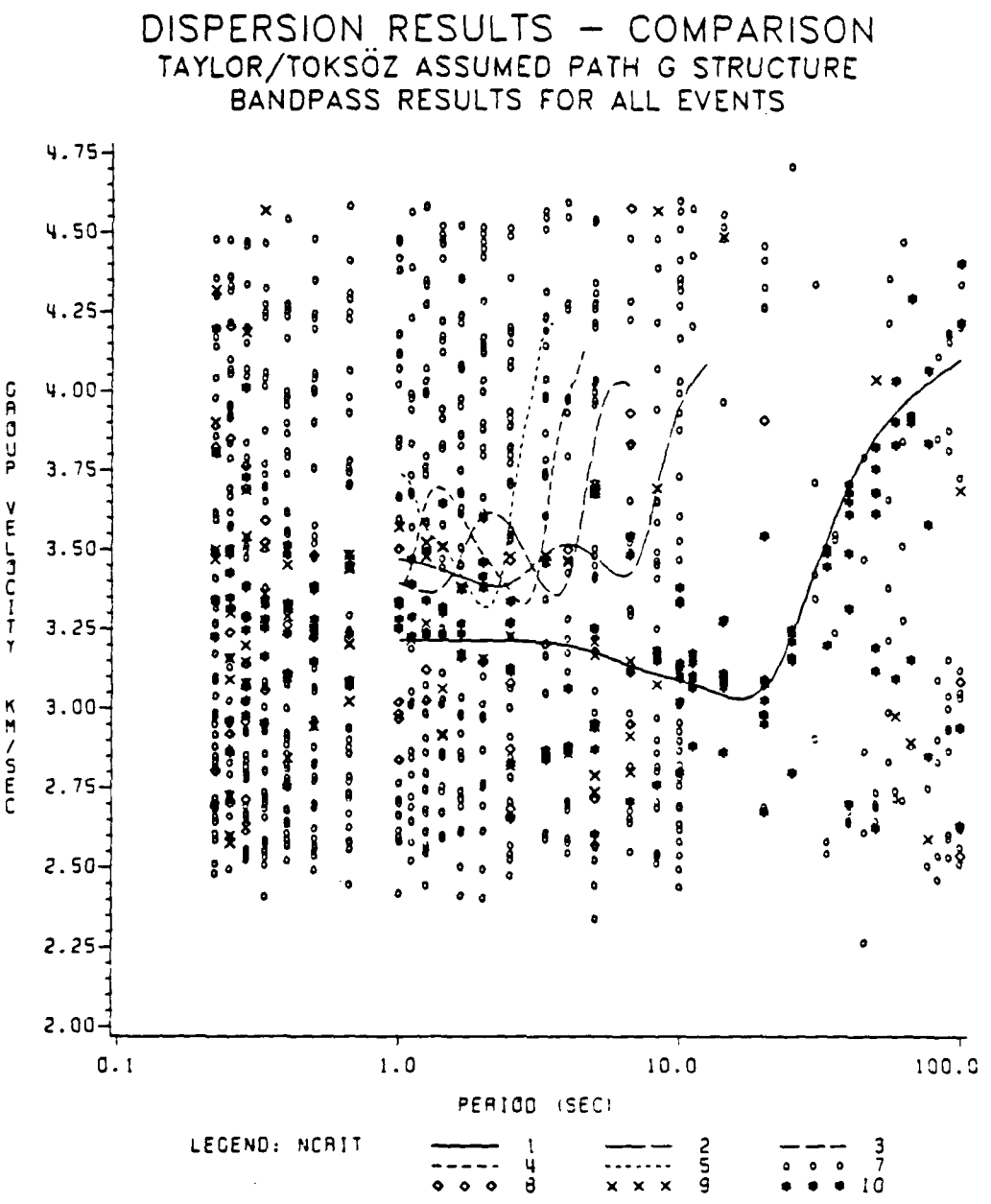

5 RAYLEIGH MODES SHOWN

Figure A4 - 1

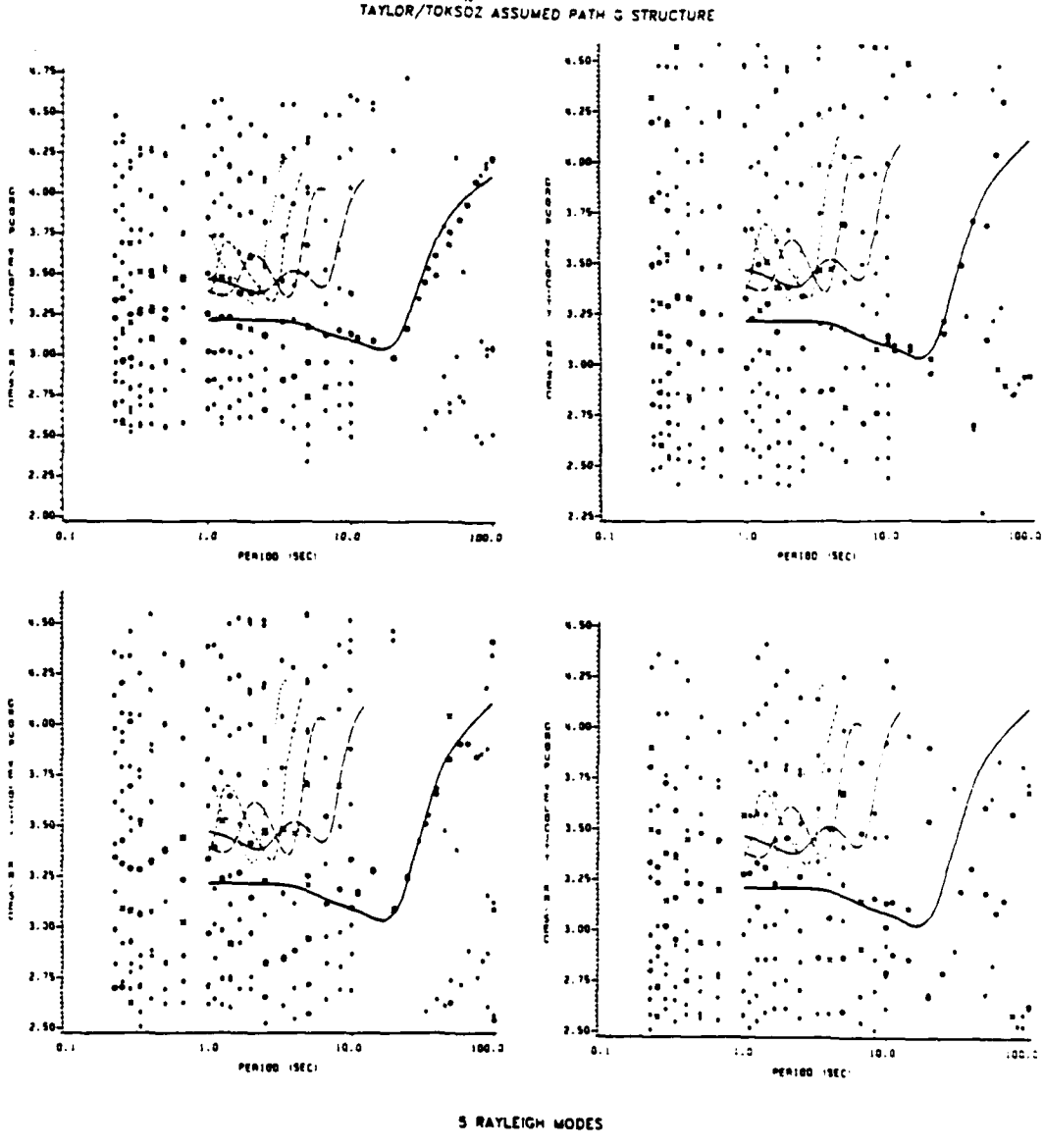
TAYLOR/TOKSÖZ ASSUMED PATH G STRUCTURE
PERIOD (SEC)
5 RAYLEIGH MODES

Figure A4 - 2

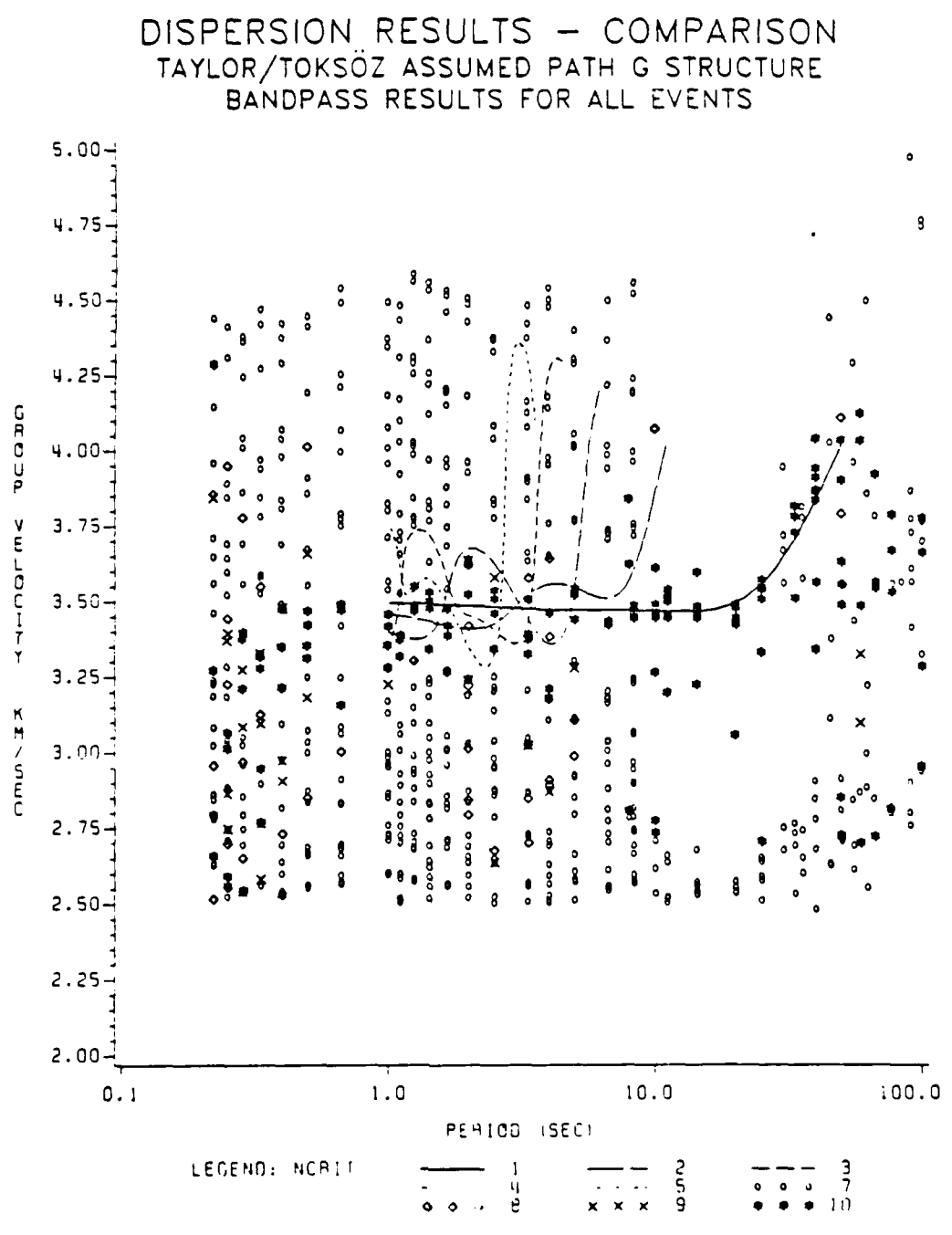
DISPERSION RESULTS – COMPARISON
TAYLOR/TOKSÖZ ASSUMED PATH G STRUCTURE
BANDPASS RESULTS FOR ALL EVENTS
GROUP VELOCITY (KM/SEC)
5.00
4.75
4.50
4.25
4.00
3.75
3.50
3.25
3.00
2.75
2.50
2.25
2.00
0.1
1.0
10.0
100.0
PERIOD (SEC)
LEGEND: NCRIT
1
2
3
4
5
7
8
9
10

Figure A4 - 3

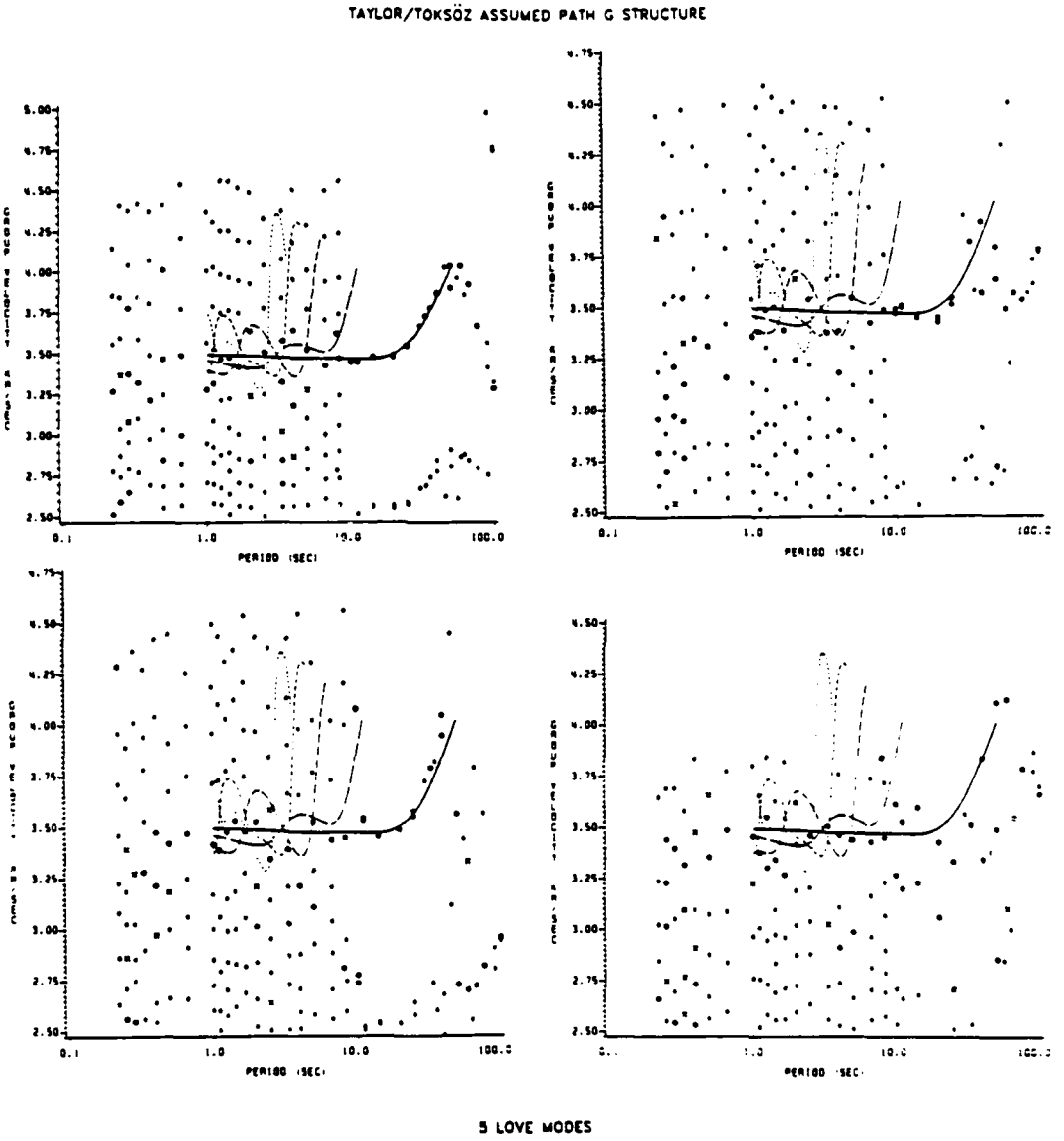
TAYLOR/TOKSÖZ ASSUMED PATH G STRUCTURE
PERIOD (SEC)
5 LOVE MODES

Figure A4 - 4

APPENDIX 5

Theoretical Spectra

And Spectral Ratios

Appendix 5 presents theoretical Love and Rayleigh spectra and Love-to-Rayleigh spectral ratios, by depth, for the four source mechanisms studied in this paper. Fundamental mode values are plotted as solid lines. Successively higher order modes are represented by lines of increasing dash-length. Depths of one to ten kilometers are considered for each model.

In each figure, (a) shows the theoretical Love amplitude spectrum; (b) shows the theoretical Rayleigh amplitude spectrum; and (c) shows the Love-to-Rayleigh spectral ratio.

Figures A5 - 1 through 5 are results for source parameters of the Choy mechanism: $\theta = 318^{o}$, $\delta = 65^{o}$, $\lambda = 70^{o}$.

Figures A5 - 6 through 10 are results for source parameters of the Nabelek mechanism: $\theta = 306^{o}$, $\delta = 34^{o}$, $\lambda = 95^{o}$.

Figures A5 - 11 through 15 are results for source parameters of the Wetmiller mechanism for the mainshock: $\theta = 318^{o}$, $\delta = 50^{o}$, $\lambda = 120^{o}$.

Figures A5 - 16 through 20 are results for source parameters of the Wetmiller mechanism for the January 11 aftershock: $\theta = 95^{o}$, $\delta = 48^{o}$, $\lambda = 59^{o}$.

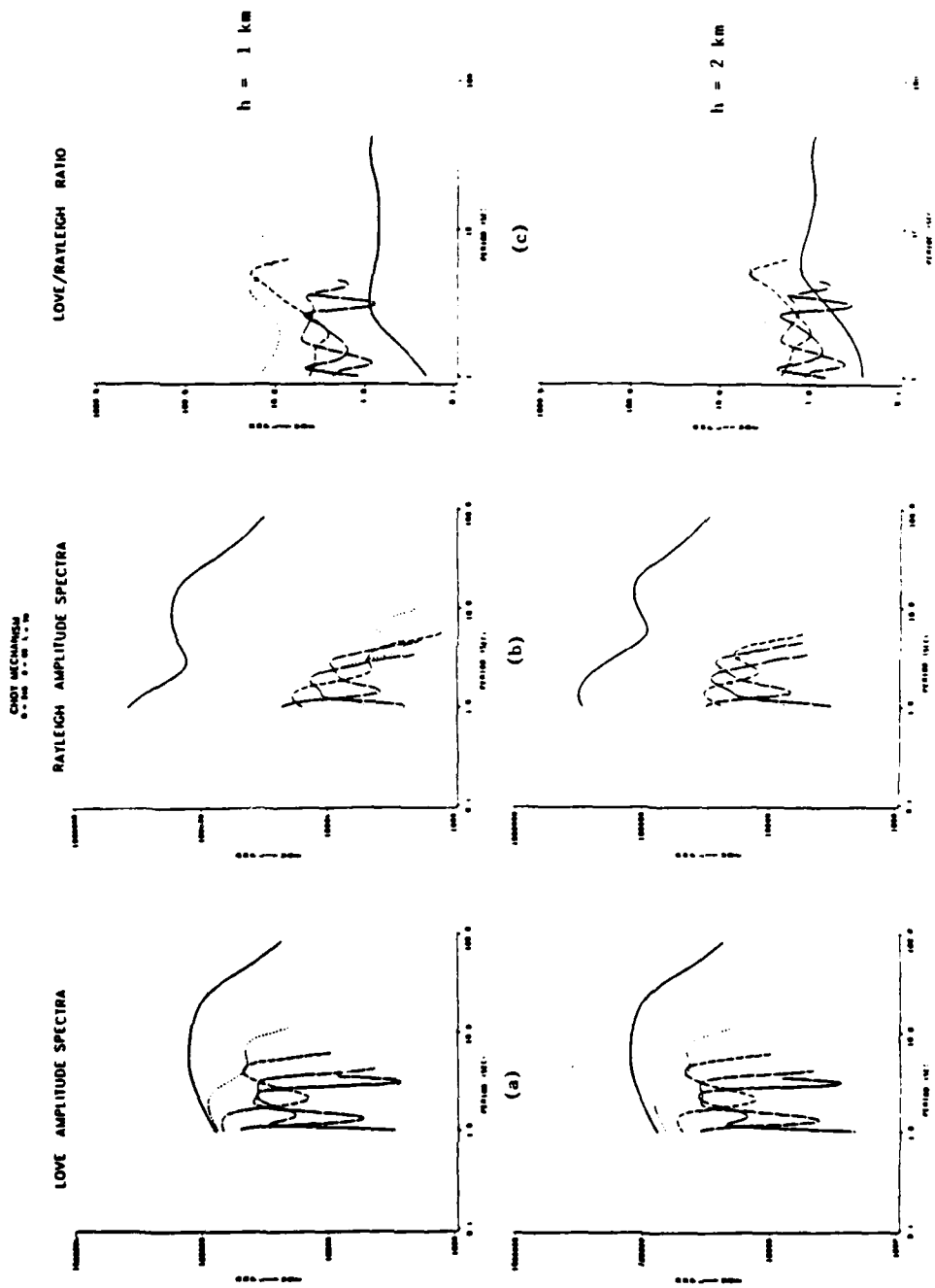
LOVE AMPLITUDE SPECTRA
RAYLEIGH AMPLITUDE SPECTRA
LOVE/RAYLEIGH RATIO
h = 1 km
h = 2 km
(a)
(b)
(c)

Figure A5 - 1

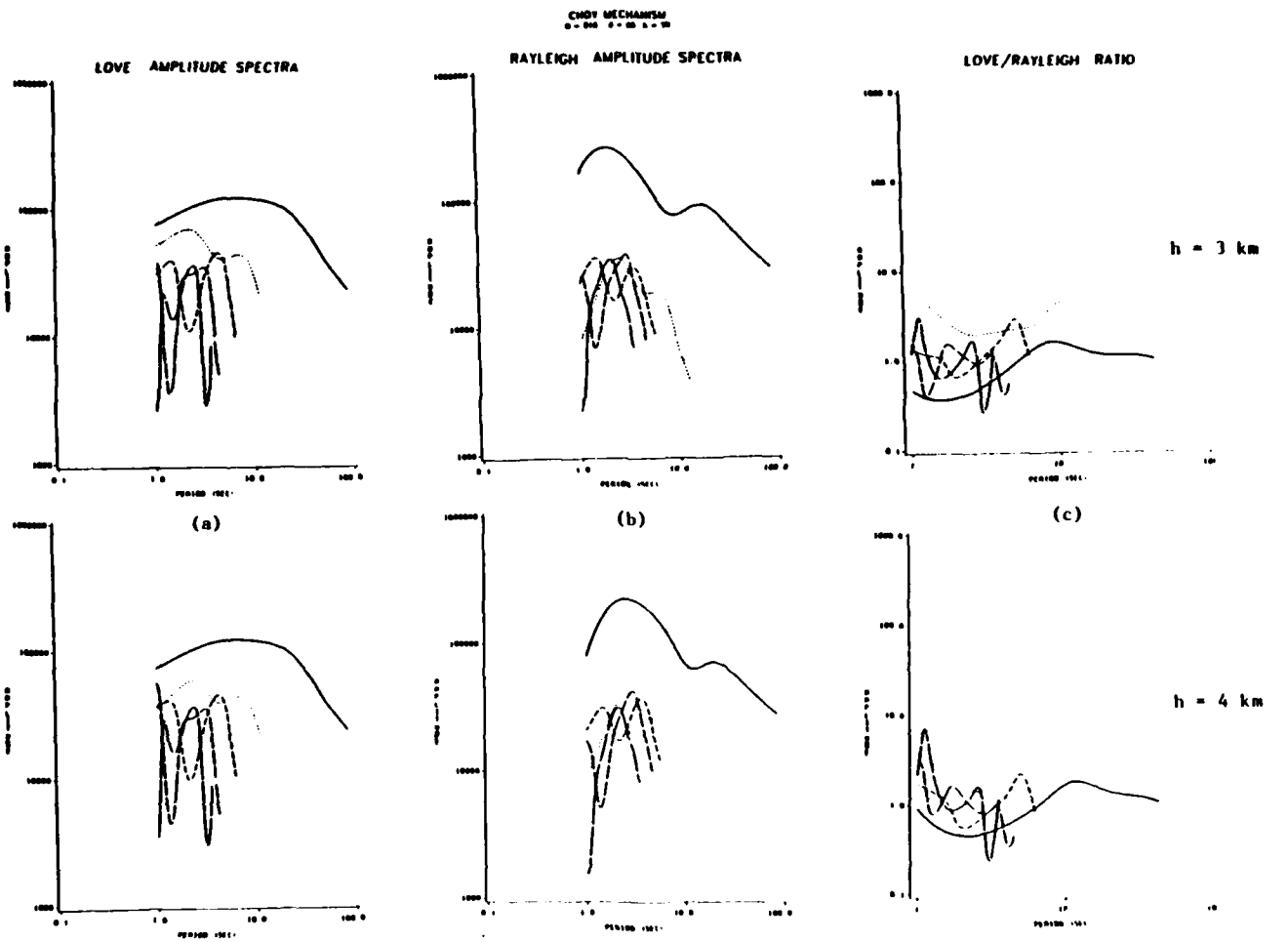
CHOY MECHANISM
LOVE AMPLITUDE SPECTRA
RAYLEIGH AMPLITUDE SPECTRA
LOVE/RAYLEIGH RATIO
h = 3 km
h = 4 km
(a)
(b)
(c)

Figure A5 -2

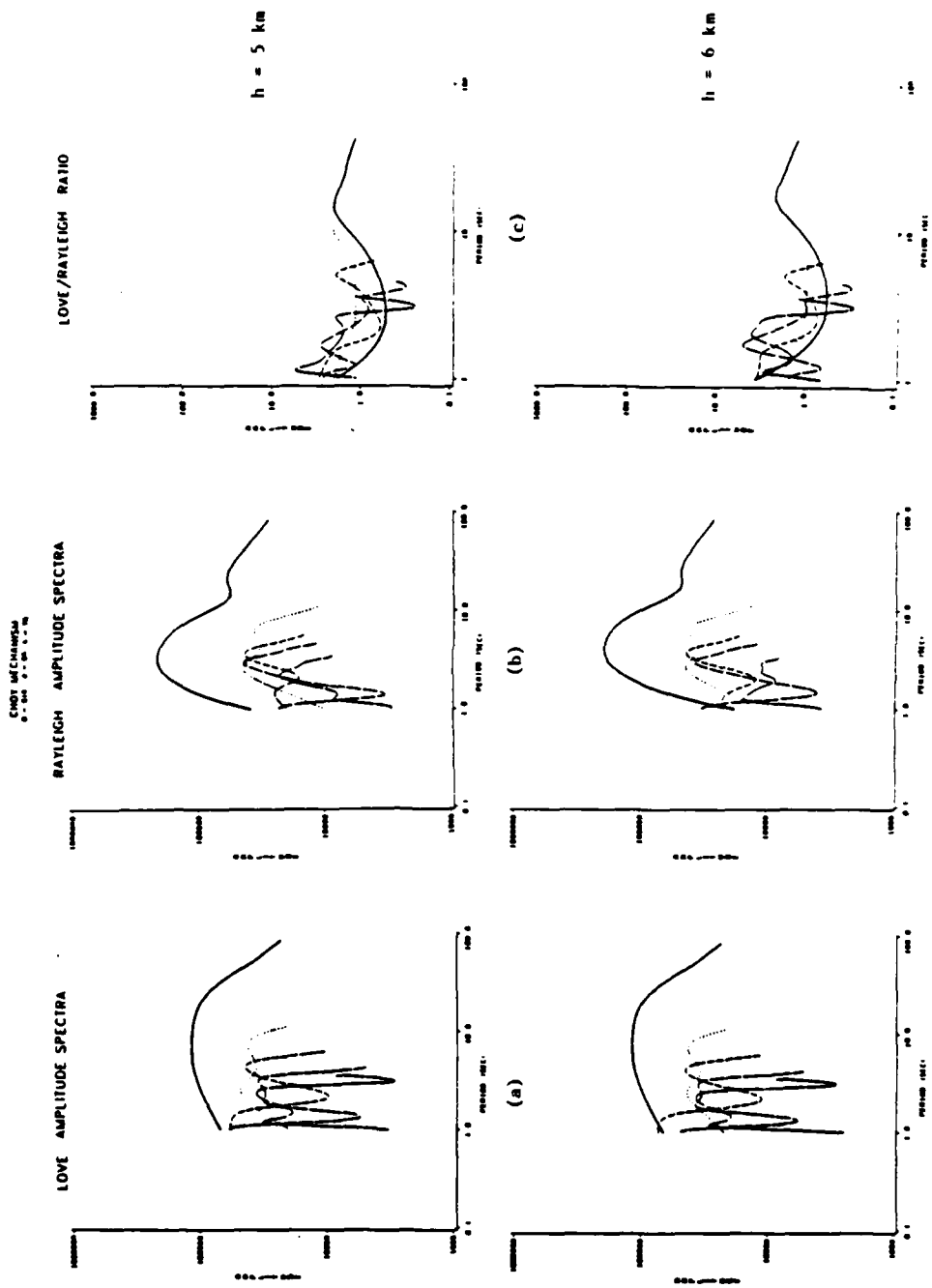
LOVE AMPLITUDE SPECTRA
RAYLEIGH AMPLITUDE SPECTRA
LOVE/RAYLEIGH RATIO
h = 5 km
h = 6 km
(a)
(b)
(c)

Figure A5 - 3

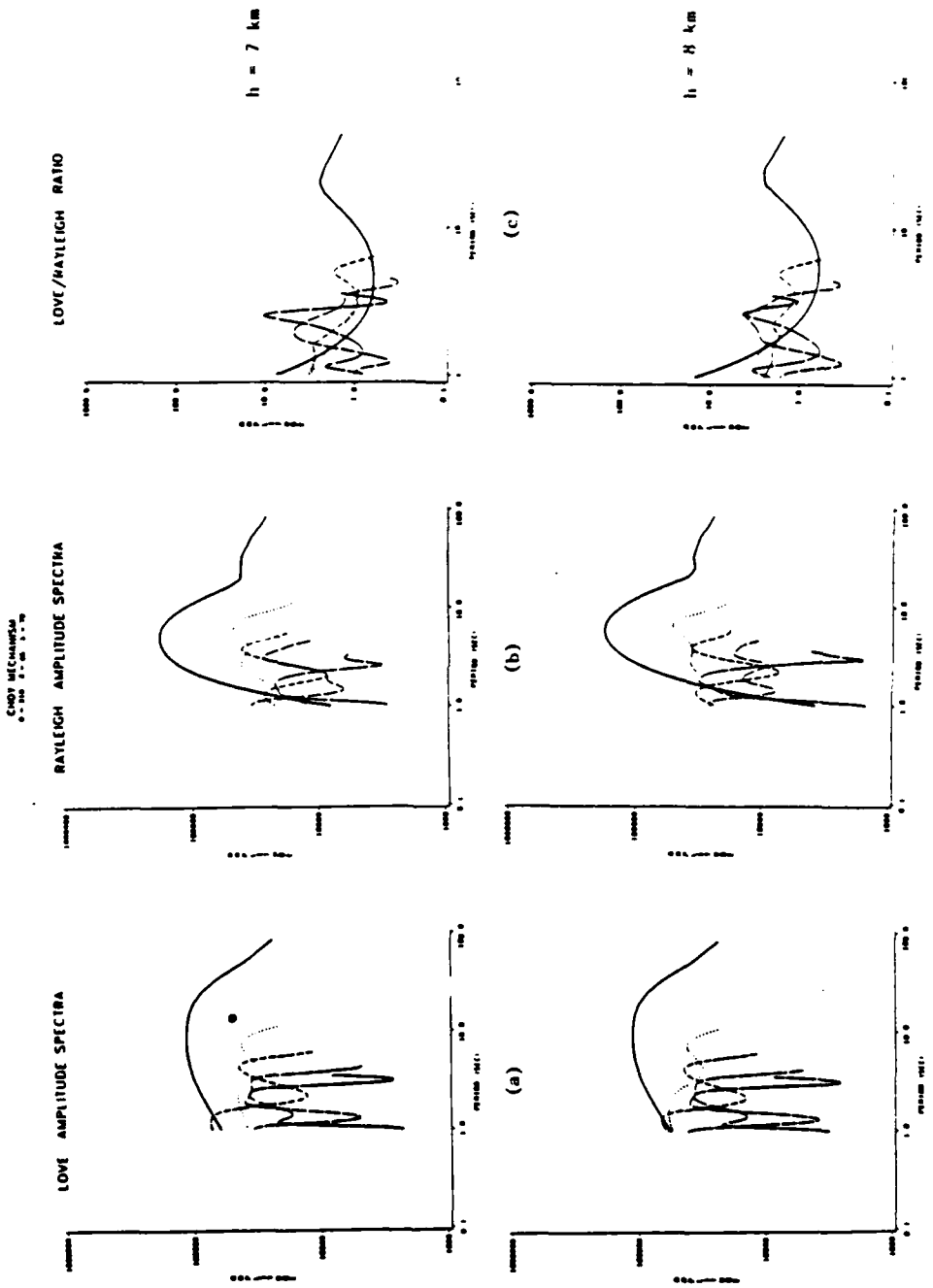
LOVE AMPLITUDE SPECTRA
RAYLEIGH AMPLITUDE SPECTRA
LOVE/RAYLEIGH RATIO
h = 7 km
h = 8 km
(a)
(b)
(c)

Figure A5 - 4

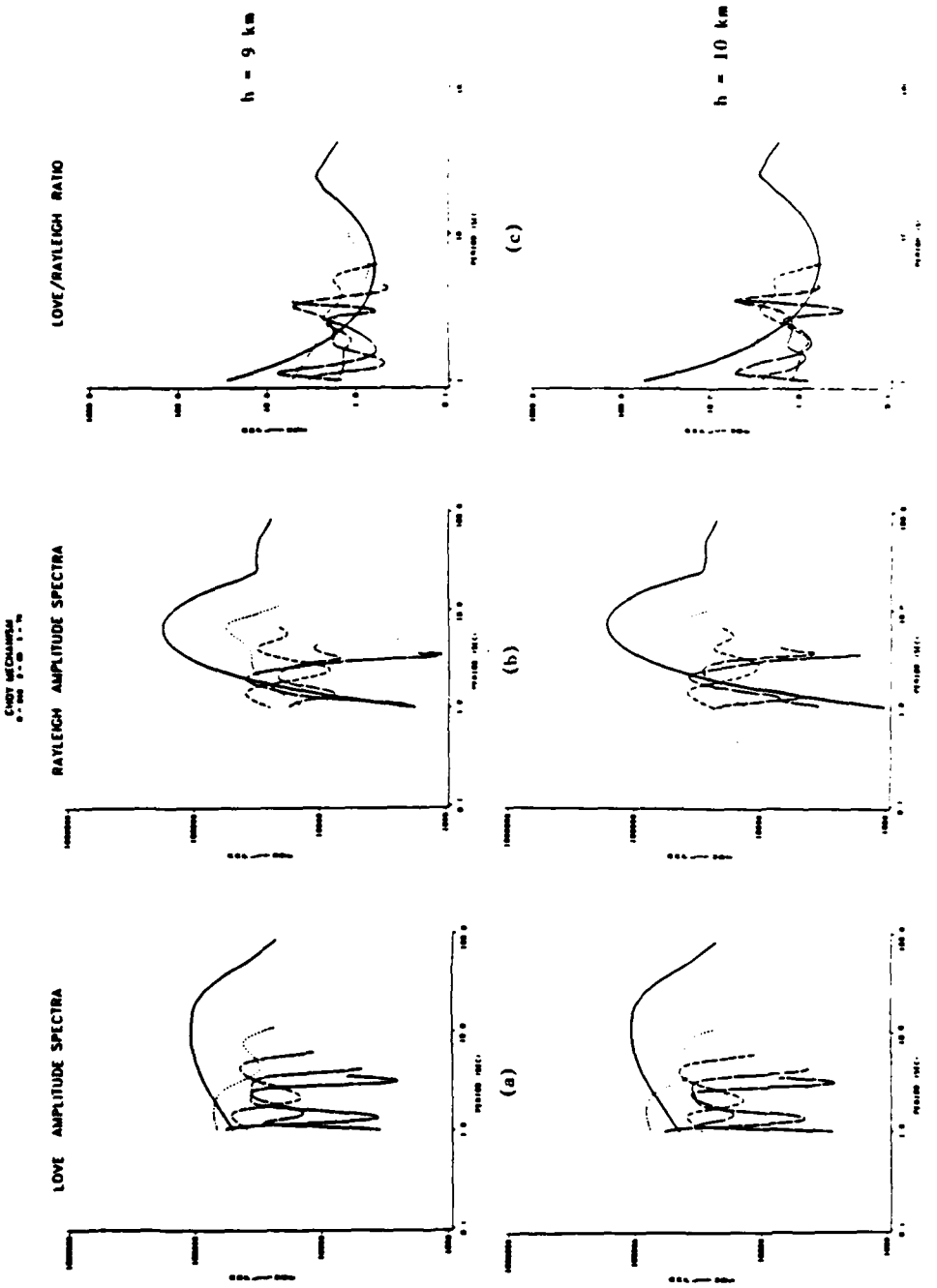
LOVE AMPLITUDE SPECTRA
RAYLEIGH AMPLITUDE SPECTRA
LOVE/RAYLEIGH RATIO
h = 9 km
h = 10 km
(a)
(b)
(c)

Figure A5 - 5

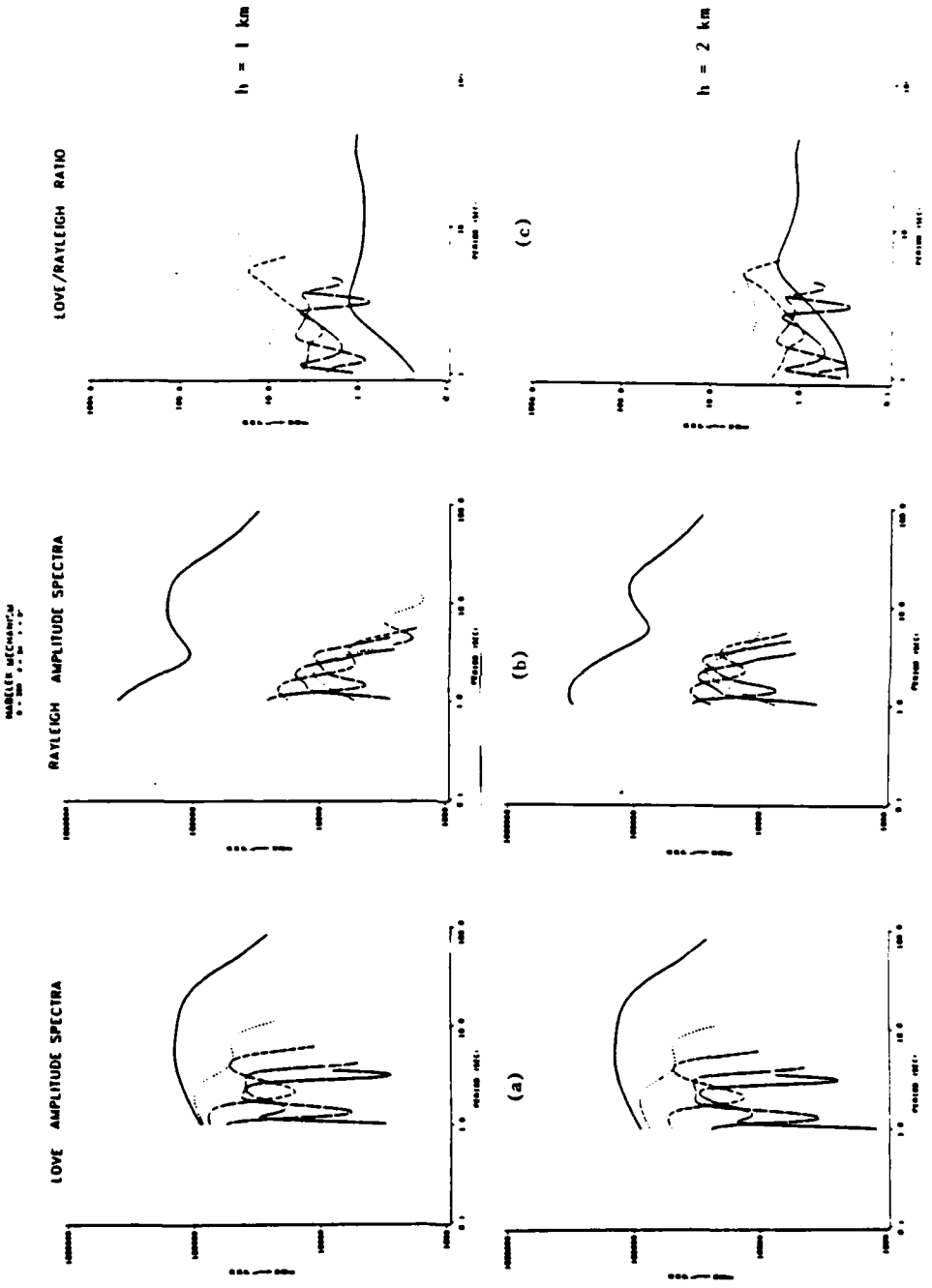
LOVE AMPLITUDE SPECTRA
RAYLEIGH AMPLITUDE SPECTRA
LOVE/RAYLEIGH RATIO
h = 1 km
h = 2 km
(a)
(b)
(c)

Figure A5 - 6

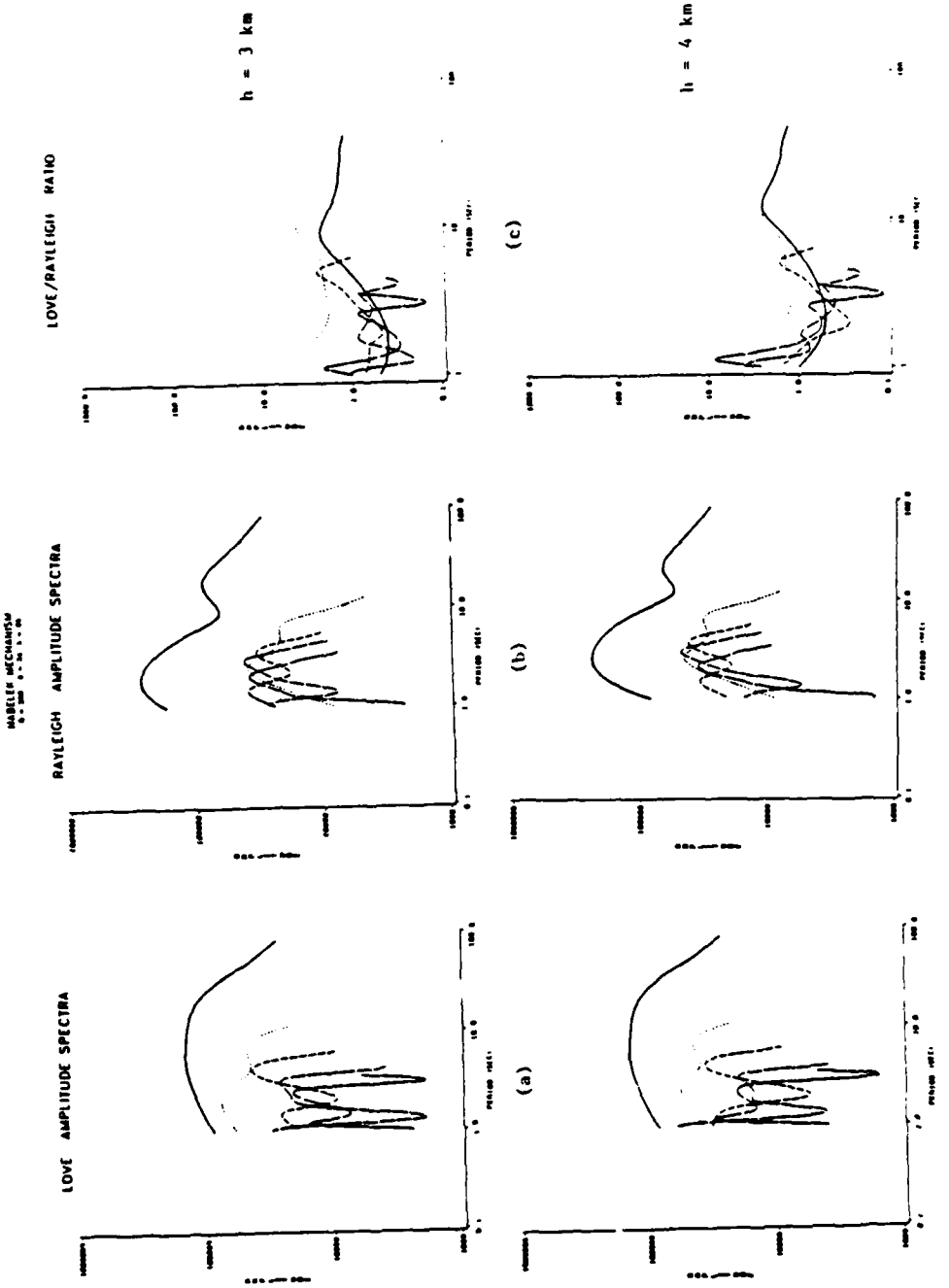
LOVE AMPLITUDE SPECTRA
RAYLEIGH AMPLITUDE SPECTRA
LOVE/RAYLEIGH RATIO
h = 3 km
h = 4 km
(a)
(b)
(c)

Figure A5 - 7

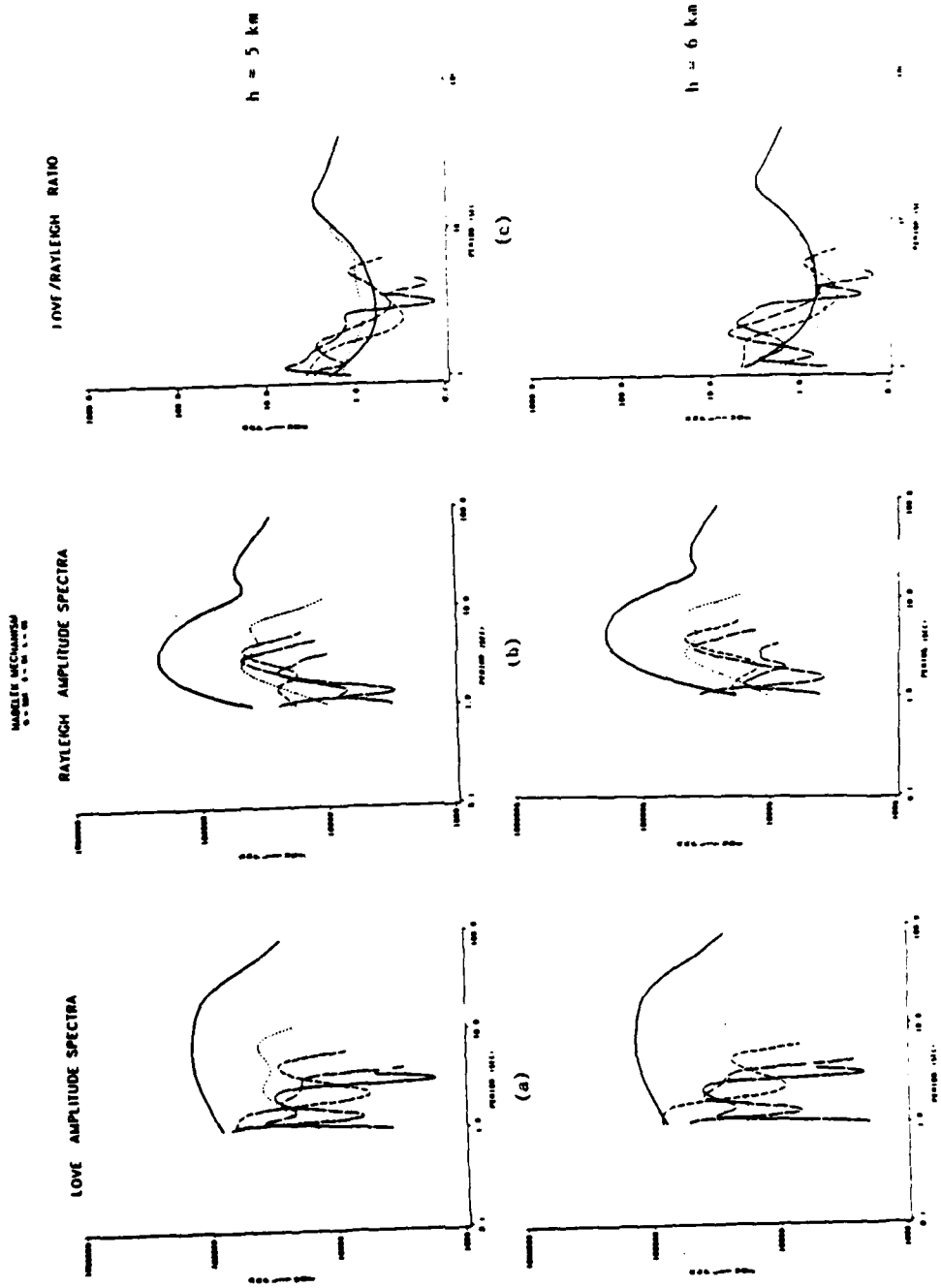
LOVE AMPLITUDE SPECTRA
RAYLEIGH AMPLITUDE SPECTRA
LOVE/RAYLEIGH RATIO
h = 5 km
h = 6 km
(a)
(b)
(c)

Figure A5 - 8

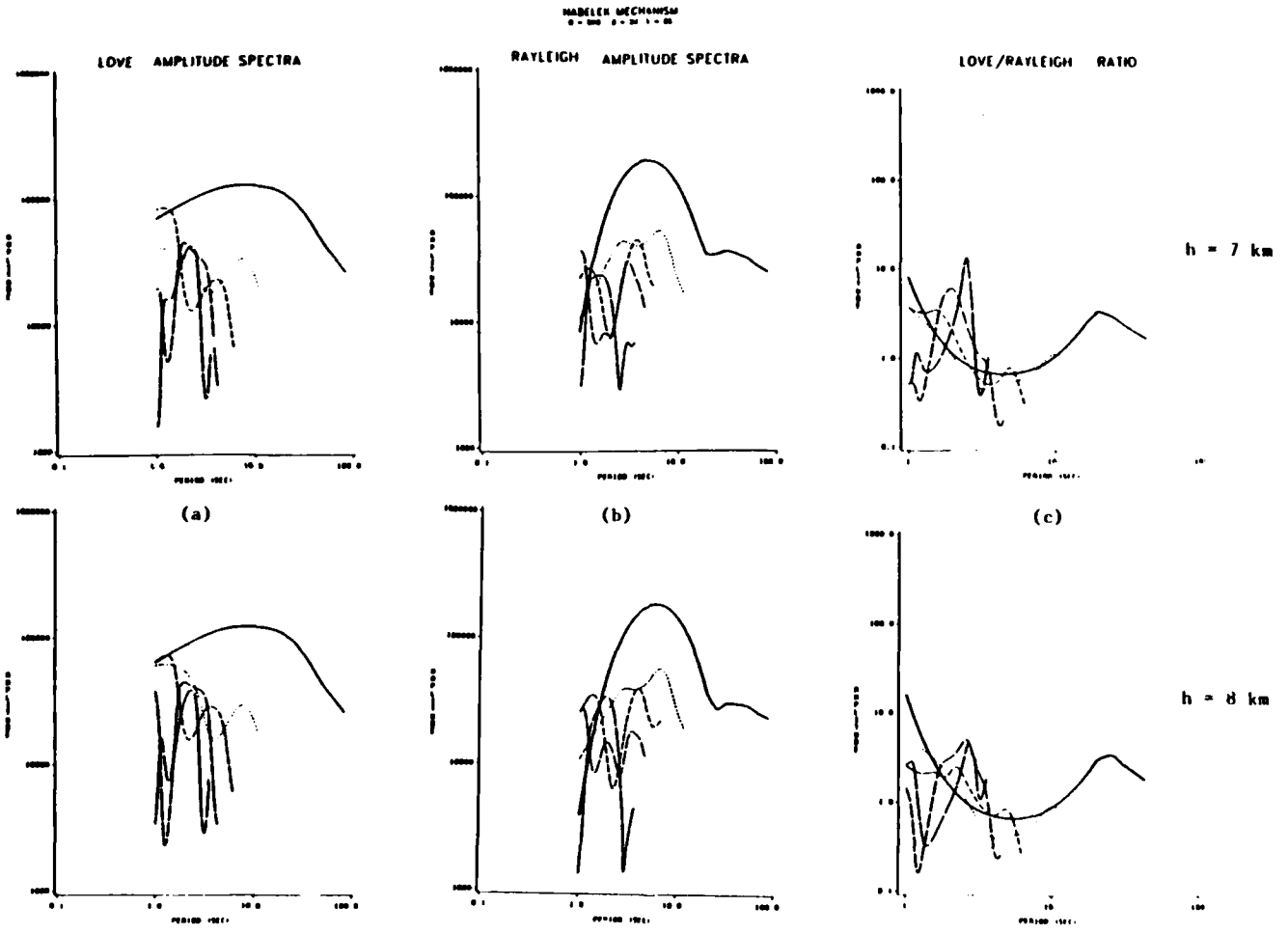
LOVE AMPLITUDE SPECTRA
RAYLEIGH AMPLITUDE SPECTRA
LOVE/RAYLEIGH RATIO
h = 7 km
h = 8 km
(a)
(b)
(c)

Figure A5 - 9

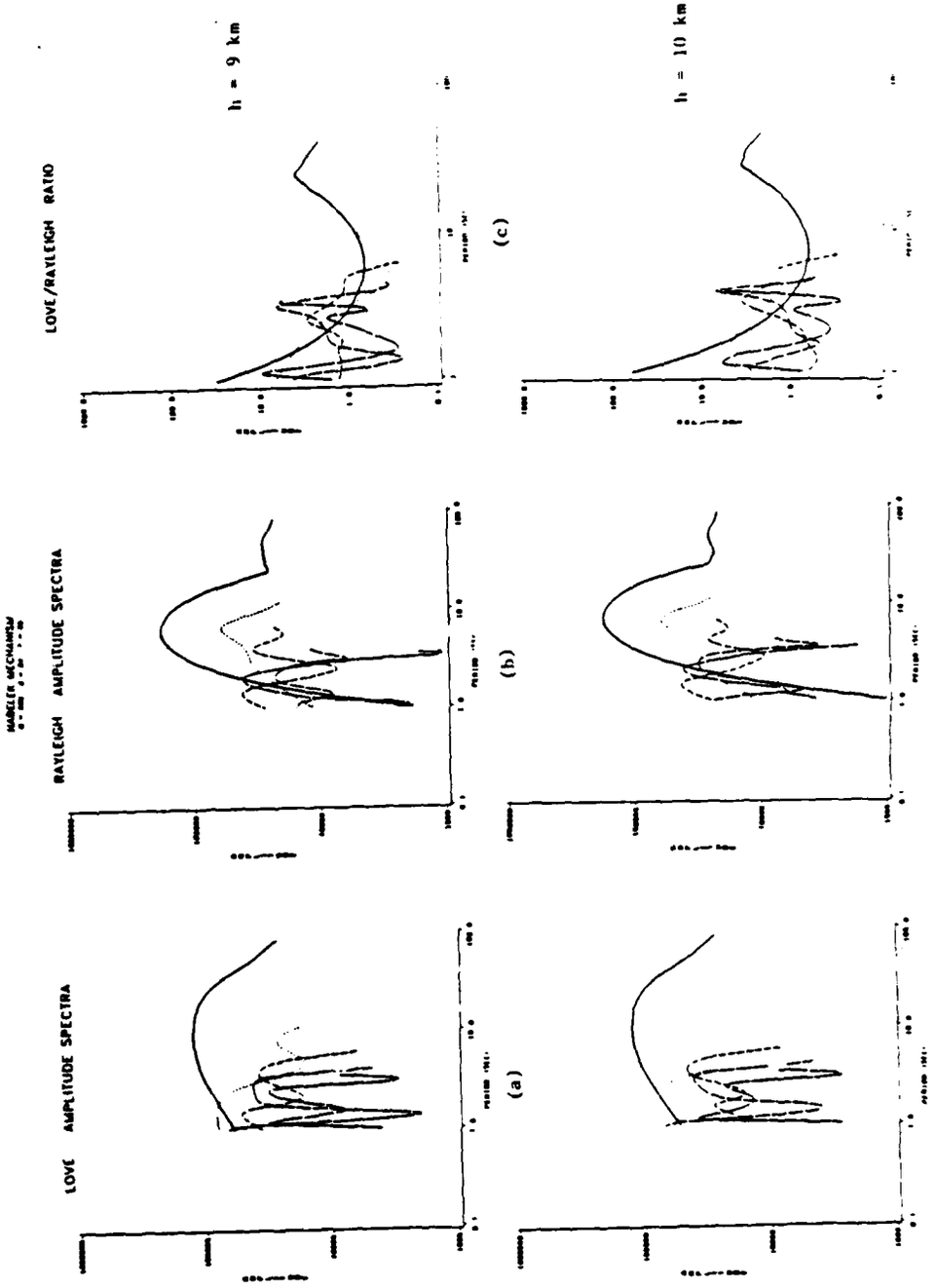
LOVE AMPLITUDE SPECTRA
RAYLEIGH AMPLITUDE SPECTRA
LOVE/RAYLEIGH RATIO
h = 9 km
h = 10 km
(a)
(b)
(c)

Figure A5 - 10

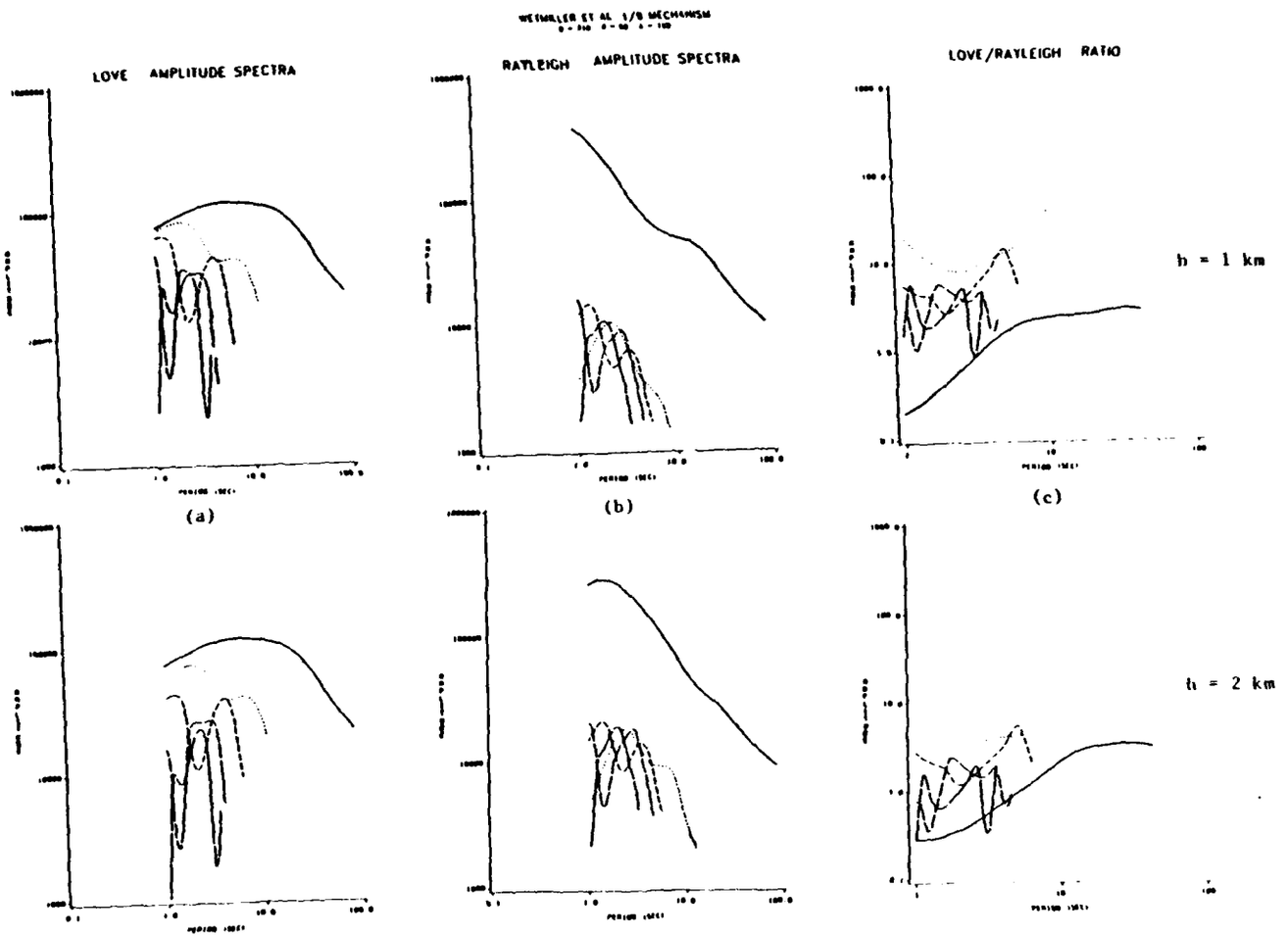
LOVE AMPLITUDE SPECTRA
RAYLEIGH AMPLITUDE SPECTRA
LOVE/RAYLEIGH RATIO
h = 1 km
h = 2 km
(a)
(b)
(c)

Figure A5 - 11

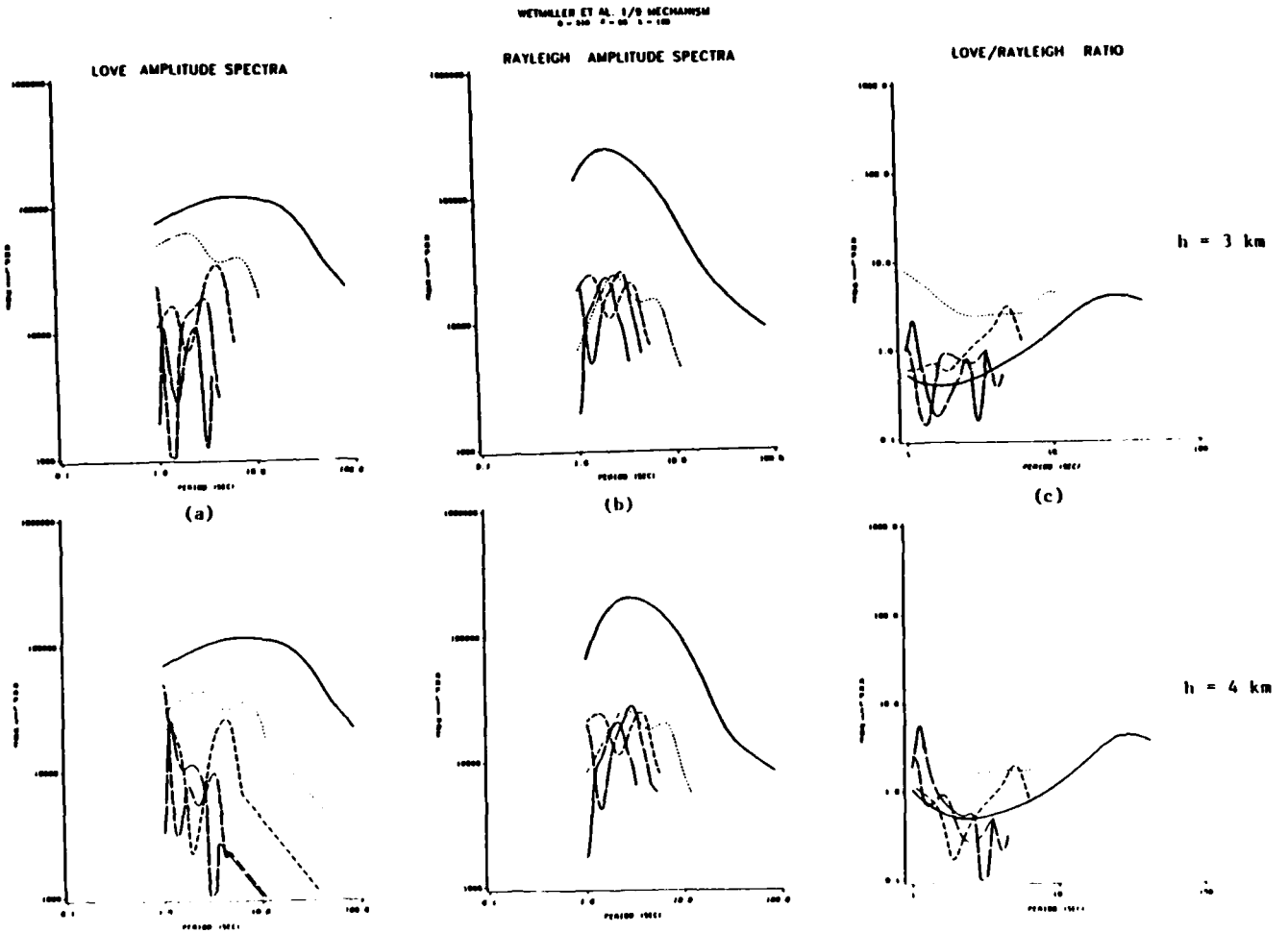
LOVE AMPLITUDE SPECTRA
RAYLEIGH AMPLITUDE SPECTRA
LOVE/RAYLEIGH RATIO
h = 3 km
h = 4 km
(a)
(b)
(c)

Figure A5 - 12

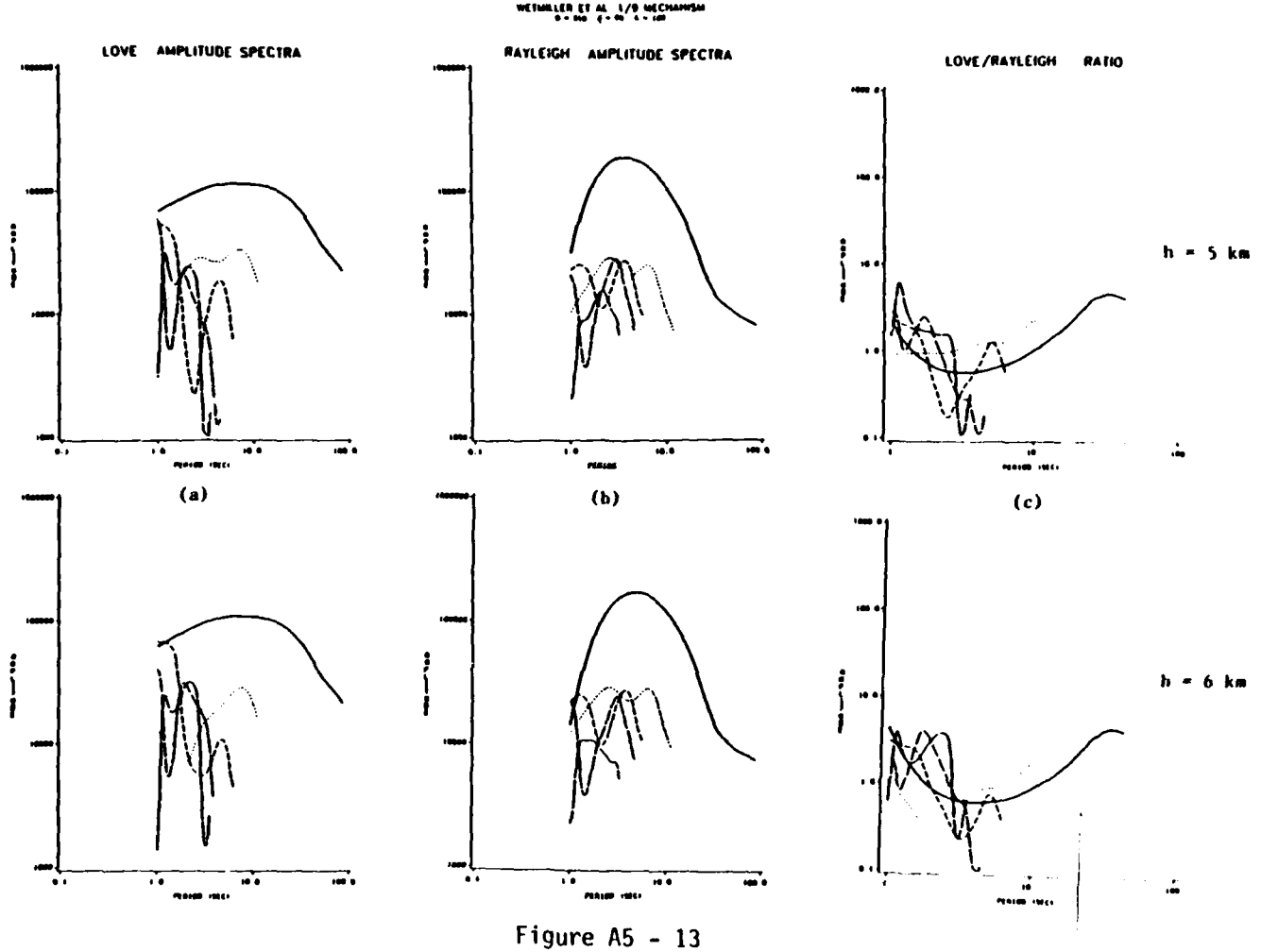
LOVE AMPLITUDE SPECTRA
RAYLEIGH AMPLITUDE SPECTRA
LOVE/RAYLEIGH RATIO
h = 5 km
h = 6 km
(a)
(b)
(c)

Figure A5 - 13

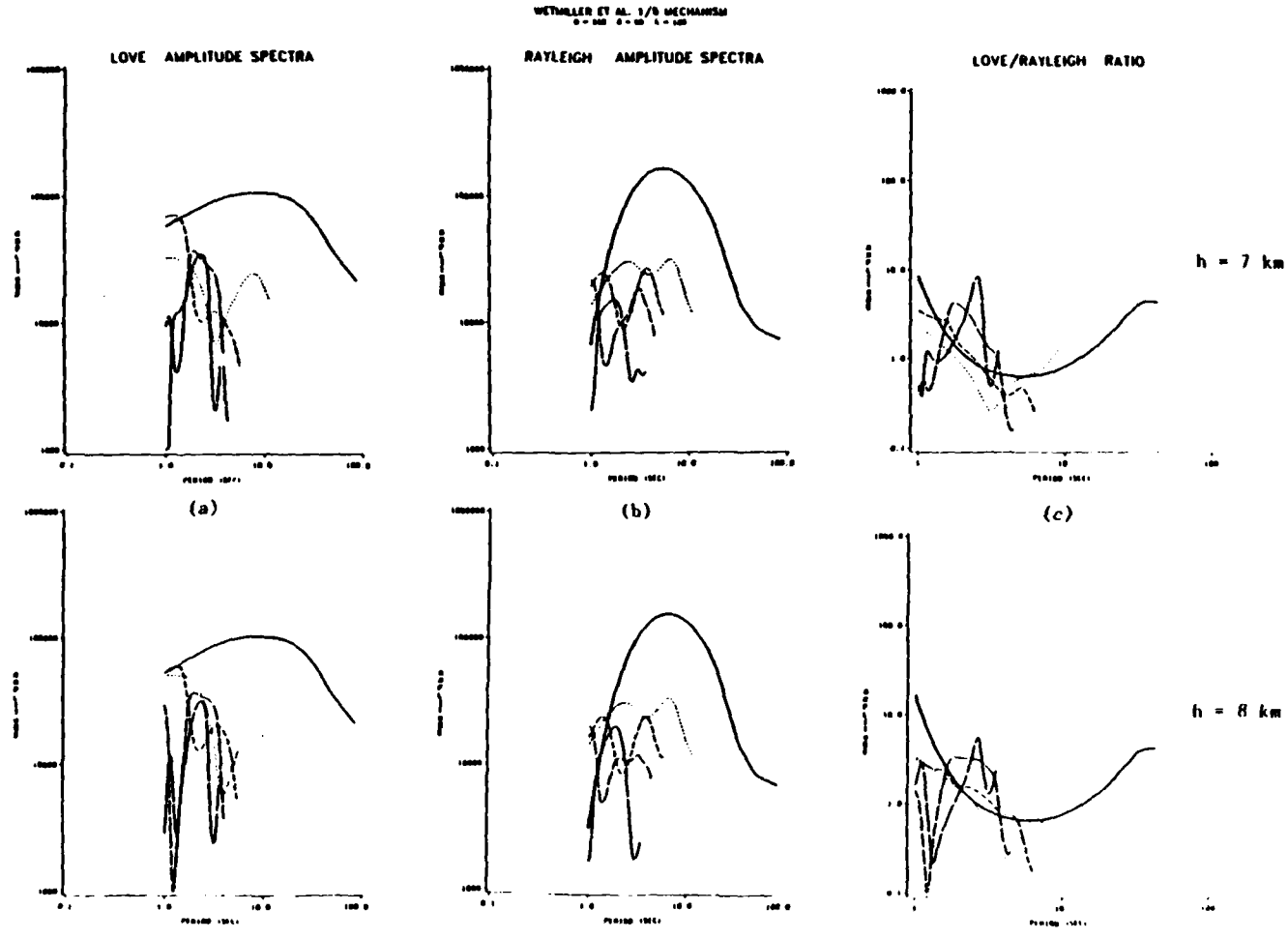
LOVE AMPLITUDE SPECTRA
RAYLEIGH AMPLITUDE SPECTRA
LOVE/RAYLEIGH RATIO
h = 7 km
h = 8 km
(a)
(b)
(c)

Figure A5 - 14

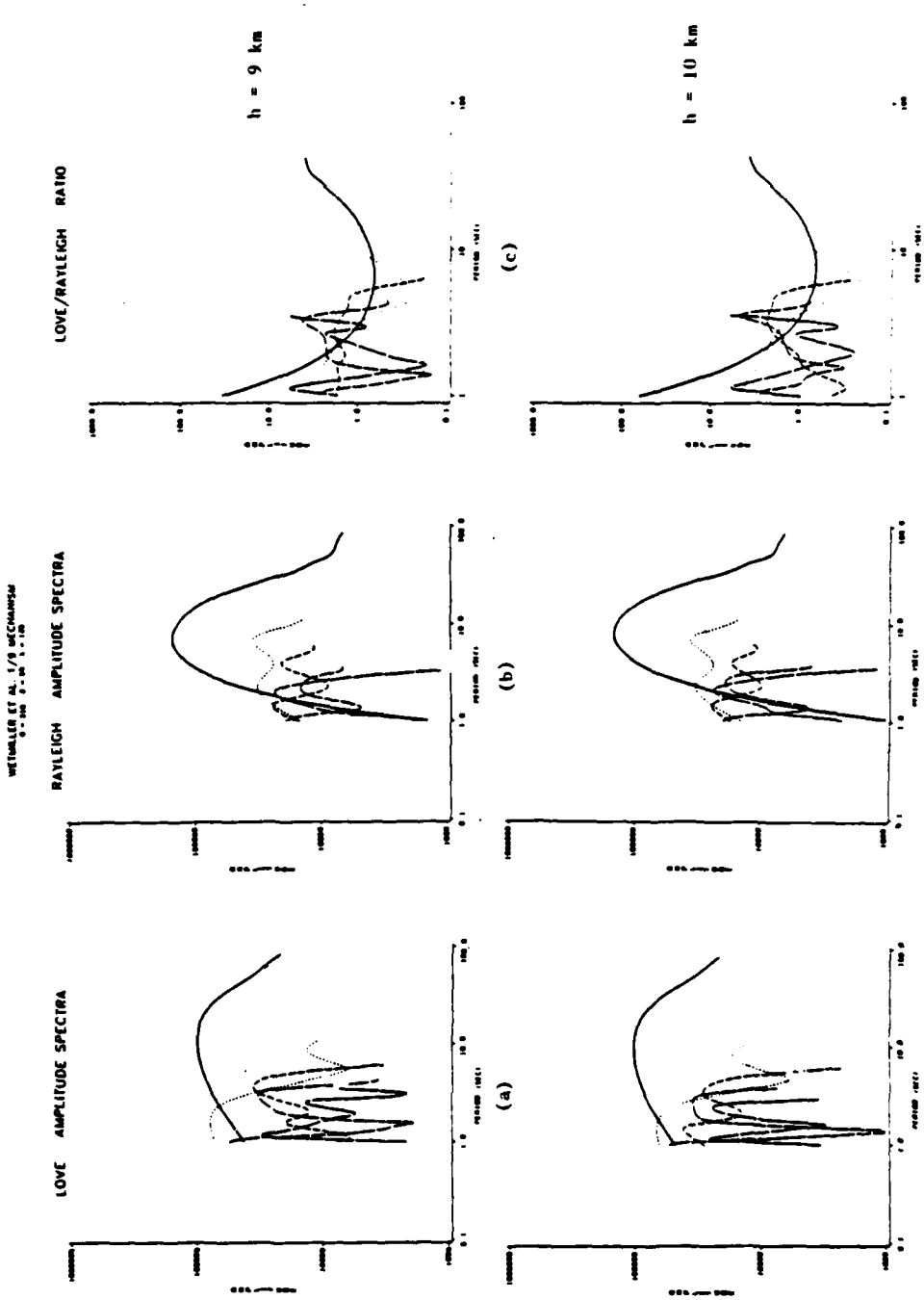
LOVE AMPLITUDE SPECTRA
RAYLEIGH AMPLITUDE SPECTRA
LOVE/RAYLEIGH RATIO
h = 9 km
h = 10 km
(a)
(b)
(c)

Figure A5 - 15

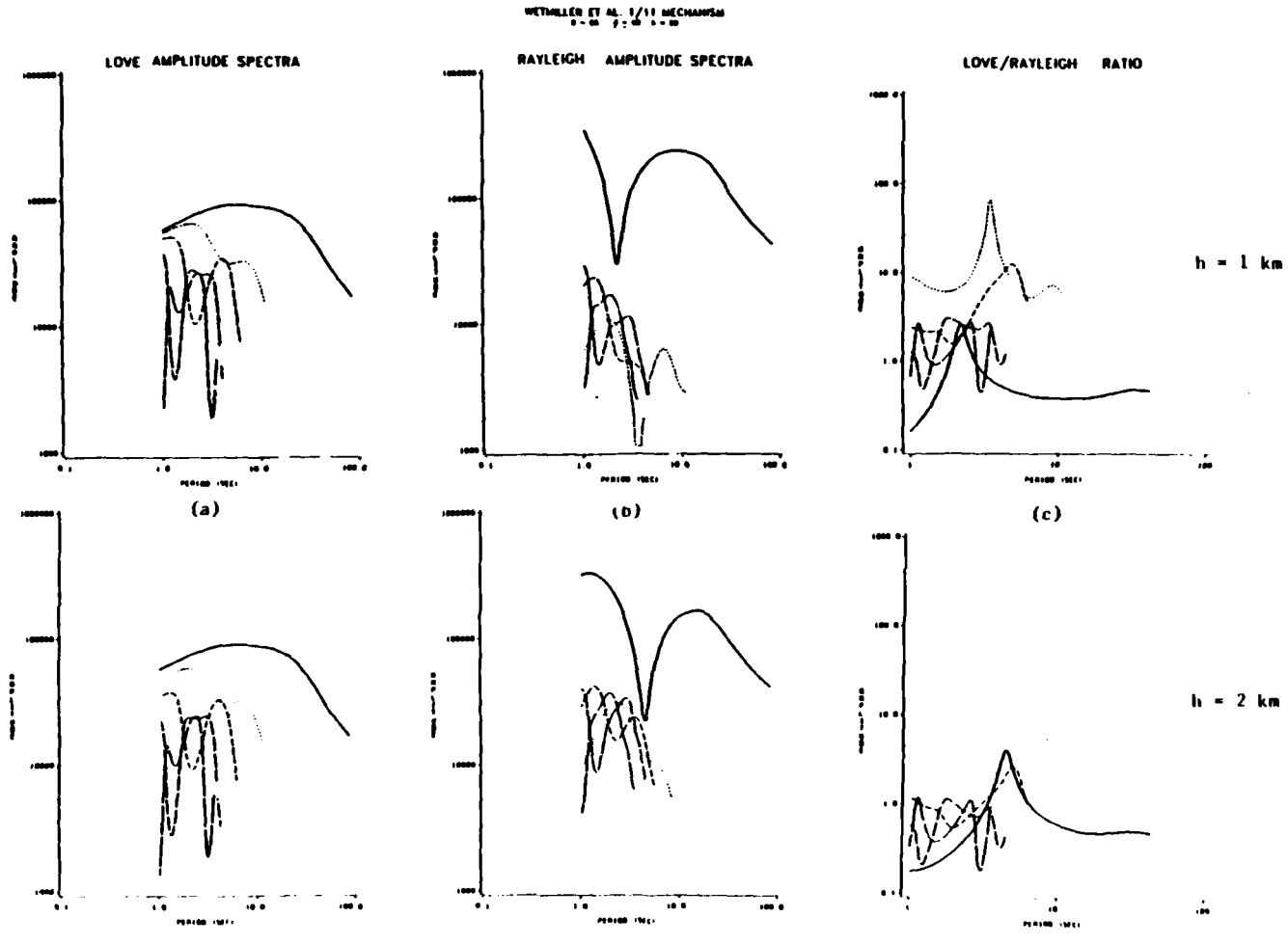
LOVE AMPLITUDE SPECTRA
RAYLEIGH AMPLITUDE SPECTRA
LOVE/RAYLEIGH RATIO
h = 1 km
h = 2 km
(a)
(b)
(c)

Figure A5 - 16

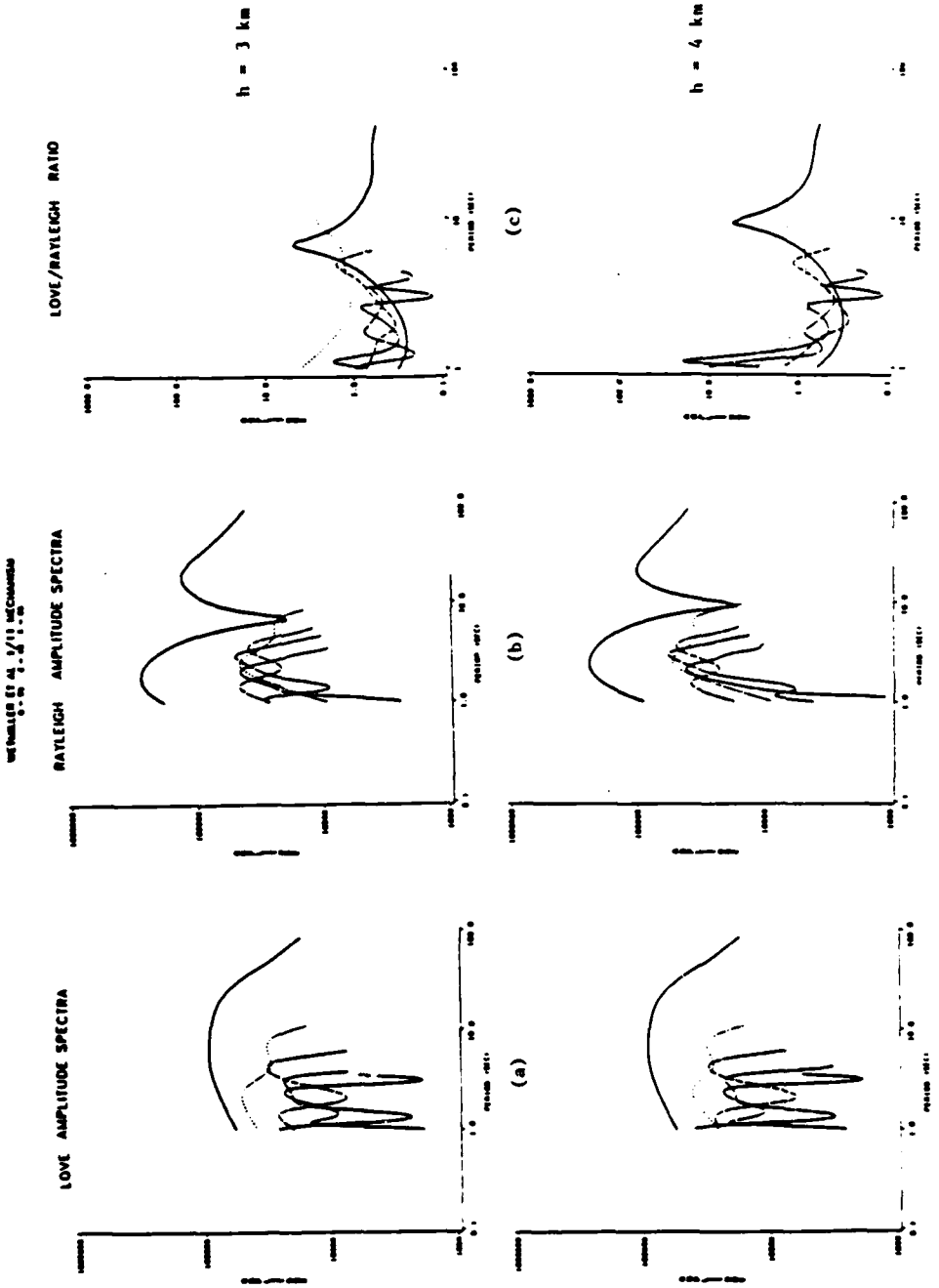
LOVE AMPLITUDE SPECTRA
RAYLEIGH AMPLITUDE SPECTRA
LOVE/RAYLEIGH RATIO
h = 3 km
h = 4 km
(a)
(b)
(c)

Figure A5 - 17

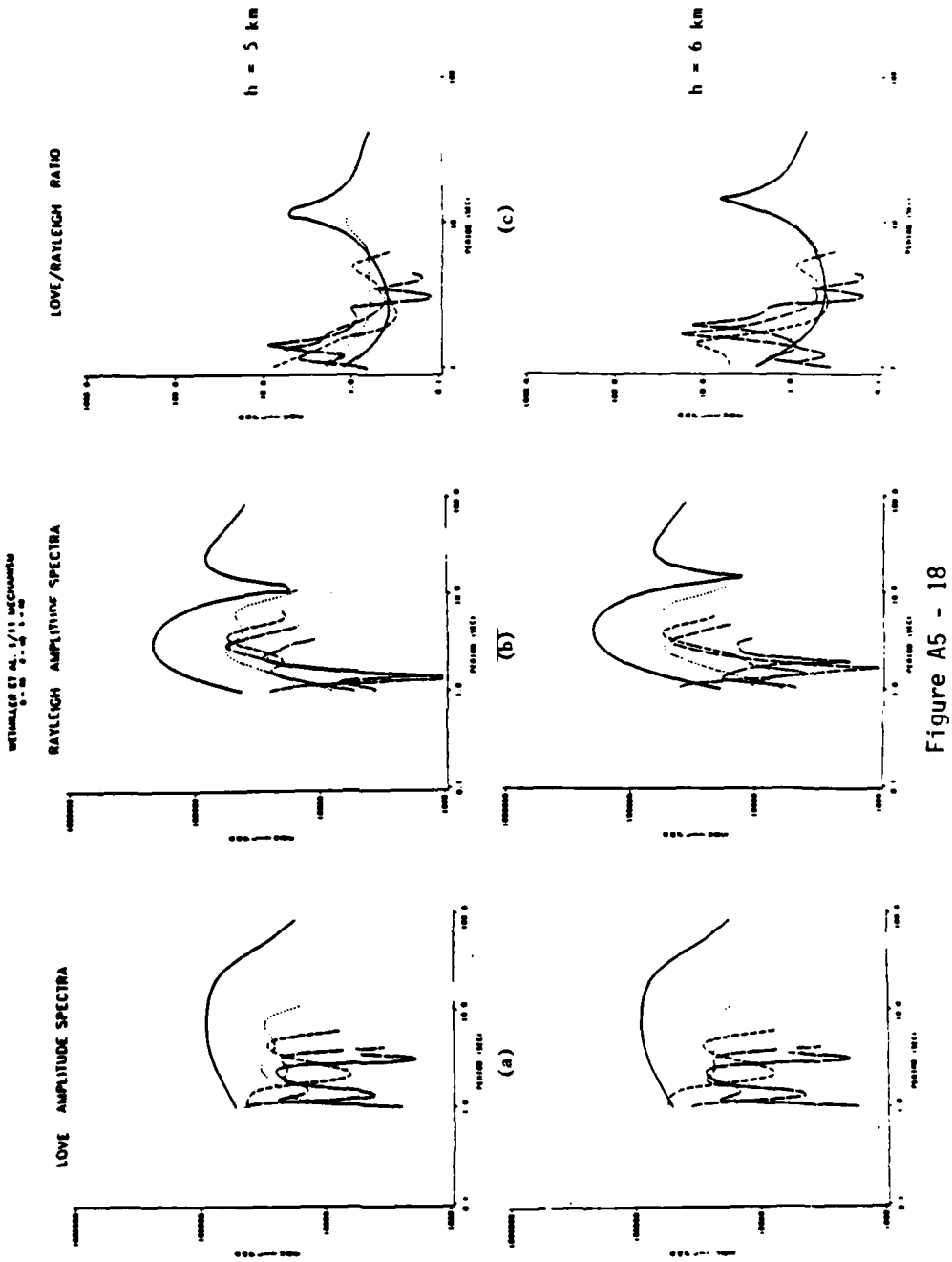
LOVE AMPLITUDE SPECTRA
RAYLEIGH AMPLITUDE SPECTRA
LOVE/RAYLEIGH RATIO
h = 5 km
h = 6 km
(a)
(b)
(c)

Figure A5 - 18

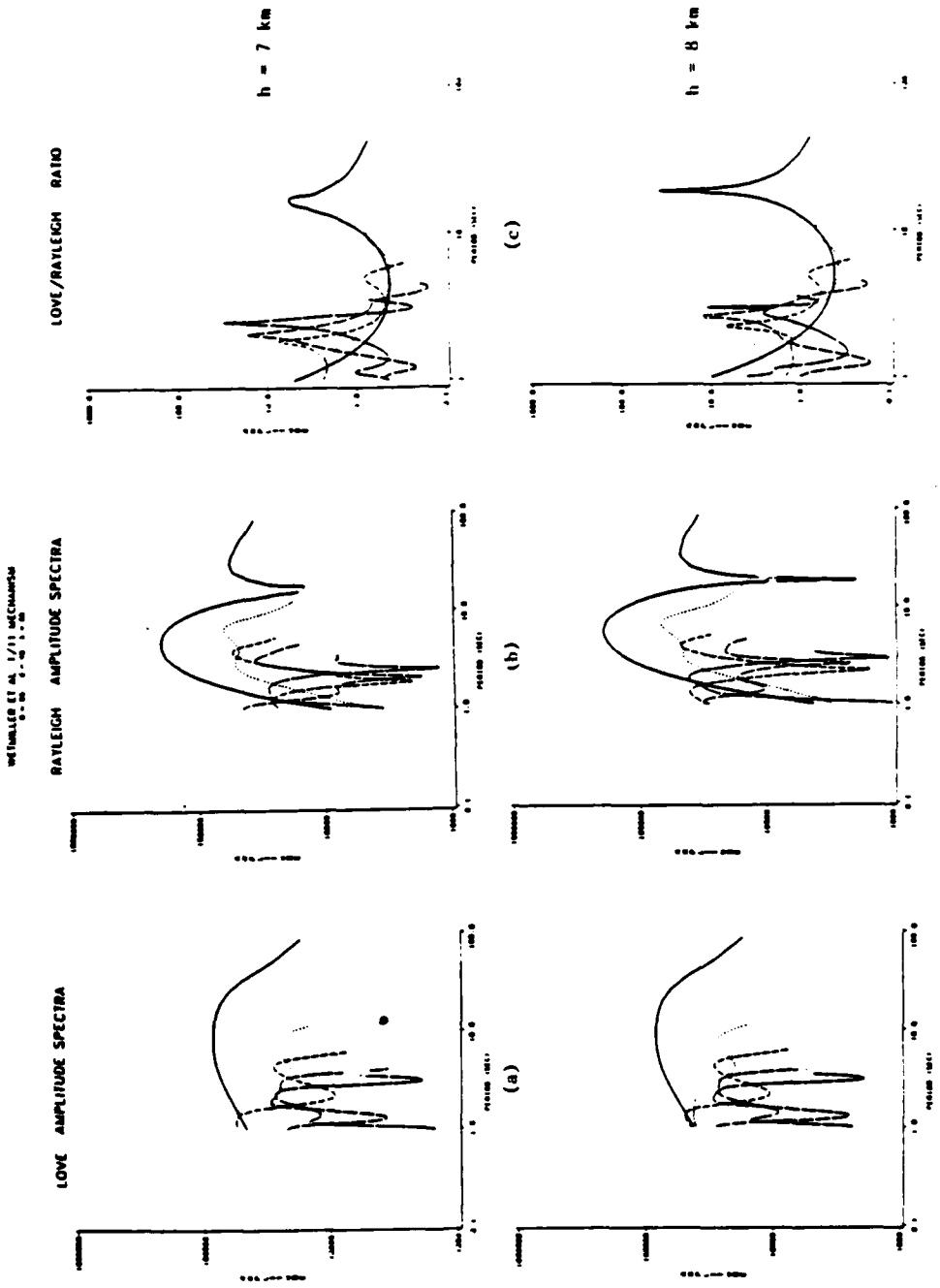
LOVE AMPLITUDE SPECTRA
RAYLEIGH AMPLITUDE SPECTRA
LOVE/RAYLEIGH RATIO
h = 7 km
h = 8 km
(a)
(b)
(c)

Figure A5 - 19

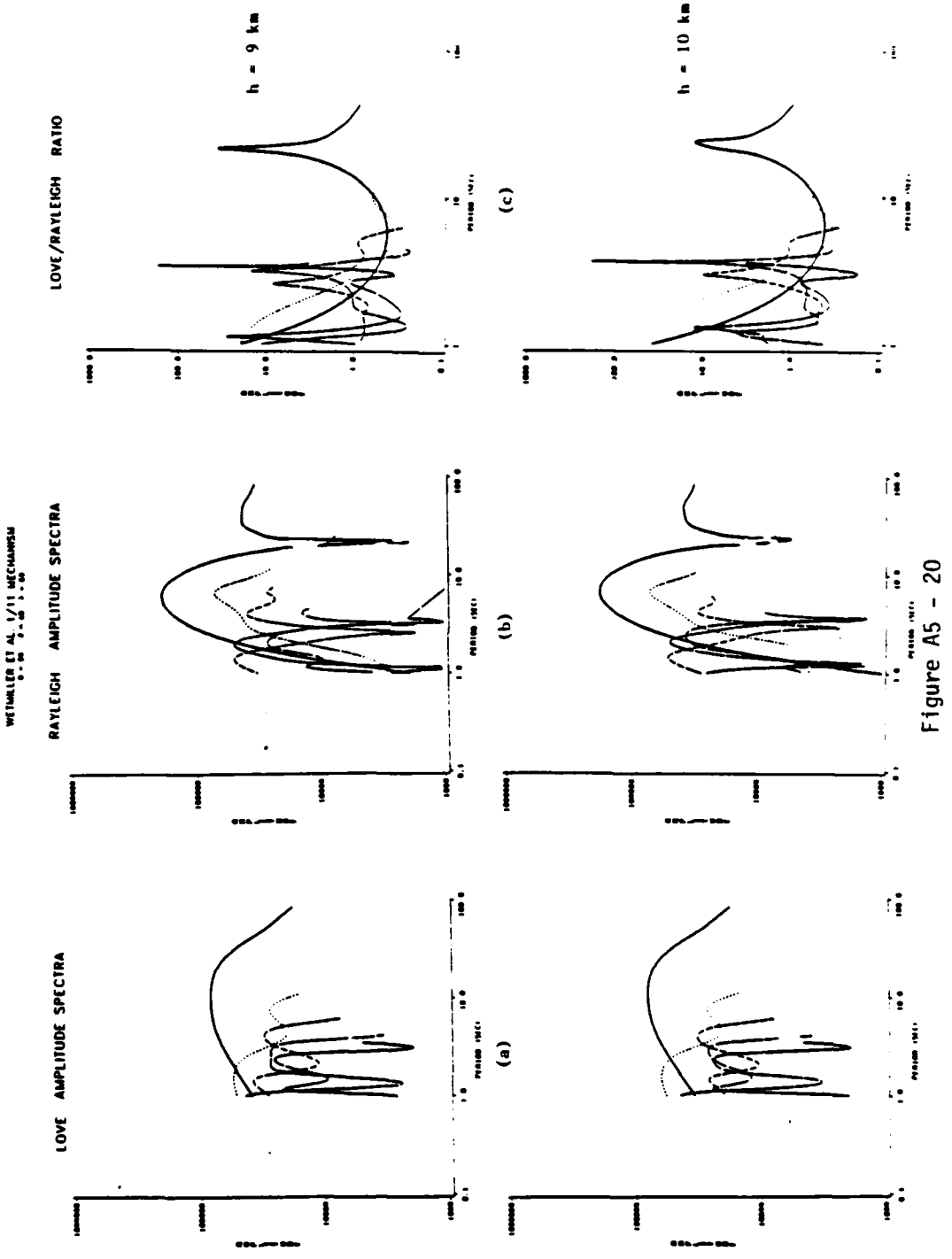
LOVE AMPLITUDE SPECTRA
RAYLEIGH AMPLITUDE SPECTRA
LOVE/RAYLEIGH RATIO
h = 9 km
h = 10 km
(a)
(b)
(c)

Figure A5 - 20

APPENDIX 6

Three-Dimensional Views
Of Spectral Amplitudes
In Group Velocity Vs. Period

Three dimensional renditions of the peak envelope amplitudes associated with the band-pass filtered seismograms were created and are displayed in Appendix 6 using a Surface II plotting routine which generates a complete grid of values from irregularly spaced points by applying a simple interpolation scheme. While a more complete three-dimensional view would result from similar processing of the entire envelope produced for each filtered signal, the amount of information anticipated from this effort vs. the expense of re-running the band-passes did not justify the undertaking. Peak amplitudes plotted against group velocity vs. period for Love (b) and Rayleigh (a) waves for each event are viewed both from a clockwise 45° and a 135° rotation of the group velocity vs. period plane, so that behavior at higher group velocities can be seen, especially when peaks at other group velocities obscure the view. Discontinuities in the lines on the plot are artifacts of instabilities in the interpolation scheme when amplitudes take on extreme values in close proximity to one another. Each three-dimensional plot is normalized to the highest amplitude value to be plotted. The long, more coarsely gridded axis represents period, with values ranging from 1 - 10 seconds; the short axis represents group velocity, spanning the window from 2.5 to 4.5 km/sec. Note that both axes are linear. Although quantitative interpretation of these plots is not feasible for obvious reasons, there is one very striking feature in the Love wave results. With the exception of the June 16 aftershock, whose features are obscured by the high amplitude arrival near ten seconds period, the three events of the January sequence show remarkable similarities in the pattern of Love wave excitation. A slightly lower amplitude in

the vicinity of one second and a more pronounced peak at about four seconds in the plot for the January 11 aftershock are the only significant differences noted(compare Figures A6-1b through 4b). This is significant considering that, for all the mechanisms tested in this study, the theoretical Love wave spectra (Appendix 5) were nearly invariant - only relative amplitudes differed. The obvious inference is that, for high frequency arrivals, Love wave relative modal excitation at the source is nearly the same from event to event and that this similarity is being preserved consistently for these events after propagating the 10.2° distance to SCP.

The Rayleigh plots (Figures A6-1a through 4a) are considerably more complicated, consistent with the character of the theoretical spectra for Rayleigh waves. The peak amplitude that so distinctly shows up at 10 seconds period is most assuredly associated with the fundamental mode, but by virtue of the controlling effect that a low velocity surficial layer will have on the higher frequency fundamental mode, it is not expected to be present in the shorter period signals for group velocities greater than 3 km/sec. It is in this shorter period higher group velocity range that it becomes possible to observe the higher mode behavior. Comparison of the theoretical spectra of the chosen mechanisms and preferred depths for the various events shows the differences that can be expected. Overlaying Figure A5-2b (for 3 or 4 km depth) and Figure A5-4b (for 7 km depth) shows that theoretically this depth difference accounts for the lower amplitude arrivals at 10 seconds period for the January 9 aftershock compared with higher amplitude contributions from both fundamental and first higher order mode at 10 seconds for the mainshock (compare Figures A6-1a and A6-2a). Figures A5-18b at 6 km for the January 11

aftershock and Figure A5-4b for the mainshock suggest that the amplitude at 10 seconds for the fundamental relative to the higher mode arrivals is smaller for the aftershock than for the mainshock. In fact, the higher order modes have comparable amplitudes to the fundamental mode amplitude for the January 11 aftershock.

In general careful comparison of the three-dimensional perspective plots in Figures A1-A4 and the corresponding band-pass filters for different events at common central frequencies (Appendix 3), shows that there is significant variation in relative excitation among the modes comprising Lg on the original vertical component seismograms. This behavior is contrast to that for the Love modes discussed earlier and is consistent with the variations in theoretical excitation of Rayleigh modes for different depths and focal mechanisms as evidenced by the theoretical results shown in Appendix 5. However, as discussed in the text, these variations

January 9, 1982
Mainshock

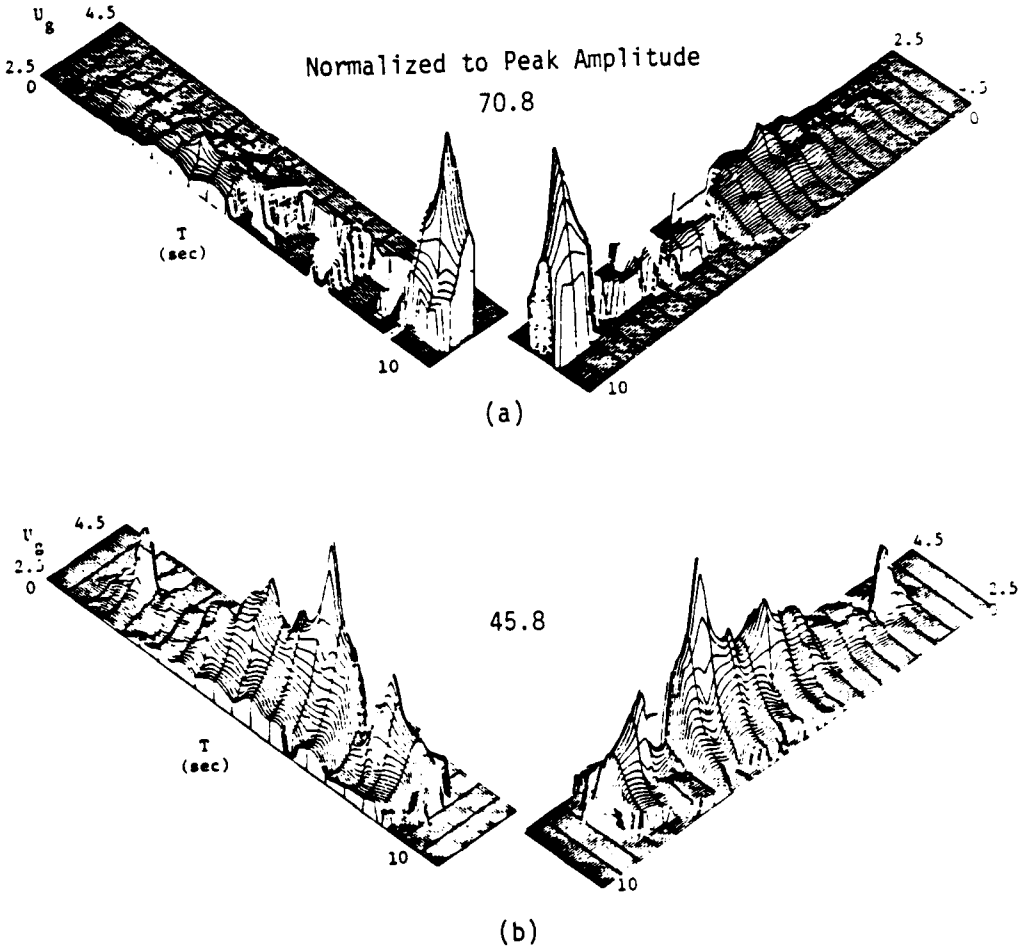

Figure A6 - 1

January 9, 1982
Aftershock

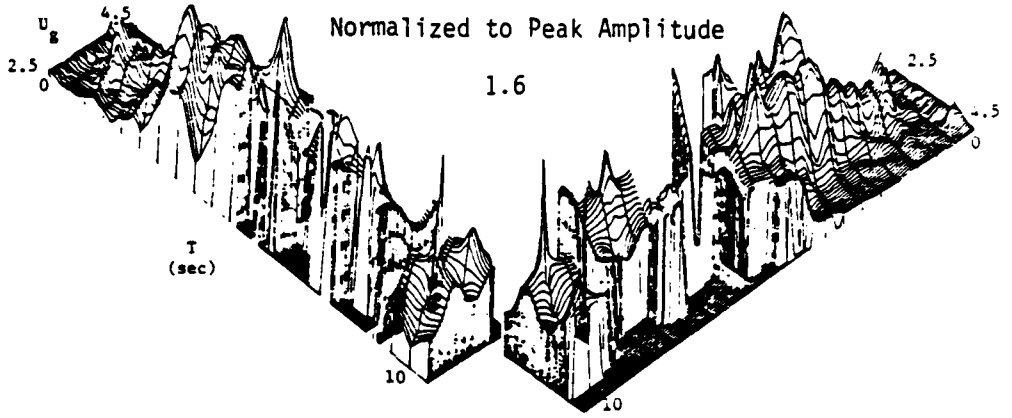

(a)

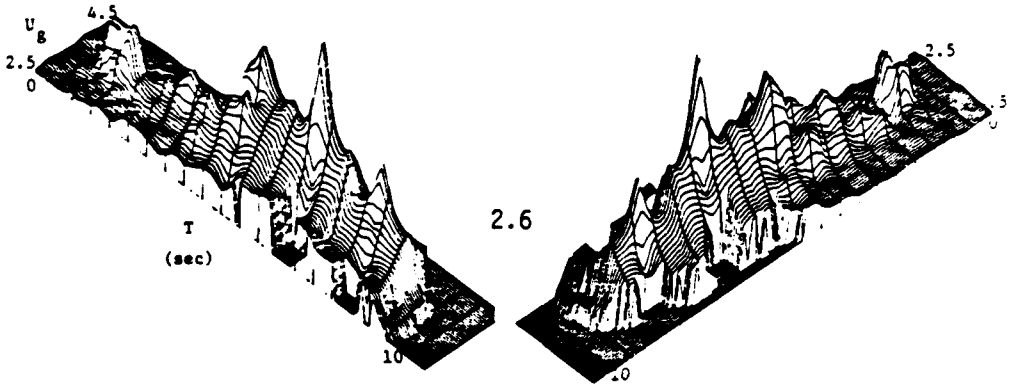

(b)

Figure A6 - 2

January 11, 1982
Aftershock

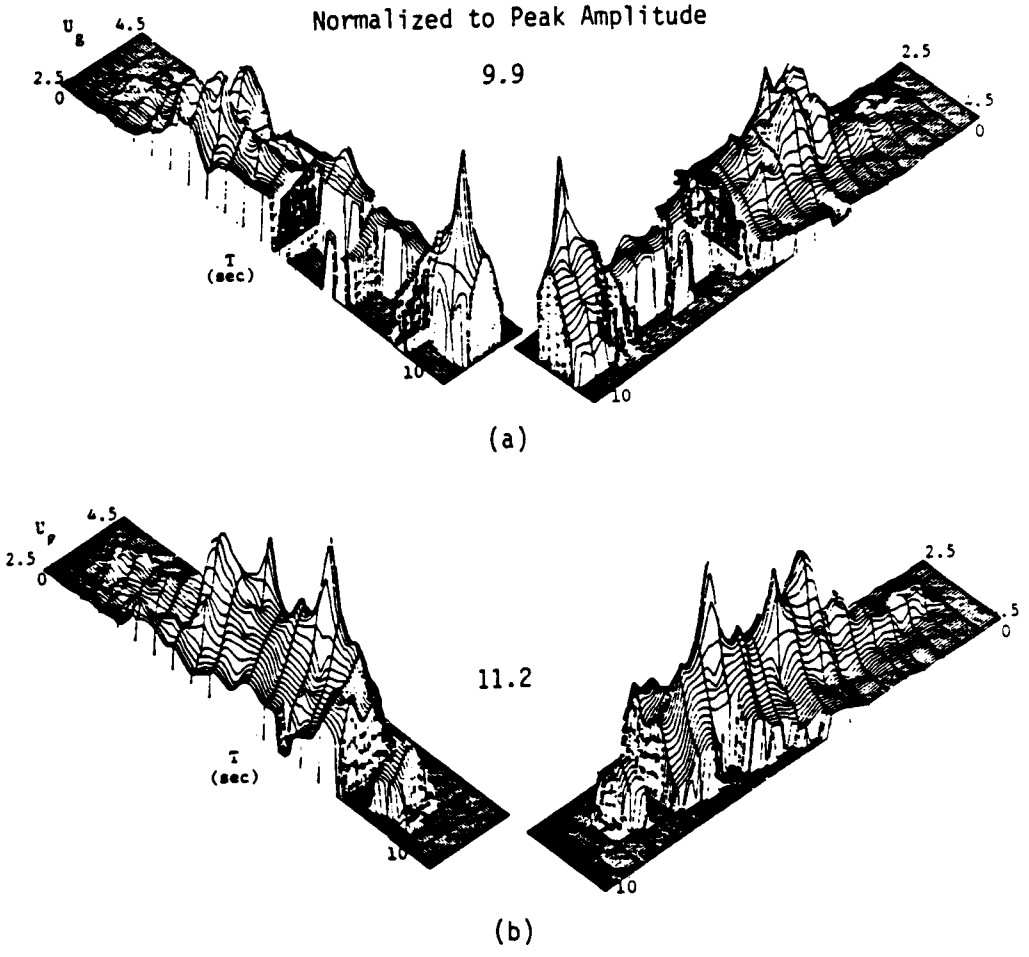

Figure A6 - 3

June 16, 1982

Aftershock

Normalized to Peak Amplitude

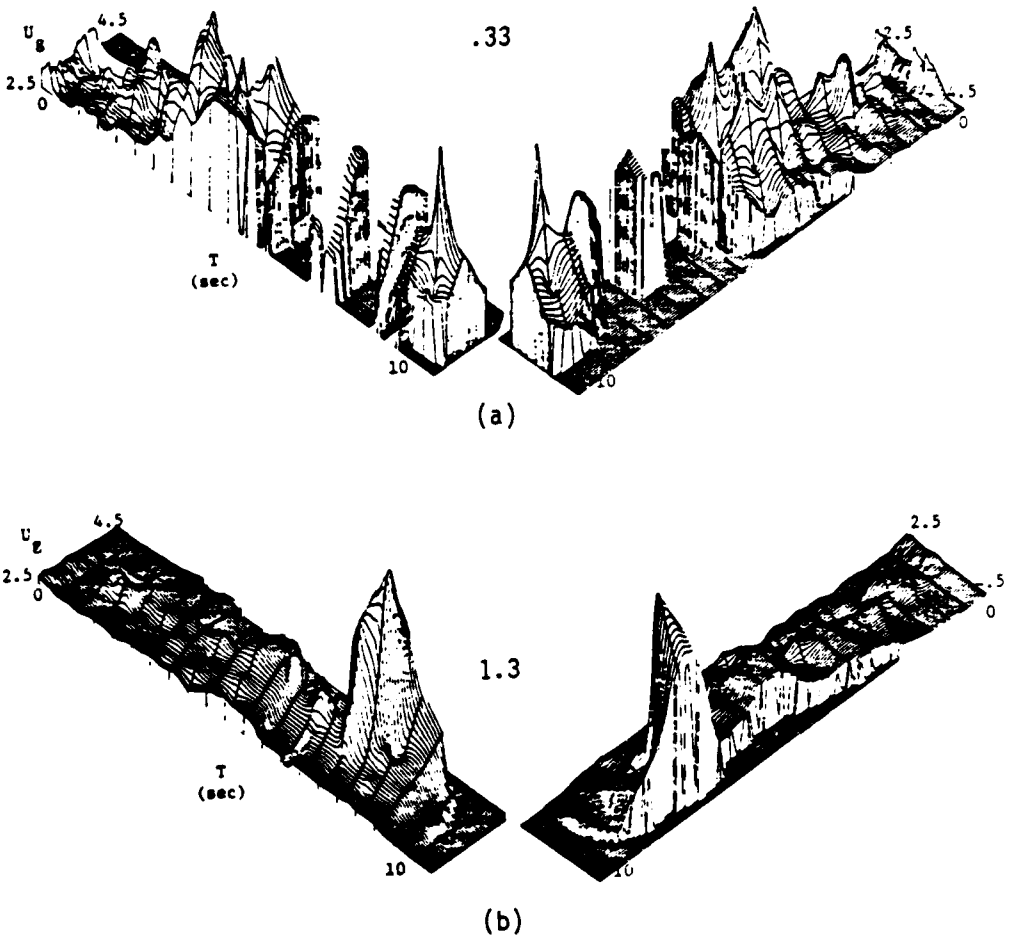

Figure A6 - 4

APPENDIX 7

Errata

Since December, 1983, when this study was concluded and defended, subsequent investigation into the New Brunswick Earthquakes has attempted to further refine source parameters using the same program but including a systematic search through incremented values of source parameters for the best match of theoretical and empirical Love/Rayleigh spectral ratios. Problems arising from this ongoing study led to pointed questioning of the published conventions of source geometry utilized by the program. What had been thought of as a reverse convention by most who studied this paper was found to be just that; it is to Lili Tang's credit that this suspicion was confirmed with Dr. Harkrider. The published convention indicated counterclockwise measurement of theta (as illustrated in Appendix 1); for subsequent programming reasons, clockwise measurement of theta from strike was preferred.

Subsequent work at The Pennsylvania State University (Yan, 1985) has yielded a best fit to the mainshock with source parameters as follows: theta equals 42 degrees, dip equals 43 degrees, and rake equals 130 degrees, most like the results proposed by Wetmiller et.al., 1983. The results of the present paper preferred the mechanism proposed by Choy (see Table 5, page 38), with strike of 195 degrees (theta = 318 degrees, or 360 - 318 degrees by the revised convention), dip of 65 degrees, and rake of 70 degrees(close to 180 minus the 130 degree rake preferred in Yan's work). Considering the equation for the radiation pattern and the dependence of the various terms and factors on theta and lambda, it's interesting to note that, except for the difference in dip values, the synthetic Love/Rayleigh amplitude ratios could be expected to be nearly the same for

the two cases. With theta now 360 degrees minus its former value and lambda now roughly 180 degrees minus its former value, the compensating effects alter the signs of all the real or imaginary terms, keeping amplitudes the same. Beyond that fortuitous relationship in the case of the mainshock, however, reasonable comparison ceases for the other events.

Acknowledgement of this error in applying the program necessitates retraction of the analyses involving comparison of synthetic spectra and empirical results obtained from the band-pass filters. With respect to the earthquakes in question, these interpretations have already been revised and improved through the subsequent work cited (Yan, 1985). Synthetic spectral ratios are, thus, submitted within the body of this paper and Appendix 5 as illustrative of the diagnostic nature of depth when using synthetic surface wave spectra in comparison with empirical Love/Rayleigh spectral ratios. They are, however, no longer indicative of the source parameters for the events studied.